

## CONTENTS

	PAGE	RUSS. ISSUE	RUSS. PAGE
Sensitization of the Photoeffect in Semiconductors by Organic Dyes Which are Acidity Indicators. <u>I. A. Akimov and Academician A. N. Terenin</u> .....	997	1	109
A Mass-Spectrometric Study of Cesium Halides. <u>P. A. Akishin, L. N. Gorokhov, and L. N. Sidorov</u> .....	1001	1	113
The Theory of Turbulent Combustion. <u>A. N. Voinov</u> .....	1005	1	117
The Thermal Properties of the Transitional Forms of Carbon. <u>V. I. Kasatochkin, V. K. Zamoluev, A. T. Kaverov, and K. Usenbaev</u> .....	1009	1	121
An Experimental Determination of the Enthalpy of Corundum ( $Al_2O_3$ ) from 500 to 2000°. <u>V. A. Kirillin, Corresponding Member, Academy of Sciences, USSR, A. E. Sheindlin, and V. Ya. Chekhovskoi</u> .....	1013	1	125
The Selective Character of Adsorption as a Function of Sorbent Structure. <u>V. S. Komarov and Academician (Academy of Sciences, Beloruss SSR) N. F. Ermolenko</u> .....	1019	1	129
The Effects of Vulcanization of Elastomers on Their Adhesion to Non-vulcanizing Polymers. <u>V. G. Raevskii and S. S. Voyutskii</u> .....	1023	1	133
The Nonlinear Thermodynamics of Irreversible Processes. <u>I. F. Bakhareva</u> .....	1027	2	350
Critical Phenomena Occurring Under the Influence of Inhibitors in Degenerative Branching Reactions. <u>A. B. Gagarina, Z. K. Maizus, and Corresponding Member of the Academy of Sciences of USSR, N. M. Emanuel'</u> .....	1033	2	354
Two Types of Plasticizing of Rigid-Chain Polymers. <u>Academician V. A. Kargin, P. V. Kozlov, R. M. Asimova, and L. I. Anan'eva</u> .....	1037	2	357
Kinetic Equations for Nonchain Monomolecular Radiation - Chemical Reactions. <u>Yu. A. Kolbanovskii and L. S. Polak</u> .....	1041	2	361
The Association of Complex Copper Ions in Solution. An Investigation by the Paramagnetic Resonance Method. <u>A. I. Ribkind</u> .....	1047	2	365
Modification of a Silver Catalyst by Organic Halogen Compounds. <u>Yu. N. Stepanov, L. Ya. Margolis, and S. Z. Roginskii, Corresponding Member, Academy of Sciences, USSR</u> .....	1051	2	369
The Theory of the Thermalization of "Hot" Hydrogen Atoms, and Their Influence on the Yield of Dimeric Product During the Radiolysis of Alkanes. <u>A. Ya. Temkin</u> .....	1055	2	373
Ring-Fluorine Chemical Shift in the Nuclear Magnetic Resonance of Fluorobenzenes with Fluorinated Substituents. <u>L. M. Yagupol'skii, V. F. Bystrov, and É. Z. Utyanskaya</u> .....	1059	2	377
A Thermographic Determination of Small Heat Changes at Temperatures Below 0° C. <u>A. G. Anikin and G. M. Dugacheva</u> .....	1065	3	634
The Heat Capacity of the Silica Gel - Water Adsorption System. <u>G. I. Berezin, A. V. Kiselev, and V. A. Sinitsyn</u> .....	1071	3	638

# CONTENTS (continued)

	PAGE	RUSS. ISSUE	RUSS. PAGE
An X-Ray Spectroscopic Study of Titanium Beryllides. <u>É. E. Vainshtein, E. A. Zhurakovskii, and I. B. Staryi</u> .....	1077	3	642
Proton Relaxation in Hydrogen Peroxide Solutions Exposed to Ultraviolet Radiation. Corresponding Member Academy of Sciences, USSR, <u>V. M. Vdovenko, E. K. Legin, O. B. Stebunov, and V. A. Shcherbakov</u> .....	1081	3	645
The Electrical Conductance of MnO <sub>2</sub> Semiconductors in the Course of Catalytic Oxidation of CO. <u>Zh. P. Kachanova, Corresponding Member of Academy of Sciences, USSR V. V. Voevodskii, and A. P. Purmal'</u> .....	1085	3	648
The Influence of Tetraalkylammonium Salts on the Capacity of the Double Layer in Butyl Alcohol Solutions. <u>P. A. Kirkov</u> .....	1089	3	651
The Assignment of Electron Configuration Types in Atoms. <u>V. M. Klechkovskii</u> .....	1093	3	655
The Saturated Vapor Pressures of Tetrachloroalkanes at Low Temperatures. <u>N. A. Malafeev, V. A. Malyusov, N. N. Urmnik, I. V. Podgornaya, and N. M. Zhavoronkov, Corresponding Member, Academy of Sciences, USSR</u> .....	1097	3	659
A Study of the Effect of Additions of Dispersed Iron as Active Filler on the Physicomechanical Properties of Polymeric Materials. <u>A. M. Smirnova, L. V. Pevzner, T. V. Raikova, and V. I. Likhman</u> .....	1101	3	663
The Problem of Reducing Basicities to a Single Standard State. An Investigation of the Basicity of Acetone. <u>Yu. L. Khaldna and V. A. Pal'm</u> .....	1105	3	667
Hyperfine Structure of the EPR Spectrum in a One-Electron System with Two Potential Wells. <u>A. I. Burshtein</u> .....	1111	4	886
The Effect of Corrosion Inhibitors on Mechanicocorrosional Abrasion. <u>E. M. Zaretskii, I. M. Katser, and O. A. Petrova</u> .....	1117	4	890
The Structure and Properties of Isotactic Polyacrylic Acid and Its Salts. Academician <u>V. A. Kargin, S. Ya. Mirlina, V. A. Kabanov, G. A. Mikheleva, and A. V. Vlasov</u> .....	1121	4	893
The Role of Longitudinal Mixing in Exchange Columns for Isotopic Separation. Academician <u>B. P. Konstantinov and L. V. Kotova</u> .....	1125	4	896
The Effect of Metallic Ions on the Corrosion of Stainless Steel in Concentrated HNO <sub>3</sub> Solutions. <u>M. M. Kurtepov and A. S. Gryaznova</u> .....	1129	4	899
The Radiolytic Reduction of Tetravalent Cerium in the Presence of Monovalent Thallium Under Irradiation at High Dosage Rates. <u>A. K. Pikaev and P. Ya. Glazunov</u> .....	1133	4	902
The Problem of the Penetration of Silver Into Tungsten. <u>V. I. Rakhovskii, A. P. Lyubimov, and V. M. Garmash</u> .....	1139	4	906
Effect of the Nature of the Cation on the Kolbe Electrosynthesis. <u>M. Ya. Fioshin, Yu. B. Vasil'ev, and E. G. Gaginkina</u> .....	1143	4	909
Investigation of Energy Transfer Along A $\sim\text{CH}_2\sim$ Chain by Luminescence Quenching. <u>V. I. Gusynin and V. L. Tal'roze</u> .....	1147	5	1160
Adsorption of Alkyl Radicals on Oxide Semiconductors. <u>I. A. Myasnikov and E. V. Bol'shun</u> .....	1151	5	1164
On A Certain Possibility in the Quantum Theory of Chemisorption. <u>V. I. Osherov</u> .....	1157	5	1168
A Method for Determining The Rates and The Kinetic Constants of Complicated Chemical Reactions in a Flow System. <u>G. M. Panchenkov and Yu. M. Zhorov</u> .....	1161	5	1172

# CONTENTS (continued)

	PAGE	RUSS. ISSUE	RUSS. PAGE
Electron Density Distribution in Germanium. <u>Academician (Academy of Sciences Beloruss SSR) N. N. Sirota and A. U. Sheleg</u> .....	1165	5	1176
Micelle Formation in Solutions of Surface-Active Substances. <u>A. B. Taubman and S. A. Nikitina</u> .....	1169	5	1179
The Capacity of the Electrical Double Layer in Molten Salts. <u>E. A. Ukshe, N. G. Bukun, and D. I. Leikis</u> .....	1173	5	1183
The Simultaneous Discharge of Metallic Ions in Real Conjugate Systems. <u>A. T. Vagramyan and T. A. Fatueva</u> .....	1177	6	1413
The Influence of Monolayers on the Evaporation of Drops. <u>Corresponding Member of the Academy of Sciences of the USSR B. V. Deryagin, S. P. Bakanov, and Yu. S. Kurgin</u> .....	1183	6	1417
Destruction and Formation of Structures of Natural Proteins During Their Transfer Through Nonporous Membranes. <u>Academician V. A. Kargin, P. V. Kozlov, S. Ya. Mirlina, and Z. A. Kapralova</u> .....	1189	6	1421
Effects of Discreteness of Charge and Properties of the Double Layer at a Metal-Solution Interphase (Consideration of the Discrete Structure of the Charge of Specifically Adsorbed Ionic Layers). <u>Corresponding Member V. G. Levich, V. A. Kir'yanov, and V. S. Krylov</u> .....	1193	6	1425
Determination of the Electrocapillary Maximum Potential of Silver. <u>D. I. Leikis</u> .....	1199	6	1429
Mechanism of the Anode Solution of Indium Amalgam in Acid Solutions. <u>V. V. Losev and A. I. Molodov</u> .....	1203	6	1432
Destruction of Molecular Chains and Disruption of Cross Links During Aging of Vulcanizates. <u>L. I. Lyubchanskaya and A. S. Kuz'minskii</u> .....	1207	6	1436
The Role of Dispersion in the Combustion of Explosives. <u>A. G. Merzhanov</u> .....	1211	6	1439
The Vibrational Distribution Function for Monatomic Molecules in Monomolecular Decomposition. <u>E. E. Nikitin</u> .....	1215	6	1442
The Relation Between the Yield of Radiochemical Reactions and the Concentration of Dissolved Substances. <u>M. A. Proskurnin</u> .....	1221	6	1446
The Relation Between the Electrical Conductivity of Organic Substances With Conjugate Bonds and the Electron Magnetic Resonance Spectra. <u>B. L. Tal'roze and L. A. Blyumenfel'd</u> .....	1225	6	1450
Author Index, Vols. 130-135, 1960 .....	1229		
Tables of Contents, Vols. 130-135, 1960 .....	1236		

2-7-77

## SENSITIZATION OF THE PHOTOEFFECT IN SEMICONDUCTORS BY ORGANIC DYES WHICH ARE ACIDITY INDICATORS

I. A. Akimov and Academician A. N. Terenin

Translated from *Doklady Akademii Nauk SSSR*, Vol. 135, No. 1, pp. 109-112,  
November, 1960

Original article submitted July 8, 1960

An earlier cycle of studies in our laboratory established and made a detailed study of the phenomenon of optical sensitization of the internal photoeffect for a number of semiconductors — oxides and halides — by organic dyes of different types [1]. In the present work the sensitizers used were organic dyes whose molecules, by combining with or releasing a proton, show a sharp color change and displacement of the position of the absorption band in the spectrum.

The condenser method [2] was used to measure the photoeffect in layers of TlI and ZnO which had been colored with dyes which are also acidity indicators: the measurements were made first in the usual way in air or in vacuo, and then after the adsorption of HCl or  $\text{NH}_3$  vapor on the materials. The vapor from concentrated hydrochloric acid and the ammonia vapor were dried thoroughly beforehand. For this purpose, concentrated sulfuric acid was added to the hydrochloric acid. The water vapor in the gases was then frozen out by passage through a trap cooled to  $-90^\circ\text{C}$ . The pressure of ammonia vapor at  $-92^\circ$  is 10 mm Hg, and pure HCl vapor gives the same pressure at  $-136^\circ$  [3]. There was no significant difference in the results of experiments carried out in air and in vacuo.

According to Putseiko's data [4], the photo-emf of ZnO in the presence of ammonia vapor at 4 mm pressure is decreased by a factor of approximately two, without change in the spectral distribution. We have established that the condenser photo-emf of an undyed layer of TlI is increased by a factor of 2-3 when HCl vapor is adsorbed, without any significant change in the spectrum.

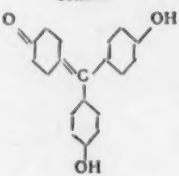
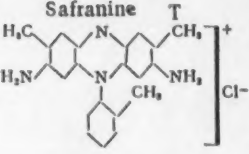
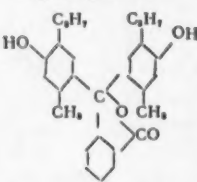
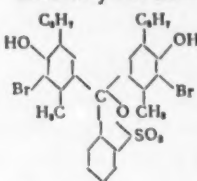
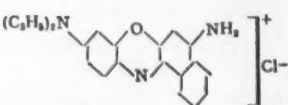
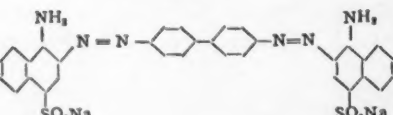
The results of experiments on the influence of gaseous HCl and  $\text{NH}_3$  on the photoeffect of TlI and ZnO colored by various indicator-dyes are shown in Table 1 and Fig. 1.\* The over-all indicator-sensitized photoeffect in TlI showed little change in magnitude after the adsorption of HCl and even decreased in some cases. The spectral distribution of the sensitized photoeffect, however, changed sharply, corresponding to the change in the absorption spectrum of the dye. After adsorption of gaseous  $\text{NH}_3$ , on the other hand, the sensitized photoeffect decreased sharply or disappeared completely in the case of TlI. Unlike the photoeffect for TlI, the sensitized photoeffect in ZnO disappears after treatment with HCl vapor. Desorption of the HCl leads to restoration of the former induced sensitivity in ZnO.

Thus, the indicator-dyes, when present in the neutral form, act as optical sensitizers of the photoeffect, both for the hole semiconductor TlI and for the electronic semiconductor ZnO. After the attachment of HCl, however, i.e., in the protonated form, the same dyes sensitize the photoeffect in TlI but lose the ability to sensitize ZnO. In the anionic form, produced by the loss of a proton under the influence of  $\text{NH}_3$ , the corresponding dye indicators sensitize the photoeffect in ZnO but lose the ability to sensitize TlI.

\* The changes in the spectral curve in the region of the noninduced sensitivity of the semiconductor are shown in a separate graph because of the difference in the scale of the ordinates.

TABLE 1

Sensitization of the Photoeffect in TlI and ZnO by Dyes Which are Also Acidity Indicators

Dyes	Color of aqueous solutions ( $\lambda_{\max}$ ) $m\mu^*$	Corresponding pH	Color of dyed TlI and ZnO	Sensitization of TlI	Sensitization of ZnO
<b>Aurin</b> 	yellow 540	6,9	yellow	+	+
	red	8,0	+ $\text{NH}_3$ , red + HCl, yellow	—	+
<b>Safranin</b> 	red 540	7,0	red + $\text{NH}_3$ , red brown (540) + HCl, blue	+	+
				—	+
				+	—
<b>Thymolphthalein</b> 	colorless	9,4	—	—	—
	blue	10,6	+ $\text{NH}_3$ , blue + HCl, colorless	—	+
<b>Bromothymol blue</b> 	brown 580, 540	6,0	brown	+	+(520)
	blue 620, 540	7,6	+ $\text{NH}_3$ , blue + HCl, yellow	—	+
				+(540)	—
<b>Nile blue</b> 	blue 630	10	blue	+	+
	pink green 680	11	+ $\text{NH}_3$ , pink + HCl, green	—	+
	red 520	5,2	red	+	—
<b>Congo red</b> 	blue 750, 540	3,0	+ $\text{NH}_3$ , violet + HCl, blue	—	+
				+	—

\* The absorption maxima of the dyes on the adsorbates TlI and ZnO are displaced slightly toward the long-wave region compared with the maxima in solutions.

The fact that TlI is not sensitized when dyed with Congo red is due to the removal of a proton from the dye when it is adsorbed on this semiconductor.

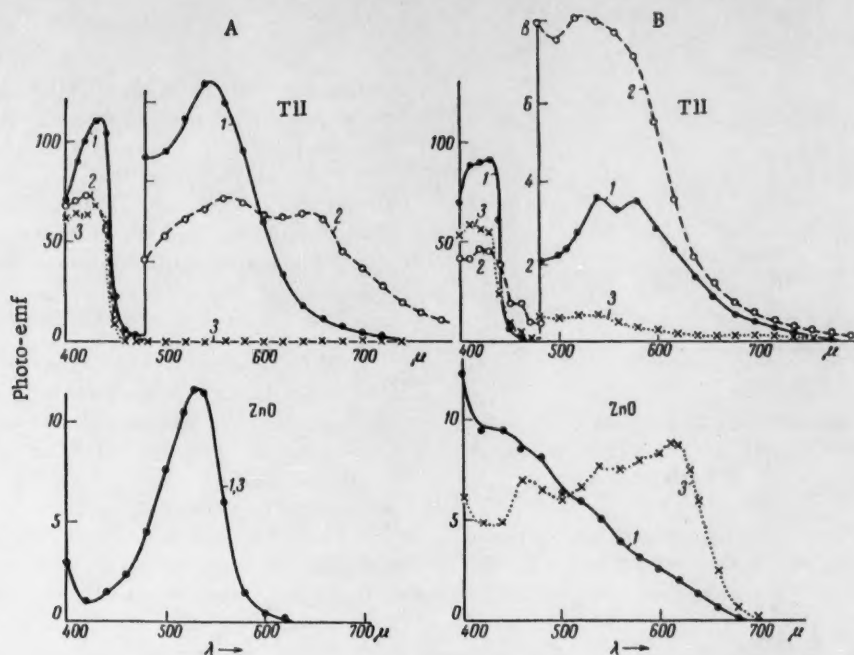


Fig. 1. The spectral distribution of the photo-emf in TlI and ZnO dyed with Safranin T (A) and Bromothymol blue (B): 1) in air; 2) after adsorption of HCl vapor; 3) after adsorption of  $\text{NH}_3$  vapor.

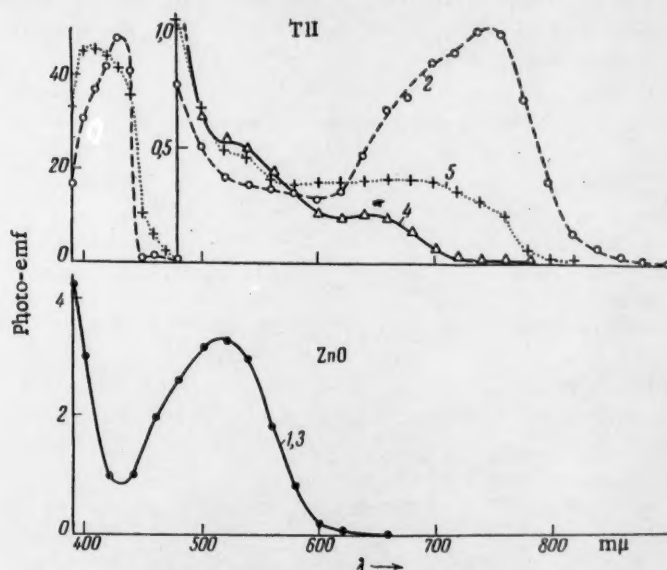


Fig. 2. The spectral distribution of the photo-emf in TlI and ZnO dyed with Congo red: 1) in air; 2) after adsorption of HCl vapor; 3) after adsorption of  $\text{NH}_3$  vapor; 4) after very slight acidification with HCl vapor; 5) after further acidification of the dye with HCl vapor.

In practice, when HCl vapor at low pressure is applied to a layer of TlI dyed with Congo red, a sensitized photoeffect is produced immediately (Fig. 2); the long-wave maximum of this effect belongs to the protonated form of the dye and the maximum at 540 m $\mu$  belongs to the neutral dye.

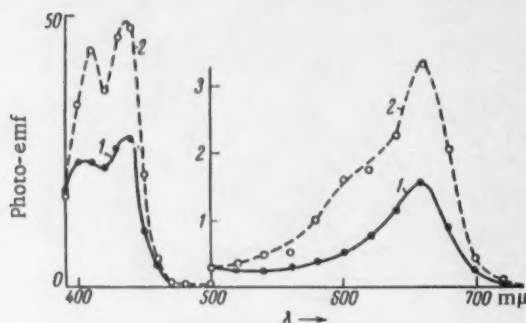


Fig. 3. The spectral distribution of the photo-emf in TlI dyed with Malachite green: 1) in vacuo, 2) in HCl vapor at 1-5 mm Hg pressure.

which are formed in ZnO by adsorbed oxygen molecules and on TlI by adsorbed molecules of iodine. According to our views [1], it is in these surface levels that the transfer of electrons to the conductivity zone takes place — in the case of ZnO by means of the energy quantum absorbed by the dye. When HCl is adsorbed, therefore, the photoeffect induced by the dye decreases. In the case of TlI, however, sensitization is accompanied by the transfer of electrons from the filled zone to the surface layer, so that their impoverishment, produced by the adsorption of protons, is favorable.

The adsorption of NH<sub>3</sub> produces the opposite effect, since it favors the filling of the surface layers of oxygen and iodine with electrons, to which the excitation energy of the dye is transferred.

This explanation is to be preferred to suggestions which bring in the height of the level reached during excitation of the dye molecule. In actual fact, as can be seen from Table 1 and the figures, the displacement of the absorption maximum toward longer wavelengths observed during protonation or deprotonation has no effect on the efficiency of the sensitization.

#### LITERATURE CITED

1. E. K. Putseiko and A. N. Terenin, *Zhur. Fiz. Khim.* **23**, 676 (1949); *Doklady Akad. Nauk SSSR* **70**, 401 (1950); E. K. Putseiko, *Radio and Electronics* [in Russian] (1956), Vol. 1, p. 1364; I. A. Akimov and E. K. Putseiko, *Doklady Akad. Nauk SSSR* **102**, 481 (1955); I. A. Akimov, *Zhur. Fiz. Khim.* **30**, 1007 (1956); *Doklady Akad. Nauk SSSR* **121**, 311 (1958);\* A. Terenin, E. Putseiko, and I. Akimov, *J. Chim. Phys.* **54**, 716 (1957).
2. E. K. Putseiko, *Doklady Akad. Nauk SSSR* **67**, 1009 (1949); *Izvest. Akad. Nauk SSSR, Ser. Fiz.* **16**, 34 (1952).
3. *Handbook of Chemistry and Physics* (Cleveland, 1956), Part 2, pp. 2151, 2157.
4. E. K. Putseiko and A. N. Terenin, *Collection, Problems of Kinetics and Catalysis* [in Russian] (Moscow, 1955), Vol. 8, p. 53.

\* Original Russian pagination. See C. B. translation.

# A MASS-SPECTROMETRIC STUDY OF CESIUM HALIDES

P. A. Akishin, L. N. Gorokhov, and L. N. Sidorov

M. V. Lomonosov Moscow State University

(Presented by Academician V. N. Kondrat'ev, June 6, 1960)

Translated from Doklady Akademii Nauk SSSR, Vol. 135, No. 1, pp. 113-116, November, 1960

Original article submitted June 3, 1960

Until recently there were no reports of molecular association in the vapor of cesium halides; it was assumed that the vapor consisted only of diatomic molecules  $\text{CsX}$ . In 1958, however, Milne, Klein, and Cubicciotti [1] and Berkowitz and Chupka [2] found by mass-spectrometric studies that when cesium chloride vapor is ionized by electrons, a comparatively small quantity of  $\text{Cs}_2\text{Cl}^+$  ions are formed, indicating the presence of dimeric  $\text{Cs}_2\text{Cl}_2$  molecules in the vapor. Eisenstadt, Rothberg, and Kusch [3] studied the velocity distribution in molecular beams of alkali metal fluorides and found that the ratio of the pressures of dimer and monomer in cesium fluoride vapor at  $T = 863^\circ \text{K}$  is  $p_d/p_m = 0.093$  and that the heat of dissociation of the dimeric molecules to monomeric molecules is  $\Delta E_T = 37.8 \pm 1.3 \text{ kcal/mole}$ . In 1959, Schoonmaker and Porter [4] used the mass-spectrometer to determine the differences in the heats of dissociation of the dimeric molecules of the alkali metal fluorides, and assuming for sodium fluoride a heat of dissociation  $\Delta H_T = 60.0 \text{ kcal/mole}$  [5] they obtained for the heat of dissociation of the cesium fluoride dimer the value  $\Delta H_T = \Delta E_T + RT = 41.4 \pm 3.7 \text{ kcal/mole}$  ( $T = 1121^\circ \text{K}$ ).

In work on the free evaporation of alkali metal halides, Rothberg, Eisenstadt and Kusch [6] detected slight dimerization of the molecules in cesium bromide vapor ( $p_d/p_m \leq 0.04$ ), but no dimerization of the iodide was observed (earlier, Miller and Kusch [7] had estimated the possible upper limit of the ratio of the pressures of dimer and monomer in the vapors of cesium chloride and bromide at 0.05 and 0.08 respectively). Thus quantitative data are available only for cesium fluoride. It was therefore considered of interest to carry out a mass-spectrometric study of all the cesium halides to determine the composition of the vapor and measure the heats of dissociation of the dimeric molecules.

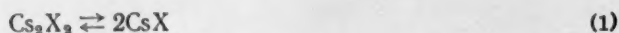
The work was carried out on an MS-4 mass-spectrometer. An ion source with double effusion chamber was used. The test specimen was placed in the lower chamber and effusion of the vapor took place from the upper chamber, which was connected to the lower chamber by a narrow channel. By heating the chambers

TABLE 1  
Mass-Spectra of Cesium Halides

Substance	Temp ° K	$\text{Cs}^+ (I_0)$	$\text{CsX}^+ (I_1)$	$\text{Cs}_2\text{X}^+ (I_2)$	$I_2/(I_0+I_1)$
Cesium fluoride	793	100,0	0,00	8,30	0,083
Cesium chloride	828	100,0	1,43	6,23	0,061
Cesium bromide	829	100,0	7,21	5,81	0,050
Cesium iodide	787	100,0	25,9	4,00	0,032

separately, it was possible to change the temperature of one while keeping the temperature of the other constant. Part of the molecular beam leaving the second chamber was ionized by means of electrons. A more detailed description of the apparatus has been given earlier [8]. Table 1 gives the mass-spectra of cesium halide vapors, obtained for the following instrument operating conditions: accelerating voltage 1.5 kv, cathode emission current 1.0 ma, and ionizing voltage 90 v. The intensity of the ion currents represent the sums of all the isotopic forms; the intensities of the weak ionic currents of  $X^+$  and  $Cs_2^+$  are not given. The mass spectra were recorded with the temperature of the upper chamber equal to that of the lower chamber, so that the data in the Table correspond to the saturated vapors.

Ionic currents for  $Cs_2X^+$  were recorded in all the spectra, indicating the presence of dimeric  $Cs_2X_2$  molecules in the vapors. In order to make allowance for the mutual superposition of the spectra of the monomers and dimers in the determination of the heats of dissociation and composition of the vapor, we found the ratios of the intensities in the spectra of the dimers of cesium fluoride and chloride. For this purpose we measured the change in the ionic currents with change in the temperature  $T_1$  of the lower chamber at constant temperature  $T_2$  in the upper chamber. Thus, the equilibrium constant for the dissociation of the dimeric molecules (in the upper chamber)



remained constant during the experiment, while the total pressure, and, hence, the degree of dissociation, changed. The formulas given in [8, 9] were used to calculate, from these measurements, the following ratios for cesium fluoride:  $I_{02}/I_2 = a_{02} = 0.7 \pm 0.3$ ;  $I_{12}/I_2 = a_{12} = 0.00$ ; for the chloride:  $a_{02} = 0.6 \pm 0.2$ ;  $a_{12} = 0.04 \pm 0.01$ . Here  $I_{02}$  and  $I_{12}$  are those fractions of the ionic currents  $I_0$  ( $Cs^+$ ) and  $I_1$  ( $CsX^+$ ) which are produced by ionization of the dimeric molecules. The value of the coefficient  $a_{02} = 0.6$ , found in experiments with the chloride, was used in subsequent calculations for cesium bromide and iodide.

The heats of dissociation of the dimeric molecules were measured as follows: the maximum superheating of the upper chamber relative to the lower chamber was established, after which the temperature  $T_2$  of the upper chamber was lowered, while the temperature  $T_1$  of the lower chamber was kept constant. The ionic currents were measured at approximately  $10^\circ$  intervals; when the point at which the temperatures of the two chambers were equal was reached ( $T_1 = T_2$ ), the temperature of both chambers was lowered further, in such a way that  $T_2 \leq T_1$ . The change in the intensities of the ionic currents  $I_0$ ,  $I_1$ , and  $I_2$  with change in  $T_2$  is shown in Fig. 1.

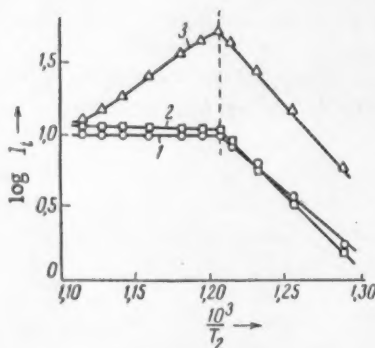


Fig. 1. Curves showing the relationship between the logarithms of the ionic currents and the reciprocal of the temperature: 1)  $Cs^+$ ; 2)  $(CsCl^{35})^+ \cdot 100$ ; 3)  $(Cs_2Cl^{35})^+ \cdot 100$ .

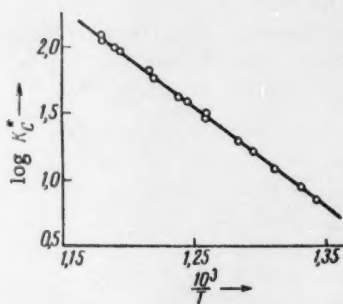


Fig. 2. Plot of  $\log K_C^*$  vs.  $1/T$  for cesium chloride.

The heats of dissociation of the dimeric molecules were calculated from the temperature dependence of the quantity  $K_C^* = I_{01}^2/I_2$ , which is proportional to the equilibrium constant for reaction (1). Here  $I_{01} = I_0 - a_{02}I_2$  is the ionic current of  $Cs^+$  from the monomer. The results of the calculations are given in Table 2. Data from one of the experiments with cesium chloride are

given in Fig. 2. The value which we found for the heat of dissociation of cesium fluoride agrees with the literature data [3, 4] within the limits of experimental error; the heats of dissociation of the dimeric molecules of cesium chloride, bromide, and iodide have been obtained for the first time.

TABLE 2

Heats of Dissociation of the Dimeric Molecules and the Composition of the Vapor of Cesium Halides

Molecule	Temp. ° K	$\Delta E_T$ , kcal/mole	$p_d/p_m$
$Cs_2F_2$	704—859	$36,4 \pm 0,9$	0,14 (793°K); 0,11 (813°K)
$Cs_2Cl_2$	745—875	$32,4 \pm 1,3$	0,07 (810°K); 0,07 (828°K)
$Cs_2Br_2$	786—909	$31,2 \pm 0,6$	0,05 (826°K); 0,03 (829°K)
$Cs_2I_2$	755—862	$31,2 \pm 0,4$	0,03 (787°K); 0,04 (820°K)

The data from the experiments on the determination of the heats of dissociation (as far as the point where  $T_1 = T_2$ ) were used to calculate the ratio of the vapor pressures of monomer and dimer  $p_d/p_m$  by the method proposed by Milne [10]. The formula used for the calculations was derived with allowance for the molecular flow of vapor along the channel connecting the upper and lower chambers [8]:

$$p_d/p_m = \frac{I_2}{I_{01} \sqrt{T_2}} \cdot \frac{I'_{01} \sqrt{T_2} - I_{01} \sqrt{T_2}}{I_2 \sqrt{T_2} - I'_2 \sqrt{T_2}} \quad (8)$$

Here  $I_{01}$  and  $I_2$  are the intensities of the ionic currents of monomer ( $Cs^+$ ) and dimer ( $Cs_2X^+$ ) at the point where the temperatures of the two chambers are equal ( $T_1 = T_2$ ), and  $I'_{01}$  and  $I'_2$  are the intensities of the same ionic currents at the point  $T'_2 > T'_1$ . This method gives the relative composition of the saturated vapor at a temperature  $T = T_1 = T_2$ . The results of the calculation are given in Table 2. Since in the case of cesium halides the heats of dissociation of the dimeric molecules are less than the heats of sublimation of the monomers, the ratio  $p_d/p_m$  should increase with increase in temperature. The deviations from this relationship shown by the data in Table 2 are due to errors in the determination of the values of  $p_d/p_m$ .

Let us examine the relationship between the intensities of the ionic currents in the mass spectra of the cesium halides and the composition of their vapors. The ions  $Cs^+$  and  $CsX^+$  are formed predominantly during the ionization of the  $CsX$  molecules, which predominate in the vapor; the ionic current  $I_2(Cs_2X^+)$  makes up approximately half of the total ionic current for ionization of the  $Cs_2X_2$  molecules. It may be assumed with sufficient accuracy that the ratio of the cross sections of ionization of the dimeric and monomeric molecules is close to two. Taking account of this fact, we reach the conclusion that the value of the ratio  $I_2/(I_0 + I_1)$  should be close to that of the ratio  $p_d/p_m$ . Comparison of the data in Tables 1 and 2 confirms this conclusion. Thus the ratio of the ionic currents can be used to determine the relative composition of the vapor of the spectra if its components are known.

In the experiments with cesium chloride, attention was paid to the fact that the ratio of the ionic currents  $I_0/I_1$  ( $Cs^+/CsCl^+$ ) decreases with increase in temperature irrespective of whether this is accompanied by an increase or decrease in the relative concentration of the dimeric molecules in the vapor (Fig. 1). Consequently, the change in the ratio  $I_0/I_1$  depends little on the contribution of the dimer to the ionic currents of  $Cs^+$  and  $CsCl^+$  and is determined chiefly by the temperature dependence of the mass-spectrum of the monomer, which can be followed more accurately from the ratio of the ionic currents of  $Cs^+$  and  $CsCl^+$  from the monomer:  $I_{01}/I_{11} = a_{01}(I_{11} = I_1 - a_{12}I_2)$ . Within a range of 100°,  $a_{01}$  varies from 86 (800° K) to 67 (900° K), i.e., by more than 20%. Thus, in this case, increase in temperature leads to an increase in the probability of formation of molecular ions  $CsCl^+$ , and this can be explained from an examination of the mutual superposition of the potential energy curves for the  $CsCl$  molecule and the  $CsCl^+$  ion. Since the intensity of the molecular  $CsCl^+$  ions in the mass-spectrum is low compared with that of the fragment ion  $Cs^+$ , it follows that  $r_c$  — the "critical"

distance of the molecular ion, at which its energy is equal to the dissociation energy — is much greater than  $r_e$  — the abscissa of the minimum on the potential energy curve for the CsCl molecule. Increase in temperature increases the population of the upper vibrational levels. The probability that the molecules occupying these levels will have internuclear distances  $r > r_c$  is high. On electron collision, therefore, transitions leading to the formation of stable molecular ions are frequent.

In the case of cesium bromide, and more particularly cesium iodide, the relative intensities of the molecular ions in the mass-spectra are much higher, indicating a smaller difference between  $r_c$  and  $r_e$  than is the case for the chloride. Increase in the population of the upper vibrational levels thus has little influence on the number of molecules forming molecular ions on electron collision. In addition, the increase in the population of the upper levels of the CsBr and CsI molecules with increase in temperature takes place more slowly, since their vibrational constants are smaller than in the case of cesium chloride (CsCl,  $\omega_e = 209 \text{ cm}^{-1}$ ; CsBr,  $\omega_e = 139 \text{ cm}^{-1}$ ; CsI,  $\omega_e = 101 \text{ cm}^{-1}$  [11]). For these reasons, the temperature coefficients of the spectra of cesium bromide and iodide are close to zero.

#### LITERATURE CITED

1. T. A. Milne, H. M. Klein, and D. Cubicciotti, *J. Chem. Phys.* **28**, 718 (1958).
2. J. Berkowitz and W. A. Chupka, *J. Chem. Phys.* **29**, 653 (1958).
3. M. Eisenstadt, G. M. Rothberg, and P. Kusch, *J. Chem. Phys.* **29**, 797 (1958).
4. R. C. Schoonmaker and R. F. Porter, *J. Chem. Phys.* **30**, 283 (1959).
5. R. F. Porter and R. C. Schoonmaker, *J. Chem. Phys.* **29**, 1070 (1958).
6. G. M. Rothberg, M. Eisenstadt, and P. Kusch, *J. Chem. Phys.* **30**, 517 (1959).
7. R. C. Miller and P. Kusch, *J. Chem. Phys.* **25**, 860 (1956).
8. P. A. Akishin, L. N. Gorokhov, and L. N. Sidorov, *Vestnik MGU, Ser. Matem., Mekh. Astron., Fiz., Khim.*, **6**, 194 (1959).
9. L. N. Gorokhov, *Vestnik MGU, Ser. Matem., Mekh., Astron., Fiz., Khim.*, **6**, 231 (1958).
10. T. A. Milne, *J. Chem. Phys.* **28**, 717 (1958).
11. S. A. Rice and W. Klemperer, *J. Chem. Phys.* **27**, 573 (1957).

# THE THEORY OF TURBULENT COMBUSTION

A. N. Voinov

Chemical Physics Institute, Academy of Sciences of the USSR

(Presented by Academician V. N. Kondrat'ev, June 6, 1960)

Translated from Doklady Akademii Nauk SSSR, Vol. 135, No. 1, pp. 117-120, November, 1960

Original article submitted May 31, 1960

The authors of the familiar theories of turbulent combustion, which are constructed on the basis of one or other of the versions of the application of the so-called "frontal model" [1-4], have started from the assumption that the front of the laminar or small-scale turbulent flame is preserved, irrespective of distortion or splitting into separate burning jets. This assumption of the nonannihilable flame front, as it were, is based on the theoretical suggestion that increase in the intensity of diffusion exchange in the flame front facilitates an increase in the rate of its propagation in accordance with the relationship  $U_f \sim \sqrt{\kappa_m \bar{W}_f}$ . For a constant average rate of reaction  $\bar{W}_f$ , the width of the combustion zone  $\delta_f$  increases, and the temperature gradient in the flame front accordingly decreases, in direct proportion to the increase in  $U_f$  (Fig. 1a). When the volume occupied by the combustion products is not restricted, however, these changes cannot change the final combustion temperature (neglecting losses by radiation), and hence cannot influence the average characteristic rate of reaction, completeness of combustion, and thermal current related to unit mass of the burnt mixture.

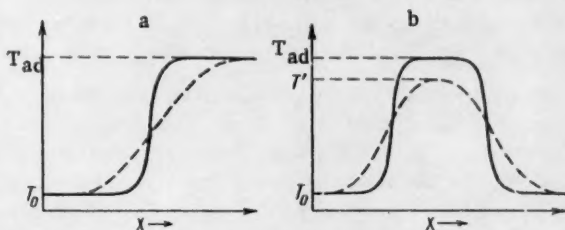


Fig. 1

It has been suggested that the action of small-scale turbulent diffusion (of scale  $l < \delta_f$ ) is in this respect exactly analogous to the increase in the molecular diffusion coefficient and hence in the same way cannot have any influence on the reaction rate and completeness of combustion, and accordingly can only facilitate an increase in the rate of propagation of the flame front. Here, however, it was not mentioned that this suggestion is applicable only so long as the volume occupied by the combustion products is large compared with the volume of the combustion zone, and in all cases almost complete combustion is achieved and a final adiabatic flame temperature  $T_{ad}$  is attained.

If, however, we are dealing with the propagation of flame from a separate tongue or jet of combustion products, surrounded by fresh burning mixture, where the dimensions of the jet are comparable with the width of the laminary flame zone, then the position proves to be quite different. When the dimensions of a jet of this type are limited, the increase in the rate of small-scale turbulent transfer, which leads to broadening of the combustion zone and increase in the flame velocity, can produce conditions where the final temperature of the

combustion products starts to decrease, so that the rate of reaction and specific thermal current also decrease (Fig. 1b). The combustion is incomplete and further increase in the rate of turbulent diffusion can create conditions where propagation of the flame becomes impossible and the flame is extinguished.

The conditions for this type of extinction of an individual isolated tongue or jet of flame of finite dimensions, thrown by the turbulent pulsation into fresh mixture, are exactly analogous to the conditions for the breakdown of stationary combustion in so-called homogeneous reaction vessels of constant volume, which have been

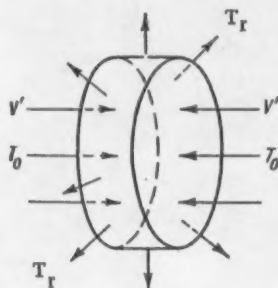


Fig. 2.

examined theoretically by Ya. B. Zel'dovich [5]. With intensification of the combustion process in restricted volume, as a result of the entry into this volume of greater quantities of fresh mixture per unit of time, the temperature in the volume starts to decrease, since combustion cannot take place completely in the time interval available. This decrease in temperature leads to retardation of the reaction, as a result of which further stationary combustion conditions become impossible at a definite rate of supply of fresh mixture in the reaction vessel.

The average temperature  $T_r$  inside the reaction volume is determined by the equilibrium between the rate of heat evolution and the consumption of heat for the combustion of fresh mixture. Breakdown of the stationary conditions takes place when the temperature decreases by a quantity

$$T_{ad} - T_r \approx \frac{RT_{ad}^2}{E}. \text{ The absolute values of } G_{crit} \text{ corresponding to}$$

breakdown prove to be proportional to the maximum reaction rates in the laminary flame front, i.e., to the maximum value of the function  $e^{-E/RT_r} (T_{ad} - T_r)^n$ . These theoretical considerations have been well confirmed in [6, 7].

Taking account of the fact that, together with the large-scale pulsations which distort the flame front or break it down into individual burning jets and which have relatively large dimensions  $l \gg \delta_{lam}$ , and small-scale pulsations with  $l < \delta_{lam}$ , which intensify the process of transfer to the front itself, there is present in any turbulent layer, to a greater or lesser extent, a whole spectrum of pulsations of intermediate scale, while the initial large-scale pulsations are later broken down into pulsations of smaller scale, we find that the above mechanism for the extinction of individual burning jets should be extremely probable. The extinction of a flame under conditions of intense turbulent exchange is confirmed by a whole series of experimental observations, particularly those made when a stream of flame gases of high velocity is directed into a burning mixture.

Although this extinction on the whole may take place in those cases where there is an excess of fresh cold mixture around the burning jets, i.e., in the start of the turbulent combustion zone, it is in these conditions that it may have a decisive influence on the rate of propagation of the leading front of the turbulent flame and the conditions for its stabilization. This rate should be determined by the probability of extinction of the individual jets of combustion products, thrown forward by the most rapid turbulent pulsations into the fresh mixture, i.e., by the possibility or impossibility of subsequent propagation of the flame from these rapid jets.

We shall attempt to carry out a quantitative analysis of the conditions for the extinction of a jet of combustion products with initial temperature  $T_{ad}$ , surrounded by original mixture of temperature  $T_0$ , making use of experimental data for the limits of the breakdown of combustion in a spherical reaction vessel [6]. Thus, for an isooctane - air mixture, for example, for an excess air factor of  $\alpha = 1.43$ , pressure 1 atm and  $T_0 = 400^\circ \text{K}$ , breakdown starts at a rate of heat evolution equal to  $222 \text{ cal/cm}^3 \cdot \text{sec}$ , which corresponds to a consumption of fresh mixture  $V_{crit} = 640 \text{ cm}^3/\text{sec}$  for  $1 \text{ cm}^3$  reaction volume.

Let us assume that the jet of combustion products has the shape of a cylinder with area of base  $1 \text{ cm}^2$  and height  $0.25 \text{ cm}$ . The fresh mixture is supplied via both bases with a velocity  $V'_0$ , and the combustion products are removed via the lateral surface of the cylinder (Fig. 2). For extinction of a jet of this type, it is necessary to supply to it  $160 \text{ cm}^3/\text{sec}$  of fresh mixture, i.e.,  $V'_0 = 0.8 \text{ m/sec}$ , which is only 1.8 times greater than the normal rate of propagation of the flame  $U_1$  in the mixture under consideration, so that even a slight increase in the small-scale turbulent exchange above the molecular conditions should lead us to expect extinction of the flame.

In the case of the stoichiometric mixture, according to the data of the same authors, breakdown took place at  $V_{\text{crit}} = 2.1 \text{ liter/sec} \cdot \text{cm}^3$ , which in our conditions would correspond to a value of  $V_0^* = 2.65 \text{ m/sec}$ , which is now 3.3 times greater than  $U_1$  for  $\alpha = 1$  ( $V_{\text{crit}} \sim W_{\text{max}}$ , whereas  $U_1 \sim \sqrt{W_{\text{max}}}$ ), so that the probability of extinction should be much less in this case.

The above mechanism for the extinction of individual burning jets of restricted dimensions under the influence of small-scale turbulent diffusion enables us to provide an extremely simple explanation for a whole series of the observed features of turbulent combustion. Thus, for example, a great deal of experimental data shows that, in complete accordance with the theory of K. I. Shchelkin [2], the rate of propagation of a turbulent flame (related to the leading boundaries of the combustion zone) as a rule proves to be proportional to the root-mean-square value of the pulsation rate  $U_t \sim \bar{U}'$ . In the progressive region this relationship becomes  $U_t \sim U_{\text{flow}}$  [8]. At the same time, however, experiment shows that in contradiction to Shchelkin's theoretical conclusions, the reaction - kinetic properties of a burning mixture influence  $U_t$  at any value of  $\bar{U}'$ , including very high values, and there is no unique relationship between  $U_t$  and  $U_1$ .

A more precise version of the relationship  $U_t = f(\bar{U}', W_r)$  is given in [9], where the authors, over a wide range of change in  $\bar{U}'$  from zero to 8 m/sec, obtained ideal straight lines corresponding to the formula

$$U_t' = a \bar{U}' + b, \quad (1)$$

where  $b \approx U_1$ , but the value of the slope  $a$  is greater the higher the combustion temperature  $T_{\text{ad}}$  and hence the reaction rate in the flame. Changes in  $T_{\text{ad}}$  have a smaller influence on the value of  $a$ , however, than on  $U_1$ .

These results prove to be quite understandable in the light of the mechanism examined above for the extinction of individual jets of flame. Assuming, as has been done repeatedly by many research workers and as appears most probable from the viewpoint of the physics of the phenomenon, that the flame in a turbulent current is carried forward into the fresh mixture at the velocity of the pulsations, we find an exhaustive explanation of the influence of the reaction - kinetic properties of the burning mixture on  $U_t$ , while still retaining the hypotheses of the frontal model. At the same time, this influence proves to be similar in many respects to the familiar relationships for homogeneous (bulk) processes.

The higher the reaction rate in the flame zone, the less probable should be the extinction of the individual burning jets thrown forward into the fresh mixture by the most rapid large-scale pulsations; or, in other words, the greater the probability that the leading boundaries of the turbulent flame will be propagated with the velocity of the most rapid pulsations. On the other hand, at a low reaction rate, the original mixture can be ignited only by the main mass of pulsations with velocities close to the root-mean-square velocity.

From this the value of the coefficient  $a$  in Eq. (1) can vary from  $a \approx 1$  (close to the limits, apparently,  $a$  may be  $< 1$ ) to certain maximum values corresponding to the ratio  $\frac{U_1' \text{max}}{\bar{U}'}$  in the given turbulent stream. In the case of normal tubular turbulency, this ratio amounts to 3.5-4 [10] and when turbulence-producing grids are present, this may rise to 6 [11], in accordance with which the rate of propagation of the turbulent flame in rapidly burning mixtures, particularly at high pressures, may be several times greater than  $\bar{U}'$ , as is in fact observed in practice. At the same time, it is no longer necessary to attribute this phenomenon to the spontaneous production of turbulence, as has been attempted by many workers [3, 13, 14].

Although, in the examination of turbulent combustion we started from the frontal model (assuming in all cases the leading part played by combustion at the boundaries of separation of the jets of fresh mixture and combustion products) and hence from an identical reaction mechanism (in both laminary and turbulent flames), it can nevertheless be seen from the proposed mechanism that the reaction rate should influence the rate of propagation of the turbulent flame only indirectly - via a change in the probability of extinction of combustion at the surface of individual rapid jets. This explains the familiar [9, 12, 14] absence of any unique relationship between  $U_t$  and  $U_1$ . Whereas the velocity of a laminar flame  $U_1 \sim \sqrt{\kappa_m \bar{W}_r}$ , the rate of propagation of a turbulent flame should be a more complex function not only of  $W_r$  but also of the characteristics of the turbulent stream, with account taken of the spectra of pulsation rates and their scale.

An explanation is also provided for the different ways in which  $U_l$  and  $U_t$  are influenced by pressure, which in the first case has a slight negative effect or zero effect, and in the second case a distinct positive effect. This is related to the influence of pressure both on the reaction rate and on the decrease in the width of the laminary flame front zone and hence the decrease in the dimensions of the burning jets, at which the extinguishing action of small-scale turbulent diffusion becomes possible.

Extremely simple explanations are also provided for the limits of stabilization of turbulent combustion by means of pilot flames behind bodies round which flow is difficult and in gas streams. The observed narrowing of the limits of combustion breakdown in stabilizers when fine networks are placed in front of them is explained by the greater probability of extinction of jets of flame of relatively small dimensions.

#### LITERATURE CITED

1. G. Damköhler, Z. Elektrochem. 46, 11, 601 (1940).
2. K. I. Shchelkin, Zhur. Tekh. Fiz. 13, 9, 520 (1943).
3. B. Karlovitz, D. W. Deniston, and T. E. Wells, IV Symposium on Combustion (1953) p. 613.
4. A. C. Scurlock and J. H. Grover, IV Symposium on Combustion (1953) p. 645.
5. Ya. B. Zel'dovich, Zhur. Tekh. Fiz. 11, 6, 493 (1941).
6. J. Longwell and M. Weiss, Ind. and Eng. Chem. 47, 8, 1634 (1955).
7. H. C. Hottel, G. C. Williamson, and M. L. Baker, VI Symposium on Combustion (1956) p. 398.
8. L. N. Khitrin, The Physics of Combustion and Explosion [in Russian] (Izd. AN SSSR, 1957) p. 223.
9. V. P. Karpov, E. S. Semenov, and A. S. Sokolik, Doklady Akad. Nauk SSSR 128, 6, 1220 (1959).\*
10. H. C. H. Townend, Proc. Roy. Soc. 145, 180 (1934).
11. L. F. G. Simmons and C. Salter, Proc. Roy. Soc. 145, 212 (1934).
12. L. S. Kozachenko, Izvest. Akad. Nauk SSSR, Energetika i Avtomatika, 2, 22 (1959).
13. A. S. Sokolik and V. P. Karpov, Doklady Akad. Nauk SSSR 129, 1, 168 (1959).\*
14. K. Wohl, Ind. and Eng. Chem. 47, 4, 825 (1955).

\* Original Russian pagination. See C. B. translation.

## THE THERMAL PROPERTIES OF THE TRANSITIONAL FORMS OF CARBON

V. I. Kasatochkin, V. K. Zamoluev, A. T. Kaverov,  
and K. Usenbaev

Institute of Mineral Products, Academy of Sciences of the USSR

(Presented by Academician M. M. Dubinin, June 10, 1960)

Translated from *Doklady Akademii Nauk SSSR*, Vol. 135, No. 1, pp. 121-124,  
November, 1960

Original article submitted April 2, 1960

The fact that carbon shows a characteristic homogeneous transition from the amorphous to the graphitic crystalline form with a continuous and extensive alteration of properties is undoubtedly related to the marked tendency of the element to polymerization. This was noted even by D. I. Mendeleev [1]. The characteristic polymeric structures which arise in the initial steps of carbonization are aggregates of layers of aromatic carbon atoms which are bound to one another by side radicals and are stable even under high temperatures [2, 3]. Homogeneous crystallization results from the polymeric nature of the carbon [4] and is an orientation process of the same type as that involved in the crystallization of many organic chain polymers [5]. The multiplicity of states assumed by carbon in homogeneous crystallization, plus a pre-crystallization state [6], determine the transitional forms of the element.

The present paper presents the results of a study of the specific heat ( $c_p$ ), coefficient of thermal diffusivity ( $a$ ), and thermal conductivity ( $\lambda$ ) of transitional forms which were obtained by high-temperature treatment of petroleum coke, and channel and thermal carbon blacks. The petroleum coke had a density of 1.405 g/cm<sup>3</sup>, and contained 0.08% ash and 5.13% volatile material. The ash content of the channel black (C 94.59%; H 0.68%; O 4.79%) was 0.09% and that of the thermal black (C 99.65%; H 0.27%; O 0.08%), 0.01%. The particle diameter was approximately 0.5 mm in the coke and <1  $\mu$  in the blacks.

The specimens were treated at various temperatures in the interval from 1000 to 3000° in a nitrogen, argon atmosphere in a furnace having graphite heating elements. Room temperature values of  $c_p$  and  $a$  were determined by the G. M. Kondrat'ev method of the regular thermal regime [7] as modified for small specimens [8]. Values of  $\lambda$  were calculated from the volume weight,  $\beta$ , and the data on  $c_p$  and  $a$  ( $\lambda = c_p a \beta$ ).

Figures 1, 2, and 3 give measured values of  $c_p$  and  $a$ , and calculated values of  $\lambda$ , for the various working substances, as functions of the temperature, the duration of treatment being 10 or 30 minutes. Figure 4 gives kinetic curves showing the relation between  $c_p$  and the time of treatment at furnace temperatures of 1600 and 2500°.

The fact that calcination under fixed conditions gives a  $c_p$  variation which differs from one carbon specimen to another indicates that each follows a different series of structural transformations. The  $a$  value for powders is markedly dependent on the density of particle packing, i.e., is dependent on the bulk weight,  $\beta$ . Observations show that channel and thermal carbon blacks differ from petroleum coke insofar as the density of particle packing is only slightly dependent on the temperature under fixed experimental conditions for the determination of  $a$ . The alteration in  $\beta$  is from 0.55 to 0.65 for the coke and from 0.23 to 0.25 for the carbon blacks.

To a considerable degree the marked difference in the absolute values of  $a$  and  $\lambda$  in the products resulting from thermal treatment of carbon blacks and petroleum coke must be due to differences in density of particle packing and structural porosity. Nevertheless, the relation between these factors and the temperature of treatment must be determined principally by the structural transformation of the carbon in each specimen.

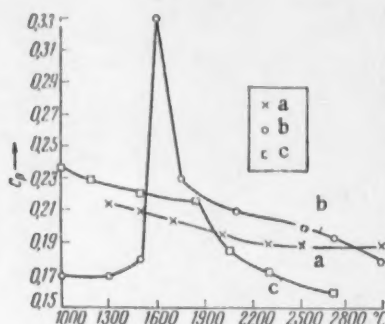


Fig. 1. The relation between specific heat and temperature of treatment: a) thermal carbon black; b) channel carbon black; c) petroleum coke ( $c_p$  in kcal/kg·°C).

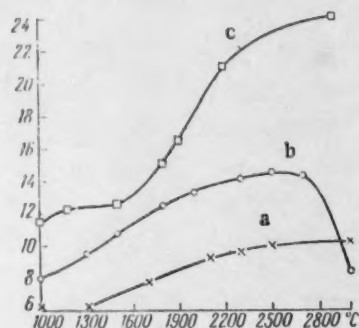


Fig. 2. The relation between thermal diffusivity and temperature of treatment. Same symbols as in Fig. 1 ( $a \cdot 10^4$ , m<sup>2</sup>/hr, plotted on the axis of ordinates).

As anticipated, not all of the side radicals enter into the polymeric carbon skeleton of the carbonized substance to form a net of valence bonds. The remaining peripheral radicals which are not incorporated into this net form a "fringe" which is bound to each layer of aromatic carbon atoms. This part of the structure markedly enriches the covalent rotational spectrum, and contributes significantly to the internal energy and to the heat capacity of the carbonized material.

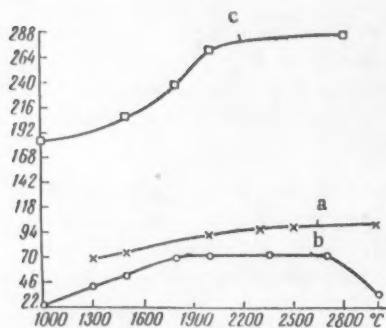


Fig. 3. The relation between the coefficient of thermal conductivity and the temperature of treatment. Same symbols as in Fig. 1 ( $\lambda$ , 10<sup>3</sup> kcal/m·hr·°C, plotted on the axis of ordinates).

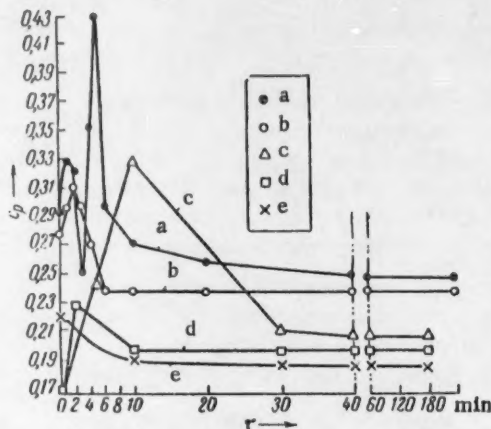


Fig. 4. Relation between specific heat and time of isothermal treatment: a) coking carbon,  $t = 500^\circ$ ; b) PS carbon,  $t = 700^\circ$ ; c) channel black,  $t = 1600^\circ$ ; d) channel black,  $t = 2500^\circ$ ; e) thermal black,  $t = 2500^\circ$  ( $c_p$ , kcal/kg·°C).

An interpretation of the thermal properties of the products obtained from thermal treatment of carbonized substances must give consideration to the changing relationships between the three basic structural factors: the plane layers of aromatic carbon atoms, the side radicals which bind these and form the spatial net, and the remaining radicals which go to make up the "fringe".

Three types of  $c_p$  vs temperature of treatment relations are observed for petroleum coke (Fig. 1) and are to be related to the existence of three different stages in the structural transformation of carbon. It is our belief that the relatively smooth fall-off of the heat capacity up to 1800° corresponds to growth of the carbon layers as the result of side radical breakdown.

The number of side radicals diminishes markedly in this stage. Nevertheless, the polymeric structure is maintained by recombination of the radical bonds as they become free and the spatial structure is continually reestablished. There is a sharp drop in  $c_p$  over the interval of pre-crystallization from 1800 to 2000°, as the result of inclusion of a second mechanism which leads to the union of neighboring layers. The possibility of layer growth is opened up in the first stage by removal of the "fringe".

The diminution of  $c_p$  in the two stages which have just been described is determined by an increase in the proportion of carbon organized into atomic planes and a decrease in the number of side radicals in the "fringe".

The diminution of  $c_p$  in homogeneous crystallization (which begins at 2000°) results from approach of the carbon layers during azimuthal orientation and is accompanied by passage from a  $d_{\max}$  of 3.42 Å in the pre-crystalline stage to a  $d_{\min}$  of 3.35 Å in the maximally graphitized carbon. It has been shown earlier [9] that the decrease in  $c_p$  is related to the degree of homogeneous graphitization resulting from approach of the carbon layers by a linear equation

$$\gamma = 3,42 - d_{002} / (3,42 - 3,35),$$

in which  $d_{002}$  is the variable interplanar spacing for the crystallization process. The relation between  $\alpha$  and  $\lambda$  and the temperature of treatment is described by S-shaped curves with a point of inflection near 1800°.

Apart from the diminution of  $c_p$ , the scattering of the elastic waves of atomic vibrations on the structural nonhomogeneities and the increase in the electronic component of  $\lambda$  resulting from the growth of the carbon layers can be considered as the principal factors leading to continuous alteration of the  $\lambda$  value of petroleum coke with rising temperature of treatment in the first two stages of the structural transformation of the carbon. The electronic component normal to the layer also determines the value of  $\lambda$  in homogeneous crystallization, as is indicated by the fact that the coefficient of thermal conductivity,  $\lambda$ , [9], and the specific resistance,  $\rho$ , [6] have been shown to vary linearly with  $\gamma$ .

TABLE 1

Treatment temperature, °C	Treatment duration, fixed temp. min.	Degree of graphitization, $\gamma$		
		petroleum coke	thermal carbon black	channel carbon black
1700	10	0	0	0
2000	10	0.10	0.04	0
2300	30	0.38	0.55	0
2420	30	0.87	—	—
2500	30	1.0	0.77	0
3000	10	1.0	0.77	0.09

Thermal carbon black has approximately the same temperature of initial crystallization (2000°) as petroleum coke, but is distinctive insofar as its crystallization at high temperature is incomplete, the maximum graphitization,  $\gamma$ , being 0.77 (Table 1).

This is clearly related to the fact that the diminution in  $c_p$  for the thermal black in homogeneous crystallization is much less pronounced. There is a common physical basis for the inability of the thermal black to undergo full crystallization and the uniform diminution in  $c_p$  prior to crystallization which distinguishes it from petroleum coke. It has been shown earlier [10] that homogeneous crystallization of carbon is impeded by the formation of a spatial net of  $=C=C=C=$  bonds between the carbon layers, since these bonds have high

thermal stability and resist breakdown at temperatures up to 3000°. This factor retards the union of the carbon layers so that there is neither a sharp fall-off of  $c_p$  over the pre-crystallization interval from 1800 to 2000° nor points of inflection on the  $\lambda$  and  $a$  curves.

The dependence of  $c_p$ ,  $\lambda$ , and  $a$  for channel black on the temperature of treatment is characterized by a very gradual diminution of  $c_p$  up to approximately 1300°, a maximum in the neighborhood of 1700°, and a diminution in  $c_p$ ,  $\lambda$ , and  $a$  over the 2700-3000° interval. The channel black differs from the other forms of carbon in that it does not undergo homogeneous crystallization and has a high initial oxygen content (4.79%). The presence of a spatial net of thermally stable bonds which are more flexible than those of the thermal black accounts for this peculiar variation of thermal properties at high working temperatures and for the almost complete inability to undergo crystallization. The formation of this net should be related to the dehydrogenation resulting from destruction of the oxygen-containing side radicals with cleavage and production of allene carbon chains to bind the carbon layers [10].

The relatively low value of  $c_p$  in channel black is determined by the fact that it contains carbonaceous materials (both initially and at working temperatures < 1300°), the oxygen in the side radicals of the latter giving rise to an additional spatial net of C-O-C bridge bonds. Breakdown of this spatial net of oxygen bonds and transition of the side radicals from the net into the "fringe" give an adequate explanation for the pronounced maximum on the  $c_p$  vs.  $t_{\text{working}}$  curve for channel black.

Destruction ("melting") of the spatial net of valence bonds of still lower thermal stability might explain the maxima on the kinetic  $c_p$  curves for mineral carbons (Fig. 4) at values of  $t_{\text{working}}$  corresponding to a temporary transition of the carbon into the liquid state [12]. Similar effects from the "melting" of a spatial net of bonds are also observed in such organic polymers as polyvinyl acetate [11] where a  $c_p$  maximum at lower temperatures corresponds to the weaker intermolecular bonding.

The results of this study have shown that the properties of carbonaceous materials are determined largely by the polymeric structure of carbon and by the nature of the spatial net of bonds. Only the maximally graphitized form of carbon ( $\gamma = 1$ ) is completely free of such a bond net.

#### LITERATURE CITED

1. D. I. Mendeleev, *Fundamentals of Chemistry* [in Russian] (Moscow, 1947) Vol. 1.
2. V. I. Kasatochkin, *Izvest. Akad. Nauk SSSR, Otdel. Tekh. Nauk* (1951) No. 9; (1953) No. 10.
3. R. E. Franklin, *Proc. Roy. Soc.* **209**, 1097, 197 (1951).
4. V. I. Kasatochkin and A. T. Kaverov, *Doklady Akad. Nauk SSSR* **117**, 837 (1957).\*
5. V. A. Kargin and G. L. Slonimskii, *Uspekhi. Khim.* **24**, 7, 785 (1955).
6. V. I. Kasatochkin and A. T. Kaverov, *Doklady Akad. Nauk SSSR* **120**, 1007 (1958).\*
7. G. M. Kondrat'ev, *The Regular Thermal Regime* [in Russian] (Moscow, 1954).
8. V. K. Zamoluev and V. I. Kasatochkin, *Izvest. Akad. Nauk SSSR, Otdel. Tekh. Nauk* **11**, 190 (1957).
9. V. I. Kasatochkin, V. K. Zamoluev, and A. T. Kaverov, *Atomnaya Energ.* **7**, 3, 272 (1959).\*
10. V. I. Kasatochkin and K. Usenbaev, *Izvest. Akad. Nauk SSSR, Otdel. Tekh. Nauk* **5**, 163 (1960).
11. S. N. Zhurkov and B. Ya. Levin, *Jubilee Collection in Honor of Academician A. F. Ioffe on His 70-th Birthday* (Izd. AN SSSR, 1950) p. 260.
12. V. K. Zamoluev, *Khim. i Tekhnol. Topliva i Masel* (1959) No. 7.

\*Original Russian pagination. See C. B. translation.

AN EXPERIMENTAL DETERMINATION OF THE ENTHALPY OF  
CORUNDUM ( $\text{Al}_2\text{O}_3$ ) FROM 500 TO 2000°

V. A. Kirillin, Corresponding Member of the Academy of  
Sciences of the USSR, A. E. Sheindlin, and V. Ya. Chekhovskoi

Translated from *Doklady Akademii Nauk SSSR*, Vol. 135, No. 1, pp. 125-128,  
November, 1960

Original article submitted August 22, 1960

The presently available experimental data on the enthalpies and heat capacities of solid substances do not generally extend beyond 1500-1600° [1, 2]. This situation results from the experimental and technical difficulties which accompany work at higher temperatures. At the same time, study of such thermophysical properties as the enthalpy and heat capacity at temperatures far above 1600° is vitally necessary for modern technology. These facts have led to the development of a technique for determining the enthalpy and heat capacity of solid substances and to the construction of an apparatus for measurements up to temperatures of the order of 2400°.

This apparatus operated on the method of mixing and involved a massive metallic calorimeter with a diathermic system for thermal measurements. The specimens were heated to high temperature in a rebuilt TVV-2 furnace which was equipped with tungsten heating elements. A separating device inserted between the furnace and the calorimeter was so constructed that a sliding door opened when the specimen fell into the calorimeter and then closed once more. Furnace and calorimeter together formed a hermetically sealed volume which was held in a vacuum of the order of  $10^{-3}$  mm of Hg or in an inert atmosphere of argon at a pressure of 1.05 atm during operation.

The calorimeter system consisted of a copper block, two platinum resistance thermometers, and a lever mechanism for closing the copper flaps in the calorimeter cover. This mechanism held these flaps open up to the instant of fall of the specimen. Once the specimen had fallen, the flaps were closed automatically by the closing of the sliding door of the separating system.

The temperature of the calorimeter system was measured on inner and outer resistance thermometers. The outer thermometer had a resistance of approximately 200 ohms and was imbedded, double wound, in a two-track groove cut into the cylindrical surface of the copper block. The inner thermometer had a resistance of approximately 50 ohms and was in the form of a spiral of platinum wire double wound on a helicoidal copper frame. This thermometer was inserted into a deep depression in the copper block. Good thermal contact between the thermometer and the block was assured by careful adjustment of the dimensions. Each thermometer was made from spectrally pure platinum wire and had a diameter of 0.05 mm.

The copper block was enclosed in a metallic jacket. The heat loss of the calorimeter system was reduced to a minimum by carefully polishing the inner surface of this jacket and by covering the copper block with a tightly stretched layer of aluminum foil. A system of polished aluminum foil screens was also interposed between the jacket and the block while the projecting portions of the calorimeter system were constructed of a textolite having low thermal conductivity.

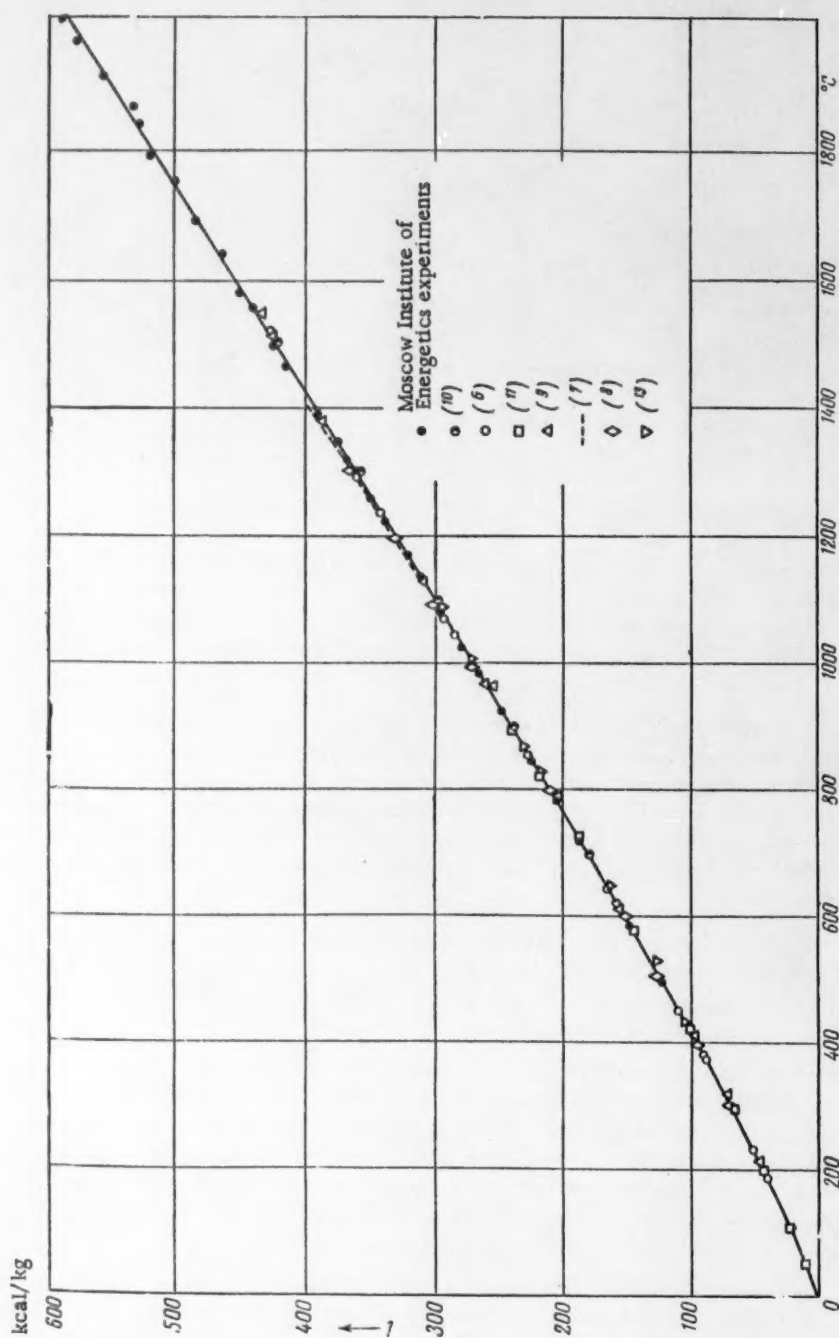


Fig. 1. The temperature dependence of the enthalpy of corundum referred to 0° C.

The calorimeter jacket was surrounded by a water bath whose temperature was held constant to within  $\pm 0.001^\circ$ .

The calorimeter was calibrated by electrical heating. The electrical work,  $Q$ , was measured potentiometrically by the compensation method, assuming that 1 abs. joule = 0.2390 cal. This calibration was used to determine the relation between the heat equivalent of the calorimeter,  $H$ , and the true change in temperature of the calorimeter system,  $\Delta t$ :

$$H = \left( \frac{Q}{\Delta t} \right)_{\text{cal}} = f(\Delta t). \quad (1)$$

Graphs showing the variation of the temperature of the calorimeter system with time were constructed from the experimental points and used in calculating  $\Delta t$ . From the averaged straight lines over the initial and final periods, the apparent temperature change in the calorimeter system  $(t - t_0)_p$  and the temperature derivatives  $(dt/d\tau)_0$  and  $(dt/d\tau)_p$  for the principal period could be found from the times  $\tau_0$  and  $\tau_p$  at its beginning and end and the corresponding temperatures  $t_0$  and  $t_p$ . The corrections for heat exchange,  $\delta t$  and  $\Delta t$ , are then given by [3]

$$\delta t = k \int_{\tau_0}^{\tau_p} (t - t_c) d\tau, \quad \Delta t = (t_p - t_0) + \delta t = t'_p - t_0, \quad (2)$$

$t'_p = t_p + \delta t$  being the corrected temperature of the system at the end of the principal period. The integral of Eq. (2) was evaluated graphically and the rate of cooling,  $k$  and the convergent temperature,  $t_c$  obtained by calculations:

$$k = - \frac{(dt/d\tau)_p - (dt/d\tau)_0}{t_p - t_0}; \quad (3)$$

$$t_c = \frac{(dt/d\tau)_p + (dt/d\tau)_0}{2k} + \frac{t_p + t_0}{2}. \quad (4)$$

The quantity of heat introduced into the calorimeter by the specimen was found from the measured value of  $\Delta t$  and the calibration function (1)

$$Q = H \Delta t = \left( \frac{Q}{\Delta t} \right)_{\text{cal}} \Delta t. \quad (5)$$

The initial temperature was the same ( $t_0 = 22^\circ$ ) in the calibration and in the experiments on the determination of enthalpy, so that Eq. (1) is a unique relation between  $Q$ ,  $H$ , and  $\Delta t$  and the values of  $\Delta t$  in the numerator and denominator of the right-hand member of Eq. (5) are identical. This method of calibration makes it possible to replace the parabolic dependence of the resistance of the platinum thermometer by a linear relation which is valid over an interval  $\Delta t \leq 10^\circ$ , at the same time keeping the error low enough [4] so that the coefficient of proportionality between temperature and resistance will be a unique function of  $\Delta t$  and will thus cancel out of the final result (5).

Thus, construction of the  $t = f(\tau)$  curves and use of Eqs. (1) - (5) for the calculation makes it possible to pass directly from the electrical resistance of the thermometers and the calorimeter calibration to the  $H = (Q/\Delta R)_{\text{cal}} = f(\Delta R)$  relation.

A total of 28 calibration points was obtained for each of the thermometers. The scatter of these points with respect to a straight line obtained by the method of least squares did not exceed  $\pm 0.2\%$  for either the outer or the inner thermometer. The mean square deviation was  $\pm 0.08\%$ . The change of the heat equivalent of the calorimeter amounted to 0.07% per degree.

The following points became clear in the course of the calibration:

1) Experiments in which the temperature curves over the principal interval were of different form agreed to within the limits of error of the calibration, even though the time required for the introduction of a fixed quantity of heat differed by a factor of 2-3.

2) The experimentally developed  $(dt/d\tau)_p = f(t_p - t_c)$  and  $(dt/d\tau)_0 = f(t_0 - t_c)$  curves indicated that the conditions of heat exchange in the calorimeter were practically independent of the direction of thermal flow and that applicability of the law of cooling upon which the calculation of  $\delta t$  from (2) was based was limited to a temperature difference  $(t - t_c) \leq 5 - 6^\circ$ . For this reason the experiments were carried out at  $\Delta t = 3 - 8^\circ$ , and the thermostat temperature was so chosen as to be almost equal to  $t_c$ , so that the value of  $\delta t / \Delta t$  did not exceed 5%.

3) The quantities of heat determined from the two thermometers were in good agreement, the deviation between them being approximately  $\pm 0.1\%$ , and use of the more convenient inner thermometers is therefore recommended in such studies.

The first experiments on the completed apparatus were devoted to an investigation of corundum, the  $\alpha$ -modification of aluminum oxide, with the aim of increasing the accuracy of the data obtained by other authors up to  $1550^\circ$  and extending the interval of study up to  $1993^\circ$ , i.e., practically up to the melting point of corundum which lies at  $2015-2050^\circ$ . Study was made of five cylindrical specimens 28-43 mm in height, and 17-21 mm in diameter. These specimens contained 99.8-99.9% aluminum oxide and weighed 17-29 g.

Temperatures up to  $1318^\circ$  were measured with a Class II platinum-platinorhodium thermocouple, while higher temperatures were determined with an optical pyrometer using a cylindrical depression in the specimen as a simulated absolute black body. This pyrometer and the triangular glass prism through which the specimen was observed were checked against a Class I reference temperature lamp in the All-Union Scientific-Research Institute of the Committee for Standards and Measuring Instruments. The specimen was suspended in the furnace on a tungsten wire which was melted electrically when it was desired to introduce the sample into the calorimeter.

In view of the special features of high temperature studies [4], an ampule was not used to contain the corundum, the heat loss of the specimen during fall into the calorimeter being calculated from the known value of the coefficient of complete radiation [5].

Thirty experimental points were obtained over the temperature interval from  $498$  to  $1993^\circ$  and through these a smooth curve was drawn. These results are represented in the graph (refer to the experiments of the Moscow Institute of Energetics) in which the experimental data of other authors have also been plotted for reference. Most of these experiments were carried out in an atmosphere of argon, the results agreeing with those control experiments which were performed in vacuum. Passage from high temperatures back to low had no effect on the results.

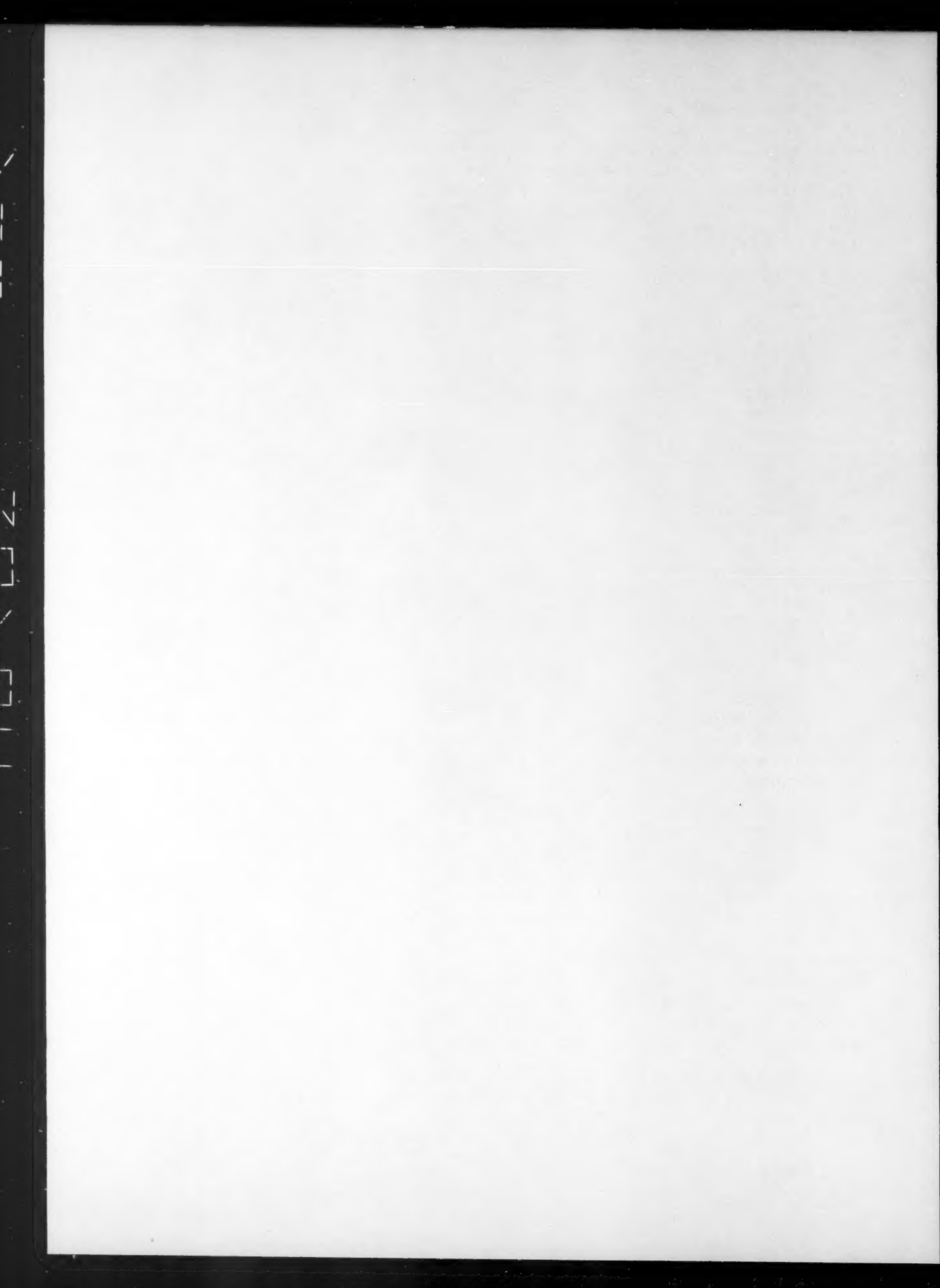
Over the working interval of temperatures, the experimental points agreed, on the average, to within  $\pm 0.5\%$  with the data of [6] ( $500 - 1514^\circ$ ), [7] ( $1100 - 1400^\circ$ ), and [8] ( $500 - 1300^\circ$ ), and to within  $\pm 1\%$  with the data of [9, 10] ( $500 - 1550^\circ$ ). New experimental data agreed with the results of [11, 12] at  $800-900^\circ$  and were higher by 1-0.2%, respectively, at  $500 - 800^\circ$ . The experimental data of [13] at  $500 - 1100^\circ$  were lower than our own by 0.5 - 1%.

The maximum relative experimental error in our determination of enthalpy was estimated to be  $\pm 0.5\%$  in cases in which the temperature was measured with the thermocouple ( $500 - 1300^\circ$ ) and  $\pm 0.9\%$  in cases in which the temperature was measured with the pyrometer ( $1300 - 2000^\circ$ ).

#### LITERATURE CITED

1. K. K. Kelley, Bureau of Mines, Bull. 476 (1949).
2. É. V. Britske, et al., The Thermal Constants of Inorganic Substances [in Russian] (Moscow, 1949).
3. M. M. Popov, Thermometry and Calorimetry [in Russian] (Moscow, 1954).
4. V. Ya. Chekhovskoi, Candidates Dissertation, Moscow Institute of Energetics [in Russian] (1958).
5. Information Circulars of the Institute of Silicate Research, Glass Ind. 36, 4, 193 (1955).

6. C. H. Shomate and B. F. Naylor, J. Am. Chem. Soc. 67, 1, 72 (1945).
7. É. N. Rodigina and K. Z. Gornel'skii, Zhur. Fiz. Khim. 29, 6, 1105 (1955).
8. E. P. Egan, J. Z. Wakefield, and K. K. Elmore, J. Am. Chem. Soc. 72, 2418 (1950).
9. N. B. Vargaftik and O. N. Oleshchuk, Teploenergetika 4 (1955).
10. H. E. Gronow and H. E. Schwiete, Z. Anorg. Chem. 216, 185 (1933).
11. G. T. Furukawa, et al., J. Res. NBS 57, 2, 67 (1956).
12. K. Z. Gornel'skii, Zhur. Fiz. Khim. 32, 8, 1859 (1958).
13. C. H. Shomate and A. J. Cohen, J. Am. Chem. Soc. 77, 285 (1955).



## THE SELECTIVE CHARACTER OF ADSORPTION AS A FUNCTION OF SORBENT STRUCTURE

V. S. Komarov and Academician (Academy of Sciences,  
Beloruss SSR) N. F. Ermolenko

Institute of General and Inorganic Chemistry, Academy of Sciences of the USSR  
Translated from *Doklady Akademii Nauk SSSR*, Vol. 135, No. 1, pp. 129-132,  
November, 1960

Original article submitted July 18, 1960

It has been shown [1-7] that the character of sorbent porosity has a considerable influence upon sorption kinetics as well as on the separation degree of mixtures. It has been found that the highest degree of separation is attained on adsorbents with small pores as a result of the fact that the adsorption potential sharply increases when the pore diameter is decreased.

Besides the sorbent structure, the nature of the mixture plays an important role when separating by means of the sorption method. We have shown [8, 9] that just the component, the addition of which causes the system to deviate from ideal behavior, is sorbed preferentially from binary mixtures. This conclusion opens new possibilities for a scientific selection of adsorbents and catalysts and for choosing the very best conditions for the purification and separation of mixtures. Consequently, the accumulation of quantitative data on the adsorption as a function of sorbent structure and nature of the medium is of known scientific and practical interest and this the more because most of the existing studies in this region of knowledge comprise only the region of diluted solutions. For this reason we have undertaken investigations in order to study more deeply the influence which narrowing of the sorbent pores has upon raising selective sorption from hydrocarbon mixtures differing in nature as well as in properties.

In this study we have investigated the adsorption from saturated vapors of the binary mixtures dichloroethane-ethyl alcohol, benzene-ethyl alcohol, chloroform-dioxane and ethyl alcohol-methyl alcohol on two silica gels with uniform pores, clay and activated wood charcoal.

The adsorption was done in the vapor phase and the concentration was varied over the whole range. The composition of the mixture adsorbed was determined from the change in the composition of the liquid. The silica gels used in this investigation were very different as regards their porosity. One (ASM) belongs to the second structure type in the classification according to A. V. Kiselev [10] and the other (MSK) to the third type. Although the catalysts chosen in this way have the same chemical nature, they must show a different selectivity for the components of the binary mixtures mentioned.

The experimental sorption data are shown in Figs. 1 and 2 in the form of equilibrium isotherms and are plotted in the coordinates: mole fraction of the component 2 in the adsorbed phase ( $N_2^a$ ) versus mole fraction of this same component in the solution at equilibrium ( $N_2$ ) (Table 1).

As can be seen in Fig. 1 a and b, the equilibrium curves have the S-shape which, as we have already noticed previously, is characteristic for binary azeotropic mixtures with positive or negative deviations from Raoult's law [8, 9].

The comparison of the data in Fig. 1 shows that a positive adsorption of alcohol from binary dichloroethane-ethyl alcohol mixtures is found at equilibrium liquid mixture compositions between 0 and 0.55 mole fraction of alcohol in the case of silica gel with narrow pores and between 0 and 0.29  $N_2$  in that of silica gel with wide pores.

TABLE 1

Selectivity of Methyl Alcohol Sorption by Silica Gel from Ethyl Alcohol—Methyl Alcohol Mixtures

Mole fraction of methyl alcohol in the solution at equilibrium	Mole fraction of methyl alcohol in sorbent phase	
	silica gel with narrow pores	silica gel with wide pores
0.092	0.156	0.103
0.262	0.324	0.293
0.415	0.495	0.459
0.555	0.636	0.611
0.680	0.771	0.719
0.794	0.848	0.825
0.904	0.942	0.935

In the system benzene—ethyl alcohol an analogous relation was found. Here, the silica gel with narrow pores shows a greater selectivity toward alcohol than does that with wide pores. To the right of the points where the composition of the adsorbent phase and that of the equilibrium liquid mixture are equal, that is, for equilibrium mixtures with a higher alcohol content, the sorbent phase is enriched in dichloroethane or benzene. Such an inversion of selectivity may be considered to result from the thermodynamic properties of binary mixtures with low-molecular components. Other conditions being equal, the selectivity of sorption depends upon whether in the sorbent are present pores with molecular dimensions (2-3 molecular diameters), which because of the superposition of the field from the opposite wall have an enhanced sorption potential.

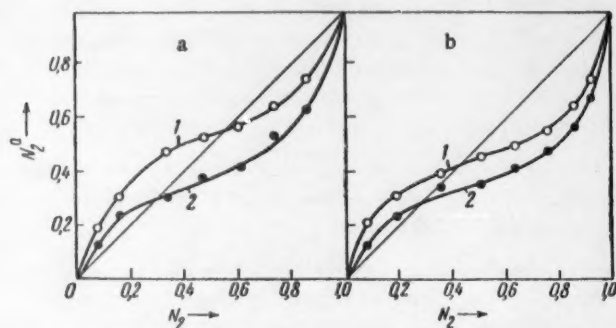


Fig. 1. Curves of the equilibrium ( $N_2^g - N_2^l$ ) between the adsorbent phase and binary dichloroethane—ethyl alcohol (a) or benzene—ethyl alcohol solutions (b). 1) On silica gel with narrow pores; 2) on silica gel with wide pores.

A. V. Kiselev and co-workers [11] have shown that upon decreasing the pore diameter of silica gel from 104 to 38 Å, the selectivity of toluene sorption from solutions in heptane is enhanced, and the maximum sorption is shifted toward more dilute solutions. For sorbents with narrow pores, the total sorption potential will be the sum of the work done by the adsorption forces when displacing a molecule from the gas phase to a given point on the sorbent surface (the adsorption potential of the sorbent surface) and the capillarity potential, which is characterized by the field energy of capillary forces referred to unit liquid mass in the porous body [12].

The first of these (referred to as unit surface area) depends upon the chemical nature of the solid surface, while the magnitude of the capillarity potential is mainly determined by the physical structure of the solid. This means that sorbents with strongly developed narrow pores will have not only high sorption potentials but also a high sorption selectivity. The capillarity potential of such sorbents will, as it were, correspond to some free surface area having a certain sorption potential and ability, obviously, to show properties analogous to those of the adsorption forces in the field of the sorbent surface. Therefore, it is difficult to expect proportionality between the selectivity of sorption and the specific surface areas of the sorbents when these refer to different structural types.

Data of I. E. Nelmark [6] on the chromatographic separation of hydrocarbons confirm this conclusion. The degree of selectivity shown by sorbents depends not only upon the magnitude of their sorption potentials but also on many other factors on which we will dwell shortly.

First as they depend upon the character and the chemical nature of the surface and the affinity for the components of the mixture, sorbents may show an enhanced or a diminished selectivity in sorption. Here two cases should be distinguished: a) when the binary mixture shows a positive deviation from Raoult's law and the sorbent has affinity for that component the addition of which causes the mixture to deviate from additivity, the degree of selectivity is enhanced; b) when the deviation of mixture properties from additivity is negative, the degree of selectivity will be diminished.

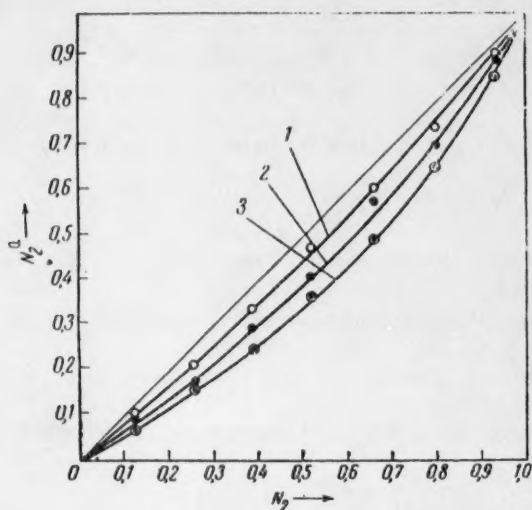


Fig. 2. Curves of the equilibrium ( $N_2^a - N_2$ ) between the adsorbent phase and a binary chloroform—dioxane solution: 1) on silica gel with narrow pores; 2) on clay; 3) on activated charcoal.

tions [15]. Such mixtures are found preeminently in those cases where the components of the solution have a raised mutual attraction, which results in the formation of solvated or chemical compounds from the mixed molecules. In other words, the mixing of two liquids with very different internal pressures will generally be accompanied by a deviation of the mixture properties from Raoult's law. From a thermodynamic point of view, such mixtures are characterized by an enhanced nonideality or, which is the same, by an excess free energy of formation per mole of real solution  $F^r$ , which is greater than that of a mole of ideal solution  $F^i$  [16]. Here, the difference  $F^o$  between these values is negative.

$$F^o = F^r - F^i.$$

Since silica gel, as mentioned above, has an enhanced affinity toward dioxane, it does work on the system such that the free energy is increased when it sorbs the latter substance. This means that in the sorption of a

In the opposite case, where the sorbent has a greater affinity for the component the dilution of which increases the ideality of the system, the degree of selectivity is diminished in systems with a positive deviation from additivity, while it is enhanced in those with a negative deviation.

To illustrate the rules given, we compare the selectivity of sorption from the binary chloroform—dioxane mixture on the silica gel with narrow pores, ASM; on clay from the region of the town Vitebsk; and on the activated wood charcoal BAU (Fig. 2).

From the data in Fig. 2 it is obvious that the silica gel with narrow pores, because of its affinity for dioxane, the component which makes the mixture deviate from ideality, shows a lower sorption selectivity than does clay or charcoal.

Let us consider the factors which determine this character of adsorption. The chloroform—dioxane mixture, just as chloroform—acetone [13] and chloroform—diethylether [14] mixtures, belongs to the systems showing a negative deviation from Raoult's law, as has been shown by thermodynamic investiga-

certain volume of the chloroform-dioxane mixture by silica gel less energy is gained than is set free upon sorbing the same volume of this mixture by clay or charcoal. An analogous relation is found also in sorption from dichloroethane-ethyl alcohol and benzene-ethyl alcohol mixtures where silica gel with narrow pores, for just the same reasons, to the right of the points where the compositions of adsorbent phase and equilibrium solution are equal, shows a smaller sorption selectivity than does silica gel with wide pores (Fig. 1).

On the other hand, in systems with a positive deviation from Raoult's law the sorption of the component which makes the system deviate from additivity is accompanied by a decrease in free energy and an increased thermodynamic stability of the mixture. Other conditions being equal, the degree of selectivity is enhanced such that the component toward which the adsorbent has greater affinity is adsorbed positively (Table 1 and Fig. 1).

In conclusion, we want to underline that sorbents with narrow pores in combination with the chemical nature of their surfaces and the thermodynamic properties of the binary solutions are responsible for the selective sorption of components from a binary mixture.

#### LITERATURE CITED

1. A. V. Kiselev and Yu. A. Él'tekov, *Doklady Akad. Nauk SSSR* **100**, 1, 107 (1955).
2. I. E. Nelmark and F. I. Khatset, *Doklady Akad. Nauk Ukr. SSR* **2**, 24 (1949).
3. A. V. Kiselev, *Trudy Komissii po Anal. Khim.* **6**, 9, 46 (1955).
4. V. P. Dreving, A. V. Kiselev and Yu. A. Él'tekov, *Doklady Akad. Nauk SSSR* **86**, 394 (1952).
5. E. A. Mikhailov and B. A. Kazanskii, Collection: Investigations in the Field of Chromatography [in Russian] (Izd. AN SSSR, Moscow, 1952), p. 155.
6. I. E. Nelmark, I. B. Slinyakova, and F. I. Khatset, Collection: Investigations in the Field of Chromatography [in Russian] (Izd. AN SSSR, Moscow, 1952), p. 98.
7. N. N. Avgul', et al., *Doklady Akad. Nauk SSSR* **77**, 77 (1951).
8. V. S. Komarov and N. F. Ermolenko, *Doklady Akad. Nauk Beloruss. SSR* **2**, 2 (1958).
9. V. S. Komarov and N. F. Ermolenko, *Doklady Akad. Nauk Beloruss. SSR* **2**, 7 (1958).
10. A. V. Kiselev, *Vestnik Moskov. Univ.* **11**, 111 (1949).
11. A. V. Kiselev, V. V. Khopina, and Yu. A. Él'tekov, *Izvest. Akad. Nauk SSSR, Otdel. Khim. Nauk* **6**, 664 (1958).\*
12. A. V. Lykov, *Heat and Mass Transfer in Drying Processes* [in Russian] (Moscow-Leningrad, 1956), p. 51.
13. J. Zawadzki, *Z. Phys. Chem.* **35**, 2, 129 (1900).
14. Guglielmo, *Atti Accad. Linc.* **1**, 1, 294 (1892). Cited from: *Technical Encyclopedia, Handbook of Physical and Chemical Values* [in Russian] (1928), Vol. 5.
15. M. L. McGlashan and R. P. Rastogi, *Trans. Farad. Soc.* **54**, 4, 496 (1958).
16. A. I. Kireev, *Zhur. Fiz. Khim.* **14**, 1456 (1940).

\*Original Russian pagination. See C. B. translation.

## THE EFFECTS OF VULCANIZATION OF ELASTOMERS ON THEIR ADHESION TO NONVULCANIZING POLYMERS

V. G. Raevskii and S. S. Voyutskii

M. V. Lomonosov Moscow Institute for Fine Chemical Technology

(Presented by Academician S. S. Medvedev, June 11, 1960)

Translated from *Doklady Akademii Nauk SSSR*, Vol. 135, No. 1, pp. 133-136,  
November, 1960

Original article submitted June 3, 1960

According to contemporary ideas [1-3], the mechanisms of adhesion and of covulcanization of rubbers have much in common. The phenomenon of covulcanization, like polymer adhesion, involves the diffusion of macromolecules and their segments, particularly so in the first stage of vulcanization when cross-linkages have not yet been formed. The only difference between covulcanization and adhesion is that, with the former, the process of interaction of molecular chains is sooner or later interrupted by the superimposed vulcanization process, which joins macromolecules or their parts by firm chemical bonds. This gives an adhesion layer considerably stronger than any layer formed by diffusing molecules, which are joined only by weak intermolecular bonds.

It is interesting to ascertain how vulcanization of elastomers will affect their adhesion to polymers which cannot form chemical bonds with them. This is a matter of great practical importance, since rubbers are frequently used in combination with vegetable and synthetic fibers, which cannot be vulcanized.

Elastomers of different molecular structure, polarity, and molecular mobility were used as adhesives: butadiene-acrylonitrile rubber (SKN-26), butadiene-styrene rubber (SKS-30A), butadiene-styrene oil-filled rubber (SKS-30ARM-15), and butyl rubber. From these we prepared a number of rubber mixes, some containing vulcanizing agent, others containing an equivalent amount of chalk as an inert filler. The best vulcanizing agents were selected for each rubber.

The substrates used were unplasticized films of Cellophane (cellulose hydrate) and Perfol PK-4 (polycaprolactam).

The adhesives were applied to the substrates as coatings on a calender, using the optimum conditions for each elastomer [4]. The products thus obtained were doubled over and vulcanized. Vulcanization was carried out in a "Berstorff" direct vulcanization apparatus, at 143° and a pressure of about 0.85 kg/cm<sup>2</sup>. The vulcanizing time was varied from 0 to 88 minutes.

Figures 1 and 2 show the variation of the specific adhesion (determined by the stripping method) of elastomer coatings to the above substrates. It can be seen that, regardless of the type of adhesive and substrate, the time for which the system was held at the vulcanization temperature had a powerful influence on the resulting adhesion. However, for coatings which did not contain vulcanizing agents, the adhesion increased continuously (though at a varying rate) with increasing time of thermal treatment, whereas, with coatings containing vulcanizing agents, the adhesion passed through a maximum.

The continuous increase in adhesion in the first case can be explained by the interaction of molecules, or of their elements, in the boundary layer. In the second case, the increasing adhesion with relatively short thermal treatments can obviously be explained in the same way. Because of the vulcanization induction period, structural changes either do not occur at this stage, or are very slight.

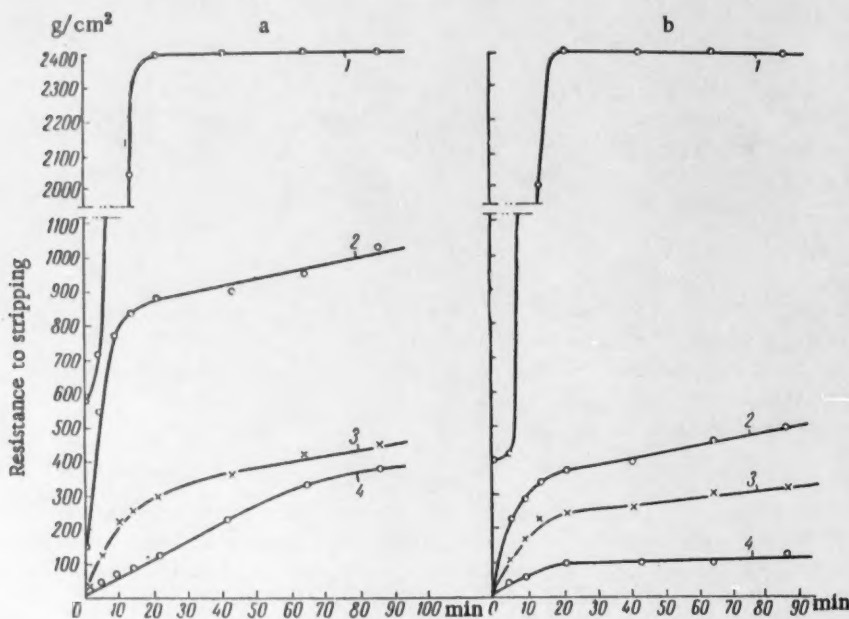


Fig. 1. The effect of thermal treatment time on the adhesion of coatings free from vulcanizing agents to: a) polyamide film PK-4 and, b) Cellophane. 1) Butyl rubber; 2) butadiene-styrene oil-filled rubber SKS-30ARM-15; 3) butadiene-styrene rubber SKS-30A; 4) butadiene-acrylonitrile rubber SKN-26.

The marked change in curve shape for vulcanization times above 12-15 minutes is probably due to two factors. One is the rapid fall in diffusion rate as the result of structural adhesion. However, even total cessation of diffusion could only mean that the adhesion would cease to increase further with heat treatment time. The reduction in adhesion must be due to the creation of an auxiliary strain in the contact zone, as the result of a contraction in the rubber coating following structural changes. This strain would reduce the force required to rupture the adhesion layer.

The results obtained enabled us to draw a number of conclusions as to the effect on adhesion of the molecular structure of the elastomers investigated.

It is well known that butyl rubber is a practically nonpolar elastomer with a linear structure, and that its molecular weight is small compared with those of the other elastomers (in our case, the mean molecular weight of the butyl rubber was 32,000). The low molecular weight of this polymer is associated with a relatively high concentration of macromolecule end groups, and it is known [5] that these are the most active in diffusion processes. This ensures that butyl rubber should have the maximum adhesion to both substrates.

The bulky styrene units and high molecular weights of butadiene-styrene elastomers account for the considerably lower values of their adhesions. It is very interesting to compare the adhesions of butadiene-styrene elastomers SKS-30A and SKS-30ARM-15. The latter only differs from the former normal low temperature butadiene-styrene rubber in containing plasticizer, which is introduced during the process of forming the copolymer. Since both the above copolymers are of the same chemical nature, it can only be supposed that the greater adhesion of the oil-filled elastomer is due to the higher mobility of its molecular chains.

In all cases, the minimum adhesion was observed with the most polar adhesive — butadiene-acrylonitrile copolymer. This circumstance can also be explained in terms of the diffusion theory of adhesion as due to the low mobility of the molecular chains and the existence of acrylonitrile units. In this case, the diffusion process definitely occurs much more slowly, as shown by the absence of any marked increase in adhesion during the initial stage of polymer interaction. Apart from this, the value of the specific adhesion in this case can largely be explained by intermolecular reaction between polar polymers in the contact zone.

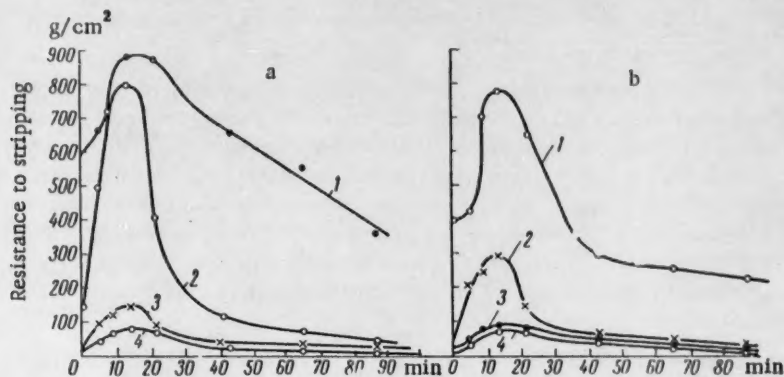


Fig. 2. The effect of vulcanization on the adhesion of rubber coatings to a) polyamide film PK-4, and b) Cellophane. The curve numbers have the same meaning as in Fig. 1.

TABLE 1

The Effects of Degree of Vulcanization on the Strength of the Bond Between Rubber and Cloth

Rubber	Cloth body type	Optimum vulcanization time, min.		Resistance to stripping, g/cm <sup>2</sup> , after vulcanization for	
		for rubber	for adhesive	35 min	15 min
SKS-30A	Percale		15	900	1500
	Caprone 1520	35	15	350	1050
	Glass cloth T <sub>1</sub>		15	600	1350
SKN-26	Percale		15	1150	2000
	Caprone 1520	35-40	15	200	700
	Glass cloth T <sub>1</sub>		15	400	1200
Butyl rubber	Percale		15	2600	3900
	Caprone 1520	40	15	2000	3600
	Glass cloth T <sub>1</sub>		15	2700	4000

It will be noted that the curves, showing the change in adhesion with time of thermal treatment for the different adhesives, are in the same order in Figs. 1 and 2. This shows that peculiarities in rubber vulcanization were not concealing adhesion effects due to the nature of the adhesives. In considering the effect of the nature of the substrate on adhesion, it is first necessary to return to the fact that nonpolar rubber can develop high adhesion to a polar substrate. This can be explained as due to local dissolution of adhesive hydrocarbon chains in a substrate consisting of polar groups together with sufficiently large nonpolar hydrocarbon chain regions [6].

Comparison showed that adhesion was always greater to caprone than to cellulose. This is probably due to the extreme stiffness of the cellulose molecular chains [7] and their high packing density as the result of

hydrogen bonds between hydroxyl groups [8]. Cellulose also differs from caprone in always being obtained only in a glassy state [7, 9]. The even structure and the physical state of cellulose provide the least favorable conditions for the diffusion of adhesive molecule elements.

Thus, vulcanization of a rubber coating requires the existence of an adhesion maximum, which corresponds to the optimum degree of vulcanization from the adhesion point of view. The existence of an optimum vulcanization for bonding strength was confirmed by us for rubberized cloth materials, using cloth made from cellulose, caprone, and glass fiber. With these materials, similar behavior was observed for the variation in adhesion with degree of rubber vulcanization. The effects of "mechanical adhesion" did not change the character of this variation, but only resulted in a higher total adhesion to the cloth as compared with the corresponding specific adhesion to foil.

The existence of an optimum vulcanization for bonding strength in rubberized cloth objects and materials can be made use of in industrial practice. At present, such objects are vulcanized under conditions corresponding to the optimum for the physicomaterial properties of the rubber. However, the optimum vulcanization time for bond strength is considerably less than for rubber properties, and objects vulcanized under the latter conditions will not show such high adhesion. Table 1 shows the corresponding values of the bond strength for cloths of different chemical nature. Bond strengths are shown after vulcanization corresponding to the optimum for rubber properties (35-40 minutes at 143°) and after vulcanization corresponding to optimum bond strength (15 minutes at 143°). According to these results, reduction in vulcanization time from 35 to 15 minutes increases the bond strength by a factor of 1.8 to 3.

A reduction in the degree of vulcanization of the surface layer (as compared with the degree of vulcanization of the main bulk of rubber) can be achieved without altering the present vulcanization time used for a given object by decreasing the vulcanizing agent content in the surface layer of the rubber. As well as increasing the strength of the "rubber-cloth" bond, this procedure will reduce the cost of the product as the result of a reduction in the content of expensive vulcanizing agent.

#### LITERATURE CITED

1. S. S. Voyutskii and B. V. Shtarkh, *Kolloid Zhur.* **16**, 3 (1954).\*
2. B. A. Dogadkin, M. S. Fel'dshtein, and D. M. Pevzner, *Collected Papers on Rubber Vulcanization* [in Russian] (Leningrad, 1954) p. 7.
3. *Collected Papers on the Bonding Strength Between Elements of Rubber-Cloth Multilayer Objects in Production and Use* [in Russian] (Leningrad, 1956) pp. 87, 118, 151.
4. M. G. Maizel's and V. G. Raevskii, *Kauchuk i Rezina* **1**, 16 (1960).
5. S. S. Voyutskii, A. I. Shapovalova, and A. P. Pisarenko, *Kolloid Zhur.* **19**, 274 (1957).\*\*
6. S. S. Voyutskii and V. L. Vakula, *Vysokomolek. Soed.* **2**, 1, 51 (1960).
7. V. A. Kargin, P. V. Kozlov, and Wang Nai-ch'ang, *Doklady Akad. Nauk SSSR* **130**, 2 (1960).\*
8. C. J. Liang and R. H. Marchessault, *J. Polym. Sci.* **35**, 129, 529 (1959).
9. V. A. Kargin, *Vysokomolek. Soed.* **2**, 3, 466 (1960).

\* See C. B. translation.

\*\* Original Russian pagination. See C. B. translation.

# THE NONLINEAR THERMODYNAMICS OF IRREVERSIBLE PROCESSES

I. F. Bakhareva

N. G. Chernyshev Saratov State University

(Presented by Academician V. N. Kondrat'ev, May 28, 1960)

Translated from *Doklady Akademii Nauk SSSR*, Vol. 135, No. 2, pp. 350-353, November, 1960

Original article submitted May 26, 1960

The kinetics of an extensive group of phenomena can be studied through a phenomenological theory of the thermodynamics of irreversible processes based on the Onsager Equations:

$$\dot{x}_i = \sum_k^n L_{ik} X_k, \quad i = 1, 2, \dots, n; \quad (1)$$

$$L_{ik} = L_{ki}, \quad (2)$$

in which  $x_1, x_2, \dots, x_n$  constitute a set of thermodynamic parameters characterizing the degree of departure of the system from equilibrium,  $L_{ik}$  are kinetic coefficients, and  $X_k$  are thermodynamic forces. For the thermally isolated system, these forces are expressed through equations of the form:

$$X_k = \frac{\partial(-\Delta S)}{\partial x_k}; \quad (3)$$

$\Delta S$  being the deviation of the entropy from its value at equilibrium.

The traditional approach to the thermodynamics of irreversible processes has been one in which second-order terms in the expansion of  $\Delta S$  have been incorporated into the expression for  $X_k$  so that the latter becomes a linear function of the thermodynamic parameters:

$$X_k = \sum_i^n g_{ik} x_i, \quad k = 1, 2, \dots, n, \quad (4)$$

and, obviously,

$$g_{ik} = g_{ki}. \quad (5)$$

Equation (4) gives a basis for rewriting the system of Eqs. (1) in the form:

$$\dot{x}_i = \sum_{k,l}^n L_{ik} g_{il} x_l, \quad i = 1, 2, \dots, n. \quad (6)$$

Thus, the thermodynamic equations of motion of Onsager are linear in both formulations, (1) and (6).

It can be shown statistically [1] that relation (2) results from symmetry in the  $b_{ik}$  matrix:

$$b_{ih} = b_{hi}, \quad (7)$$

The elements of this matrix enter into the expression for the dissipative function,  $D$ :

$$D = \frac{1}{2} \sum_{i,h}^n b_{ih} \dot{x}_i \dot{x}_h, \quad (8)$$

which resembles the "production of entropy,"  $\sigma$ ,

$$\sigma = \frac{d(\Delta S)}{dt} = \sum_i^n \dot{x}_i X_i, \quad (9)$$

Insofar as it is a measure of energy dissipation.

It can be shown readily that

$$D = \frac{\sigma}{2}. \quad (10)$$

By taking (7), (8), (9), and (10) into account, we obtain

$$L_{ih} = b_{ih}^{-1}. \quad (11)$$

The linear form of the kinetic relation expressed through the system of Eqs. (6) is valid only in the neighborhood of equilibrium since it was developed for condition (4). This limitation is always vitally significant except for transfer phenomena and similar effects. In general, the system (6) cannot be extended to the entire kinetic region of the phenomenon in question but begins to come into play at times close to  $t = \infty$  when equilibrium is established in the system.

The kinetic relation expressed through the system of linear equations (1) with condition (6) will be designated as linear-linear. It will be shown below that the linearity of (6) will break down in the next stage of approximation while that of (1) is maintained.

If the earlier definition of the thermodynamic forces in the form of (3) is retained and account taken of third-order members in the expansion of  $\Delta S$ , the result is:

$$X_h = \sum_i^n g_{ih} x'_i + \frac{1}{2} \sum_{i,l}^n m_{ihl} x'_i x'_l, \quad (12)$$

from which it is obvious that

$$g_{ih} = g_{hi}, \quad m_{ihl} = m_{hil} = m_{nli} = m_{ilh}. \quad (13)$$

It will be quickly noted that the form of the function  $\sigma$  is independent of the number of members in the expansion of  $\Delta S$ , i.e.,

$$\sigma' = \sum_i^n \dot{x}_i X'_i. \quad (9')$$

Under these conditions, the kinetic equations can be brought into linear form once more:

$$\dot{x}'_i = \sum_h^n L'_{ih} X'_h, \quad i = 1, 2, \dots, n. \quad (1'')$$

It will be assumed further that the dissipative function, which resembles  $\sigma$  in determining the dissipation of energy, can be expressed as before

$$D' = \frac{1}{2} \sum_{i, h}^n b'_{ih} \dot{x}_h \dot{x}_i, \quad (8')$$

with

$$D' = \frac{\sigma'}{2}. \quad (10')$$

It must be supposed that

$$b'_{ih} = b_{ih}. \quad (14)$$

if the function  $D'$  is to pass over into  $D$  when  $\dot{x}'_k \rightarrow \dot{x}_k$ .

Equations (7), (8'), (9'), (10') and (14) give

$$L'_{ih} = L_{ih}. \quad (15)$$

The kinetic Eq. (1\*) takes the form

$$\dot{x}_i = \sum_h^n L_{ih} X'_h, \quad (1')$$

and relation (2) is fulfilled by the  $L_{ik}$ .

When the  $X'_k$  are expressed as functions of the thermodynamic parameters of (12) the result is a system of nonlinear kinetic equations of the form

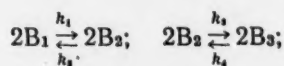
$$\dot{x}_i = \sum_{h, m}^n L_{im} g_{ih} x'_h + \frac{1}{2} \sum_{m, l, h} L_{im} m_{ihl} x'_h x'_l. \quad (6')$$

The kinetic relation covered by Eqs. (1') and (6') will be designated as linear-nonlinear.

It is natural to suppose that the linear-nonlinear form of the kinetic relation has greater generality and possibly embraces the entire kinetic region for certain processes in which the linear-linear form is applicable over only a limited interval near the equilibrium state.

It is readily noted that (6') passes over into (6) when nonlinear members can be neglected.

By way of illustration we will consider a system subject to chemical reactions since this is the most typical instance of limited applicability of the linear-linear relation. For simplicity we will select a definite reaction involving two consecutive reversible bimolecular steps:



$k_i$  being the rate constant for the  $i$ -th reaction;

$$x_i = c_i - c_i^0 = \Delta c_i; \quad (16)$$

$c_i$  is the concentration of the  $i$ -th component at the instant in question, and  $c_i^0$  is the concentration of this same component at equilibrium.

If this reaction is carried out at fixed temperature and volume, it will follow that [2]

$$X_i = \frac{\partial(\Delta F)}{\partial(\Delta c_i)}; \quad (17)$$

$\Delta F$  being the departure of the free energy from its equilibrium value.

In view of the fact that superposition effects are absent in chemical reactions [3], i.e., that

$$L_{ih} = L_{hi} = 0, \quad (18)$$

the independent concentrations will be covered by the kinetic equations

$$\begin{aligned} \frac{1}{2} \frac{d(\Delta c_1)}{dt} &= L_1 X_1, \\ \frac{1}{2} \frac{d(\Delta c_3)}{dt} &= L_2 X_2. \end{aligned} \quad (19)$$

Supposing the chemical potential to be expressed by

$$\mu_i = RT \ln \frac{c_i}{c_i^0} + \mu_i^0, \quad (20)$$

and considering third-order members in the expansion of  $\Delta F$ , we obtain

$$\begin{aligned} \frac{1}{2} \frac{d(\Delta c_1)}{dt} &= L_1 \left\{ 2 \left( \frac{1}{c_2^0} - \frac{1}{c_1^0} \right) \Delta c_1 + \frac{2}{c_2^0} \Delta c_3 + \left[ \frac{1}{(c_2^0)^2} - \frac{1}{(c_1^0)^2} \right] \Delta c_1^2 + \right. \\ &\quad \left. + \frac{2}{(c_2^0)^2} \Delta c_1 \Delta c_3 + \frac{1}{(c_2^0)^2} \Delta c_3^2 \right\}; \\ \frac{1}{2} \frac{d(\Delta c_3)}{dt} &= L_2 \left\{ \frac{2}{c_2^0} \Delta c_1 + 2 \left( \frac{1}{c_2^0} - \frac{1}{c_3^0} \right) \Delta c_3 + \frac{1}{(c_2^0)^2} \Delta c_1^2 + \right. \\ &\quad \left. + \frac{2}{(c_2^0)^2} \Delta c_1 \Delta c_3 + \left[ \frac{1}{(c_2^0)^2} - \frac{1}{(c_3^0)^2} \right] \Delta c_3^2 \right\}. \end{aligned} \quad (21)$$

Taking account of the fact that

$$L_1 = k_1 (c_1^0)^2, \quad L_2 = k_3 (c_2^0)^2, \quad (22)$$

and using (16) to bring the variables  $c_i$  into the system (21), gives

$$\begin{aligned} \frac{1}{2} \frac{dc_1}{dt} &= -k_1 c_1^2 + k_2 c_2^2, \\ \frac{1}{2} \frac{dc_3}{dt} &= k_3 c_2^2 - k_4 c_3^2, \end{aligned} \quad (23)$$

a result which is in complete agreement with the Law of Mass Action.

Thus, in this case the linear-nonlinear relation applies over the entire kinetic region ranging from initiation of reaction (at  $t = 0$ ,  $c_1 = c_0$ ,  $c_2 = c_3 = 0$ ) to equilibrium.

It is readily noted that the linear form of the formulation (1) results from the use of (3) as definition of the thermodynamic forces. The range of applicability of the thermodynamic method is limited by this definition. The conditions of the physical problem in question will dictate the number of members which must be taken into account in the expansion of  $\Delta S$ . It can be shown that the linear-linear relation obtained by considering second-order members in the expansion of  $\Delta F$  is applicable over the entire kinetic region of each monomolecular step. Bimolecular steps require that third-order members in the decomposition of  $\Delta F$  be taken into account while trimolecular steps necessitate consideration of fourth-order terms in conformity with the Law of Mass Action.

The author wishes to take this opportunity of expressing her deep appreciation to A. D. Stepukhovich for his continual interest in this work and for valuable comments and advice.

#### LITERATURE CITED

1. L. Landau and E. Lifshits, *Statistical Physics* [in Russian] (1951).
2. K. Popov, *Doklady Akad. Nauk SSSR* 106, 3 (1956). \*
3. S. R. DeGroot, *Thermodynamics of Irreversible Processes* [Russian translation] (1956).

\* See C. B. translation.



# CRITICAL PHENOMENA OCCURRING UNDER THE INFLUENCE OF INHIBITORS IN DEGENERATIVE BRANCHING REACTIONS

A. B. Gagarina, Z. K. Maizus, and Corresponding Member  
of the Academy of Sciences of the USSR N. M. Émanuél'

Institute of Chemical Physics, Academy of Sciences of the USSR

Translated from Doklady Akademii Nauk SSSR, Vol. 135, No. 2, pp. 354-356,  
November, 1960

Original article submitted July 22, 1960

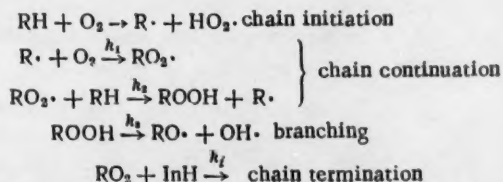
The nature of the critical phenomena which have been disclosed during the study of branching chain reactions is essentially that at certain values of experimental parameters (dimensions of vessel, temperature, and pressure), a very small change in these may produce a sudden alteration in the nature of the process taking place. The theory of critical phenomena for rapid branching chain reactions, associated with the ignition of the reaction mixtures, has been developed by N. N. Semenov [1].

It follows from the Semenov theory of slow chain reactions with degenerative branching that critical phenomena are to be expected under these conditions. As far as gaseous reactions are concerned, the conclusions of the theory have been vindicated for the oxidation of arsine [2], of ethane [3], of acetylene [4], and of some other hydrocarbons (methane, propane, ethylene and propylene) [5], for which the occurrence of the critical phenomena when the dimensions of the reaction vessel are changed has been established.

During a recent study of the oxidation of n-decane in the presence of copper stearate, it has been shown that critical phenomena are also present for the oxidation processes in the liquid phase [6]. It was observed that the copper stearate plays a dual role in this process: small quantities exert an accelerating effect, but increase in the copper stearate ( $\text{CuSt}_2$ ) concentration leads to the observation of a distinct retarding effect. A critical concentration of the copper stearate has been established, beneath which the autoaccelerative process is developed with a measurable induction period (2 to 4 hours), and above which the induction period increases rapidly and produces a practically complete cessation of the reaction.

The authors explained the existence of a critical concentration of copper stearate within the framework of the generally accepted scheme of oxidation on the assumption of branching and breaking of chains on the  $\text{CuSt}_2$  molecules. N. N. Semenov, considering the mechanism of chain degenerative branching reactions, has expressed the opinion that in liquid phase oxidations a critical inhibitor concentration ought to exist, above which the process will be found to be stationary, and above which it will be autooxidative [7].

The scheme for the oxidation process in the presence of an inhibitor may be represented in the following manner:



(where InH denotes the inhibitor).

In the current work it may be taken as established that the destruction of radicals on the inhibitor molecules occurs practically exclusively by means of chain termination up to the point of almost complete exhaustion of the inhibitor. The system of differential equations which describes the kinetics of the process has the form:

$$\begin{aligned}\frac{d[\text{RO}_2\cdot]}{dt} &= w_0 + k_3[\text{ROOH}] - k_i[\text{InH}][\text{RO}_2\cdot]; \\ \frac{d[\text{ROOH}]}{dt} &= k_2[\text{RO}_2][\text{RH}] - k_3[\text{ROOH}].\end{aligned}$$

At constant inhibitor concentration the solution of this system of differential equations is given by the following functions:

$$\begin{aligned}[\text{RO}_2] &= A_0 + A_1 e^{\lambda_1 t} + A_2 e^{\lambda_2 t} = f_1(t); \\ [\text{ROOH}] &= B_0 + B_1 e^{\lambda_1 t} + B_2 e^{\lambda_2 t} = f_2(t),\end{aligned}$$

where  $A_0, A_1, A_2, B_0, B_1,$  and  $B_2$  are parameters whose value depends on the initial conditions but are independent of  $t$ ; while  $\lambda_1$  and  $\lambda_2$  are the roots of the characteristic equation

$$\lambda^2 + [k_i[\text{InH}] + k_3]\lambda + k_i[k_i[\text{InH}] - k_2[\text{RH}]],$$

which is obtained by equating to zero the determinant of the system:

$$\begin{vmatrix} -k_i[\text{InH}] - \lambda & k_3 \\ k_2[\text{RH}] & -k_3 - \lambda \end{vmatrix} = 0.$$

The condition that the roots of the characteristic equation shall pass through zero is fulfilled by equating to zero the free term

$$k_i[\text{InH}] - k_2[\text{RH}] = 0.$$

For negative values of  $\lambda_1$  and  $\lambda_2$ , which are found when  $k_i[\text{InH}]$  is greater than  $k_2[\text{RH}]$ , a slow, stationary development of the process should be observed. If, however, one of the values of  $\lambda$  becomes positive,  $k_i[\text{InH}]$  is less than  $k_2[\text{RH}]$ , the process then becomes autoaccelerative.

The current work has had the objective of obtaining experimental indication of the existence of the phenomenon of a critical concentration for the inhibitor in the oxidation of hydrocarbons, using typical inhibitors of radical-chain processes, and to measure the magnitude of this concentration.

The reaction chosen for investigation was the oxidation of n-decane in the presence of  $\alpha$ -naphthol as inhibitor, the concentration of the latter in the reaction mixture being maintained constant during the course of an experiment. The inhibitor was introduced into a mixture in which reaction was already taking place at some definite time in the reaction,  $t_1 = 2$  hours, when the concentration of hydroperoxides in the reacting mixture had reached the value of 0.17 mole %.

The course of the reaction was followed by means of the kinetic curve for the hydroperoxide accumulation. Constancy of concentration for the  $\alpha$ -naphthol was attained by addition of the inhibitor to the reaction vessel in quantities which compensated for the destruction of the  $\alpha$ -naphthol as the

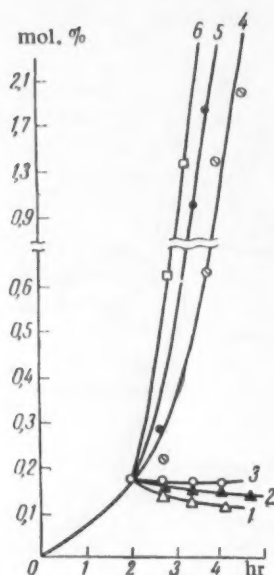


Fig. 1. Kinetic curves for the accumulation of hydroperoxides during the oxidation of n-decane at 130° for different concentrations of  $\alpha$ -naphthol (in mole/ml). 1)  $8.2 \cdot 10^{-7}$ ; 2)  $4.4 \cdot 10^{-7}$ ; 3)  $3.3 \cdot 10^{-7}$ ; 4)  $2.9 \cdot 10^{-7}$ ; 5)  $3.1 \cdot 10^{-7}$ ; 6)  $1.0 \cdot 10^{-7}$ .

reaction proceeded. The inhibitor was added in the form of a solution in n-decane (at the same stage of oxidation as the decane in the reaction vessel) at the rate of 1 ml/hr. Fluctuations in the stationary concentration of the inhibitor during the dropping in of its solution did not exceed 0.5-1.5%. The level of the liquid in the reaction vessel during the entire experiment was practically constant, since the removal of samples for analysis corresponded to the volume of the inhibitor solution in decane which was added.

The concentration of the  $\alpha$ -naphthol was determined spectrophotometrically by the absorption maximum at 5830 Å, after it had been extracted from the sample by an alcoholic solution of alkali and coupling with paranitrophenyl diazonium chloride. The rate of destruction of the inhibitor under the conditions of the reaction was determined by special experiments.

The kinetic curves for the accumulation of hydroperoxides for different concentrations of  $\alpha$ -naphthol are given in Fig. 1. The phenomenon of a critical concentration of the inhibitor is perfectly plain by these data. Within the  $\alpha$ -naphthol concentration range from  $8.2 \cdot 10^{-7}$  to  $3.3 \cdot 10^{-7}$  mole/ml, practically complete inhibition of the oxidation of n-decane is observed. The kinetic curves for the change of hydroperoxide concentration in this region give indication only of the decomposition of the hydroperoxides.

However, in passing from  $3.3 \cdot 10^{-7}$  to  $3.1 \cdot 10^{-7}$  mole/ml of  $\alpha$ -naphthol, that is, for a very small reduction in the inhibitor concentration, an abrupt change in the character of the process occurs. The inhibited oxidation is replaced by a rapid reaction, which takes place according to an autocatalytic law similar to the process which occurs in the absence of inhibitor.

The data which have been obtained confirm the theoretical considerations set out above concerning the existence of critical phenomena under the influence of inhibitors, in the case of slow chain branching processes (reaction with degenerative branching).

#### LITERATURE CITED

1. N. N. Semenov, Chain Reactions (Leningrad, 1934) [in Russian].
2. P. S. Shaitarovich, Zhur. Fiz. Khim. 10, 700 (1937).
3. P. Ya. Sadovnikov, Zhur. Fiz. Khim. 9, 575 (1937).
4. R. Spence, J. Chem. Soc. (1932) p. 686.
5. R. G. W. Norrish and J. D. Reagh, Proc. Roy. Soc. A-176, 429 (1940).
6. L. G. Chuchukina, D. Z. Knorre, and N. M. Émanuéli', Zhur. Fiz. Khim. 33, 877 (1959).
7. N. N. Semenov, Some Problems of Chemical Kinetics and Reactivity [in Russian] (Izd. AN SSSR, 1958) p. 632.
8. S. Palkin and H. Wales, J. Am. Chem. Soc. 46, 1488 (1924).



## TWO TYPES OF PLASTICIZING OF RIGID-CHAIN POLYMERS

Academician V. A. Kargin, P. V. Kozlov, R. M. Asimova,  
and L. I. Anan'eva

M. V. Lomonosov Moscow State University

Translated from *Doklady Akademii Nauk SSSR*, Vol. 135, No. 2, pp. 357-360,  
November, 1960

Original article submitted August 12, 1960

Plasticizing of polymers is usually regarded as a technological method of improving the elastic and plastic properties of a material, i.e., decreasing its brittleness as a result of the introduction of specially chosen low-molecular substances, namely, plasticizers. This lowers the transition points of the polymer from one physical state to another or broadens the temperature range in which it is in a highly elastic state [1]. In the first case, there is weakening of the intermolecular bonds as a result of blocking by plasticizer molecules of the active groups of the polymeric chains responsible for these bonds and in the second case there is blocking of the active groups of the polymer chain units responsible for the rigidity of the chains as a whole. This plasticizing therefore increases the flexibility of the polymeric macromolecules without changing the transition point from the highly elastic to the ductile state.

The two plasticizing mechanisms presented follow from contemporary ideas on the model of a polymer macromolecule and its behavior during deformation [2]. It is not difficult to see that these explanations of the plasticizing action of plasticizers are based on the molecular interaction of the components of the system: polymer macromolecules and plasticizer molecules. The molecular mechanism of this action is described by the law of molar [3] or, in the general form, of volume [4] proportions. This interpretation of the phenomenon of plasticizing is correct for all cases where there is unlimited compatibility of the plasticizer and polymer, i.e., when the plasticizer is soluble in the polymer. However, for rigid-chain polymers in particular there are many cases of low compatibility or even complete incompatibility of plasticizer and polymer. At the same time, in such cases the introduction of low-molecular substances into the polymer produces a decrease in brittleness of the polymeric material, which appears to the greatest extent at low temperatures and under impact.

One of us [1] put forward the hypothesis that the mechanism of this third form of plasticizing is caused by loosening of the molecular chains of the polymer as a result of the introduction of low-molecular substances with the improvement in the mechanical properties of the material in this plasticizing caused by the appearance of the elasticity of the macromolecules. However, these ideas on the mechanism of the action of plasticizers which are partly miscible or completely immiscible with the polymer, which are close to the truth, are also based on the behavior of the molecular chains of the polymer and plasticizer molecules. At the same time, these ideas make no allowance for the structure of the polymeric material, which apparently plays an important part in plasticizing, especially in cases of limited miscibility of plasticizers with the given polymer.

It seemed interesting to examine the mechanism of the plasticizing action of plasticizers in the light of contemporary ideas on the structure of amorphous polymers on the example of the most rigid-chain natural high-molecular substance, namely cellulose. For this purpose we used an industrial sample of sulfite cellulose with a mean molecular weight of about 200,000. The cellulose was first reduced to a powdered state by solution in triethylphenylammonium oxide with subsequent precipitation with 2% acetic acid solution. The precipitate

obtained was washed carefully with water, then acetone, and finally ethanol and dried to constant weight in a drying cupboard at 80°. The plasticizers we chose were low-molecular compounds of limited miscibility with cellulose, with one of them (guanidine thiocyanate) mixing with cellulose somewhat better than the other (urea).

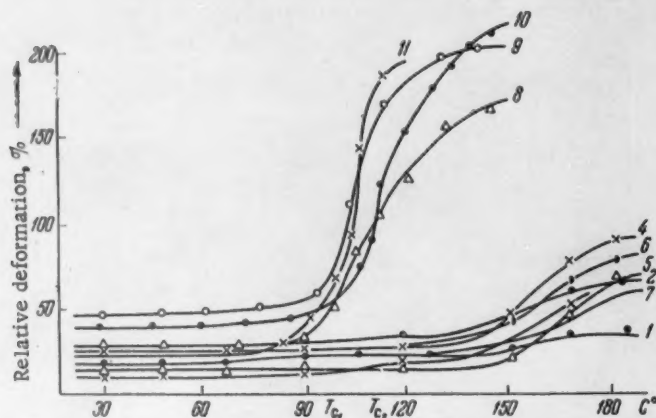


Fig. 1. Thermomechanical curves of cellulose samples plasticized with guanidine thiocyanate. Amount of plasticizer to mixture weight: 1) 8%; 2) 10%; 3) 12%; 4) 15%; 5) 17%; 6) 18%; 7) 20%; 8) 30%; 9) 40%; 10) 50%; 11) 60%.

The plasticizers were introduced into the cellulose as ethanol solutions; cellulose impregnated with alcoholic plasticizer solutions of given concentrations was kept at room temperature for 2-3 days for better distribution of the plasticizer in the cellulose. The samples were then dried at 60° to an air-dried state and tablets pressed from them at 130-140° and 75 atm. The pressed tablets were kept at the given temperature and pressure for 30 minutes and then cooled. Thermomechanical curves were obtained on dynamometric balances with a variable load [5]. The temperature was raised at 1° C per minute. The load on samples with large amounts of plasticizer (20% and above) was increased to 200 g/mm<sup>2</sup> and with small amounts of plasticizer (up to 20%) to 300 g/mm<sup>2</sup>. Thermomechanical curves of cellulose plasticized with various amounts of guanidine thiocyanate (8-60% by weight) are given in Fig. 1. The presence of polar groups in guanidine thiocyanate makes possible some reaction with cellulose, leading to limited compatibility. The presence of a plasticizing effect is indicated by a certain reduction in the vitrification point ( $T_v$ ) of the cellulose. However, this reduction in  $T_v$  is comparatively small and is not characterized by the direct dependence typical of plasticizers of unlimited miscibility with the polymer. Simple calculation showed that the plasticizing effect of this plasticizer does not correspond to the rules of molar or volume proportions.

An analogous picture was observed in the plasticizing of cellulose with urea, whose reaction with cellulose is even weaker and as a result of this, the reduction in  $T_v$  of cellulose plasticized with urea was even less appreciable than with guanidine thiocyanate. This is illustrated by Fig. 2, which shows the change in  $T_v$  of cellulose plasticized with various amounts of guanidine thiocyanate and urea compared with the change in  $T_v$  of cellulose plasticized with various amounts of triethylphenylammonium oxide, which we studied previously [6]. As in [6], Fig. 2 gives curves of the change in  $T_v$  of plasticized cellulose in relation to the amount of plasticizer for the beginning of the bend on the thermomechanical curves  $T_{v1}$  (curves 1, 3, and 5) and for the inflection point on these curves  $T_{v2}$  (curves 2, 4, and 6). As was shown in [6], the first series of curves characterize the production in the plasticized cellulose of the minimum mobility of the chains, determining the first signs of highly elastic deformation. The second series gives the vitrification temperatures of plasticized cellulose at which rubber-like elasticity of the material arose at a given rate of application of the deforming stresses.

Thus, the data obtained in the present investigation and in the previous work [6] show that we are dealing with two very different types of plasticizing of cellulose. In one case, the introduction of plasticizer leads to regular reduction of  $T_v$  of cellulose and as calculations show, the molecular mechanism of plasticizing completely reflects the accuracy of the rules of molar and volume proportions. This plasticizing occurs in all cases of unlimited miscibility of plasticizer and polymer, i.e., in our case, in the plasticizing of cellulose with triethylphenylammonium oxide. In the other case, the introduction of plasticizer leads away from the rules presented above and the plasticizing effect cannot be explained by the interaction of plasticizer molecules with polymer macromolecules. This plasticizing occurs when the plasticizer is not infinitely miscible with the polymer, i.e., in our case, in the plasticizing of cellulose with guanidine thiocyanate and urea.

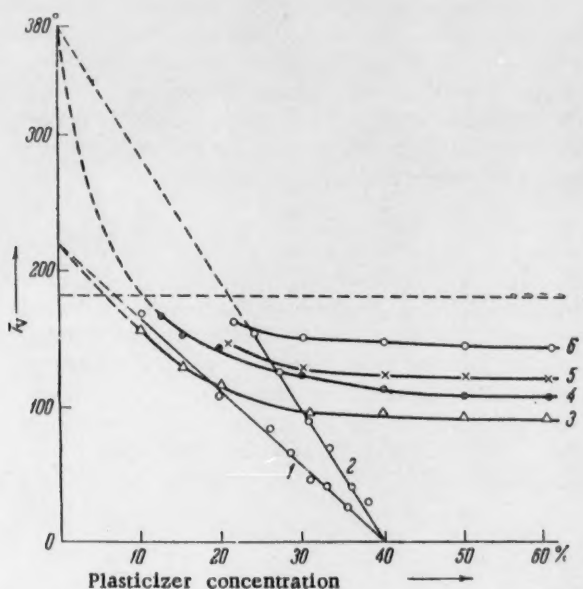


Fig. 2. Relation of the vitrification points  $T_v$  of cellulose to the amount of plasticizer introduced, determined from thermomechanical curves from the beginning of the bend (odd numbers) and from the point of inflection (even numbers). 1,2 Triethylphenylammonium oxide; 3,4) guanidine thiocyanate; 5,6) urea.

It seems to us that the plasticizing action of this type of plasticizer is best interpreted on the basis of modern ideas on the structure of amorphous polymers [7]. In actual fact, if we assume that amorphous polymers in the condensed phase consist of highly ordered, secondary structural formations — micelles of highly oriented chains — then we are correct in considering two possible types of plasticizing. One of these types, namely, intramolecular plasticizing occurs if the reaction of plasticizer molecules with the active groups of the polymer chains is more than the intermolecular reaction in the polymer itself. The plasticizing action of such plasticizers as are infinitely miscible with the polymer leads to destruction of any secondary structural formations in the polymer and we are essentially dealing with a solid solution of polymer and plasticizer. The picture changes sharply if the reaction of plasticizer molecules with the active groups of the polymer chains is substantially weaker than the intermolecular reaction in the polymer itself. Then the plasticizer may react only with molecules on the surface of secondary structural formations in the polymer and this type of plasticizing should be called intermolecular plasticizing.

The mechanical properties of polymeric materials obtained as a result of intra- and intermolecular plasticizing apparently should also differ substantially. With intramolecular plasticizing we are correct to expect that with the application of deforming stresses there will be a fall in the mechanical strength of the

material and a substantial increase in elongation, based on the appearance of the highly elastic properties of the polymer for which the vitrification point will be lowered in proportion to the plasticizer introduced. Consequently, with this plasticizing there will appear in the material all the relaxation processes which are given by changes in the conformation of the molecular chains. An increase in temperature also leads to viscous flow as with intramolecular plasticizing there is a substantial fall in the temperature at which the polymer changes from the highly elastic to the ductile state. For rigid-chain polymers such as cellulose, this is the only way of achieving its temperature transitions as for the pure polymer these points lie above the chemical decomposition point of the product [6].

With intermolecular plasticizing, we will probably have a different effect on the mechanical properties of the polymer. In the ideal case of this plasticizing, the vitrification point of the polymer should not be lowered at all in the presence of plasticizer. Consequently, the mechanical strength, which is caused by micelles of highly oriented polymer chains, is then high. At the same time, the elasticity of the plasticized polymer is determined by the flexibility of the micelles, which have very asymmetric forms, i.e., is determined by the elasticity of the form of these secondary structural formations. This plasticizing is apparently more suitable for the production of frost-resistant polymeric materials with a high impact strength, i.e., for those conditions of polymer use where the material is required to have the highly flexible properties caused by the elasticity of the form of the structural elements of the material.

#### LITERATURE CITED

1. P. V. Kozlov and E. F. Russkova, Coll.: High-Molecular Compounds [in Russian] (1952) No. 12, p. 44.
2. V. A. Kargin and G. L. Slonimskii, Doklady Akad. Nauk SSSR 62, 239 (1948).
3. S. N. Zhurkov and R. I. Lerman, Doklady Akad. Nauk SSSR 47, 109 (1945).
4. V. A. Kargin and Yu. M. Malinskii, Doklady Akad. Nauk SSSR 73, 967 (1950).
5. V. A. Kargin and T. I. Sogolova, Zhur. Fiz. Khim. 23, 530 (1949).
6. V. A. Kargin, P. V. Kozlov, and Van Naichan, Doklady Akad. Nauk SSSR 130, 356 (1960).\*
7. V. A. Kargin, A. I. Kitaigorodskii, and G. L. Slonimskii, Kolloid. Zhur. 19, 131 (1957).\*

\* Original Russian pagination. See C. B. translation.

# KINETIC EQUATIONS FOR NONCHAIN MONOMOLECULAR RADIATION-CHEMICAL REACTIONS

Yu. A. Kolbanovskii and L. S. Polak

Institute of Petrochemical Synthesis of the Academy of Sciences of the USSR

(Presented by Academician A. V. Topchlev, June 3, 1960)

Translated from Doklady Akademii Nauk SSSR, Vol. 135, No. 2, pp. 361-364,  
November, 1960

Original article submitted June 3, 1960

During recent years numerous papers have been published describing experimental work on the investigation of radiation-chemical reactions which take place according to a chain mechanism. In individual papers devoted to concrete reactions, the derivation of the kinetic equations is given. However, for a series of cases of great practical importance, such, for example, as the inhibited radiolysis of hydrocarbons, or radiolysis with the use of large aggregate doses, both the total and the partial kinetic equations are lacking.

The present communication is devoted to the consideration of nonchain, monomolecular radiation-chemical processes involving the participation of some substance X. It is assumed that the substance X may exist in two forms in the excited state,  $X^*(1)$  and  $X^*(2)$  and may decompose in some arbitrary number  $m$  ways.\* All the equations relate to the rate of decomposition of the initial substance.

1. Region of low integral doses. 'Low dose' is here used to denote doses sufficiently small to permit us to neglect the decomposition of the starting substance and the inhibiting effect of the final products.

In this region the following processes take place (considering initially only one type of excitation):

- 1)  $X \xrightarrow{h\nu} X^*$ : excitation by means of irradiation.
- 2)  $X^* \rightarrow X (+h\nu)$ : dissipation and scattering of radiation.
- 3)  $X^* \rightarrow$  products ( $m$  ways of decomposition or isomerization).

Accordingly, we have:

$$W_1 = K_1 I, \quad (1)$$

where  $I$  is the differential power of the dose in  $\text{ev/cm}^2 \text{ sec}$ ;

$$W_2 = K_2 [X^*]; \quad (2)$$

$$W_3 = \sum_{i=1}^m K_i [X^*]. \quad (3)$$

For stationary conditions:

$$W_1 = W_2 + W_3. \quad (4)$$

\* If we follow the assumptions made in [1], then  $X^*(1)$  and  $X^*(2)$  may be considered as triplet and singlet excitation types.

When Eqs. (1) to (3) are inserted in (4) we obtain

$$[X^*] = \frac{K_1 I}{\sum_{i=2}^m K_i} \quad (5)$$

Eliminating  $[X^*]$  from (3) and (5), we obtain:

$$W_3 = -d[X]/dt = K_1 I \sum_{i=2}^m K_i / \sum_{i=2}^m K_i \quad (6)$$

Since the development of each of the forms of excitation proceeds independently, an equation analogous to (6) may also be written down for the decomposition of the substance X by means of other types of excitation. Hence, in the general case, the desired rate of decomposition of the substance X may be represented as the sum of two equations of the form (6).

Combining the constants, we obtain:

$$W_3 = I \left( \frac{K_{(1)1} \bar{K}_{(1)3}}{K_{(1)2} + \bar{K}_{(1)3}} + \frac{K_{(2)1} \bar{K}_{(2)3}}{K_{(2)2} + \bar{K}_{(2)3}} \right) \quad (7)$$

Since  $W_3 = G(-X)I$ , where  $G(-X)$  is the radiation-chemical decomposition of the substance X in molecules per 1 ev of absorbed energy, then:

$$G = \frac{K_{(1)1}}{K_{(1)2} / \bar{K}_{(1)3} + 1} + \frac{K_{(2)1}}{K_{(2)2} / \bar{K}_{(2)3} + 1} \quad (8)$$

It follows from (8) that the value of the radiation-chemical yield depends on two parameters:  $K_1$ , which determines the yield of excited molecules per unit dose intensity, and  $K_2/\bar{K}_3$ , which is the ratio of the rate constant for dissipation and scattering to the sum of the rate constants of the elementary decomposition process. It is evident that, for molecules with a system of coordinated bonds, and especially luminophores, the ratio  $K_2/\bar{K}_3$  will be relatively larger, and the value of G correspondingly smaller, than for molecules which do not possess such a bond system.

We note that if one or several of the means of decomposition are reversible, then, in the direct portions of (6) and (7), there ought also to be inserted terms, with a negative sign, giving relationships corresponding to the sum of the rates (rate constants) of the reverse reactions.

II. Kinetics of radiation-chemical reactions with low concentrations of inhibitor which exercises a protective influence of the "sponge" type.\* The term "low concentration" is here to be understood as meaning such an inhibitor concentration as will permit us to neglect the change in concentration of the initial substance X, so that the absorption of energy may be completely attributed to the basic substance.

In such a system, in addition to the processes considered above, it is also necessary to take into account the process of transfer of excitation energy, which may be written in the form:

4)  $X^* + B \rightarrow X + B^*$ , where B is the inhibitor molecule. The rate of this process is:

$$W_4 = K_4 [X^*] [B]^{n/3} \quad (9)$$

\* The "sponge" type of inhibition — a literal rendering of the Russian — denotes inhibition by absorption of excitation energy prior to the reaction of the activated particle, as distinct from inhibition by destruction of a reactive species — Publisher's note.

For reactions in the gas-phase,  $n = 3$  (in general  $\underline{n}$  is a whole number not greater than 3), and so the form of Eq. (9) is the normal form for a bimolecular reaction. It is known, however, that the mechanism of excitation energy transfer in condensed systems is not connected with collision processes (see, for example [2]). The consideration of possible values for  $\underline{n}$  in condensed systems is a special problem, lying outside the framework of our present communication.

III. Radiation-chemical reactions with intermediate integral dosage, with accumulation among the reaction products of excitation energy acceptors exercising a protective function of the "sponge" type. Under this heading we contemplate the range of integral dosages within which it is impossible to neglect the retardation of the reaction by means of the end products, though we may still neglect the destruction of the initial substance X.

In our treatment, we assume that the acceptors of excitation energy are formed by the decomposition of one of the forms of excited molecule, for example  $X_{(2)}^*$ , and that these then inhibit the decomposition by the other route, using the excited form  $X_{(1)}^*$ . Then

$$W_{(2)3} = \bar{K}_{(2)3} [X_{(2)}^*] = \frac{d[A]}{dt}, \quad (10)$$

where A is the excitation energy acceptor.

It is also necessary to take into account the process:

5)  $X_{(1)}^* + A \rightarrow A^* + X$ , the rate of which is

$$W_5 = K_5 [X_{(1)}^*] [A]^{n/3}, \quad (11)$$

where  $\underline{n}$  has the values indicated above. Taking this process 5 into account:

$$W_3 = W_{(2)3} + (W_{(1)3} - W_5). \quad (12)$$

The condition for stationary concentration of  $[X_{(1)}^*]$  will be

$$W_{(1)1} = W_{(1)2} + W_{(1)3} + W_5, \quad (13)$$

so that,

$$[X_{(1)}^*] = \frac{K_{(1)1} I}{K_{(1)2} + \bar{K}_{(1)3} + K_5 [A]^{n/3}}. \quad (14)$$

If we now insert in (13) the appropriate values and equate the coefficients, we obtain,

$$W_3 = I \left( \bar{K}_{(2)3} + \frac{1}{\bar{K}_{(1)1} + \bar{K}_A [A]^{n/3}} \right). \quad (15)$$

In such a case, as Eq. (15) shows, the reaction rate diminishes with time (that is, with dosage) since [A] increases with increase in the integral dosage.

IV. The general equation. In the general case, it is necessary to take into account not only the accumulation of excitation energy acceptors among the reaction products but also the destruction of the initial substance. Equation (15) should then be rewritten in the form

$$W_3 = I [X] \left( \bar{K}_{(2)3} + \frac{1}{\bar{K}_{(1)1} + \bar{K}_A [A]^{n/3}} \right). \quad (16)$$

It follows from this general Eq. (16) that the rate of reaction in the region of large integral dosages is diminished very rapidly, since simultaneously there occur the reduction of [X] and increase in the concentration of excitation energy acceptors.

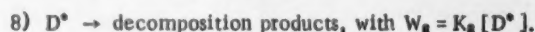
V. The kinetics of a radiation chemical reaction inhibited by low concentrations of added substances which exercise protection by a "sacrificial" mechanism.\* In considering such a system we shall take account of a process similar to 5, above:



If the probability of the decomposition of  $D^*$  is taken as equal to unity, then the final equation will have the same form as (15):

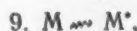
$$W_3 = I \left( \bar{K}_{(2)} + \frac{1}{\bar{K}_{(1)} + \bar{K}_D [D]^{n/3}} \right) \quad (17)$$

with this difference, however, that [D] diminishes with time. In the more general case, when the probability of the decomposition of  $D^*$  is not equal to unity, we have:

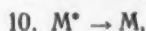


The destruction of D then depends, not only on  $W_8$ , but also on the ratio  $\frac{W_8}{W_7} = \frac{K_8}{K_7}$ . The ratio of these constants can be expressed as a new constant  $K_D$ , and the form of Eq. (17) remains unchanged.

VI. The kinetics of a monomolecular radiation chemical reaction of an added substance X in a medium in which the energy transfer takes place from the medium M to the added substance.\*\* In the case in which we may not neglect the direct influence of the irradiation on the substance X itself, we must employ processes 1-3 and also the processes:



$$W_9 = K_9 I,$$



$$W_{10} = K_{10} [M^*],$$



$$W_{11} = K_{11} [M^*] [X]^{n/3}.$$

In the case under consideration two conditions may be written down to define stationary states with respect to  $M^*$  and  $X^*$ , respectively:

$$W_9 = W_{10} + W_{11}, \quad (18)$$

$$W_1 + W_{11} = W_2 + W_3. \quad (19)$$

From (18) and (19), we may determine the concentrations of the excited species as:

$$[M^*] = \frac{K_9 I}{K_{10} + K_{11} [X]^{n/3}}; \quad (20)$$

$$[X^*] = \frac{K_{11} [X]}{K_2 + K_3} + \frac{K_{11}}{K_2 + K_3} [M^*] [X]^{n/3}. \quad (21)$$

\* That is, a mechanism in which the inhibitor absorbs the excitation energy, and so undergoes destruction instead of the particle whose energy it has absorbed — Publisher's note.

\*\* The consideration is carried out on the assumption that the decomposition of the molecules of the medium is negligibly small. In the general case  $K_{10}$  will be the aggregate rate constant of the two processes.

If we now eliminate  $[M^*]$  between (20) and (21), and multiply both parts of (21) by  $K_9$ , we obtain the desired equation:

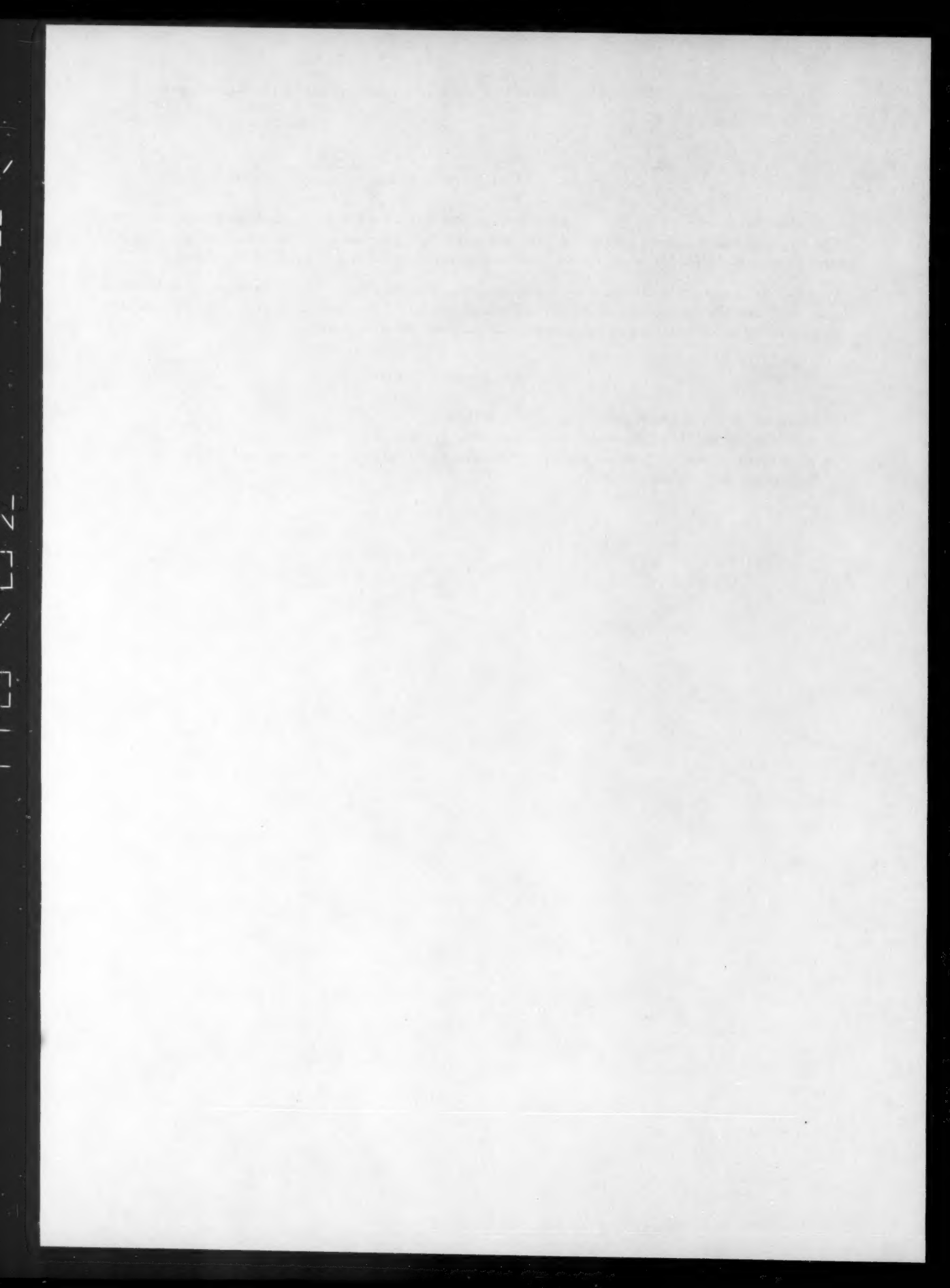
$$W_3 = K_3 [X^*] = \frac{K_1 K_3 I [X]}{K_2 + K_3} + \frac{K_3 K_9 K_{11} I [X]^{n/3}}{(K_2 + K_3) (K_{10} + K_{11} [X]^{n/3})} \quad (22)$$

When  $K_2 = 0$  and  $n = 3$ , Eq. (22) becomes identical with that derived by V. A. Krongauz for the radiolysis of benzoyl peroxide in benzene solution [3]. The authors of [3], unfortunately, did not discuss the situation in which  $K_2$  may be regarded as  $\ll K_9$ , nor the concentration region in which  $n = 3$  (in the liquid phase).

We note in conclusion that the relationships produced above encompass all the basic classes of monomolecular, nonchain radiation chemical reactions; and that this permits of the construction of experiments specially directed toward the investigation of the parameters of radiation chemical processes.

#### LITERATURE CITED

1. M. Burton, et al., J. Chem. Phys. **26**, 1337 (1957).
2. S. C. Ganguly and N. K. Chaudhury, Rev. Mod. Phys. **31**, 990 (1959).
3. V. A. Krongauz and Kh. S. Bagdasar'yan, The Influence of Irradiation on Inorganic and Organic Systems [in Russian] (Izd. AN SSSR, 1958).



# THE ASSOCIATION OF COMPLEX COPPER IONS IN SOLUTION

## AN INVESTIGATION BY THE PARAMAGNETIC RESONANCE METHOD

A. I. Ribkind

The Physicotechnical Institute, Kazan Branch of the Academy of Sciences  
of the USSR

(Presented by Academician A. E. Arbuzov, June 1, 1960)

Translated from *Doklady Akademii Nauk SSSR*, Vol. 135, No. 2, pp. 365-368,  
November, 1960

Original article submitted May 26, 1960

During an investigation of the superfine structure of the electronic paramagnetic resonance spectra obtained from dilute solutions of complex copper ions, we have encountered anomalous behavior which could not be explained on the basis of the theory of spectra and, as further investigation showed, is to be attributed to the association of the complex particles.

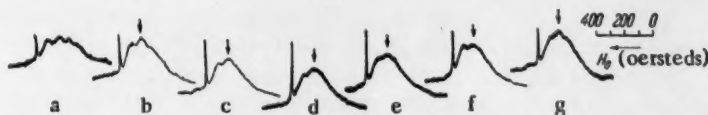


Fig. 1.

Figures 1 to 3 give the oscillogram electronic paramagnetic resonance curves obtained at a frequency of oscillation of the magnetic field of  $\nu_0 = 9395$  Mh and at room temperature, for solutions of some amine complexes of bivalent copper. The narrow lines to the left of the curves are signals from free radicals of  $\alpha, \alpha$ -diphenyl- $\beta$ -picrylhydrazyl, which was used for the calibration of the constant magnetic field  $H_0$ . Figure 1 refers to 0.15 M solutions of monoethanolamine complexes. It had been shown earlier, using the method of protonic magnetic resonance [1], that monoethanolamine in solution forms with cupric ions simple internally complexed compounds, of which those with a coordination number three possess the greatest stability. These are assumed to possess the formula  $\text{CuEtm}_3^-$ , where the symbol  $\text{Etm}^-$  denotes the monoethanolamine ion,  $\text{NH}_2\text{CH}_2\text{CH}_2\text{O}^-$ . In the preparation of the solutions we have used a sufficiently large excess of monoethanolamine (see below) to ensure the formation of complexes of this formula, and we shall therefore conditionally denote them by the formula  $\text{CuEtm}_3^-$ . The oscillograms given in Fig. 1a-f show the change in the form of the spectra which takes place when the solvent is varied in the sequence: methanol (Fig. 1a); ethanol (Fig. 1b); propanol (Fig. 1c); isopropanol (Fig. 1d); butanol (Fig. 1e); and benzyl alcohol (Fig. 1f).

The alcohols used as solvents in this work have approximately the same dipole moment,  $\sim 1.7$  D, but their dielectric constants diminish from  $\epsilon \approx 33$  for methanol to  $\epsilon \approx 13$  for benzyl alcohol. Under the strong field conditions which are obtained at the chosen value of the frequency  $\nu_0$ , the spectra should consist of four components of superfine structure, corresponding to the value of the nuclear spin of  $\text{Cu}^{63}/\text{Cu}^{65}$  of  $3/2$ . For the solution of  $\text{CuEtm}_3^-$  in methyl alcohol (Fig. 1a), all the components are resolvable. The spectrum displays appreciable asymmetry: the extreme right hand superfine component, corresponding to a value of  $I_z = +3/2$  (where  $I_z$  is the nuclear magnetic quantum number), is wider, and therefore less intense, than the remainder.

The asymmetry of the superfine structure spectra has been observed repeatedly for solutions of magnetically anisotropic complexes [2, 3], and arises when the characteristic frequency of the Brownian rotation of the complexes,  $\nu_c$  is less than the Larmour frequency  $\nu_0$ . The asymmetry of the spectra is enhanced by continued reduction of  $\nu_c$  and, conversely, disappears if  $\nu_c$  is greater than  $\nu_0$ . These conclusions, drawn in [4], will be employed in the subsequent discussion.

When we turn our attention from the solution in methyl alcohol to that in ethyl alcohol (dielectric constant about 24),\* the picture changes abruptly (Fig. 1b). There is superimposed on the superfine structure spectrum an exchange curve with  $g_{\text{eff}} = \sim 2.09$ ,\*\* which corresponds to the position of the superfine structure component  $I_z = -1/2$  (second from the left). In addition to this, the superfine structure itself is extremely asymmetrical: the breadth of the superfine component increases rapidly with increase in  $I_z$ . Because of the latter, the superfine component  $I_z = +3/2$  (which should be at the extreme right) is greatly broadened and cannot be detected. The intensity of the exchange peak, in comparison with that of the superfine structure rises for the solution in propyl alcohol (dielectric constant  $\approx 20$ ), is approximately at the same level for the solution in isopropyl alcohol (dielectric constant  $\approx 18$ ), and diminishes slightly in moving to solutions in butyl alcohol (dielectric constant  $\approx 17$ ) and benzyl alcohol ( $\approx 13$ ). See Figs. 1 c-f, respectively.

The presence of the exchange peaks points quite unequivocally to the formation of associated particles containing at least two complex copper ions, while the time during which the ions remain in the associated state must be greater than the reciprocal of the Larmour frequency. In an 0.15 M solution of  $\text{CuEtm}_3^-$  complexes in methyl alcohol (Fig. 1a) no exchange occurs, but if the dielectric constant of the solution is reduced, as by replacing half of the methanol by ether (dielectric constant of ether  $\approx 4.3$ ), association arises and an exchange peak appears (Fig. 1g).\*\*\*

The fact that the exchange peak arises as a result of reduction in the dielectric constant of the solutions is evidence of the important role played by Coulomb (electrostatic) effects in the formation of the complex particles.

The association of  $\text{CuEtm}_3^-$  ions when we move from the solution in isopropyl alcohol (Fig. 1d) to that in butyl alcohol (Fig. 1e) and benzyl alcohol (Fig. 1f) is somewhat weakened, although, judging from the value of the dielectric constant in these alcohols, we should have expected it to continue to increase. It is necessary, however, to take into account the fact that the diminution of the dielectric constant of the solutions (Fig. 1a-f) is accompanied by an increase in their volume viscosity of the same order.\*\*\*\* The latter factor, which diminishes the probability of ionic collisions, seems to be the most likely cause of retardation in the formation of associated particles.

The association of singly charged complex ions under the influence of Coulomb forces may be regarded as taking place through the mutual polarization of the complexes when they come within close range of each other. A complete explanation of the phenomenon is impossible, however, with the present insufficient experimental data.

We have also observed the association phenomenon for a range of other complex copper ions. Figure 2a gives the electronic paramagnetic resonance oscillogram for an 0.15 M aqueous solution of the ammoniacal complexes  $\text{Cu}(\text{NH}_3)_4^{2+}$ . The form of the curve is that corresponding to a nonresolved superfine structure. For a relatively small increase in the viscosity of the solution, by substituting about 25% of the aqueous solvent by glycerol (by volume), the time of relaxation is extended, and this leads to a contraction of the superfine component, and the appearance of a clearly discernible superfine structure (Fig. 2b) [4]. However, the effect is quite different if the complex ions  $\text{Cu}(\text{NH}_3)_4^{2+}$  are dissolved in a solvent with a sufficiently low dielectric constant.

\* All the dielectric constants given refer to the solvent.

\*\* The position of the exchange peak here, and on the other oscillograms of the spectra, where they occur, is denoted by a vertical arrow.

\*\*\* During the preparation of this solution, the content of the complexing agent, monoethanolamine, was somewhat increased also. See the method of preparing the solutions, below.

\*\*\*\* The range of viscosity increase ( $\eta$ ) can be gathered from the following values (in cp): for methanol:  $\eta_{20^\circ} = 0.55$ ; for benzyl alcohol,  $\eta_{15^\circ} = 7.76$ .

We have prepared 0.15 M solutions of the complex ions  $\text{Cu}(\text{NH}_3)_4^{2+}$  in  $\sim 90\%$  by volume aqueous methanol,  $\sim 84\%$  by volume aqueous ethanol,  $\sim 65\%$  by volume aqueous propanol, and  $\sim 60\%$  by volume aqueous dioxane (for the last of which the dielectric constant  $\approx 2.2$ ). Measurements carried out on all these solutions give identical exchange curves with  $g_{\text{eff}} \sim 2.10$ , and with width  $\Delta H \sim 219$  oe; one of these curves is shown in Fig. 2c. Since the superfine structure obtained from the monomeric ions is completely absent, we may conclude that almost all the complex particles are combined into dimeric or more complicated structures. Similar results have also been obtained for solutions of ethylenediamine complexes of  $\text{CuEn}_2^{2+}$  (where En denotes the ethylenediamine molecule,  $\text{NH}_2\text{CH}_2\text{CH}_2\text{NH}_2$ ). Using 0.15 M solutions of the  $\text{CuEn}_2^{2+}$  complex in water (Fig. 2d), and also in methanol, no association was found, but if ethanol was used as solvent, an exchange peak was found on the basis of the superfine structure (Fig. 2e).

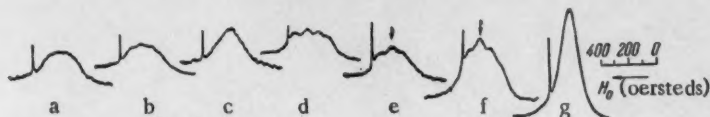


Fig. 2.

It is evident that, the more concentrated the solution, the larger should be the probability of association. This relationship can be applied very successfully to aqueous solutions of  $\text{CuEn}_2^{2+}$  complex ions, in which high concentrations can be attained. In moving from 0.15 M to 0.3 M concentrations of the complexes  $\text{CuEn}_2^{2+}$ ,

an exchange peak is superimposed on the superfine structure oscillogram (Fig. 2f). The height of the exchange peak increases with further increase in the concentration of the aqueous solutions of  $\text{CuEn}_2^{2+}$ , until in a 1.2 M solution (Fig. 2g), only the intensive exchange curve can be observed ( $g_{\text{eff}} \sim 2.07$ ;  $\Delta H \sim 150$  oe), without any indication of superfine structure.

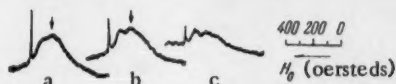


Fig. 3.

Association of the  $\text{CuEtm}_3^-$  complexes in alcoholic solutions (Fig. 1) is hindered by the addition of small quantities of water

(dielectric constant  $\approx 80$ ), which cause an increase in the aggregate dielectric constant. This is shown in Fig. 3a-c. In an 0.15 M solution of  $\text{CuEtm}_3^-$  complexes in butanol, containing  $\sim 5\%$  by volume of water (Fig. 3b), the intensity of the exchange peak (in comparison with that of the superfine structure) is appreciably less than in the same concentration of solution in absolute butanol (Fig. 3a).<sup>\*</sup> For even greater water concentration ( $\sim 10\%$  by volume), the exchange peak is completely extinguished, and the curve takes on the asymmetrical form shown in Fig. 3c. It is evident that the abruptly asymmetrical form of the curve in Fig. 3c must be considered as a direct precursor of the phenomenon of the exchange peak. And therefore, as we have remarked, the development of asymmetry in the spectra is a consequence of the reduction of the characteristic frequency of the Brownian rotation of the complexes,  $\nu_c$ , and it may be concluded that the observed association precedes the reduction in the frequency  $\nu_c$ . It appears that reduction of the dielectric constant of the solutions initially causes the formation of associated particles with a lifetime  $t_i$  which is less than the reciprocal of the Larmor frequency (that is,  $t_i < 1/\nu_0 \sim 10^{-10}$  sec.). These associates, which are constantly dissolving and reforming, would be expected to hinder the Brownian rotation of the complex ions. Further reduction in the dielectric constant causes a strengthening of the bonding of the associated particles, and when the lifetime of the complex ions in the associated state,  $t_i$ , begins to exceed the value of  $1/\nu_0 \sim 10^{-10}$  sec. an effective exchange interaction comes into operation, and an exchange peak arises on the oscillograms of the superfine structure. The value of  $t_i = 1/\nu_0 \sim 10^{-10}$  sec. is the lower limit of the lifetime of the associated particles which are revealed by the existence of the exchange peaks at the frequency of the oscillating magnetic field (of the order of  $10^4$  Mh).

<sup>\*</sup> This curve is given in Fig. 1e. It is here repeated for convenience in comparing it with Figs. 3b and 3c.

### Method of Preparation of Solutions

All the solutions were prepared by dissolving weighed portions of cupric chloride or nitrate and predetermined volumes of the necessary reagents (monoethanolamine, concentrated aqueous ammonia, and ethylenediamine) in the appropriate solvents. The salt usually used was the chloride,  $\text{CuCl}_2 \cdot 2\text{H}_2\text{O}$ . The only exceptions were aqueous solutions of  $\text{CuEn}_2^{2+}$ , for which the starting salt was the nitrate,  $\text{Cu}(\text{NO}_3)_2 \cdot 3\text{H}_2\text{O}$ . Calculating on the basis of 0.15 M concentration of the complexes, the following quantities of the reagents were taken (in percentages of the volume of all the solutions): for aqueous solutions of  $\text{CuEn}_2^{2+}$ , 5%; for methanol-ether solution of  $\text{CuEtm}_2^+$ , 15%; for all the remaining cases, 10%.

### LITERATURE CITED

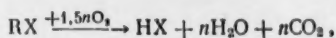
1. A. I. Ribkind, Zhur. Neorg. Khim. 2, 1263 (1957).
2. B. R. McGarvey, J. Phys. Chem. 60, 71 (1956).
3. T. Vännngard and S. Akerström, Nature 184, 183 (1959).

## MODIFICATION OF A SILVER CATALYST BY ORGANIC HALOGEN COMPOUNDS

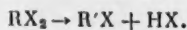
Yu. N. Stepanov, L. Ya. Margolis, and S. Z. Roginskii,  
Corresponding Member of the Academy of Sciences, USSR

Institute of Physical Chemistry, Academy of Sciences of the USSR  
Translated from Doklady Akademii Nauk SSSR, Vol. 135, No. 2, pp. 369-372,  
November, 1960  
Original article submitted July 22, 1960

Formerly, we have shown that nonmetal admixtures which when introduced into silver enhance the selectivity in the oxidation of ethylene to ethylene oxide are partially eliminated from the catalyst by their interaction with ethylene [1]. Therefore, modification of the catalyst by volatile organic halide admixtures, which are added to the gaseous reaction mixture is a more rational method of regulating the selectivity. In literature [2-5], there have been published data on the influence of organic halides upon the selectivity in the oxidation of ethylene to ethylene oxide, but the mechanism by which the admixtures act has not been investigated. The aim of this paper is to explain the behavior of these admixtures on the silver surface. Under the conditions of the catalytic process the organic halide admixtures may be oxidized:



where R is the radical  $C_nH_{2n+1}$ , X the halogen: Cl, Br, I or S etc. Dissociation of the molecule containing halogen might also occur:



The character of their absorption on silver may also play an important role.

The oxidation of the admixtures was investigated in the following way. Air which had been purified from carbon dioxide was saturated by the volatile organic additions to various concentrations and passed through the silver catalyst bed at temperatures between 150 and 350° in a flow system. The oxidation of the admixture yields carbon dioxide, which is sorbed by a  $Ba(OH)_2$  solution and then titrated. After each experiment the chlorine ion concentration in the silver was determined turbidimetrically or gravimetrically. If there is only oxidation of the organic halide, the amount of carbon dioxide will be equivalent to the chlorine content of the silver. Therefore, by drawing the balance of  $CO_2$  and chlorine in the silver the ratio in which the admixtures are oxidized and dissociated can be determined. In Table 1 are given data on the oxidation of a series of organic halogen compounds on silver. At a temperature 180-200° carbon tetrachloride and pentachloroethane are oxidized for more than 50%. Dichloroethane, chlorobenzene, etc. are oxidized much less. After these admixtures had been oxidized on the silver, the latter was investigated by x-rays (diffraction from a tablet with an area of 0.78 cm<sup>2</sup>). On the tablet surface a considerable concentration of silver chloride was found. After the surface layer had been removed to a depth of 0.2 mm, silver chloride was no longer detected in the sample. It should be remarked that in this method of modifying there is observed a drop in the AgCl concentration not only along the depth of the tablet but also along the length of the catalyst bed. So, an examination of the silver catalyst

on its chlorine ion content after it had been treated with dichloroethane ( $10^{-5}\%$ ) showed that besides a considerable increase in the selectivity of the oxidation of ethylene into ethylene oxide, there is found an unequal distribution of the halogen along the bed (see Table 2). The results obtained when analyzing layers of the silver catalyst bed are given in Table 2 and they show that in the first layer the chlorine ion concentration is considerably higher than in the succeeding ones.

TABLE 1

The Oxidation of Organic Admixtures on Silver at 180-200°

Admixture	Admixture conc. in air, volume, %	Temp. of catalysis, °C	CO <sub>2</sub> content of the gas, volume, %	Cl <sup>-</sup> conc. in silver weight, %	Degree of admixture oxidation	
					from CO <sub>2</sub>	from halogen
CCl <sub>4</sub>	$5,5 \cdot 10^{-2}$	200	0,34	0,2 — 0,7	~62,0	~68,0
CH <sub>2</sub> Cl <sub>2</sub>	$3,2 \cdot 10^{-2}$	180	traces	$3 \cdot 10^{-3}$ — $6 \cdot 10^{-3}$	—	~3,0
ClCH <sub>2</sub> — CH <sub>2</sub> Cl	$1,7 \cdot 10^{-2}$	180	traces	$3 \cdot 10^{-3}$ — $5 \cdot 10^{-3}$	—	~4,0
C <sub>2</sub> H <sub>5</sub> Cl <sub>2</sub>	$2,3 \cdot 10^{-2}$	200	0,0033	$1,3 \cdot 10^{-3}$	~7,0	~5,0
HOCH <sub>2</sub> CH <sub>2</sub> Cl	$3,3 \cdot 10^{-2}$	180	traces	$4 \cdot 10^{-3}$ — $1 \cdot 10^{-2}$	—	~9,0
HCCl <sub>3</sub> — CCl <sub>3</sub>	$1,8 \cdot 10^{-2}$	200	0,0109	$1,4 \cdot 10^{-1}$	~59,0	~52,0
Cl <sub>2</sub> CF — CFCI <sub>2</sub>	$4,0 \cdot 10^{-2}$	180	traces	$1 \cdot 10^{-3}$ — $3 \cdot 10^{-2}$	—	~4,0*
FCCl <sub>2</sub> CF <sub>2</sub> Cl	$3,3 \cdot 10^{-2}$	180	traces	$4 \cdot 10^{-3}$ — $2 \cdot 10^{-2}$	—	~3,0*
C <sub>6</sub> H <sub>5</sub> Cl	$3,3 \cdot 10^{-2}$	180	0,0224	$4 \cdot 10^{-3}$ — $1 \cdot 10^{-2}$	~11,0	~7,0
C <sub>6</sub> H <sub>5</sub> Br	$3,3 \cdot 10^{-2}$	180	0,0079	$7 \cdot 10^{-3}$ — $1 \cdot 10^{-2}$	~4,0	~4,0**

Note. The mean chlorine content of the silver was used in calculating the degree of oxidation from halogen.

\* The degree of admixture oxidation was calculated from the Cl-ion content; the F-ion was not considered.

\*\* Calculated from the Br-ion content.

TABLE 2

Distribution of the Modifying Admixture Along the Catalyst Bed

Reaction temperature, °C	Yield of C <sub>2</sub> H <sub>4</sub> O in %		Cl concentration in wt. %		
	on C <sub>2</sub> H <sub>4</sub> fed	on C <sub>2</sub> H <sub>4</sub> converted	layer I, 20 mm	layer II, 30 mm	layer III, 30 mm
220	33.0	45.5	} $8.6 \cdot 10^{-3}$	$6.5 \cdot 10^{-3}$	$4.1 \cdot 10^{-3}$
255	35.0	70.5			
265	37.0	68.5			

When oxygen is absent in the reacting mixture, the additions decompose on silver (see Table 3). At 250°C the highest degree of decomposition is found for pentachloroethane (approximately 42%) and the lowest for chlorobenzene (approximately 8%).

Oxidation curves of 1,2-dichloroethane and chlorobenzene are shown in Fig. 1. When the initial concentration of the organic admixtures is varied by about two times, the degree of oxidation does not change and the rate of this process practically does not depend upon the original admixture concentration.

It should be remarked that the oxidation rate is found to decrease sharply in the course of time. So, the oxidation rate of 1,2-dichloroethane over 30 minutes after the start of the experiment is three times greater than that over two hours. The decrease in oxidation rate of organic halides on silver probably can be explained by the formation of a silver chloride layer on the surface of the tablet. Experiments which we carried out on pure AgCl under the same conditions proved that organic halides are not oxidized. The activation energies of the

oxidation on Ag, as determined from the initial rates, are: 3 kcal/mole for pentachloroethane, 4 kcal/mole for chlorobenzene and 6 kcal/mole for dichloroethane.

TABLE 3

Decomposition of Organic Halide Admixtures at 250° in the Absence of Oxygen

Admixture	Admixture conc. in nitrogen, volume %	Degree of decomposition calc. from Cl' data, %	Cl content in silver, %
Without admixture	—	—	0,0012
CCl <sub>4</sub>	$9,7 \cdot 10^{-2}$	27,0	0,3
CH <sub>3</sub> —CHCl	$5,4 \cdot 10^{-1}$	15,0	0,18
CH <sub>3</sub> —CHCl <sub>2</sub>	$2,8 \cdot 10^{-2}$	42,0	0,14
ClCH <sub>2</sub> —CH <sub>2</sub> Cl	$1,4 \cdot 10^{-1}$	16,5	0,12
FCCL <sub>2</sub> —CFCL <sub>2</sub> *	$1 \cdot 10^{-1}$	32,0	0,366
C <sub>6</sub> H <sub>5</sub> Cl *	$3,4 \cdot 10^{-2}$	8,0	0,0055

\* Calculated from Cl' only.

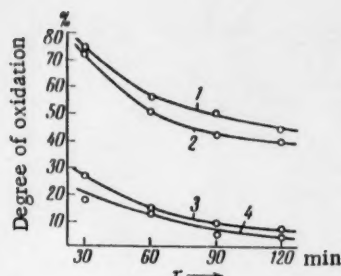


Fig. 1. Change of oxidation degree with time. Space velocity  $4000 \text{ hr}^{-1}$ ,  $t = 250^\circ$ . 1) Initial chlorobenzene concentration  $1,7 \cdot 10^{-2}$  vol. %; 2) the same,  $9,2 \cdot 10^{-3}$  vol. %; 3) initial dichloroethane concentration  $3,8 \cdot 10^{-2}$  vol. %; 4) the same,  $5,9 \cdot 10^{-2}$  vol. %.

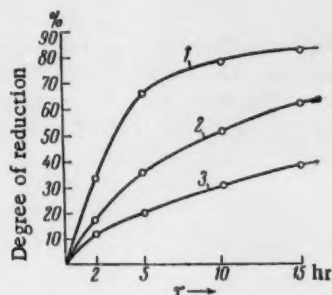


Fig. 2. Degree of AgCl reduction on a silver surface by a 3% ethylene-air mixture at  $t = 200^\circ$ . Chlorine concentration in silver: 1) 0.005, 2) 0.01, 3) 0.02 wt. %.

The rate of reducing chlorine ions introduced during the preparation of the silver catalyst is considerably lower than the oxidation rate. By determining the rate of reducing in a 3% ethylene-air mixture the silver chloride formed during the oxidation of the organic admixture it was shown that this rate is considerably higher than that of reducing the chlorine ions introduced into the silver during the preparation from inorganic salt solutions and has nearly the same value as the oxidation rates of the organic admixtures. In Fig. 2 are shown the kinetic curves found when reducing in a 3% ethylene-air mixture three silver samples containing AgCl only on the surface (the chlorine ion contents referred to the entire sample were 0.005; 0.01 and 0.02 wt. %). The rate of AgCl removal from the surface is proportional to the chlorine ion content. So, at the Cl' content of 0.005% the initial rate in relative units is equal to 17.5 and for samples with 0.02% Cl' the rate is lowered by three times. In Fig. 3 the logarithms of the initial oxidation rates of organic halide admixtures ( $\text{C}_2\text{H}_5\text{Cl}$ ,  $\text{C}_6\text{H}_5\text{Cl}$  and  $\text{C}_2\text{H}_4\text{Cl}_2$ ) and those of the initial AgCl reduction (chlorine concentration  $\sim 0.01$  weight %) are plotted versus reciprocal temperature.

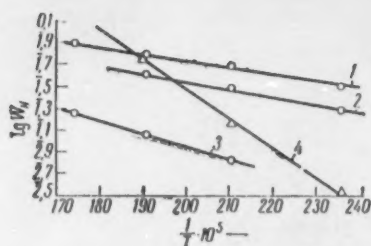


Fig. 3. Logarithms of initial rates plotted versus reciprocal temperature. 1)  $C_2H_5Cl_2$  oxidation, 2)  $C_6H_5Cl$  oxidation, 3)  $C_2H_4Cl_2$  oxidation, 4) reduction of AgCl on a silver surface (0.01 weight % Cl referred to the weight of the silver) in a 3% ethylene-air mixture.

organic admixture the ratio between its oxidation rate and the rate of AgCl reduction determines under which circumstances (concentration, temperature) its modifying action gives the highest selectivity in the oxidation of ethylene to ethylene oxide.

The difference between the activation energies of organic halide admixture oxidation ( $E = 4-6$  kcal/mole) and that of AgCl reduction ( $E = 15$  kcal/mole) indicates that in the temperature range 200-230° (at which the catalytic reaction takes place) the rate of chlorobenzene oxidation is higher than the reduction rate and in this case chlorine ions may accumulate on the surface and poison the catalyst. Raising the temperature to 240° results in an increased reduction rate and in order to maintain the required chlorine ion concentration on the surface the amount of admixture has to be increased. For dichloroethane, which in the temperature range 200-250° is oxidized with a considerably higher rate than is  $C_6H_5Cl$ , the rate of reduction surpasses that of oxidation and, therefore, the modifying of the silver can be adjusted only by feeding with a definite  $C_2H_4Cl_2$  concentration. The reduction and oxidation rates may vary for various silver samples because the latter may contain different amounts of chlorine ions on their surface. For each volatile

#### LITERATURE CITED

1. Yu. N. Stepanov, L. Ya. Margolis, and S. Z. Roginskii, *Doklady Akad. Nauk SSSR* **133**, 1384 (1960).\*
2. V. A. Pokrovskii, *Uspekhi Khim.* **25**, 1446 (1956).
3. F. T. McBee, H. B. Hass, and P. A. Wiseman, *Ind. and Eng. Chem.* **37**, 5, 432 (1945).
4. L. I. Beckhan, U. S. Patent 2,734,906 (1956).
5. A. I. Kurilenko, N. V. Kul'kova, V. E. Ostrovskii, and M. I. Temkin, *Doklady Akad. Nauk SSSR* **123**, 878 (1958).\*

\* Original Russian pagination. See C. B. translation.

THE THEORY OF THE THERMALIZATION OF "HOT"  
HYDROGEN ATOMS AND THEIR INFLUENCE ON THE  
YIELD OF DIMERIC PRODUCT DURING THE  
RADIOLYSIS OF ALKANES

A. Ya. Temkin

Institute of Petroleum Synthesis of the Academy of Sciences of the USSR

(Presented by Academician A. V. Topchiev, June 3, 1960)

Translated from *Doklady Akademii Nauk SSSR*, Vol. 135, No. 2, pp. 373-376,  
November, 1960

Original article submitted June 3, 1960

When ionizing radiation interacts with organic compounds, there are formed excited molecules and excited ions, a portion of which subsequently decomposes into smaller fragments, such as free radicals, ions, ion-radicals and the like. If the reactions whereby the excited molecules or excited ions decompose takes place in the gas phase, then it is easy to show from the laws of conservation of energy and of momentum that a portion of the energy liberated during such a reaction is converted into kinetic energy of translation of the fragments produced. As a result of this the fragments may be "hot", that is, they may acquire kinetic energy considerably in excess of the mean energy of thermal movement at the given temperature. If the excited molecule decomposes into fragments with different masses, then the particles with the lowest masses will possess the greatest kinetic energy. Thus, as an example, during the radiolysis of alkanes, "hot" alkyl radicals will only be produced by rupture of C-C bonds, while rupture of C-H bonds only produces "hot" hydrogen atoms. In this article we shall, for the sake of precision, only concern ourselves with hot hydrogen atoms.

The movement of a hot hydrogen atom through a gaseous hydrocarbon is accompanied by elastic and nonelastic collisions between it and the molecules of the gas, during which a portion of the energy of the hot atom is lost. Ultimately, the initially hot atom becomes a thermal atom. During nonelastic collision with a molecule, the hot atom may produce excitation in this molecule, or initial chemical reaction. As a result of this, the presence of hot atoms will change the course of the radiolytic process and affect the yield of the final products.

Since the energy thresholds of chemical reactions are different, the rates at which the reactions initiated by hot atoms will proceed will be determined by their energy spectrum at each point in the medium and at each moment of time. The determination of the over-all energy distribution may be carried out by solving Boltzmann's gas-kinetic equation, but this is a very complex procedure. We have therefore adopted an approximate method for this purpose, the so-called energy group method, which is often used in the theory of the retardation and thermalization of neutrons[1, 2]. This method consists in describing the course of the hot hydrogen atoms by means of a system of equations for the diffusion of various groups of atoms of uniform energy ("monoenergetic groups"), in which the atoms may be transferred from groups with higher energy to those with lower.

1. We shall limit ourselves initially to a two-group approximation and consider only the hot hydrogen atom group and the thermal hydrogen atom group. We shall suppose that, with nonelastic collisions with a molecule, the hot hydrogen atom causes the appearance of a new radical. This, of course, does not exhaust the possible reactions of the hot hydrogen atom with a paraffin molecule, but the essential characteristics of

radiolysis in the presence of hot atoms may be most simply developed by means of such a model as this. We note that, owing to the shortness of the lifetime of the hydrogen atom in the "hot" state, we may neglect collisions between hot hydrogen atoms and the radiolysis products, which will include hydrogen atoms and alkyl radicals. Therefore, the equation for the hot atom group will only contain the density of the hot atoms, and will thus be linear. Actually, the radiolysis products are appreciably less than the molecules of the starting substance, and the retardation of the hot atoms (their transition to the thermal group) takes place on collision with any molecules, and their velocity is, in consequence, practically determined by the number of collisions with the molecules of the starting substance. In other words, a hot atom, before it would be likely to collide, for example, with another hydrogen atom, would be able to undergo a sufficient number of collisions with molecules of the starting substance to go over into the thermal group.

The application of the two group method is, in the case which we are considering, equivalent to the assumption that the hot and thermal hydrogen atoms are particles of two different species, while the particles of one kind are able to undergo transformation into particles of the other. Hence, in the case of nonoverlapping tracks, the system of equations for one track, describing diffusion, recombination and the development of free radicals of different types, and also the process of thermalization of hot hydrogen atoms, may be written down in the following fashion:

$$\frac{\partial n_i}{\partial t} = D_i \Delta n_i - \sum_{j=1}^m a_{ij} n_i n_j - a_{iH} n_i n_H + A_i n_h + S_i, \quad (1a)$$

$$\frac{\partial n_h}{\partial t} = D_h \Delta n_h - \Lambda n_h + S_h, \quad (1b)$$

$$\frac{\partial n_H}{\partial t} = D_H \Delta n_H - \sum_{i=1}^m a_{iH} n_i n_H - a_{HH} n_H^2 + (\Lambda + \Lambda_H) n_h + S_H, \quad (1c)$$

where  $D_i$  is the diffusion coefficient of radicals of the  $i$ th type,  $a_{ij}$  is the recombination coefficient of radicals of the  $i$ th and  $j$ th types,  $S_i$  is the quantity of radicals of the  $i$ th type created in unit time in unit volume of track of ionizing particles;  $A_i$  is the macroscopic effective section of the formation of the free radical of the  $i$ th type by the hot hydrogen atom;  $\Lambda$  is the macroscopic effective section of the collisions of the hot atom with the molecules of the gas, accompanying its transition into the thermal group;  $n_i$  is the density of radicals of the  $i$ th types; all the magnitudes which refer to the hot hydrogen atom are designated by the index  $h$ , and all those to the thermal atoms by the index  $H$ . The term  $\Lambda_H n_h$  describes the development of thermal hydrogen atoms by decomposition of molecules which have been excited by means of the hot hydrogen atoms. Atomic hydrogen, because of its great mobility, diffuses rapidly from the track into the surrounding medium, where the density of alkyl radicals is small. Hence, the terms  $a_{iH} n_i n_H$  may be neglected. The system of Eqs. (1a) and (1b) is then independent of Eq. (1c), and we shall consider these two equations only.

We consider an example. Let hot atoms be formed at a time  $t_0$  (when the track is initiated) and at a point with radius vector  $r_0$ ; while within a sphere of radius  $R$ , with its center at the same point, free radicals of only one type are produced (so that we can omit the index  $i$ ). Then  $S = Q \delta(t - t_0) \eta(R - |r - r_0|)$ ;  $S_h = q \delta(t - t_0) \delta(r - r_0)$ ; where  $Q$  and  $q$  are constants; the value of  $\eta(x) = 1$  when  $x > 0$ , and  $\eta(x) = 0$  when  $x < 0$ . Considering the model of a spherical track, this resembles one "bead" of the electronic track. In addition, the qualitative yields ought not to depend on the shape of the track, though calculation for the case of a spherical track is considerably simpler than, for example, a cylindrical track. If we solve the system of Eqs. (1a) and (1b) by the method of successive approximations [3], we obtain Eq. (12) given in paper [3] for  $w = \text{constant}$ , and to a first approximation find that the yield of the dimeric product is given by the formula:

$$\begin{aligned}
\rho = & \frac{aQ^2w}{(4\pi)^{3/2}D^{3/2}Vt} \int_0^t dt_0 \int_V d\mathbf{r}_0 \int_V d\mathbf{r}'' \int_V d\mathbf{r}' \int_0^\infty dt'' \times \\
& \times \frac{\eta(R-|\mathbf{r}'-\mathbf{r}_0|)}{(t''-t_0)^3(t-t'')^{1/2}} \exp\left\{-\frac{(\mathbf{r}''-\mathbf{r}')^2}{2D(t''-t_0)}-\frac{(\mathbf{r}-\mathbf{r}'')^2}{4D(t-t'')}\right\} + \\
& + \frac{2aQAqw}{(4\pi)^{3/2}D^3D_h^{3/2}Vt} \int_0^t dt_0 \int_V d\mathbf{r}_0 \int_V d\mathbf{r}'' \int_V d\mathbf{r}' \int_0^\infty dt'' \int_0^\infty dt' \times \\
& \times \frac{\exp\{-\Lambda(t'-t_0)\}\eta(R-|\mathbf{r}'-\mathbf{r}_0|)}{(t''-t_0)^{3/2}(t'-t_0)^{1/2}(t''-t')^{1/2}(t-t'')^{1/2}} \times \\
& \times \exp\left\{-\frac{(\mathbf{r}''-\mathbf{r}')^2}{4D(t''-t_0)}-\frac{(\mathbf{r}'-\mathbf{r}_0)^2}{4D_h(t'-t_0)}-\frac{(\mathbf{r}''-\mathbf{r}')^2}{4D(t''-t')} - \frac{(\mathbf{r}-\mathbf{r}'')^2}{4D(t-t'')}\right\} + \\
& + \frac{aA^2wq^2}{(4\pi)^{3/2}D^{3/2}D_h^3Vt} \int_0^t dt_0 \int_V d\mathbf{r}_0 \int_V d\mathbf{r}'' \int_V d\mathbf{r}' \int_0^\infty dt'' \int_0^\infty dt' \frac{\exp\{-2\Lambda(t'-t_0)\}}{(t'-t_0)^3(t''-t')^3(t-t'')^{1/2}} \times \\
& \times \exp\left\{-\frac{(\mathbf{r}'-\mathbf{r}_0)^2}{2D_h(t'-t_0)}-\frac{(\mathbf{r}''-\mathbf{r}')^2}{2D(t''-t')} - \frac{(\mathbf{r}-\mathbf{r}'')^2}{4D(t-t'')}\right\}. \quad (2)
\end{aligned}$$

The first term in (2) gives the yield of dimeric product in the absence of hot atoms. The second and third terms give the additional yield of dimer owing to the effect of the hot hydrogen atoms.  $\Lambda = A + F$ , where  $F$  is the macroscopic section of the elastic scattering of the hot hydrogen atoms on the gas molecules. It can be seen from Eq. (2) that, for example, the addition of helium atoms would lead to a reduction in the effect of the hot hydrogen atoms, since, with increase in  $\Lambda$ , the two last integrals diminish, while the first integral is independent of  $\Lambda$ .

A more detailed investigation of formula (2) is in general difficult. Calculations on the basis of this formula may be carried out by numerical methods if the values of all the coefficients occurring in it are known.

2. In the case in which the power of the ionizing radiation dose is so great that the tracks are completely overlapping, and the reaction takes place not in these tracks only but in the entire irradiated volume, the group equations are greatly simplified, and the use of a multi-group method makes it easy to calculate the yield of various chemical reactions produced by the hot atoms. Actually, when there is homogeneous distribution of the hot atoms in the system, the diffusion terms vanish. If, under these conditions, we consider the stationary distribution of the hot atom which is set up, then all the time-dependent derivatives in the group equations reduce to zero.

We shall use the following notation:  $n_i$  is the stationary density of the hot atoms with energy  $E_i$  (in relation to the  $i$ th group);  $N$  is the number of molecules of the starting substance in unit volume;  $S_i$  is the number of hot atoms in the  $i$ th group created in unit volume and unit time by the ionizing radiation;  $\sigma_i$  is the effective section of elastic scattering of a hot atom of the  $i$ th group at a molecule, leading to its transition to the  $(i+1)$ -th group;  $\sigma_{ik}$  and  $\sigma_{ic}$  are the total effective sections of all nonelastic collisions of a hot atom of the  $i$ -th group, leading to its transition to the  $k$ th group (where  $k > 1$ ), or, to absorption, respectively. Then the system of group equations can be written thus:

$$N\left(\sigma_i + \sum_{k=i+1}^n \sigma_{ik} + \sigma_{ic}\right)n_i = N\left[\sigma_{i-1}n_{i-1} + \sum_{k=1}^{i-1} \sigma_{ik}n_k\right] + S_i \quad (1 \leq i \leq m-1); \quad (3a)$$

$$N\sigma_{mc}n_m + a_{HH}n_m^2 + \sum_i a_{H\mu}n_m n_{R,\mu} = N\left(\sigma_{m-1}n_{m-1} + \sum_{k=1}^{m-1} \sigma_{mk}n_k\right) + S_m \quad (3b)$$

(where  $n_{R,\mu}$  is the density of free radicals of the type  $\mu$ ). Equation (3b) refers to the thermal hydrogen atom.

When the algebraic system (3) is solved, it is easy to write the relationship which determines  $\rho^{(\alpha)}$ , the number of elementary acts of the various reactions taking place in unit volume and unit time. For reactions of the type  $H + M$ , where the hydrogen atom disappeared, we find:

$$\rho^{(\alpha)} = N \sum_{i=1}^m \sigma_{ic}^{(\alpha)} n_{i0} \quad (4)$$

while for reactions which accompany the transition of the hot atom from the  $i$ th group to the  $k$ th, we may write:

$$\rho^{(\alpha)} = N \sum_{i=1}^{m-1} \sigma_{ik}^{(\alpha)} n_i. \quad (5)$$

If the reaction threshold,  $E^{(\alpha)}$  satisfies the inequality  $E_{i_0} < E^{(\alpha)} \leq E_{i_0-1}$ , then all the values of  $\sigma^{(\alpha)}_{ik}$  and  $\sigma^{(\alpha)}_{ic}$  in Eqs. (4) and (5) for which  $i > i_0 - 1$  reduce to zero.

The method here described may be employed also in the investigation of the kinetics of processes which take place with the participation of hot molecules, radicals or ions. It may be used in radiochemistry, photochemistry and thermochemistry.

In conclusion, we wish to express our sincere thanks to L. S. Polak and N. Ya. Chernyak for their discussion of the results of this work.

#### LITERATURE CITED

1. S. Glasstone and M. Edlund, The Bases of the Theory of Nuclear Reactors [Russian translation] (Moscow, 1954).
2. M. V. Kazarnovskii, A. V. Stepanov, and F. L. Shapiro, Second International Conference on the Peaceful Uses of Atomic Energy (Geneva, 1958); Communications of Soviet Scientists, Nuclear Physics [in Russian] (Moscow, 1959) Vol. 1, p. 469.
3. L. S. Polak and A. Ya. Temkin, Doklady Akad. Nauk SSSR 125, 584 (1959).\*

\* Original Russian pagination. See C. B. translation.

# RING-FLUORINE CHEMICAL SHIFT IN THE NUCLEAR MAGNETIC RESONANCE OF FLUOROBENZENES WITH FLUORINATED SUBSTITUENTS

L. M. Yagupol'skii, V. F. Bystrov, and É. Z. Utyanskaya

Institute of Organic Chemistry, Academy of Sciences of the USSR;

Institute of Chemical Physics, Academy of Sciences of the USSR

(Presented by Academician V. N. Kondrat'ev, June 1, 1960)

Translated from Doklady Akademii Nauk SSSR, Vol. 135, No. 2, pp. 377-380,

November, 1960

Original article submitted May 25, 1960

In the last few years a great number of aromatic compounds have been synthesized with various fluorinated side-chains. Their physicochemical properties have barely been explored. The purpose of this work was to determine the effects of fluorinated substituents on the electron density distribution in a benzene ring and to correlate the structure of these compounds with their reactivity by means of nuclear magnetic resonance (n.m.r.).

Fluorine chemical shifts in monosubstituted fluorobenzenes are measured with reference to the fluorine resonance line in unsubstituted fluorobenzene and can be defined by the equation:

$$\delta = \frac{H_X - H_{C_6H_5F}}{H_{C_6H_5F}} \cdot 10^6, \quad (1)$$

TABLE 1

Ring-Fluorine Chemical Shifts in the n.m.r.  
Spectra of Substituted Fluorobenzenes



Substituent X	o	m	p	3,4
SO <sub>2</sub> CF <sub>3</sub>	-8,7	-4,7	-15,1	
SCF <sub>3</sub>	-7,8	-2,3	-4,7	
OCF <sub>3</sub>	+17,4	-2,3	+2,8	
CH=CH-CF <sub>3</sub>			-2,4	
				+3,9
				-8,6

where  $H_X$  and  $H_{C_6H_5F}$  are the external magnetic fields, at which the  $F^{19}$  resonance is observed in the substituted and unsubstituted fluorobenzene, respectively. The instrument had a resolution of approximately  $1 \cdot 10^{-6}$ , and the chemical shifts could be measured accurately to within  $\pm 0.3 \cdot 10^{-6}$ . The experimental samples consisted of pure liquids. We used an external standard in all of our measurements. The investigated samples had an effective volume of approximately 80 mm<sup>3</sup>, while the standard had an approximate 20 mm<sup>3</sup> volume. No corrections were applied for the diamagnetic susceptibilities of our samples. A 4530 gauss uniform magnetic field was maintained. The n.m.r. technique and instrumentation have been described in detail elsewhere [1]. The measured ring-fluorine chemical shifts are listed in Table 1.

Any redistribution of the electron densities in a benzene ring induced by a substituent will not only affect the fluorine chemical shift in substituted fluorobenzenes [2] but will also be reflected in the chemical reactivity of these benzene derivatives [3]. The general quantitative relationship between the nature of a substituent meta or para to a reaction center

and the reactivity of a side chain can be expressed by the well-known Hammett equation [3]:

$$\lg \frac{k}{k_0} = \sigma \rho, \quad (2)$$

where  $k$  and  $k_0$  are the rate (or equilibrium) constants for the substituted and unsubstituted benzene derivatives respectively;  $\rho$  is a constant determined by the conditions and type of reaction, but it also depends on the nature of the side chain;  $\sigma$  is a constant determined solely by the nature and position of the substituent. An approximate empirical relationship has been established [2] between the magnitude of the chemical shift  $\delta$  and the Hammett  $\sigma$ -constant,

$$\delta_m = -5,92 \sigma_m, \quad (3)$$

$$\delta_p = -17,9 \sigma_p + 4,84. \quad (4)$$

A further development of the theory of chemical reactivity of benzene derivatives [4] yielded a new, more precise quantitative relationship between the  $\delta$  and  $\sigma$ -functions [5]. Taft showed that the effect of a substituent on the reactivity of a meta or para-substituted benzene derivative can be expressed as a sum of the two independent contributions: from the inductive and the conjugation effects,

$$\sigma_p = \sigma_i + \sigma_c, \quad (5)$$

$$\sigma_m = \sigma_i + \alpha \sigma_c, \quad (6)$$

where  $\alpha$  is a constant which depends on the type of reaction [6]. The following quantitative relationship between the  $\sigma$  and  $\delta$  functions can readily be derived [5]:

$$\delta_m = -5,83 \sigma_i + 0,20, \quad (7)$$

$$\delta_p = -5,83 \sigma_i - 18,80 \sigma_c + 0,80. \quad (8)$$

TABLE 2

Substituent	$\sigma_i$	$\sigma_p$ from pK <sub>a</sub>	$\sigma_c$ Eq. (5)	$\sigma_m$ Eq. (6)	$\sigma_m$ from pK <sub>a</sub>	$\sigma_c$ (n.m. r.)	$\sigma_m$ Eq. (3)	$\sigma_p$ Eq. (4)
OCF <sub>3</sub>	0,43	0,32	-0,11	0,38	0,36	-0,24	0,39	0,11
OCH <sub>3</sub>	0,25 <sup>(*)</sup>	-0,27 <sup>(*)</sup>	-0,52	0,10	0,12 <sup>(*)</sup>	—	—	—
SCF <sub>3</sub>	0,43	0,38	-0,05	0,41	0,35	0,16	0,39	0,53
SCH <sub>3</sub>	0,27 <sup>(*)</sup>	0,01 <sup>(*)</sup>	-0,26	0,16	0,15 <sup>(*)</sup>	—	—	—
CF <sub>3</sub>	0,41 <sup>(*)</sup>	0,54 <sup>(*)</sup>	0,13	0,46	0,43 <sup>(*)</sup>	0,19 *	0,35 *	0,56 *
CH <sub>3</sub>	-0,05 <sup>(*)</sup>	-0,17 <sup>(*)</sup>	-0,12	-0,08	-0,07 <sup>(*)</sup>	—	—	—
SO <sub>2</sub> CF <sub>3</sub>	0,84	1,03	0,19	0,92	0,79	0,58	0,79	1,12
SO <sub>2</sub> CH <sub>3</sub>	0,58 <sup>(*)</sup>	0,72 <sup>(*)</sup>	0,14	0,64	0,65 <sup>(*)</sup>	—	—	—
CH=CH-CF <sub>3</sub>	—	0,23	—	—	—	—	—	0,40
CF <sub>3</sub> -C(=O)-	—	0,36	—	—	—	—	—	0,05
O-CF <sub>2</sub> -	—	0,81	—	—	—	—	—	0,75

\* In these calculations we used the values of  $\delta_m = -2,1$  and  $\delta_p = -5,1$  [6].

However, in the case of strong electronegative groups (for example, CN, NO<sub>2</sub>, and COCH<sub>3</sub>, etc.) the  $\sigma_p$ -constants calculated from chemical shifts by the use of Eqs. (7), (8), and (5) come out considerably greater than the standard  $\sigma_p$ -constants [5, 6]. Recently, it has been shown that the standard  $\sigma_p$ -constants are only valid

TABLE 3

Substituent	SO <sub>2</sub> CF <sub>3</sub>	NO <sub>2</sub>	SO <sub>2</sub> CH <sub>3</sub>	CN	CF <sub>3</sub> CF <sub>2</sub> O	COCH <sub>3</sub>	CF <sub>3</sub>	SCF <sub>3</sub>	CH=CH-CF <sub>3</sub>	I	Br	Cl	OCF <sub>3</sub>	CF <sub>3</sub> O	F	SCF <sub>3</sub>	CH <sub>3</sub>	OCH <sub>3</sub>
$\delta_p$	-15,1	-10,8	—	-9,6	-8,6	-6,6	-5,1	-4,7	-2,4	1,2	2,3	2,4	2,8	3,9	6,4	—	5,5	11,4
$\sigma_p$	1,03	0,78	0,72	0,66	0,81	0,50	0,54	0,38	0,23	0,23	0,23	0,23	0,32	0,36	0,06	0,01	-0,17	-0,27
$\lambda_{\max}$ (l), m $\mu$ (in ethanol)	476	475	445	—	450	447	430	432	435	—	420	420	419	420	—	419	408	407

TABLE 4

Substituent	SO <sub>2</sub> CF <sub>3</sub>	NO <sub>2</sub>	SO <sub>2</sub> CH <sub>3</sub>	CN	CF <sub>3</sub>	F	Cl	Br	I	SCF <sub>3</sub>	OCF <sub>3</sub>	SCF <sub>3</sub>	OCH <sub>3</sub>	CH <sub>3</sub>
$\delta_m$	-4,7	-3,3	—	-3,0	-2,8	-3,1	-2,1	-2,4	-2,6	-2,3	-2,3	—	-1,3	+0,9
$\sigma_m$	0,79	0,71	0,65	0,56	0,43	0,34	0,37	0,39	0,35	0,35	0,36	0,15	0,12	-0,07

in cases where there is either no direct conjugation between the para-substituent and the functional group or very little of it [6, 7]. If such conjugation does exist we would expect a continuous series of  $\sigma_p$ -constants for the various substituents since the deviation of any one value from the standard  $\sigma_p$ -constant depends on the magnitude of the para-conjugation effect.

Equation (7) has been shown to hold for all the previously investigated groups without exception [5, 6]. Using this equation we evaluated the  $\sigma_I$ -constants for the substituents examined by us (Table 2) while the  $\sigma_p$ -constants listed in the table were obtained from Eq. (2) by using the  $pK_a$  values of corresponding substituted benzoic acids [10]; we have, of course, assumed that there is very little para-conjugation between the carboxyl group and the substituents. The  $\sigma_c$ -constants corresponding to these  $\sigma_p$  values were calculated from Eq. (5) and are also included in Table 2. Substituents with positive  $\sigma_c$ -constants are meta-directors in electrophilic ring-substitution reactions, while those with negative  $\sigma_c$ -constants are ortho, para-directors [4]. Indeed, only the meta-substituted product is obtained when the  $CF_3$  and  $SO_2CF_3$  derivatives of benzene are nitrated; at the same time we get 65% para and 35% ortho-substitution in the case of the  $SCF_3$  derivative, while the  $OCF_3$  derivative gives a 90% yield of the para-nitro compound. The agreement between the  $\sigma_m$ -constants computed from Eq. (6) and those determined from the dissociation constants of the corresponding benzoic acids is as good as one could expect from the Hammett equation. The  $pK_a$  values of the  $CH_3$  and  $OCH_3$  derivatives of benzoic acid were determined in aqueous solutions ( $\alpha = 0.29$  [6]), while those of the remaining derivatives were measured in a 50% ethanol solution ( $\alpha = 0.42$  [6]). Table 2 also includes the n.m.r.  $\sigma_c$ -values calculated with the help of Eqs. (7) and (8). Since the n.m.r. measurements yield considerably larger values of  $\sigma_c$  for the  $SO_2CF_3$ ,  $CF_3$ , and  $SCF_3$  groups, it seems that the effect of para-conjugation with fluorine is more pronounced than with a carboxyl group. On the other hand an  $OCF_3$  group exhibits less para-conjugation with fluorine than with a  $COOH$  group. We have also listed in Table 2 the values of  $\sigma_m$  and  $\sigma_p$  calculated from Eqs. (3) and (4).

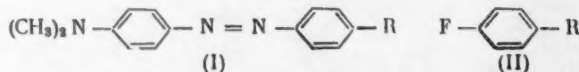
For the sake of comparison, we have also included in Table 2 the  $\sigma$ -constants of the corresponding unfluorinated derivatives. In all the cases the introduction of fluorine increases the induction effect of the corresponding substituent. When the hydrogens in substituents such as  $OCH_3$  and  $SCH_3$  ( $\sigma_c < 0$ ) are replaced by fluorine the conjugation between the ring and the group decreases considerably, while in the case of  $SO_2CH_3$  ( $\sigma_c > 0$ ) the conjugation slightly increases due to the fact that fluorine pulls away some electrons from the oxygen and sulfur atoms. The conjugation effects of the  $CH_3$  and the  $CF_3$  groups though similar in magnitude are reverse in sign. It seems that in this case a fluorine tends to attract electrons through a  $\sigma - \sigma$  interaction to about the same extent as the hydrogens tend to repel them.

To compare the effects of the investigated substituents on the benzene ring with the ones previously reported we have tabulated in Tables 3 and 4 the ring-fluorine chemical shifts  $\delta_m$  and  $\delta_p$  [2, 6], and the  $\sigma$ -constants of these substituents [8]. The groups were arranged in order of decreasing electronegativities. Tables 3 and 4 show that the  $SO_2CF_3$  group is the most electronegative substituent known. As far as their effect on the benzene ring is concerned the  $OCF_3$ ,  $SCF_3$ , and  $CH=CH-CF_3$  groups resemble halogens,  $CF_3$  resembles

$COCH_3$  and  $CN$ ,  $O \begin{smallmatrix} \diagup \\ \diagdown \end{smallmatrix} CF_2$  resembles  $OCF_3$ , and  $CF_2 \begin{smallmatrix} \diagup \\ \diagdown \end{smallmatrix} O$  resembles  $CF_3$ . The  $CH=CH-CF_3$  group (the vinylog

of benzyl trifluoride) is less electronegative than a  $CF_3$  group. A similar relationship exists between the  $CH=CH-COOH$  and the  $COOH$  groups.

One can also note in Table 3 that there seems to be a relationship between the wavelength of the absorption maximum in the visible spectrum of 4'-substituted dimethylaminoazobenzenes (I) [9] and the fluorine chemical shift in the corresponding parafluorobenzenes (II).



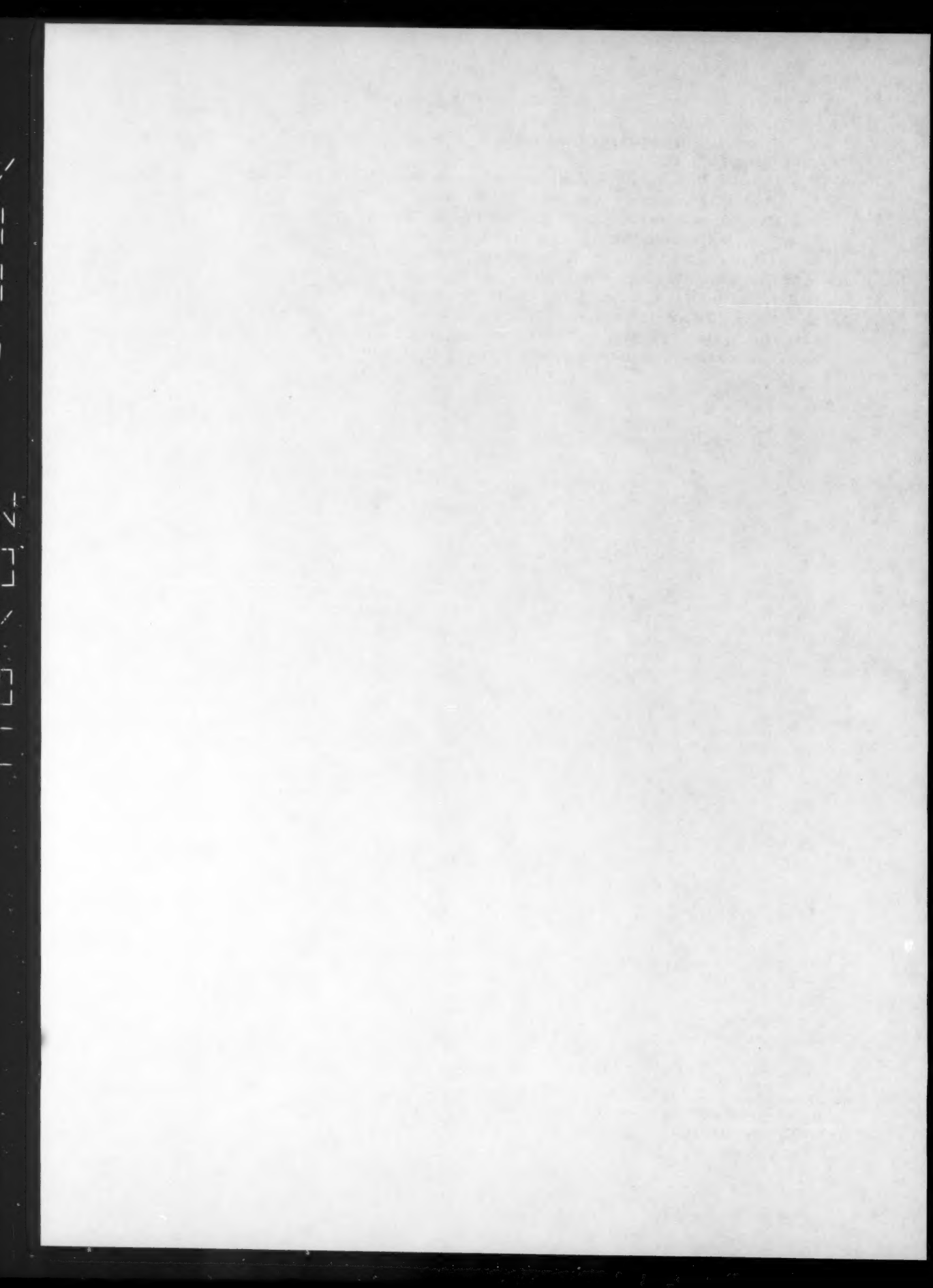
This relationship apparently results from the fact that the same type of electron displacement is responsible for both the fluorine chemical shift (in the para derivative) and the shift in the absorption maximum in the visible spectrum.

# LITERATURE CITED

1. V. F. Bystrov, L. L. Dekabrun, Yu. N. Kul'yanov, A. U. Stepanyants, and É. Z. Utyanskaya, *Pribor. i Tekh. Eksp.* No. 1 (1961).
2. H. S. Gutowsky, D. W. McCall, B. R. McGarvey, and L. H. Meyer, *J. Am. Chem. Soc.* **74**, 4809 (1952).
3. L. P. Hammett, *Physical Organic Chemistry* (1940); H. H. Jaffe, *Chem. Rev.* **53**, 191 (1953).
4. R. W. Taft, in: M. S. Newman, *Steric Effects in Organic Chemistry* (1959) Chap. 13.
5. R. W. Taft, *J. Am. Chem. Soc.* **79**, 1045 (1957).
6. R. W. Taft and I. C. Lewis, *J. Am. Chem. Soc.* **81**, 5343, 5352 (1959).
7. H. Van Bekkum, P. E. Verkade, and B. M. Webster, *Rec. trav. chim.* **78**, 815 (1959).
8. D. H. McDaniel and H. C. Brown, *J. Org. Chem.* **23**, 420 (1958).
9. L. M. Yagupol'skli and M. S. Marinets, *Zhur. Obshch. Khim.* **27**, 1395 (1957); \* I. N. Zhmurova, *Zhur. Obshch. Khim.* **27**, 2704 (1957); \* E. Sawicki, *J. Org. Chem.* **22**, 915 (1957); L. M. Yagupol'skli and L. N. Yagupol'skaya, *Doklady Akad. Nauk SSSR* **134**, 6 (1960). \*\*

\* Original Russian pagination. See C. B. translation.

\*\* See C. B. translation.



# A THERMOGRAPHIC DETERMINATION OF SMALL HEAT CHANGES AT TEMPERATURES BELOW 0° C.

A. G. Anikin and G. M. Dugacheva

M. V. Lomonosov Moscow State University

(Presented by Academician P. A. Rebinder, June 20, 1960)

Translated from *Doklady Akademii Nauk SSSR*, Vol. 135, No. 3, pp. 634-637,  
November, 1960

Original article submitted June 15, 1960

There are two methods for the quantitative determination of heat changes — the calorimetric and the thermographic. The calorimetric method requires more complicated equipment and it takes more time for the completion of an experiment, but this is compensated by the high accuracy. The thermographic method though simpler and more rapid is, on the other hand, less precise.

The literature lists quite a number of thermographic determinations of heats of fusion [1, 2], heats of recombination of frozen free radicals [3], heats of reaction of solid hydrogen peroxide [4], etc., and in no case was a determination faced with a shortage of available material. However, in many cases one has to deal with very minute samples of material. But microcalorimetric work though extremely precise is at the same time very difficult and takes a long time [5]. These methods become even more complex and the accuracy further declines when materials are investigated at temperatures below zero. Several attempts have recently been made to render the thermographic method more accurate while preserving its basic simplicity and rapidity. The work described in this paper represents one such attempt applied to small samples (hundredths of grams) at temperatures below 0° C (down to the liquid nitrogen temperature\*).

The temperature recording part of our apparatus consisted of a copper-constantan thermocouple, a low-resistance potentiometer (model PMS-48) and a rebuilt electronic self-recording potentiometer (model ÉPP-09) with a sensitivity of  $\pm 0.07^\circ/\text{mm}$  which was used as a reference instrument. When heat was evolved or absorbed temperature was automatically recorded against time on a special graph paper.

The thermocouple leads were either fused by the short circuit shock method [6] or simply soldered with lead. The fused wires were 0.1 mm in diameter; at about 5 cm from the junction these fine wires were soldered to some thicker wires, 0.25 mm in diameter. The small dimensions of the wires and of the junction are essential for reducing the thermocouple inertia.\*\*

To get temperatures between  $-190^\circ$  and  $-70^\circ$  and above we built a small cryostat. The cryostat made it possible to record the temperatures of our samples as they were heated at a fixed and controllable rate. This was achieved by using radiant heat. The apparatus had the following structural features: a test-tube-shaped glass vessel was plugged with a ground joint stopper into which two copper wires about 0.6 mm in diameter were sealed (Fig. 1, I).

\* The method is not restricted to this temperature range. Very small alterations will permit the recording of curves at temperatures above zero.

\*\* At the same time to prevent the thermocouple from acquiring excessively high resistance we did not use fine wire throughout the apparatus.

We then wrapped heating wires around a glass tube, placed the tube rigidly on a stopper inside the test tube, and connected the wires with the copper wires fused into the ground joint. The heating element consisted of a simple 0.2 mm nichrome wire with the successive strands separated from each other by glass wool threads and the whole unit was coated with bakelite varnish. The heater had a resistance of about 50 ohms.

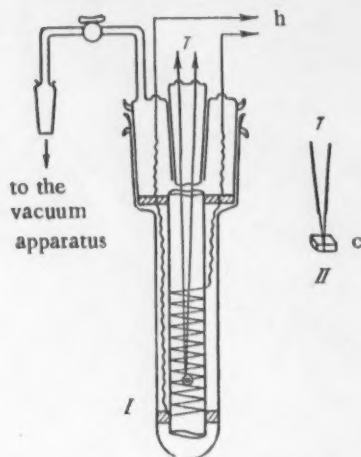


Fig. 1. The heating apparatus and the container used for thermal analysis (I) and the cup for the determination of heats of fusion (II); the thermocouple wires are denoted by T, the heater wires by h, and c is a copper foil cup.

TABLE 1

Experimental Results Obtained from the Heating Curve of a Solid Cyclohexane Drop in the Region of a Phase Transition ( $t_{tr}$ , °C [7];  $\Delta H_{tr}$ , cal/g [7])

Expt. Nos.	g, in g	L, in mm	$\Delta H_{tr}$ , °g, in cal.	A, in cal/mm
1	0,009	18	0,17	0,009 <sub>5</sub>
2	0,019	41	0,36	0,009
3	0,022	43	0,42	0,010
4	0,027	51	0,52	0,010
5	0,045	110	0,86	0,008

nitrogen temperature and evacuated to a pressure of  $(1-5) \cdot 10^{-2}$  mm Hg. At this low pressure the thermal conductivity of the air inside the test tube was reduced to such an extent that the exchange of heat between the liquid nitrogen and the sample became very slow, reducing substantially the heat losses from the sample during the evolution or absorption of heat. After the vessel was evacuated a 0.15 amp current was sent through the heating coil. A current of this magnitude allowed for even heating and a steady rate of temperature increase over a temperature range of about 100° C. Since the samples had no contact with the heater they received only radiant heat. This also reduced heat losses during the evolution or absorption of heat. Hence, whenever a process accompanied by a heat change occurred in the sample most of the evolved or absorbed heat would be conducted through the thermocouple and duly recorded by our instruments.

Since the main stopper was hollow inside and could accommodate another ground joint, a solid plug into which the copper and the constantan thermocouple leads were sealed was inserted so as to effectively seal the entire apparatus. The thermocouple junction was located inside the hollow shell of the heater in such a way that the number of heating coils below and above it was the same. The thermocouple wires were encased in three stoppers. The stoppers had a diameter 1 mm smaller than the inside diameter of the heating tube. All three stoppers were placed inside the tube to keep the thermocouples from coming into contact with the walls.

When studying any solid state processes accompanied by the evolution or absorption of heat we condensed the materials directly on the thermocouple junction. Thus the junction would be located right in the middle of a spherically shaped solid product. The samples weighed from 0.005-0.05 g. For the determination of heats of fusion of compounds initially powdered which decompose on melting, and in other similar cases, we used a special cup made of copper foil (Fig. 1, II). We would seal the thermocouple junction to the bottom of the cup so that the cup and the thermocouple would constitute one unit. Since the copper cup increased the thermocouple inertia the sensitivity of our measurements was slightly reduced. Liquid compounds were poured into the cup by means of a volumetric pipette calibrated to within 0.005 ml. If the density of the material was known the weight could be readily computed; the weight had to be known in order to obtain all heat changes per unit weight.

The material condensed on the junction was weighed by melting it into a previously weighed container; these weighings were accurate to within  $\pm 0.001$  g. Hence, the errors in the weights of samples weighing 0.05-0.01 g constituted 2-10% of the total weight. When the cup was used the weighings were accurate to within  $\pm 0.0005$  g. Since we also dealt in these cases with larger samples (0.01-0.15 g) the relative errors were correspondingly smaller (2-0.3%).

After the material was either condensed on the junction or poured into the cup the entire vessel (with the heater wires disconnected from the main circuit) was cooled to liquid

The instrument was calibrated under similar conditions (of heating current, pressure, temperature, and amount of refrigerant) by using compounds with known heat changes taking place at various points of our temperature scale. From the ratio of heat evolved (or absorbed) to the length of the plateau on the heating curves of known compounds we can construct a calibration curve of temperature versus calories per millimeter. Using this curve together with the experimentally determined length of the plateau on the heating curve of the investigated compound and the sample weight we can calculate the unknown heat change from the equation:

$$\Delta H_x = AL_x \frac{1}{g_x}, \quad (1)$$

where  $g_x$  is the weight of the investigated compound (in grams);  $\Delta H_x$  is the heat change (in cal/g);  $L_x$  is the length of the plateau (in mm);  $A$  is a conversion factor determined from the calibration curve (in cal/mm) at the temperature at which heat is evolved or absorbed.

TABLE 2

Experimental Results Obtained from the Heating Curves of Samples Placed in the Cup

Compound	Expt. Nos.	$g$ , in g	$\Delta H_{tr} \cdot g$ , in cal.	$L$ , in mm	$A$ , in cal/mm
Cyclohexane ( $\Delta H_f = 19.14$ cal/g at $-87.06^\circ [7]$ )	1	0,0325	0,62	32	0,020
	2	0,0450	0,86	41	0,021
					$0,020 \pm \pm 0,0005$
n-Hexane ( $\Delta H_f = 36.1$ cal/g at $-95.35^\circ [8]$ )	1	0,0149	0,54	27	0,020
	2	0,0321	1,16	52	0,022
	3	0,0380	1,37	63	0,022
	4	0,0487	1,76	78	0,022
					$0,021 \pm \pm 0,0015$
n-Heptane ( $\Delta H_f = 33.5$ cal/g at $-90.6^\circ [8]$ )	1	0,0194	0,65	32,5	0,020
	2	0,0278	0,94	48	0,020
	3	0,0427	1,44	64	0,022
	4	0,0575	1,92	85	0,022
					$0,021 \pm 0,001$
Toluene ( $\Delta H_f = 17.2$ cal/g at $-94.99^\circ [8]$ )	1	0,0309	0,52	26	0,020
	2	0,0488	0,86	42	0,020
	3	0,0515	0,90	43	0,021
	4	0,0602	1,03	47	0,022
					$0,021 \pm 0,001$

The factor  $A$  can also be determined without a calibration curve. If the investigated heat change occurs at a temperature  $\underline{t}$  then it is sufficient to record the melting curve of any compound which melts at a temperature close to  $\underline{t}$  and the  $\Delta H_{f,a}$  of which is known. Then,

$$A = \frac{\Delta H_{f,a} g_a}{L_a}, \quad (2)$$

where  $\Delta H_{f,a}$  is the heat of fusion of compound  $\underline{a}$  (in cal/g),  $g_a$  is its weight (g), and  $L_a$  is the length of the plateau on the melting curve of the compound (in mm).

We condensed a cyclohexane drop on the thermocouple junction and studied the heat changes accompanying solid phase transitions (transition temperature  $-87.06^\circ [7]$ ). The cyclohexane samples ranged in weight

from 0.009 to 0.045 g. Since the transition temperature is known (19.14 cal/g [7]) it is easy to see that we were dealing in our samples with heat changes of the order of 0.2 to 0.9 cal (Table 1). The value of A was about the same in each experiment and averaged  $0.0095 \pm 0.0015$  cal/mm. Consequently, it is possible to measure heat changes of 0.1-0.2 cal in our apparatus with an error of 10-15%.

All these data, of course, pertain to experiments where a 0.15 amp heating current was used. If the current is changed the heating rate of the material will change and consequently the plateau will have a different length.

The cup was used to study the heat change associated with the solid phase transition of the same cyclohexane and for the determination of the heats of fusion of n-hexane, n-heptane, and toluene. The sample weights ranged from 0.015 to 0.15 g. The results are tabulated in Table 2. In all these cases the precision was about  $0.021 \pm 0.001$  cal/mm. We carried out 2-3 measurements on each sample to make sure that the plateau lengths and temperatures were reproducible.

TABLE 3  
Thermographically Determined Heats of Fusion

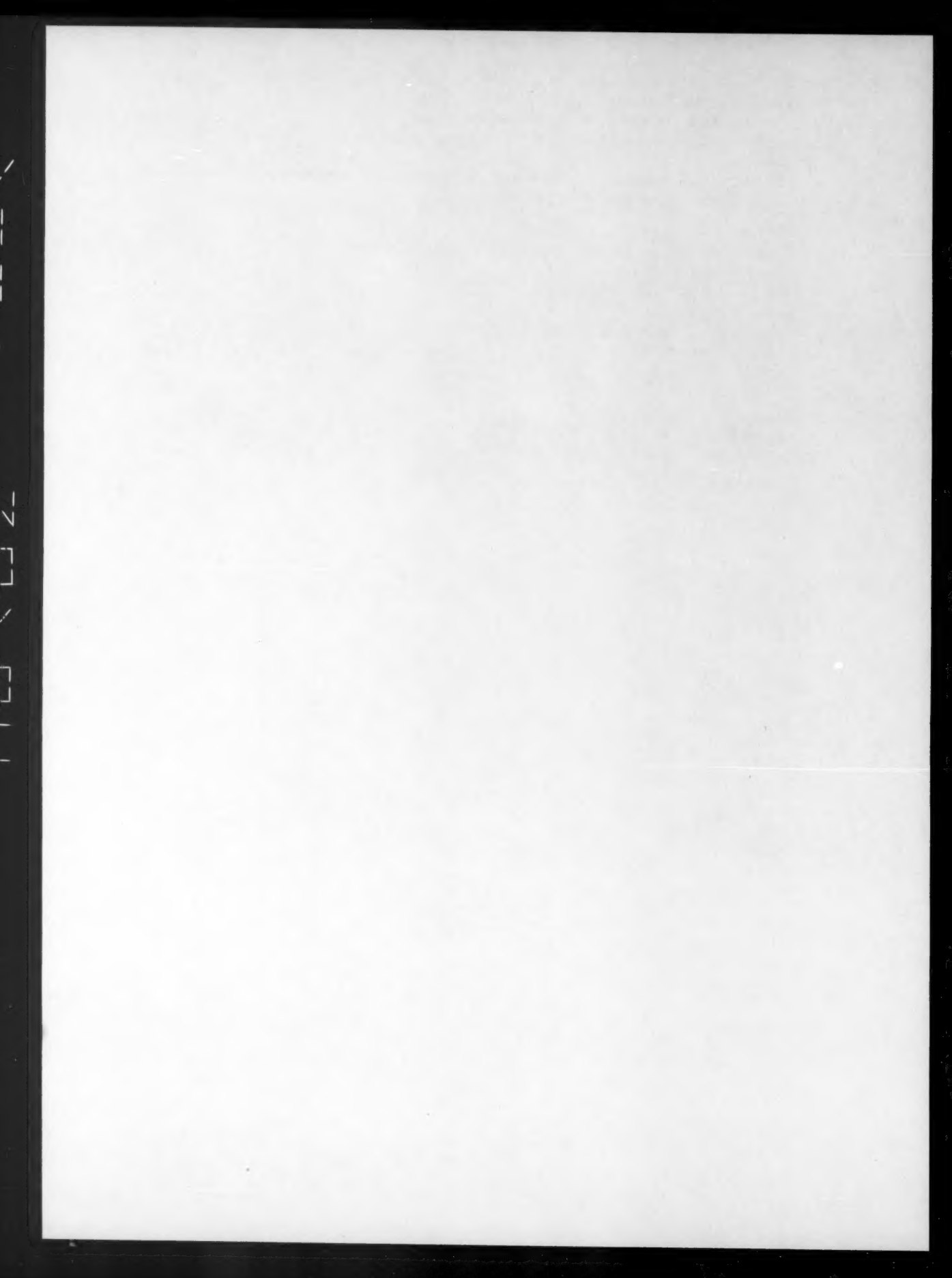
Compound	$g_x$ , in g	$L_x$ , in mm	$\Delta H_{f,a}$ , in cal/g [8]	$\Delta H_{f,a}$ , $\cdot g_a/L_a$ in cal/mm (from Table 2)	$\Delta H_x$ , in cal/g	
					from melting curves	from literature data [8]
Toluene (x)	0,0515	43	33,5	0,021	17,5	17,2
n-Hexane (a)	0,049	42			18,0	
	0,031	26			17,6	
n-Hexane (x)	0,038	63	17,2	0,021	$17,7 \pm 0,3$	36,1
Toluene (a)	0,032	52			34,8	
	0,015	27			34,1	
n-Heptane(x)	0,0575	85	17,2	0,021	$35,6 \pm 2$	33,5
Toluene (a)	0,043	64			35,2	
	0,028	48			36,2	
	0,020	32,5			31,5	
					31,0	
					$33,5 \pm 2,5$	

Using Eq. (1) we computed the heats of fusion of toluene, n-hexane, and n-heptane, all of which melt very close together. Toluene was taken as the known reference compound a with a known heat of fusion. The heat of fusion of toluene was in turn calculated by using n-hexane as the reference compound a. Table 3 shows that the differences between our results and the literature data lie within the range of experimental errors. The experimental errors were in all cases  $\leq 10\%$ . Thus, the described method is quite adequate for the determination of heat changes accompanying any physicochemical transitions. At the same time samples weighing only a tenth or a hundredth of a gram can be used and heat changes on the order of tenths of a calorie can be determined with a 10% accuracy.

#### LITERATURE CITED

1. B. J. Mair, A. R. Glasgow, and F. D. Rossini, J. Res. Nat. Bur. Stand. **26**, 591 (1941).
2. D. G. Barnard-Smith and P. T. White, Anal. Chim. Acta **17**, 1, 125 (1957).
3. M. A. Hogg and J. E. Spice, J. Chem. Soc. **9**, 3971 (1957).
4. H. P. Broida and O. S. Lutes, J. Chem. Phys. **24**, 484 (1956).

5. É. Kal've, Zhur. Fiz. Khim. 33, 6, 1161 (1959).
6. A. G. Anikin, Zhur. Fiz. Khim. 30, 3, 685 (1956).
7. Handbook of Physicochemical Properties of Pure Hydrocarbons (Ed. by M. D. Tillicheeva) [in Russian] (Moscow, 1954) Vol. 5.
8. F. D. Rossini, et al., Selected Values of Physical and Thermodynamic Properties of Hydrocarbons and Related Compounds (Pittsburgh, 1953).



## THE HEAT CAPACITY OF THE SILICA GEL - WATER ADSORPTION SYSTEM

G. I. Berezin, A. V. Kiselev, and V. A. Sinitsyn

Institute of Physical Chemistry, Academy of Sciences of the USSR

(Presented by Academician V. I. Spitsyn, May 12, 1960)

Translated from *Doklady Akademii Nauk SSSR*, Vol. 135, No. 3, pp. 638-641,

November, 1960

Original article submitted May 7, 1960

The current theory of adsorption equilibria is based on the presumed existence of adsorption complexes [1, 2]. To fully solve the problems connected with adsorption it is important that we not only be able to calculate the potential energy curves [3] and obtain the infrared spectra of the components involved [4], but also determine the thermodynamic properties of adsorption systems, particularly their heat capacities. A quantitative evaluation of entropies requires knowledge of heat capacities at low temperatures. These have only been determined for very few simple systems [5]. However, the study of heat capacities of adsorption systems at ordinary temperatures and for various degrees of surface covering is also very interesting since the heat capacity is frequently very sensitive to changes in the state of matter. On top of that, heat capacity measurements will provide information about the change in the heat of adsorption with temperature.

The dependence of heat capacity on the degree of surface covering has only been studied at ordinary temperatures in the case of water adsorbed on porous crystals [6], and it has been found that the heat capacity gradually declines below about 30 cal/mole  $\cdot$   $^{\circ}$ C with increasing surface coverage. However, the mean molar heat capacities reported in [6] were not very accurately determined, with errors ranging from 2-20%. Since we wanted to determine the heat capacities at low concentrations of adsorbate, it was necessary to construct a very sensitive and reliable calorimeter.

The reference method [7] for the precise determination of heat capacity changes in either liquids or solids requires no knowledge of the amount of heat introduced into the system or of the accompanying temperature changes; as a result a constant error is usually introduced into the measured heat capacity. The method [7], however, combines the advantages of a differential calorimeter [9] with those of steady heating [8]. Essentially, it involves the equalization of the heating rates of two materials, one with a known heat capacity  $C_1$  and the other with an unknown  $C_2$ . The two substances are heated under adiabatic conditions by means of heaters  $R_1$  and  $R_2$ , respectively (Fig. 1a). By varying the resistance of either  $R_1'$  or  $R_2'$  we can achieve equal heating rates when

$$W_1/W_2 = C_1/C_2, \quad (1)$$

where  $W_1$  and  $W_2$  are the respective power outputs of the two heaters. It follows from Eq. (1) that,

$$\frac{C_1}{R_1} (1 + R_1/R_1')^2 = \frac{C_2}{R_2} (1 + R_2/R_2')^2. \quad (2)$$

If the condition demanded by Eq. (1) is not satisfied a temperature gradient will arise between the two substances. By varying  $R_1'$  we can render this gradient very small.

The calorimeter (Fig. 1) consisted of a partitioned copper container containing adsorbent 1 with a total heat capacity  $C_2$  and a large heavy brass cylinder 2 with a heat capacity  $C_1$ . Temperature gradients between the container and the insulating mantle were immediately detected by means of four spiral batteries of copper - constantan thermocouples 3 [10]; each battery contained 1000 junctions and had a sensitivity of  $10^{-6} \text{ }^\circ\text{C}$ . Cylinder 2 served both as a reference material  $C_1$  and as an adiabatic mantle for the container 1.

The calorimeter was placed inside air chamber 4 which was maintained at the same temperature as the mantle by means of a similar set of thermocouples 5 and a heater 6. The optimum heating rate was found to be  $4 \text{ }^\circ\text{C/hr}$ . In all of our experiments, we varied only  $R'_1$ , i.e., the heating rate of the brass mantle  $C_1$ , since it acquired a constant temperature distribution more rapidly. The container with the adsorbent was a poor conductor and hence to maintain a constant temperature distribution the current had to be maintained very steady by means of a PPTN potentiometer (which was attached at points a and b) and a resistance box 8 connected in parallel with the reference resistance 7.

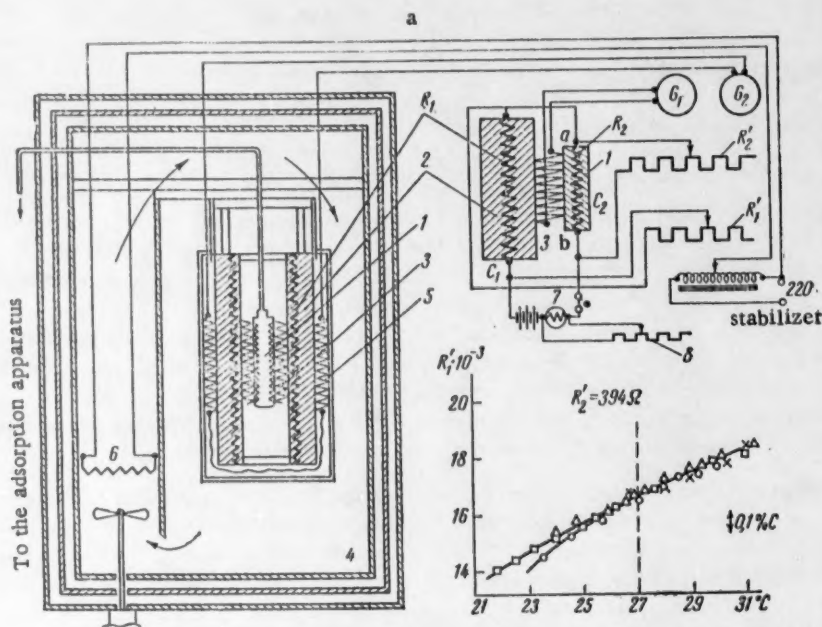


Fig. 1. a) A schematic drawing of the calorimeter and b) some curves of  $R'_1$  vs. temperature.

To find the unknown heat capacity  $C_2$  from Eq. (2) we have to evaluate the  $C_1/R_1$  ratio. To obtain the latter we first calibrated the calorimeter by using compounds of known heat capacities. The  $C_1/R_1$  ratios obtained with various amounts of mercury were verified by measuring the heat capacity of KCl; we get  $0.1621 \text{ cal/mole} \cdot ^\circ\text{C}$  for the latter while the literature value is  $0.1623 \pm 0.0006$  [11]. Before beginning the main experiment, the determination of the heat capacity of the adsorption system, we recalibrated the calorimeter with water at temperatures between 25 and  $30^\circ\text{C}$ .

The values of  $R'_1$  obtained in four such experiments are shown in Fig. 1b.  $R'_2$  was not varied. From the values of  $R'_1$  and  $R'_2$  we determined  $C_1/R_1$  as a function of temperature by using Eq. (2). Subsequent determinations were done at  $27^\circ\text{C}$ .

For our first project we chose an adsorbent with a large specific surface - microporous silica gel No. 8 [12], and a material strongly adsorbed on hydrated silica - water. A 53.56 g sample of silica gel was placed inside container 1 and pumped on for 45 hours at  $110^\circ\text{C}$ . Silica gel has a heat capacity  $c_s = 0.206 \text{ cal/g} \cdot ^\circ\text{C}$ ; that this value exceeds that of quartz by 10% [3] is not surprising if one considers the random orientation of particles which constitute the loose silica gel network and also the surface hydration. The water vapor adsorbed on silica

gel was introduced into the container by means of a vacuum microburette [14]. After each adsorption (or desorption) interval the system was allowed to equilibrate (with small fractions of surface covered, 24 hours, with large, 10-12 hours), the equilibrium relative water vapor pressure  $p/p_s$  was determined, and the heat was turned on.

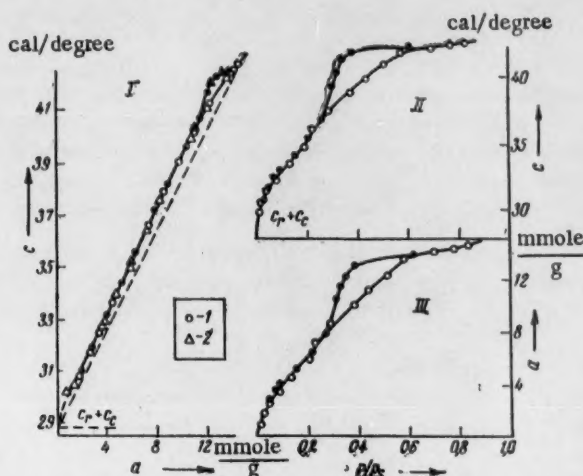


Fig. 2. Changes produced in the heat capacity  $\bar{c}$  of the calorimeter system by the adsorption of water vapor  $\bar{a}$ . I)  $\bar{c}$  as a function of  $\bar{a}$ ; II)  $\bar{c}$  as a function of  $p/p_s$ ; III) adsorption isotherm. 1 and 2 represent two sets of experiments. The solid markings represent desorption.

We could thus measure simultaneously the specific heat as a function of the amount of adsorbed material  $\bar{a}$  and of the ratio  $p/p_s$  and consequently determine the adsorption isotherm. Errors introduced by the absorption

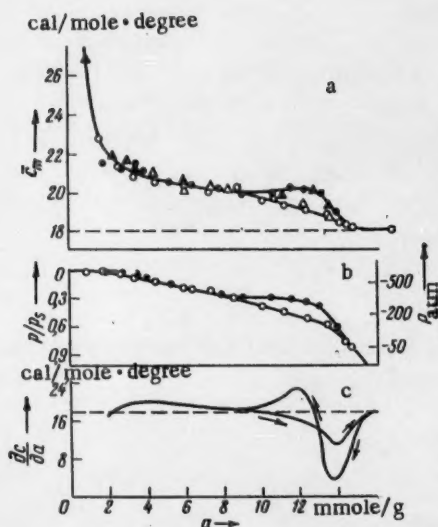


Fig. 3. The heat capacity of adsorbed water as a function of the fraction of surface covered. a) Mean molar heat capacity  $\bar{c}_m$ ; b) adsorption isotherm; c) differential molar heat capacity  $\bar{c}_a$ .

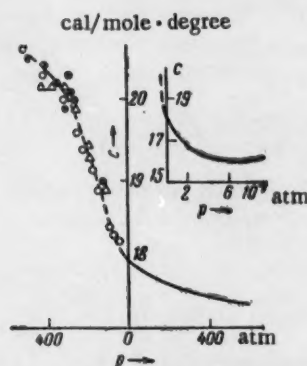


Fig. 4. Heat capacity of water as a function of pressure. The dotted portion of the curve was obtained from data in Fig. 3a and b, while the solid line is reproduced from [17].

of the desorption heat during the heating did not exceed 1% of the heat capacity. The total specific heat of the container, adsorber, and adsorbate could be determined with an error of only 0.05%.

In Fig. 2 we have plotted the heat capacity of the container plus silica gel and adsorbed water ( $c$ ) as a function of  $\underline{a}$  and  $p/p_s$ , and we also included the adsorption isotherm. The heat capacity of our system exceeds the sum of the individual capacities of silica gel and liquid water. The heat capacity isotherm is reversible to a certain point, then it has a hysteresis higher up which resembles the hysteresis observed on the adsorption isotherm.

In Fig. 3a, we have plotted the mean molar heat capacity of adsorbed water  $\bar{c}_m = (c_2 - c_c - c_s)/a$  as a function of the fraction of surface covered  $\underline{a}$ ;  $c_c$  is the heat capacity of the container (17,636 cal/°C and  $c_s$  that of the silica gel (11,154 cal/°C). We assumed that  $c_c$  was independent of  $\underline{a}$ , or in other words, that the difference between the heat capacity of the adsorption system and that of dry silica gel  $c_s$  plus normal liquid water ( $c_l = 18$  cal/°C) was due exclusively to the changed heat capacity of water.

Figure 3a shows that (just as has previously been observed [6])  $\bar{c}_m$  is everywhere greater than 18, and that with increasing  $\underline{a}$  the heat capacity declines, at first very rapidly then gradually and upon saturation becomes almost equal to 18 (the heat capacity of liquid water). This behavior is connected with the complex relationship between  $\underline{a}$  and the differential heat capacity of adsorbed water,  $c_a = \frac{\partial c}{\partial a}$  (Fig. 3c). With increasing  $\underline{a}$  this function passes through a negative minimum; integration of the function  $c_a = f(a)$  yields a value close to 18 cal/mole · °C, indicating that when  $p/p_s = 1$  the water in the pores is in a state very close to that of normal liquid water.

For the sake of comparison, we have also plotted the adsorption isotherms (Fig. 3b and 2, III). Since the heat capacity hysteresis was apparently connected with the capillary-condensation hysteresis, it seemed worthwhile to check if the increase in  $\bar{c}_m$  which accompanies the decline in  $p/p_s$  (or  $\underline{a}$ ) could not have been the result of some changes in the negative pressure  $P$  which the concave menisci at the mouth of each pore (in the silica gel grains) exert on the liquid inside [15].

Figures 2 III and 3b give the values of  $P \approx \frac{\Delta\mu}{v_m} = \frac{RT \ln p/p_s}{v_m}$  [16], where  $\Delta\mu$  is the change in partial molar free energy, and  $v_m$  is the molar value of the liquid (assumed to be independent of  $P$ ). In Fig. 4 we have plotted  $\bar{c}_m$  as a function of  $P$ . In this case the adsorption and desorption points fall on the same curve. This portion of the curve, which gives the heat capacity as a function of liquid expansion, can be extended by using the data given in [17] to give a curve representing heat capacity as a function of liquid compression.

Thus, the heat capacity measurements show that under our experimental conditions the adsorbate exists in the pores in the form of a strongly expanded liquid.\* We would like to point out that capillary condensation makes it possible to measure the heat capacity of a liquid under high negative pressures.

The large  $\bar{c}_m$  at low  $\underline{a}$  seems to be due to a great degree of vibrational freedom and extensive migration of water molecules in the adsorption complexes formed on the surface of silica gel.

The authors express their gratitude to N. N. Avgul' and I. A. Lygina for their interest in the work and assistance rendered toward its completion.

#### LITERATURE CITED

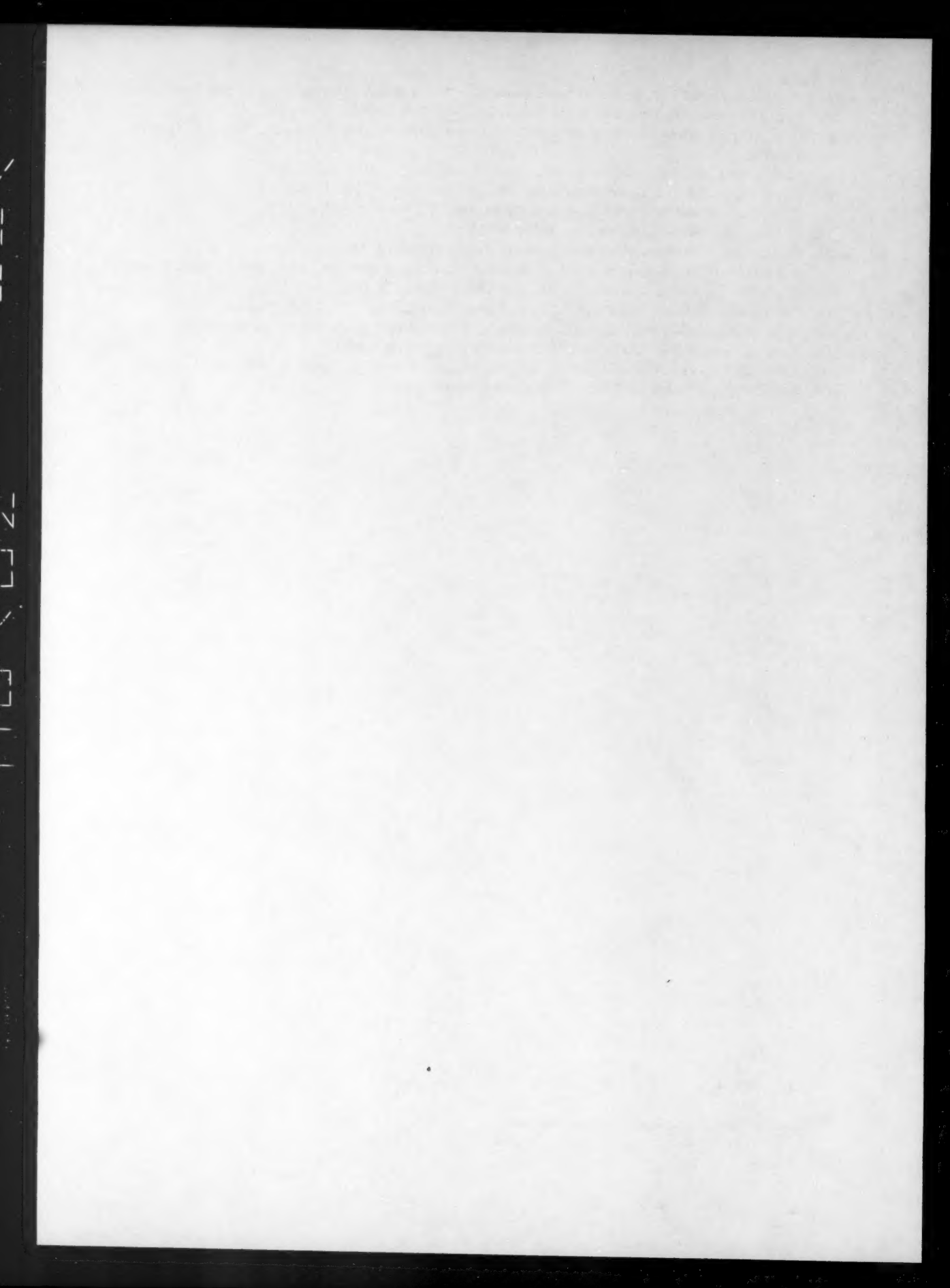
1. A. V. Kiselev, *Vestnik Akad. Nauk SSSR* 10, 43 (1957).
2. A. V. Kiselev and D. P. Poshkus, *Doklady Akad. Nauk SSSR* 132, 876 (1960).\*\*
3. N. N. Avgul', A. V. Kiselev, I. A. Lygina, and D. P. Poshkus, *Izvest. Akad. Nauk SSSR, Otdel Khim. Nauk* 1314 (1957);\*\* 1196 (1959).\*\*

\* The same explanation has previously been used to explain the maximum heat of absorption at the completion of capillary condensation [14, 15].

\*\* Original Russian pagination. See C. B. translation.

4. A. V. Kiselev and V. I. Lygin, *Kolloid. Zhur.* 22, 403 (1960);\* 23 (1961) [to be published].
5. L. E. Drain and J. A. Morrison, *Trans. Farad. Soc.* 49, 654 (1953).
6. G. L. Kington, *The Structure and Properties of Porous Materials*, Ed. D. Everett, F. Stone (London, 1958) p. 247.
7. G. I. Berezin, *Izvest. Akad. Nauk SSSR, Otdel Khim. Nauk*, 1143 (1959).\*
8. M. M. Popov and G. L. Gal'chenko, *Zhur. Obshch. Khim.* 21, 2220 (1951).\*
9. T. W. Richards and J. T. Gucker, *J. Am. Chem. Soc.* 47, 1876 (1925).
10. G. I. Berezin, *Zavodskaya Lab.* 4, 484 (1959).\*
11. M. M. Popov, *Thermometry and Calorimetry* [in Russian] (Izd. MGU, 1954).
12. O. M. Dzhigit, A. V. Kiselev, and I. E. Nelmark, *Zhur. Fiz. Khim.* 28, 1804 (1954); L. D. Belyakova, O. M. Dzhigit, and A. V. Kiselev, *Zhur. Fiz. Khim.* 31, 1577 (1957).
13. *Handbook of Chemistry and Physics* (Chem. Rubber Publish. Co., 1955-1956) 37th ed.
14. O. M. Dzhigit, A. V. Kiselev, and G. G. Muttik, *Kolloid Zhur.* 23 (1961) [to be published].
15. A. A. Isrikyan and A. V. Kiselev, *Zhur. Fiz. Khim.* 32, 679 (1958).
16. A. V. Kiselev, *Proc. Second Internat. Congress on Surface Activity* (London, 1957) No. 2, p. 189.
17. P. S. Épshtein, *Thermodynamics* [in Russian] (Moscow, 1948).

\* Original Russian pagination. See C. B. translation.



## AN X-RAY SPECTROSCOPIC STUDY OF TITANIUM BERYLLIDES

É. E. Vainshtein, E. A. Zhurakovskii, and I. B. Staryi

V. I. Vernadskii Institute of Geochemistry and Analytical Chemistry of the Academy of Sciences of the USSR and the K. D. Ushinskii Odessa Pedagogical Institute

(Presented by Academician A. P. Vinogradov, June 16, 1960)

Translated from *Doklady Akademii Nauk SSSR*, Vol. 135, No. 3, pp. 642-644, November, 1960

Original article submitted June 8, 1960

The inadequate understanding of the interatomic forces operating in the transition metal beryllides, the contradictory theories of various workers [1, 2], and the great importance which beryllium alloys have assumed in modern technology [3], all combine to make a thorough study of these compounds a very practical and interesting problem.

The current work was devoted to the investigation of the fine structure in the x-ray absorption and emission spectra of the transition metal in titanium beryllides. The phase diagram of the Ti-Be system has only been examined very superficially, which makes the available data highly questionable in many respects. According to Ehrlich [4] at low Be concentrations (up to 9.1 at. %) solid substitution solutions are formed in titanium which possess a hexagonal crystal lattice very similar to that of pure titanium. Single-phase regions were also observed in alloys containing about 43 and 66 at. % Be. Ehrlich was unable to establish the crystal structure of the first one of the two. The second one corresponds in composition to the intermetallic compound  $\text{TiBe}_2$ , which according to Misch [5] is isomorphous with  $\text{MgCu}_2$  and is related to the so-called Laves phases [6]. It forms a complex cubic lattice ( $c/a = 6.42$ ) with 24 atoms in a unit cell which can be represented as two interlaced subcells, one of only titanium, the other of beryllium atoms. The beryllium atoms are located at the junctions of the tetrahedra which are interconnected through their apices. Each Be is surrounded by six Ti atoms so that the total coordination number of beryllium is 12. Each titanium atom is surrounded by four like atoms and by 12 Be atoms at a slightly greater distance. Hence, the total coordination number of titanium is 16. The phase composition of alloys containing large amounts of Be (more than 80%) is extremely complex. There are some indications that entirely new intermetallic compounds may be formed. According to Rauechle [7] one of these has the formula  $\text{TiBe}_{12}$ . On the other hand, the data of P. I. Kripyakevich and E. I. Gladyshevskii\* indicate that a compound of the composition  $\text{Ti}_2\text{Be}_{17}$  is formed. This compound has a structure of the  $\text{Th}_2\text{Zn}_{17}$  type and resembles structurally  $\text{ThMn}_{12}$ , to which according to [7] the structure of  $\text{TiBe}_{12}$  is also related.

In the present work we examined the x-ray spectra of two well established and thoroughly investigated phases with compositions close to the intermetallic compounds of the TiBe and  $\text{TiBe}_2$  type. For the samples, which were prepared at the Institute of Metaloceramics and Special Alloys of the Academy of Sciences Ukrainian SSR, we are deeply indebted to G. V. Samsonov. Both alloys were made by sintering a mixture of titanium metal and beryllium. The two components were combined together at the proper ratio, mixed thoroughly for 2 hours, passed through a sieve, and compressed into ingots at a pressure of 1000 kg/cm<sup>2</sup>. The

\* Private communication.

resulting ingots were placed into a quartz cylinder inside a resistance furnace and maintained for one hour in an atmosphere of argon at 1200° C. A control chemical analysis of the sintered material indicated that the actual concentration of beryllium was in good agreement with the calculated. In Table 1 we have listed the concentrations of impurities detected by optical spectroscopy in the original titanium and in the alloys.

TABLE 1

	Mg	Al	Si	Mn	Fe	Cu
Ti <sub>met</sub>	0,01	0,01	0,01	—	0,02	0,0001
TiBe	0,01	0,03	0,01	0,003	0,03	0,01
TiBe <sub>2</sub>	0,03	0,03	0,02	0,003	0,05	0,01

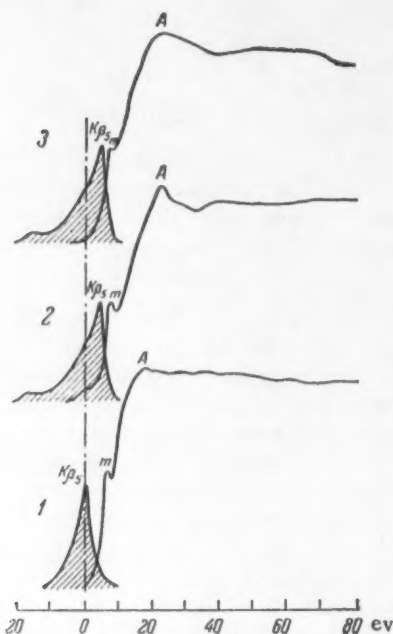


Fig. 1. X-ray K absorption spectra and  $K\beta$  emission bands of titanium: 1) in pure metal; 2) in TiBe; 3) in TiBe<sub>2</sub>.

lengths by more than three times as much as in the first absorption edge, the short-wave tail of the emission band and the absorption edge of titanium overlap much more in the spectra of beryllides than they do in the spectrum of pure titanium metal; moreover the distance between the  $K\beta$ -band maximum and point m in the absorption spectrum is appreciably reduced in the alloys. It has also been found that the  $K\beta$  emission band of titanium becomes much wider in beryllides and that its asymmetry increases; at the same time there are some noticeable changes in the relative intensities of various portions of the main absorption edge of titanium which are connected with transitions of the 1s' electrons (of the metal) into various zones of common 3d and 4sp energy bands in the alloy. The energy of the absorption maximum A increases appreciably (approximately 5 ev) in beryllides; this maximum arises from the transition of a photoelectron into a hybridized energy band (of the alloy) with a predominant p-symmetry. It is quite probable that the remarkable increase in the energy of the 4p state of titanium observed in the alloys results from the 5% shortening of the Ti-Ti distance (the distance in the beryllides is 0.15 Å shorter than in pure metal). The shift of point A in the absorption spectra of these titanium alloys is also accompanied by a general increase in the width of the observed K-edge.

We checked the structure of our alloys by comparing their x-ray diffraction patterns with the corresponding literature data [4].

The apparatus and the experimental technique used in our x-ray spectroscopic study have been described elsewhere [8, 9]. We investigated the fine structure in both the absorption spectra and the fluorescence spectra of titanium. In the first case most satisfactory spectra were obtained when a 15 kv 40 ma current was used for 4-6 hours; in the second case, where we studied the fine structure of the  $K\beta$  emission line of titanium, a 20-40 hour exposure at 15 kv and 70  $\mu$ a yielded best results. Under these experimental conditions no substantial re-absorption effects were observed in the fluorescence spectra. In working with the absorption spectra, we used a gold anode, while a chromium anode was used for the fluorescence spectra. The absorption spectra of titanium in the beryllides were recorded on samples in which the absorbing atom had a density of 5 ml/cm<sup>2</sup>. After determining photometrically the intensities at various sites of the spectrum and averaging corresponding values we plotted the relative absorption coefficients as a function of the energy (in ev) of x-ray quanta. The energies could be determined with an accuracy of 0.2 ev.

In Fig. 1 we have placed the absorption and emission spectra of pure titanium metal below the corresponding spectra (first order reflections) of the same element in beryllides of the TiBe and the TiBe<sub>2</sub> composition. The zero on the energy scale was chosen to coincide with the maximum of the  $K\beta$  emission band in titanium metal. It is apparent that in beryllide alloys the  $K\beta$  emission band and the K absorption edge of titanium are both shifted toward shorter wavelengths, with the shift being different for the  $K\beta$ -band and individual points on the absorption edge. The extent of this shift is tabulated in Table 2. Because the emission band is shifted toward shorter wave-

In sharp contrast with all these changes the position and the shape of the K absorption edge in the region of initial absorption (from the beginning of the K-edge to position  $\underline{m}$ ), which is currently believed to be connected with the transition of a K-electron into an unfilled part of a hybridized 3d energy band of titanium, remains practically the same in the beryllides as in the metal. Point  $\underline{m}$  is only slightly shifted (0.5-0.8 ev) toward shorter wavelengths, and the absorption maximum is somewhat less intense in the diberyllide. This last observation can probably be explained by the fact that the dsp energy levels of titanium and beryllium in this alloy overlap much less than they do in alloys containing less beryllium and consequently the probability for a photoelectron transition into the region of common energy bands is decreased. Judging from the position of the long-wave maximum on the investigated edges, the degree of screening produced by the 3d electrons on titanium nuclei seems to be no different in either beryllide from what it is in the pure metal, so that it is impossible to assume that the valence shell electrons of beryllium penetrate the 3d orbital of the transition metal

TABLE 2

	Relative position on the energy scale, ev		
	K $\beta_1$ max.	point $\underline{m}$	point A
Metal	0	6.7 $\pm$ 0.2	17.8 $\pm$ 0.5
TiBe	3.8 $\pm$ 0.2	7.5 $\pm$ 0.2	23.0 $\pm$ 0.3
TiBe <sub>2</sub>	3.8 $\pm$ 0.2	7.2 $\pm$ 0.2	22.6 $\pm$ 0.3

when these alloys are formed. On the contrary, all of the observations pertaining to the fine structure of the x-ray spectra of titanium in these alloys together with the physical properties of these alloys are in full accord with the relative electronegativities of titanium and beryllium and indicate that the best interpretation has to assume true metallic bonding and common sharing of the valence shell electrons of both components of the alloy. At the same time there seems to be very little donor - acceptor type interaction between the 2s electrons of beryllium and the 3d electrons of titanium.

#### LITERATURE CITED

1. U. Dehlinger and G. Schulze, Z. Metallkunde **33**, 157 (1941).
2. G. B. Bokii and É. E. Vainshtein, Izvest. Akad. Nauk SSSR, Ser. Khim. **4**, 241 (1943).
3. V. N. Eremenko, Titanium and Its Alloys [in Russian] (Kiev, 1960).
4. P. Ehrlich, Z. anorg. Chem. **1**, 259 (1949).
5. Z. Misch, Metallwirtschaft **15**, 163 (1936).
6. F. Laves, Crystal Structure and Atomic Dimensions [Russian translation] (1956).
7. R. F. Rauechle and R. E. Rundle, Acta Crystallogr. **5**, 85 (1952); **6** (1), 107 (1953).
8. É. E. Vainshtein and E. A. Zhurakovskii, Izvest. Akad. Nauk SSSR, Otdel Khim. Nauk **8**, 1493 (1959).\*
9. E. A. Zhurakovskii and É. E. Vainshtein, Doklady Akad. Nauk SSSR **129**, 1269 (1959).\*

\* Original Russian pagination. See C. B. translation.

222-1111

## PROTON RELAXATION IN HYDROGEN PEROXIDE SOLUTIONS EXPOSED TO ULTRAVIOLET RADIATION

Corresponding Member of the Academy of Sciences of the  
USSR, V. M. Vdovenko, E. K. Legin, O. B. Stebunov, and  
V. A. Shcherbakov

V. G. Khlopin Radium Institute, Academy of Sciences of the USSR  
Translated from *Doklady Akademii Nauk SSSR*, Vol. 135, No. 3, pp. 645-647,  
November, 1960  
Original article submitted June 23, 1960

Some recent work on the proton relaxation time in aqueous solutions exposed to ionizing radiation has shown that the relaxation times in such solutions become shorter than they were in nonirradiated solutions. Thomas and Duffy [1] have found that the proton relaxation time  $T_1$  in water containing 20% tritium is reduced to one-third its normal value. Vdovenko and Shcherbakov [2] made similar observations in various aqueous solutions irradiated by means of an external or internal  $\beta$ ,  $\gamma$ -ray source. They concluded that the radiolysis of the investigated solutions gives rise to paramagnetic particles, which instead of disappearing as soon as irradiation ceases persist for a considerable length of time. While studying the thermal decomposition of hydrogen peroxide Dekabrun and Purmal' [3] also detected a shortening in the proton relaxation time and attributed the effect to the accumulation of a great amount of  $\text{HO}\cdot$  and  $\text{HO}_2\cdot$  free radicals, the paramagnetism of which interferes with the relaxation time ( $T_1$ ) of the solution protons.

It is a well-known fact [4] that  $\text{H}_2\text{O}_2$  undergoes a rapid decomposition when exposed to ultraviolet radiation and that the photochemically induced chain reaction yields a great number of free radicals. Hence, in view of what has been discussed above the study of proton relaxation in such a system seemed worthwhile. The first results of our work in this field are reported in this communication.

The method used in this work has been described before [2]. Standardized manganese sulfate solutions were used for the determination and calibration of the amplification of our apparatus. Measurements were done on the linear portion of the calibration curve (from  $0.1 \cdot 10^{-4}$  to  $4.0 \cdot 10^{-4}$  M  $\text{Mn}^{++}$ ). Chemically pure  $\text{H}_2\text{O}_2$  was used in all experiments. The reagent was concentrated by distilling the 30% hydrogen peroxide under a 15-20 mm pressure in a quartz apparatus fitted with a fractionation column. The exact concentration was determined by titration with a standardized permanganate solution. A PRK-2 tube without filters served as a radiation source. Experiments were done at room temperature in sealed quartz tubes.

As in the case of thermal decomposition one would expect a decrease in  $T_1$  when  $\text{H}_2\text{O}_2$  is exposed to ultraviolet radiation. And indeed, this was noted even in the preliminary experiments. In Fig. 1, we have plotted several curves showing the growth of the signal (the signal ratio between irradiated and nonirradiated solutions) as a function of radiation time at various concentrations of hydrogen peroxide. All the curves are of the same type and resemble what is known as a "saturation" curve.

Figure 2 shows  $\alpha$ , which represents the "saturation" level on the curves in Fig. 1, as a function of  $\text{H}_2\text{O}_2$  concentration. The curve shows that the effect can be observed over a wide range of concentrations and that its intensity ( $\alpha$ ) behaves in a very distinct manner. The signals were measured both immediately after irradiation

as well as after a time interval required to transfer the sealed tube from the radiation source to the generator loop (5-10 sec). Since free radicals usually have very short half-lives, one would think that if the signal were partially or entirely caused by the paramagnetism of free radicals, it would sharply decline soon after irradiation is stopped. As can be seen in Fig. 3a nothing of the sort was observed; instead, the products responsible for the shortened  $T_1$  do not disappear at once but over an extended period of time. Even if we did have some free radicals left in the irradiated peroxide the apparatus failed to detect any signal changes directly attributable to an increased number of paramagnetic particles (represented by these same free radicals). Since our apparatus could only detect concentrations exceeding  $0.1 \cdot 10^{-4}$  M (the sensitivity was checked with standardized  $Mn^{++}$  solutions), the concentration of free radicals had to be less than  $1.2 \cdot 10^{-4}$  M if we assume an effective magnetic moment  $\mu_N = 1.7 \beta$  (where  $\beta$  is the Bohr magneton; the value was estimated by following the procedure described in [5]).

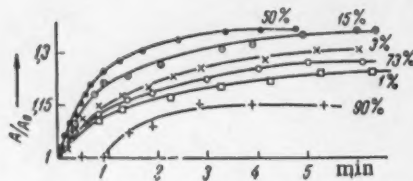


Fig. 1.

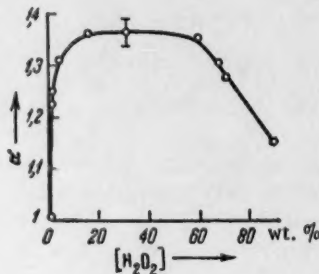


Fig. 2

Thus the detected effect was not caused by the free radicals themselves but by some other products whose origin could be traced to these radicals. It has actually been found that if a small amount of acrylonitrile (which is polymerized by free radicals and thus removes them effectively from solution) is introduced into the peroxide solution before irradiation the relaxation time is still reduced.

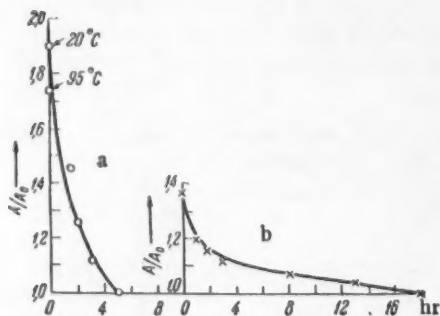


Fig. 3. Decline in signal intensity with time: a) after irradiation is stopped; b) in the case of thermal decomposition.  $H_2O_2$  concentration was the same in both cases.

Experiments involving the thermal decomposition of  $H_2O_2$  (30 %) have shown that the relaxation time is shortened much more than in the case of the photochemical reaction induced by ultraviolet radiation. It is noteworthy that a subsequent drop in temperature (back to the initial) did not restore the initial value of the signal. The manner in which the signal disappears (Fig. 3b) indicates a certain common character in all these effects.

Mechanical agitation of the irradiated peroxide (such as stirring at various rates) reduced the signal at a rate determined by the vigor of the agitation; this effect was observed over the entire range of concentrations studied by us. At the same time bubbles of the oxygen formed in the photolysis were evolved. When we calculated the amount of  $O_2$  needed to account for the observed time  $T_1$  in the irradiated  $H_2O_2$  we found that the investigated solutions had to be strongly supersaturated with oxygen. In solutions of average peroxide

concentration supersaturation could lead to oxygen concentrations 10-20 times the amount dissolved on exposure to air at a pressure of one atmosphere; in the thermal dissociation experiments the supersaturation was even greater (30-50 times).

These estimates were based on the assumptions that the  $\mu_N$  of  $O_2$  in  $H_2O_2$  was the same as in water ( $1.2 \beta$  [6]) and that the solubility of oxygen in  $H_2O_2$  solutions was also the same as in water. Considering that the peroxide solutions are more dense than water the figures given above are probably too low (may have to be increased by a factor of 1.5-2). It is interesting to note that at high  $H_2O_2$  concentrations (70-80%) the heavy evolution of oxygen was not initially accompanied by any noticeable decrease of the signal intensity.

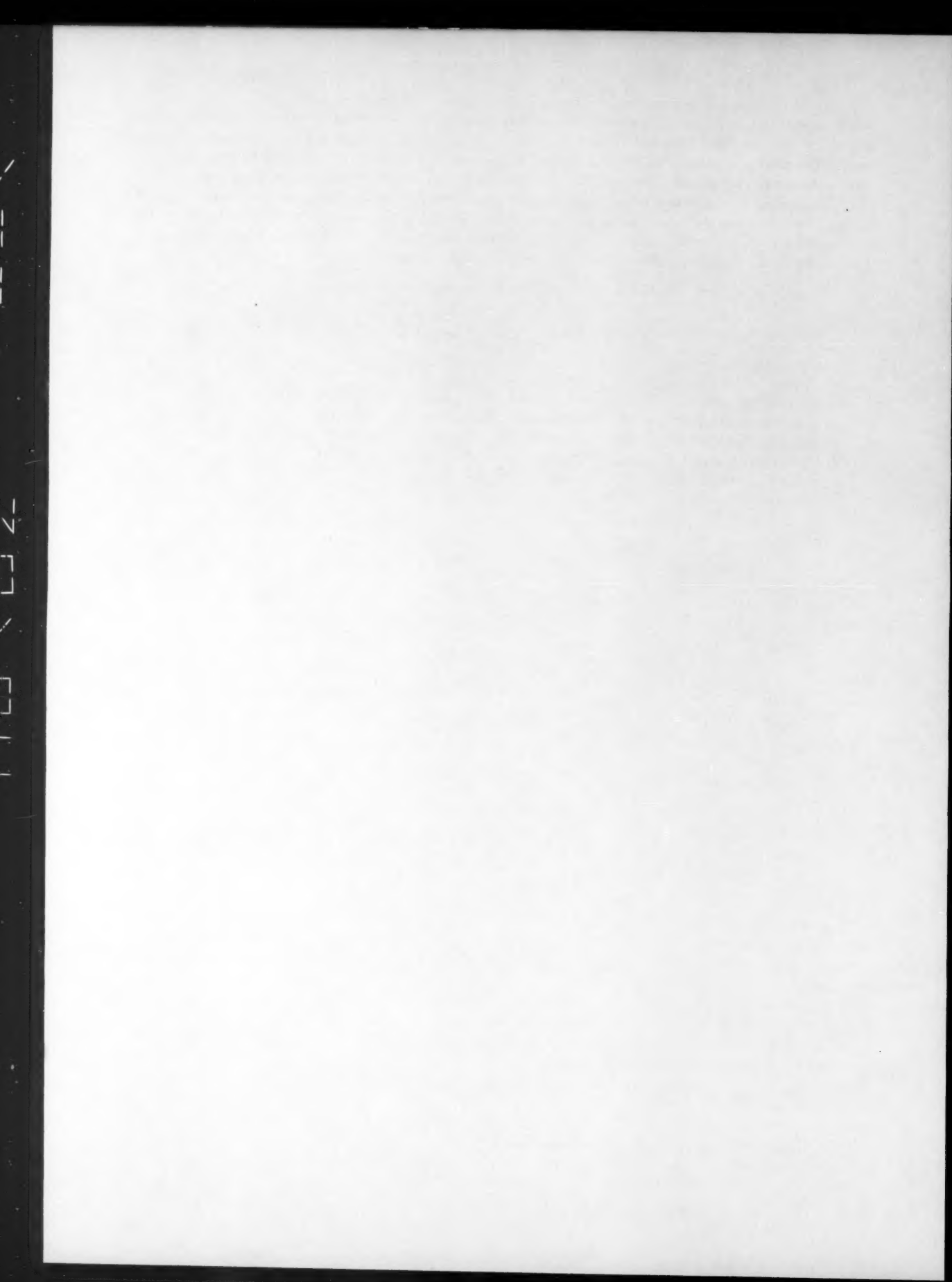
All of our experimental results could be readily explained by attributing the observed effects to the dissolved  $O_2$ . The curves in Fig. 1 would then owe their shape to the supersaturation limits under various conditions. The beginning and the end of the curve shown in Fig. 2 could be attributed to two opposing effects: increasing quantity of oxygen evolved with increasing peroxide concentration and a declining supersaturation level at higher concentrations. However, the curves shown in Fig. 3 seem to indicate the existence of two reactions proceeding at different rates. Right after the irradiation is stopped one notes a sharp decline in signal intensity; subsequently the signal decreases at a moderate rate and disappears entirely after 15-20 hours. Observations are somewhat different in the case of the thermal decomposition of peroxides. It is quite probable that the observed phenomena can not be wholly attributed to the removal of oxygen from solution.

The authors are very grateful to Yu. V. Gurikov for his valuable comments and advice.

#### LITERATURE CITED

1. W. Thomas and J. Duffy, *Bull. Am. Phys. Soc.* **2**, 4, 250 (1959).
2. V. M. Vdovenko and V. A. Shcherbakov, *Doklady Akad. Nauk SSSR* **127**, 127 (1959).\*
3. L. L. Dekabrun and A. P. Purmal', *Doklady Akad. Nauk SSSR* **116**, 983 (1957).\*
4. W. Schumb, C. Satterfield, and R. Wentworth, *Hydrogen Peroxide* [Russian translation] (IL, 1958).
5. V. M. Kozyrev and A. I. Rivkind, *Zhur. Eksp. i Teoret. Fiz.* **27**, 69 (1954).
6. G. Chiarotti and L. Giulotto, *Phys. Rev.* **93**, 1241 (1954).

\* Original Russian pagination. See C. B. translation.



# THE ELECTRICAL CONDUCTANCE OF $\text{MnO}_2$ SEMICONDUCTORS IN THE COURSE OF CATALYTIC OXIDATION OF CO

Zh. P. Kachanova, Corresponding Member of the Academy  
of Sciences of the USSR V. V. Voevodskii, and A. P. Purmal\*

Institute of Chemical Physics, Academy of Sciences of the USSR

Translated from *Doklady Akademii Nauk SSSR*, Vol. 135, No. 3, pp. 648-650,  
November, 1960

Original article submitted June 18, 1959

According to several recent theories there is a definite relationship between the catalytic and electronic properties of semiconductor catalysts [1-13]. In most of the earlier investigations attempts were made to correlate the catalytic activities of various compounds with their electronic properties, which were regulated by varying the stoichiometry or by adding impurities. Considerably less work has been devoted to the investigation of changes produced in the electronic properties of semiconductor catalysts during the catalytic process itself. Among the workers in the field of semiconductor catalysis there is still no consensus of opinion as to whether the reaction itself produces any reversible changes in electronic properties of the catalyst.

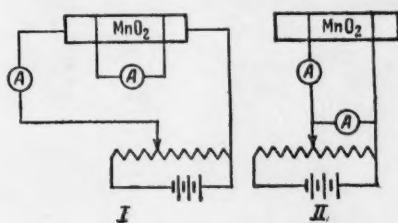


Fig. 1. Circuit diagrams of the apparatus used for the determination of the electrical conductance of  $\text{MnO}_2$ .

According to a general theory developed by one of the authors [14] the catalyzed reaction induces a reversible excited state in the catalyst. Several workers have reported observing [9] a striking increase in the electrical conductance of a catalyst during a reaction. Their effect, however, was connected with certain macrochemical changes produced in the samples. Lyashenko and Stepko [12, 13] have found that the electrical conductance of their catalyst (a  $\text{CuO}$  film) increased in the course of a reaction carried out under conditions precluding any macrochemical changes. In the present work we have undertaken a quantitative study of these effects.

For our study we selected  $\text{MnO}_2$  (a catalyst for the oxidation of CO), since it does not undergo any macrochemical changes in the temperature range used in this work (60-140°C). The experiments were carried out in a vacuum apparatus with automatically regulated pressure; the reactants flowing through the system were recycled after  $\text{CO}_2$  was removed by condensation. The catalyst consisted of electrolytic finely dispersed  $\text{MnO}_2$  with a specific surface of 150  $\text{m}^2/\text{g}$  compressed into a pellet ( $P = 2.5 \text{ tons/cm}^2$ ,  $d = 9 \text{ mm}$ ,  $l = 13 \text{ mm}$ ). The temperature was measured with a chromel-alumel thermocouple which was attached to the side of the pellet by means of a Teflon clamp. In exactly the same way we attached 4 golden contact electrodes for the determination of electrical conductance. Two types of circuits were used in our measurements (Fig. 1); these yielded either  $R_{\text{spec}}$  or  $R_{\text{Au-MnO}_2}$  (the resistance of the surface layer). Our work showed that  $R_{\text{Au-MnO}_2}$  has the same value during the reaction as it does when the reactants are simply adsorbed on the catalyst. Measurements of the Hall effect and of the thermoelectric potential indicated that  $\text{MnO}_2$  is a P-type semiconductor.\* The sample

\* Measurements were carried out by T. I. Kolomenskaya at the Institute of Physics, Academy of Sciences of the USSR.

had a specific resistance ranging from  $0.8 - 2.2 \cdot 10^3 \text{ ohm} \cdot \text{cm}$ .

The preliminary treatment of the samples can be subdivided into two stages. The catalytic activity is very low at first, but it increases after each successive experiment. A sample used in the reaction would have the same electrical conductance as it normally has in vacuo. It is noteworthy that under these conditions the oxygen present in the reaction mixture affected the electrical conductance of the sample only during the reaction whereas normally the adsorption of  $\text{O}_2$  greatly decreases the conductance of a sample. This observation can either be explained by the absence of adsorbed oxygen (adsorption of CO or  $\text{CO}_2$  does not alter the electrical conductance relative to the value in vacuo) or by assuming that at every temperature and pressure the drop in conductance caused by the adsorption of oxygen is compensated by an equivalent increase produced by the reaction. The latter case seems very unlikely. The second stage is characterized by the constant level of catalytic activity under standard processing conditions, namely half an hour of heating under oxygen and half an hour of pumping at  $200^\circ \text{C}$ . The specific effects of  $\text{O}_2$ , CO, and  $\text{CO}_2$  adsorption and of the reaction on the electrical conductance are shown in Fig. 2. The data given in Fig. 2 indicate that the electrical conductance in the course of the reaction greatly exceeds the conductance of the same sample in vacuo. This change  $\sigma$  is reversible; it appears when the reaction mixture is introduced into the system and disappears completely when the mixture is rapidly pumped out. Under the influence of oxygen the electrical conductance decreases considerably, while the adsorption of CO produces a very insignificant increase. The sample had the same electrical conductance activation energy during the reaction as it did in vacuo (2-3 kcal/mole in different sets of experiments). This indicates that no new levels are formed during the reaction; instead, the effective occupancy of some upper levels already present in vacuo is increased.

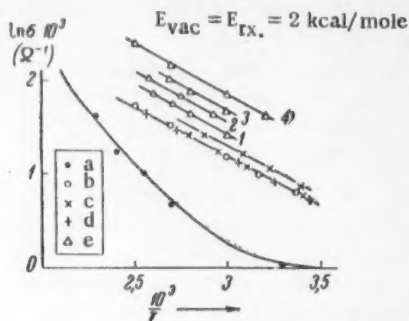


Fig. 2. Variation in the electrical conductance of  $\text{MnO}_2$  with temperature. a) In oxygen; b) in vacuo; c) in carbon monoxide; d) in carbon dioxide; e) in the course of reaction. Stoichiometric mixtures were used in all reactions; 1) 10 mm; 2) 20 mm; 3) 45 mm; 4) 85 mm.

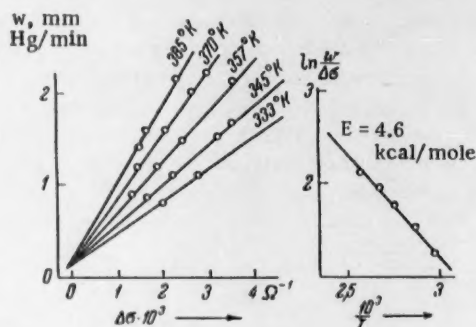


Fig. 3. The increase in the electrical conductance of  $\text{MnO}_2$  (relative to the value in vacuo) as a function of reaction rate at various temperatures.

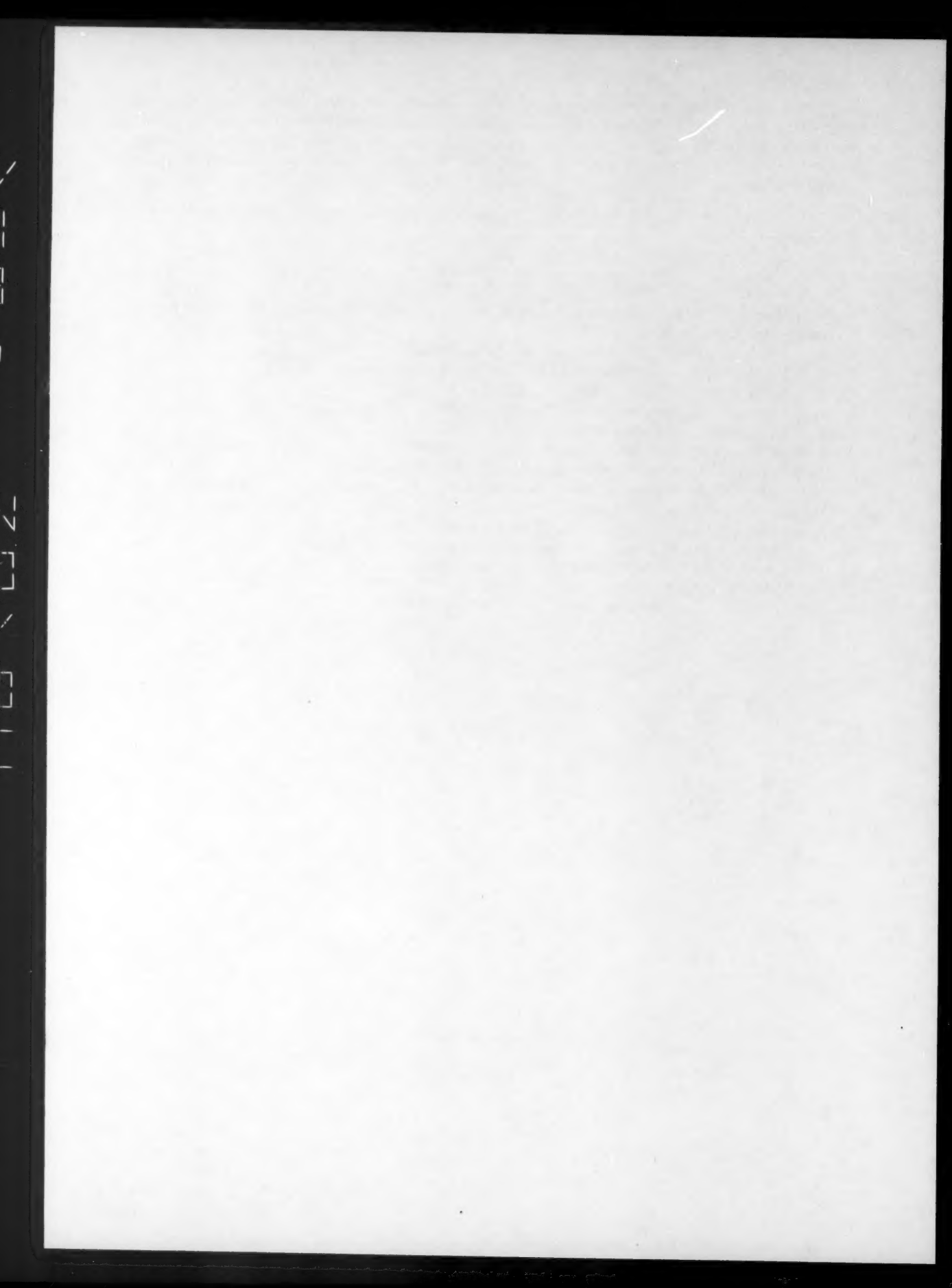
In Fig. 3 we have plotted  $\Delta \sigma$  against  $w$  (rate in arbitrary units) at various temperatures and the ratio  $w/\Delta \sigma$  against reciprocal temperature ( $\Delta \sigma$  is the difference between the electrical conductance during the reaction and the value in vacuo). The  $\Delta \sigma/w$  ratio gives the extent by which the catalyst deviates from the thermodynamic equilibrium state under the influence of the reaction. As the temperature increases so does the rate of energy dissipation processes which lead to the establishment of a thermodynamic equilibrium state, and the  $\Delta \sigma/w$  ratio declines accordingly. Only mixtures in which the CO content was between 30% and 80% gave reactions with  $\Delta \sigma$  linearly dependent on  $w$ ; moreover as the oxygen content of the mixtures was increased  $\Delta \sigma/w$  decreased rapidly making the determination of  $\Delta \sigma$  very difficult in mixtures strongly diluted with oxygen. The decreased  $\Delta \sigma/w$  in experiments involving oxygen-rich mixtures is not connected with the adsorption of oxygen, since the extrapolation of the  $\sigma$  vs.  $w$  line gives  $\sigma_{\text{vac}}$  for  $w=0$ , whereas normally the electrical conductance is appreciably reduced even at very low  $\text{O}_2$  pressures (few hundredths of mm Hg) and results in saturation at 0.1-1 mm. In mixtures with a large excess of CO the relationship between  $w$  and  $\Delta \sigma$  becomes very complex.

Thus our work has clearly demonstrated that a semiconductor catalyst ( $\text{MnO}_2$ ) remains in an electronically excited state during a catalytic reaction ( $\text{CO} + \text{O}_2$ ), or in other words the catalyst does not remain in a state of thermodynamic equilibrium. Under any set of conditions a definite relationship exists between the reaction rate and the extent of deviation from the equilibrium state. During the oxidation of CO on  $\text{MnO}_2$  no oxygen adsorption is observed.

The authors wish to thank B. P. Bruns for kindly providing us with samples of electrolytic manganese dioxide.

#### LITERATURE CITED

1. V. V. Voevodskii, F. F. Vol'kenshtein, and N. N. Semenov, Problems in Chemical Kinetics and Reactivity [in Russian] (1955) p. 423.
2. S. Z. Roginskii, Problemy Kinetiki i Kataliza 8, 5, (1955).
3. F. F. Vol'kenshtein, Problemy Kinetiki i Kataliza 8, 79 (1955).
4. F. F. Vol'kenshtein, Zhur. Fiz. Khim. 23, 917 (1949).
5. F. F. Vol'kenshtein, Zhur. Fiz. Khim. 21, 1317 (1947).
6. F. F. Vol'kenshtein, Zhur. Fiz. Khim. 26, 1962 (1952).
7. F. F. Vol'kenshtein, Zhur. Fiz. Khim. 27, 159, 167 (1953).
8. Coll. Catalysis, Electronic Phenomena [Russian translation] (IL, 1959).
9. L. Bielian'ski, G. Deren', and G. Gabar, Bull. Polish Acad. Sci., Div. 3, 3, 4, 221 (1955); 9, 491 (1955).
10. I. A. Myanikov and S. Ya. Pshezhetskii, Problemy Kinetiki i Kataliza 8, 175 (1955).
11. K. I. Matveev and G. K. Borekov, Problemy Kinetiki i Kataliza 8, 165 (1955).
12. V. I. Lyashenko and I. I. Stepko, Problemy Kinetiki i Kataliza 8, 180 (1959).
13. V. I. Lyashenko and I. I. Stepko, Zhur. Fiz. Khim. 29, 401 (1955).
14. V. V. Voevodskii, Problemy Kinetiki i Kataliza 8, 97 (1955).



# THE INFLUENCE OF TETRAALKYLAMMONIUM SALTS ON THE CAPACITY OF THE DOUBLE LAYER IN BUTYL ALCOHOL SOLUTIONS

P. A. Kirkov

(Presented by Academician A. N. Frumkin, June 17, 1960)

Translated from *Doklady Akademii Nauk SSSR*, Vol. 135, No. 3, pp. 651-654, November, 1960

Original article submitted June 9, 1960

The effects of tetraalkylammonium salts on the electrode processes have already been studied by Frumkin and co-workers [1-3]. The strong adsorption of these cations on a mercury electrode helped explain some of the results obtained in these systems.

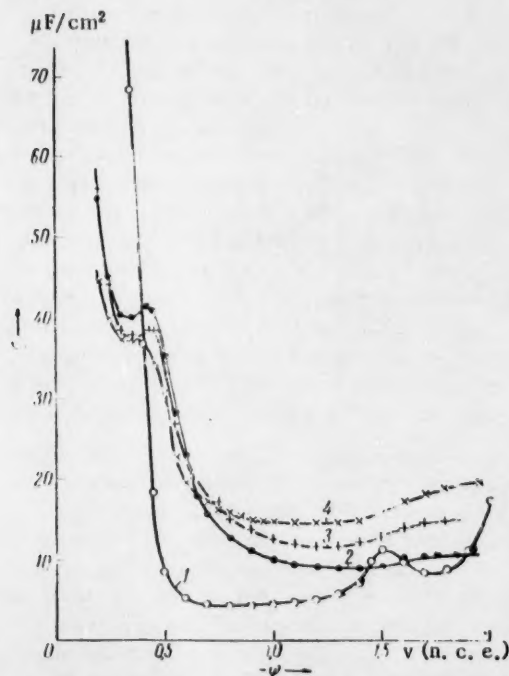


Fig. 1. Differential capacity curves at 750 cps in 0.01 N solutions of: 1)  $N(C_4H_9)_4Br$ ; 2)  $N(C_2H_5)_4Br$ ; 3)  $N(CH_3)_4Br$ ; 4)  $KBr$ .

It seemed worthwhile to examine the combined action of a neutral organic molecule and a surface-active organic cation on the differential capacity. Consequently, an investigation was undertaken to determine the effects of potassium bromide and tetraalkylammonium salts on the capacity of the double layer in the presence of butyl alcohol.

We used a mercury drop electrode and the impedance bridge method [4-7] in our work. A 750 cps alternating current was used. All measurements were carried out at room temperature. A normal calomel electrode (n.c.e.) was used as reference.

All the salts were recrystallized three times from twice-distilled water.  $KBr$  was heated at elevated temperatures, while  $N(CH_3)_4Br$  and  $N(C_2H_5)_4Br$  were dried at 100-120°C, and the samples thus treated gave reproducible results. The differential capacity was measured at three concentrations of the electrolyte: 1, 0.1, and 0.01 N, while the butyl alcohol concentrations were varied from  $5.5 \cdot 10^{-4} M$  to  $5.5 \cdot 10^{-1} M$ . Butyl alcohol was purified in the manner prescribed by Lund and Beirum [8].

The curves of  $C = f(\varphi)$  recorded on a mercury drop electrode in aqueous solutions are plotted in Fig. 1. The capacity at negative polarizations depends on the cations of the supporting electrolyte and declines in the order  $K^+ > [N(CH_3)_4]^+ > [N(C_2H_5)_4]^+ > [N(C_4H_9)_4]^+$  due to increasing cationic radius and decreasing effective

dielectric constant in the electric double layer. One can see in Fig. 1 that the curves of  $C = f(\varphi)$  recorded in solutions of  $N(CH_3)_4Br$  and  $N(C_2H_5)_4Br$  under conditions of low positive surface charge exhibit a small "hump", which is characteristic of aqueous solutions of inorganic salts [9], while the capacity on this portion of the graph increases as one proceeds from  $K^+$  to  $N(C_2H_5)_4^+$ . The reversed order is due to the fact that the specific adsorption of the cation leads to an increased  $Br^-$  concentration in the double layer and consequently to a higher differential capacity.

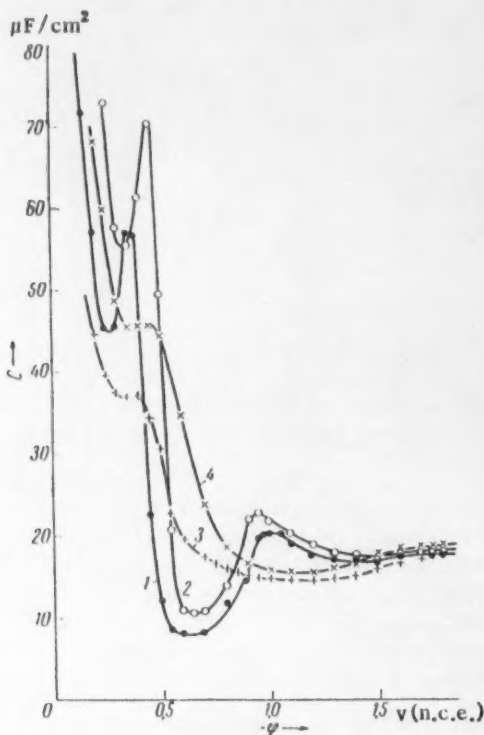
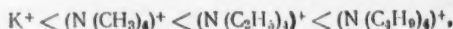


Fig. 2. Differential capacity curves at 750 cps in solutions of: 1) 0.01 N KBr +  $5.5 \cdot 10^{-2}$  M  $C_4H_9OH$ ; 2) 0.1 N KBr +  $5.5 \cdot 10^{-2}$  M  $C_4H_9OH$ ; 3) 0.01 N KBr; 4) 0.1 N KBr.

as the concentration of  $N(C_2H_5)_4Br$  is increased. Addition of butyl alcohol brings out well defined minima on the  $C = f(\varphi)$  curves in the vicinity of the electrocapillary zero and near the adsorption and desorption maxima.

The potentials at which the minima and the adsorption maxima occur, as well as the capacities at these potentials depend on the nature of the supporting cation, and the concentrations of butyl alcohol and the electrolyte (Figs. 2, 3, and 4). Thus, for example, a high concentration of alcohol reduces the capacity at the minimum point and broadens the curve in the vicinity of the minimum, while the adsorption and desorption maxima increase. The magnitude of these effects depends on the electrolyte and supporting cation concentrations: at high concentrations of the supporting electrolyte the capacity at the minimum increases while the curve becomes sharper in that region. Essentially, these effects result from increased  $Br^-$  adsorption at higher electrolyte concentrations. At the same time it is important to consider the various ways in which the supporting cation affects the adsorption of  $Br^-$ . A high butyl alcohol concentration has a progressively diminishing effect on the curve shape as the cation radius increases in the series:



Though an increased concentration of the supporting electrolyte raises the capacity along the positive branch of the  $C = f(\varphi)$  curve, the curve still retains its original shape.

In the case of KBr the curve retains the "hump" at higher concentrations, and the capacity on this portion of the curve is higher due to an increased adsorption of the  $Br^-$  anion. At the same time when the concentration of either  $N(C_2H_5)_4Br$  or  $N(CH_3)_4Br$  is raised (for example from 0.01 to 0.1 N) the "hump" on the capacity curve is replaced by an inflection point.

The specific adsorption of the organic cations somehow leads to increased  $Br^-$  adsorption which is responsible for the observed effects.

The effects of increased supporting electrolyte concentration also show up on the cathode branch of the  $C = f(\varphi)$  curve. In the case of KBr an increase in concentration shifts the minimum toward more negative potentials and increases the capacity over the entire cathode branch of the  $C = f(\varphi)$  curve (Fig. 2). When the  $N(C_2H_5)_4Br$  concentration is raised from 0.01 to 0.1 N the capacity declines over a certain range of potentials, but at large negative polarizations the two curves approach each other (Fig. 3). These observations can be explained in the following way. When we change from KBr to  $N(C_2H_5)_4Br$  an excess of the undissociated dipolar specie  $[N(C_2H_5)_4Br]$  accumulates in the electric double layer displacing water molecules. Apparently this process reduces the dielectric constant inside the double layer and results in decreased capacity over a certain range of potentials

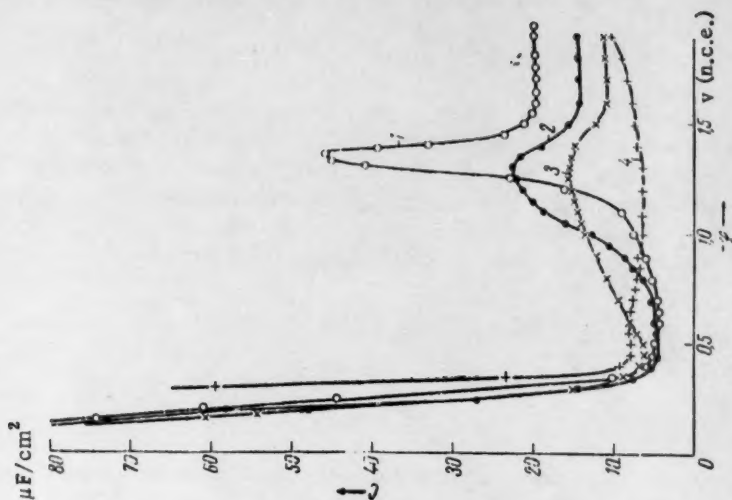


Fig. 4. Differential capacity curves at 750 cps in solutions of:  $5.5 \cdot 10^{-1}$  M  $C_4H_9OH$  with 0.01 N supporting electrolytes; 1) KBr; 2)  $N(CH_3)_4Br$ ; 3)  $N(C_2H_5)_4Br$ ; 4)  $N(C_4H_9)_4Br$ .

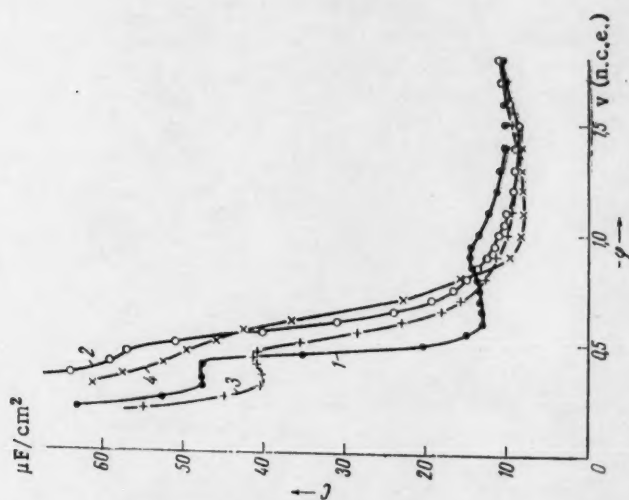
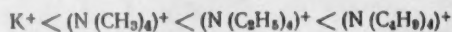


Fig. 3. Differential capacity curves at 750 cps in solutions of: 1) 0.01 N  $N(C_2H_5)_4Br + 5.5 \cdot 10^{-2}$  M  $C_4H_9OH$ ; 2) 0.1 N  $N(C_2H_5)_4Br + 5.5 \cdot 10^{-2}$  M  $C_4H_9OH$ ; 3) 0.01 N  $N(C_2H_5)_4Br$ ; 4) 0.1 N  $N(C_2H_5)_4Br$ .

(Figs. 2, 3, and 4). The relative concentrations of the organic cation and of butyl alcohol can be so chosen as to completely eliminate the minimum on the  $C = f(\varphi)$  curve (Curve 2 in Fig. 3 and curve 4 in Fig. 4).

According to a theory proposed by Frumkin [10], the greater the difference between the capacity in a pure solution of supporting electrolyte and the capacity in a solution to which an organic compound has been added the more thoroughly will the organic compound be desorbed from the mercury surface. On the basis of data presented in Fig. 1 one would expect the desorption of butyl alcohol to be most pronounced when KBr is used as a supporting electrolyte. The capacity decreases with increasing cation radius in the order:



and consequently the desorption of butyl alcohol should become less and less pronounced in the same order. Indeed, as can be seen in Fig. 4, the height of the desorption maximum does decline, while the maximum itself spreads out as we change from  $K^+$  to  $(N(C_2H_5)_4)^+$ , indicating less and less desorption of butyl alcohol. Since the maximum is entirely absent on the curve of  $(N(C_4H_9)_4)^+$ , these cations apparently do not promote the desorption of butyl alcohol, which fact is in full accord with the theory. These effects may possibly also reflect the van der Waals attraction between the hydrocarbon radicals in the tetraalkylammonium ion and the butyl alcohol molecules.

We wish to thank Academician A. N. Frumkin for his interest in this work and B. B. Damaskin for his valuable advice.

#### LITERATURE CITED

1. A. N. Frumkin, V. S. Bagotskii, Z. I. Iofa, and B. N. Kabanov, *The Kinetics of Electrode Processes* [in Russian] (Moscow, 1952).
2. N. V. Fedovich and B. B. Damaskin, *Trans. of the Conference on Corrosion* [in Russian] (Vilnius, 1957) p. 33.
3. B. B. Damaskin, *Dissertation* [in Russian] (MGU, 1959).
4. D. C. Grahame, *J. Am. Chem. Soc.* **63**, 1207 (1941); **68**, 301 (1946).
5. V. I. Melik-Gaikazyan, *Zhur. Fiz. Khim.* **28**, 560 (1952).
6. V. I. Melik-Gaikazyan and P. I. Dolin, *Doklady Akad. Nauk SSSR* **66**, 409 (1949).
7. B. B. Damaskin, *Zhur. Fiz. Khim.* **32**, 2199 (1958).
8. N. Lund and J. Beirum, *Ber.* **64**, B. 210 (1931).
9. D. C. Grahame, *Chem. Rev.* **41**, 441 (1947).
10. A. N. Frumkin, *Z. Physik* **35**, 792 (1926).

# THE ASSIGNMENT OF ELECTRON CONFIGURATION TYPES IN ATOMS

V. M. Klechkovskii

(Presented by Academician V. N. Kondrat'ev, March 26, 1960)

Translated from Doklady Akademii Nauk SSSR, Vol. 135, No. 3, pp. 655-658,  
November, 1960

Original article submitted March 22, 1960

The electron configuration of atoms is intimately connected with the fundamental concepts underlying the theory behind the periodic nature of chemical and certain physical properties of elements (such as atomic spectra) which result from the repetition of a given type of electron configuration in analogous elements. Yet, so far nobody has come up with a function which could be rigorously determined by some physical means and the values of which would at the same time uniquely define all the types of electron configurations found in the periodic system of elements. And it is precisely such a function that we have in mind, a function which would depend on the ground state electron distribution of atoms and consequently assume identical values in elements with analogous electron configurations.

If we started from the scheme known as "the ideal system of elements" [1], which is based on the assumption that the electronic levels of atoms are filled in an order corresponding to the consecutive filling of the electron cloud layers (from the smallest value of the principal quantum number  $n$  to the largest), then the electron configuration of an atom could be related to a number such as the number of valence shell electrons, or under certain circumstances the number of electrons which fill the levels with the highest value of  $n$  for the atoms of a given element. However, in a real periodic system the number of valence shell electrons, as the term is now defined, can not unequivocally define the actual electron configuration that an atom assumes. The reason this is so is that as  $Z$  increases the actual order in which the electronic levels of atoms are filled does not strictly correspond to the ideal system, but is regulated instead by another law which becomes apparent when the quantum levels are grouped together according to the sum of the principal and orbital quantum numbers and is expressed in the rule of consecutive filling of  $(n + l)$ -subshells [2].

With the help of this rule we have managed to solve several problems pertaining to the relationship between  $Z$  and the electron distribution in atoms [3-5]. In this communication an attempt will be made to show how by grouping the quantum levels according to the sum of the principal and orbital quantum numbers one can derive a set of numbers, each with a direct correspondence to the electron configuration type characterizing the atoms (in their ground state) of a given set of analogous elements; this set is valid over the entire periodic system and on the basis of the rule of consecutive filling of  $(n + l)$ -subshells can be rationally expressed as a periodic function of  $Z$ .

We are going to make use of the following terms. Let  $N_{n+l}$  be the number of electrons occupying the levels with the designated principal and orbital quantum numbers of a given atom, and  $E_{n+l}$  will then be the number of free (not filled with electrons) quantum states with the same value of  $n + l$ ; we will define  $E_{n+l}$  as the filling deficiency of a  $(n + l)$ -subshell [6]. We will now use  $\delta_{n+l}$  to denote the filling deficiency of only those  $(n + l)$ -subshells which are already partially filled, or in other words,

$$\delta_{n+l} = E_{n+l}, \text{ when } N_{n+l} > 0. \quad (1)$$

We will now introduce  $\delta_k$  to denote the total filling deficiency of all partially filled  $(n + l)$ -subshells, i.e.,

$$\mathcal{E}_k = \sum \mathcal{E}_{n+l}, \quad (2)$$

where we sum only over those values of  $n + l$  for which  $N_{n+l} > 0$  [see Eq. (1)]. We will call  $\delta_k$  the configuration index for the ground state electron structure of atoms, or simply the configuration index. Accordingly  $\delta_k$  can be defined as the number of missing electrons in the atom required to fill the partially filled  $(n + l)$ -subshell. It can be easily demonstrated that the configuration index  $\delta_k$  assumes the same value for all electronically analogous elements (see Table 1).

TABLE 1

The Configuration Index  $\delta_k$  for the Ground State Electron Structure of Atoms

$\mathcal{E}_k$	Elements	$\mathcal{E}_k$	Elements	$\mathcal{E}_k$	Elements
0	He, Be, Mg, Ca, Sr, Ba, Ra	11	Co, Rh, Ir	22	Dy, Cf
1	H, Li, Na, K, Rb, Cs, Fr	12	Fe, Ru, Os	23	Tb, Bk
2	Ne, Ar, Kr, Xe, Rn	13	Mn, Tc, Re	24	Gd, Cm
3	F, Cl, Br, I, At	14	Cr, Mo, W	25	Eu, Am
4	O, S, Se, Te, Po	15	V, Nb, Ta	26	Sm, Pu
5	N, P, As, Sb, Bi	16	Ti, Zr, Hf	27	Pm, Np
6	C, Si, Ge, Sn, Pb	17	Sc, Y, Lu	28	Nd, U
7	B, Al, Ga, In, Tl	18	Yb (102)	29	Pr, Pa
8	Zn, Cd, Hg	19	Tm, Mv	30	Ce, Th
9	Cu, Ag, Au	20	Er, Fm	31	La, Ac
10	Ni, Pd, Pt	21	Ho, E		

According to the rule of consecutive filling of  $(n + l)$ -subshells the levels of each  $(n + l)$ -subshell become completely filled when the  $s$ -subshell is filled (which yields the  $s^2$  configuration), which leads to an  $\delta_k = 0$  for the ground state of He, Be, Mg, Ca, Sr, Ba, and Ra atoms. The presence of the element He in this series can be justified on the grounds that it has the same configuration ( $s^2$ ) as all the other members, even though the chemical properties require that helium be placed in another group of the periodic system; this constitutes the only instance where elements with the same configuration index are located in different groups of the Mendeleev Periodic System.\*

As we proceed from any of the above-listed elements by increasing  $Z$  and begin to fill the levels of a new  $(n + l)$ -subshell in Li, B, Al, Sc, Y, La, and Ac,  $\delta_k$  increases in discrete steps of integral numbers, and the more  $n, l$ -subshells contained in the respective new  $(n + l)$ -subshell the greater the value of the index. As the levels of each individual  $(n + l)$ -subshell fill up  $\delta_k$  decreases and again becomes zero when all the levels of a particular  $(n + l)$ -subshell (and of all the preceding ones) become filled. From the rule of consecutive filling of  $(n + l)$ -subshells one can derive a mathematical relationship between  $\delta_k$  and  $Z$ . Let  $y$  be a parameter which assumes only such integral values as satisfy the inequality

$$\frac{1}{6} y^3 + y \left( \frac{1}{2} \cos^2 \frac{1}{2} \pi y - \frac{1}{6} \right) < Z \leq \frac{1}{6} (y + 1)^3 + (y + 1) \left( \frac{1}{2} \sin^2 \frac{1}{2} \pi y - \frac{1}{6} \right), \quad (3)$$

\* Let us point out that in certain modified tables of elements, particularly when an attempt is made to show the relationship between the electron distribution in atoms and the position of the elements in the periodic system, helium is placed in Group II [7] or listed twice — in the zero and in the 2nd group.

then

$$\mathcal{E}_k = \frac{1}{6}(y+1)^3 + (y+1)\left(\frac{1}{2}\sin^2\frac{1}{2}\pi y - \frac{1}{6}\right) - Z. \quad (4)$$

The double term appearing on the right-hand side of Eq. (4) and inequality (3) gives the number of non-identical quantum states for all the values of  $n+l$  not exceeding  $n+l=y$ , while the corresponding term on the left-hand side of inequality (3) is the total number of nonidentical quantum states for all the values of  $n+l$  smaller than  $y$  [5, 6]. It should be pointed out that expressions (3) and (4) do not represent a properly chosen combination of empirical formulas connecting  $\mathcal{E}_k$  and  $Z$ , but follow from the definition of  $\mathcal{E}_k$ , the rule of consecutive filling of  $(n+l)$ -subshells, and the Pauli exclusion principle.

When  $\mathcal{E}_k$  is evaluated by means of expressions (3) and (4) (for any  $Z$  within the limits of the real system of elements) it always agrees with the corresponding  $\mathcal{E}_k$  derived from empirical electron distribution data in neutral atoms and defined as the total filling deficiency of all partially filled  $(n+l)$ -subshells. This agreement persists despite the fact that in several instances the electrons become variously redistributed between the  $\underline{d}$  and  $\underline{s}$  or  $\underline{d}$  and  $\underline{f}$ -subshells; the redistribution makes the actual arrangement of electrons in several  $\underline{d}$  and  $\underline{f}$ -subshell elements differ somewhat from that predicted by the usual rules. These small differences (for example,  $d^5s^1$  instead of  $d^4s^2$  in chromium,  $d^{10}s^1$  instead of  $d^9s^2$  in copper,  $d^{10}$  instead of  $d^9s^2$  in palladium,  $f^7d^1$  instead of  $f^8$  in gadolinium, etc.) never go beyond the limits of any set of levels with partially filled  $(n+l)$ -subshells, and hence they do not show up in the value of  $\mathcal{E}_k$ . Thus, the configuration index  $\mathcal{E}_k$  provides a generalized form of the electron configuration type of atoms, since a given  $\mathcal{E}_k$  may stand for several specific configurations which can not be always represented in a similar way (by the number of  $\underline{d}$  and  $\underline{s}$  or  $\underline{d}$  and  $\underline{f}$  electrons) and hence can not always be described by the same principal term symbol. At the same time one encounters certain cases where the different values of  $\mathcal{E}_k$  indicate different configuration types despite an apparent formal analogy. This refers specifically to elements such as Sc, Y, La, Lu, and Ac. Normally, all these five elements could be assigned a  $d^1s^2$  configuration. Yet scandium, yttrium, and lutetium have an  $\mathcal{E}_k = 17$ , whereas lanthanum and actinium have an  $\mathcal{E}_k = 31$ . A close examination of this particular case will show that  $\mathcal{E}_k$  is related to certain properties of the atomic electron cloud which would otherwise be overlooked if the usual designation of configuration type were used.

The difference between the configuration of Sc, Y, and Lu and that of La and Ac can be readily explained by considering not only the filling of levels by electrons but also certain combinations of "vacant" levels. Both La and Ac ( $5d6s^2$  and  $6d7s^2$ , respectively, in their ground state) contain vacant  $\underline{f}$ -levels (4f in La and 5f in Ac) among the levels belonging to a partially filled  $(n+l)$ -subshell, which fact accounts for the very large value of  $\mathcal{E}_k$ . On the other hand, Sc, Y, and Lu do not have any such vacant  $\underline{f}$ -levels in their partially filled  $(n+l)$ -subshells. This is not a strictly formal distinction, since it involves the possibility of a transition from a  $d^1$  ground state to an energetically very close  $f^1$  state in the case of La and Ac, whereas in Sc, Y, and Lu this is not feasible and a transition from a  $d^1$  to a  $f^1$  state would indicate a high degree of excitation.

Consequently a given value of the configuration index  $\mathcal{E}_k$  defines not only the general features of a group of real and different configurations of a single type in a set of analogous elements, but at the same time it also represents certain combined properties of the actual configurations for the ground state and a state close to the ground state of a given element.

In general, it can be stated that just as the number  $Z$  of an atom defines precisely an element regardless of the mass number or the radioactive and other nuclear properties of a given isotope, so the configuration index  $\mathcal{E}_k$  defines precisely the electron configuration type of atoms among analogous elements regardless of any variations in the actual configurations which might arise not only due to different total number of electrons but also sometimes as a result of electron redistribution between  $\underline{d}$  and  $\underline{s}$  or  $\underline{d}$  and  $\underline{f}$ -subshells, provided of course the redistribution does not go beyond the limits of the partially filled  $(n+l)$ -subshells. The introduction of the configuration index concept enables one in all these cases to clearly distinguish a difference between configuration types from the differences between some of the various actual configurations belonging to a particular type.

# LITERATURE CITED

1. A. Sommerfield, Atomic Structure and Spectra [Russian translation] (Moscow, 1956); É. V. Shpol'skii, Atomic Physics [in Russian] (1951), Vol. 2.
2. V. M. Klechkovskii, Doklady Akad. Nauk SSSR 80, 4 (1951); Zhur. Eksp. i Teoret. Fiz. 23, 1 (1952); Yeou Ta, Ann. Phys. 1, 1 (1946).
3. V. M. Klechkovskii, Zhur. Fiz. Khim. 27, 8 (1953); Izvest. Timiryazevskoi Selskokhozyaistvennoi Akad. (1953), No. 1; (1954), No. 2 (6); R. Hakala, J. Phys. Chem. 56, 2 (1952).
4. V. M. Klechkovskii, Doklady Akad. Nauk SSSR 92, 5 (1953); 95, 6 (1954); Zhur. Eksp. i Teoret. Fiz. 26, 6 (1954).
5. V. M. Klechkovskii, Zhur. Eksp. i Teoret. Fiz. 30, 1 (1956); Optika i Spektroskopiya 2, 1 (1957); Izvest. Timiryazevskoi Selskokhozyaistvennoi Akad. 1 (14) (1957).
6. V. M. Klechkovskii, Izvest. Timiryazevskoi Selskokhozyaistvennoi Akad. (1958), No. 5 (24); L. Marson, Nature 177, 4521 (1956).
7. V. I. Semishin, Zhur. Obshch. Khim. 25, 13 (1955).

# THE SATURATED VAPOR PRESSURES OF TETRACHLOROALKANES AT LOW TEMPERATURES

N. A. Malafeev, V. A. Malyusov, N. N. Umnik,

I. V. Podgornaya, and N. M. Zhavoronkov, Corresponding  
Member of the Academy of Sciences of the USSR

L. Ya. Karpov Physicochemical Institute

Translated from *Doklady Akademii Nauk SSSR*, Vol. 135, No. 3, pp. 659-662,  
November, 1960

Original article submitted July 27, 1960

The literature does not as yet contain data on the low-temperature saturated vapor pressures of the various tetrachloroalkanes which are obtained by telomerization of carbon tetrachloride with ethylene. V. M. Olevskii has measured vapor pressures ranging from 2 to 760 mm of Hg for those compounds of this series whose molecules contain 3, 5, 7, and 9 carbon atoms (from  $C_3$  to  $C_9$ ).

The present paper will present data on the saturated vapor pressures for tetrachloroalkanes ranging from  $C_9$  to  $C_{17}$  in the low-pressure interval from  $1 \cdot 10^{-4}$  to  $5 \cdot 10^{-2}$  mm of Hg. Such data are indispensable for calculations on molecular and high-vacuum distillation of mixtures of these compounds. There are various methods which have been widely applied for the determination of the vapor pressures of high-boiling liquids and certain solid materials, e.g., the dynamic method, the effusional method, the Langmuir method, etc. Among these we selected a variant of the static method based on the direct measurement of the force exerted by the vapor on unit surface area. This method was employed, first by Hickman [1] and then by other investigators [2, 3], for measuring the saturated vapor pressures of esters of phthalic and sebacic acids, various plasticators, fats, diffusion pump oils, etc. It has the advantage of being free of those errors which arise in all techniques of determining vapor pressures which require that the accommodation coefficient for vaporization in high vacuum be known and that certain assumptions concerning the structure and degree of association of the vaporized molecules be made.

This method is based on the fact that the apparatus (tensimeter) is constructed in such a manner that the vapors of the working material pass out of a vaporizer through a nozzle covered by a light disk suspended on a fine wire and thereby gives this disk a certain angular displacement.

The movement of the disk from its original "null" position is compensated by rotating the tensimeter through the same angle.

The principal portion of the tensimeter\* (Fig. 1) was prepared from molybdenum glass. The bottom of the tensimeter contained the vaporizer 1 and the nozzle 2, the latter having an internal diameter of 30 mm. The edge of the nozzle was carefully polished.

\* This apparatus for the measurement of vapor pressures was built from plans prepared by the All-Union Scientific Research Vacuum Institute.

The suspension holder 5 was affixed to the end of the molybdenum bar 4, 5 mm in diameter, which was fused into the ground fitting 3. A light duraluminum disk 6, 0.1-0.3 mm thick was attached to this support by two thin molybdenum wires, 35  $\mu$  in diameter, which had been heated in vacuum. The upper portion of the apparatus served as a condenser. The condensate collected in a ring-shaped groove in the condenser and then flowed back into the vaporizer through the thin tube 7 which had a capillary construction. The tensimeter was joined to the vacuum system through the ground connecting joint 8.

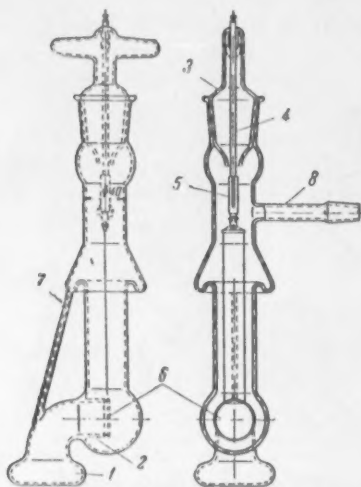


Fig. 1. Tensimeter for the measurement of vapor pressures.

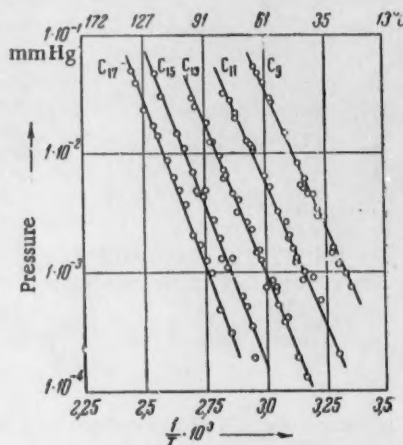


Fig. 2. The temperature dependence of the vapor pressures of tetrachloroalkanes.

The tensimeter was mounted in the socket of a specially constructed swivel head so that it could be rotated smoothly in either of two mutually perpendicular directions. During operation, the tensimeter was immersed in an oil bath whose temperature was held constant to within  $\pm 0.2^\circ \text{C}$ . Observation of the position of the tensimeter disk was carried out through a viewing window in the thermostat wall, using a horizontally mounted long-focus microscope. Vacuum was maintained in the system by a VN-461-M forepump and a two-stage SDN-1 glass oil pump. The accuracy of measurement of the angle of rotation of the tensimeter was increased by reflecting a ray of light from a mirror attached to the head onto a scale. The scale and source of illumination were one meter from the apparatus. The earlier tensimeters were so constructed [1, 2] that the angle of rotation was measured directly on a circular scale with a vernier and the error of measurement was therefore considerable.

Determinations of the vapor pressures of liquids were carried out in vacuum, the pressure of residual gases in the system being less than  $1 \cdot 10^{-4}$  mm Hg. The evaporator was filled with 6-7  $\text{cm}^3$  of the working liquid.

During operation, the tensimeter was rotated into such a position that the effective weight of the disk was just balanced by the pressure of vapors in the vaporizer. The position of the light ray reflected from the mirror was then marked on the scale. The vapor pressure was evaluated from the equation:

$$P = 0,735 \frac{m}{S} \sin \left( \frac{1}{2} \arctg \frac{n_1 - n_0}{Z} \right),$$

$P$  being the vapor pressure in mm Hg,  $m$  is the weight of the disk;  $S$  is the cross-sectional area of the nozzle,  $\text{cm}^2$ ;  $n_0$  is the null-point scale reading at room temperature, in mm;  $n_1$  is the scale reading at the working temperature, in mm; 0.735 is the conversion factor for passage from  $\text{g/cm}^2$  to mm Hg; and  $Z$  is the distance from the mirror to the scale.

Mean values of several readings, all at the same temperature, were substituted for  $n_0$  and  $n_1$ .

The apparatus was given a preliminary test by using it for measurements on substances whose vapor pressures were already known from the literature. Di-2-ethylhexylsebacinate and dibutylphthalate were chosen as standards. The results obtained on these materials agreed quite closely with the data of the literature [1, 3].

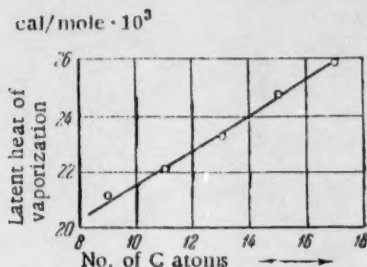


Fig. 3. The dependence of the latent heat of vaporization of tetrachloroalkanes on the number of carbon atoms.

molecular column of the ladder type [4, 5]. The compounds obtained from a second distillation were of adequate purity and had the physicochemical constants shown in Table 1.

TABLE 1

Tetra-chloro-alkanes	Experimental data				Data of the literature			
	$n_D^{20}$	$d_4^{20}$	viscosity at 20°C, centistokes	Molecular wt.	$n_D^{20}$	$d_4^{20}$	viscosity at 20°C, centistokes	molecular weight, calculated
C <sub>9</sub>	1,4820	1,1942	7,57	268,0	1,4821 (°)	1,1856 (°)	7,45 (°)	266
C <sub>11</sub>	1,4813	1,1479	10,95	290,4	1,4827 (°)	1,1476 (°)	11,5 (°)	294
C <sub>13</sub>	1,4807	1,1150	15,6	323,7	1,4801 (°)	1,1166 (°)	14,61 (°)	322
C <sub>15</sub>	1,4802	1,083	21,4	349,0	1,4795 (°)	1,0935 (°)	19,65 (°)	350
C <sub>17</sub>	—	—	26,5	—	1,4795 (°)	1,0773 (°)	21,89 (°)	378

Chromatographic analysis of specimens of the tetrachloroalkanes obtained in this manner was carried out in the State Institute for the Nitrogen Industry and showed the presence of certain contaminants whose peaks on the chromatogram fell between those of the compound under study and those of the tetrachloroalkane with next lower number of carbon atoms. It was not possible to eliminate these contaminants through a second molecular distillation. Thus, it could be assumed that their vapor pressures were approximately the same as those of the working material so that their presence could have no significant effect on the measured values.

The results obtained in the measurements of the saturated vapor pressures of these tetrachloroalkanes are plotted in Fig. 2 in the coordinates  $\lg P$ ,  $1000/T$ ,  $T$  being the absolute temperature. Straight lines drawn through the experimental points could be represented by an equation of the general form:

$$\lg P = -\frac{A}{T} + B.$$

The interval of temperature over which these vapor pressures were measured was narrow (50-60° C) and the latent heat of vaporization could be considered as constant to within the limits of experimental error. Thus  $A = L/2,302 R$ , where  $L$  is the latent heat of vaporization and  $R$  is the molar gas constant, 1,986 cal/° C.

\* V. I. Baranova and N. P. Abramova participated in the preparation of the pure tetrachloroalkanes.

Latent heats of vaporization of tetrachloroalkanes calculated in this way are presented in Table 2. Figure 3 shows the dependence of these values on the number of carbon atoms per molecule. It is clear that the relation between these quantities is very close to being linear.

TABLE 2

Tetra-chloro-alkane	A	B	Latent heat of vaporization, cal/mole
C <sub>9</sub>	4650	12,48	21200
C <sub>11</sub>	4830	12,22	22100
C <sub>13</sub>	5088	12,25	23280
C <sub>15</sub>	5405	12,43	24730
C <sub>17</sub>	5640	12,55	25600

The authors wish to express their indebtedness to M. L. Alashkevich for his valuable advice and counsel in mounting and testing the apparatus used in measuring these vapor pressures.

#### LITERATURE CITED

1. K. C. D. Hickman, J. C. Hecker, and N. D. Embree, *Ind. and Eng. Chem. Anal.*, Ed. 9, 6, 264 (1937).
2. F. H. Verhoek and A. L. Marshall, *J. Am. Chem. Soc.* **61**, 10, 2797 (1939).
3. E. S. Perry, W. H. Weber, and B. F. Daubert, *J. Am. Chem. Soc.* **71**, 11, 3720, 3726 (1949).
4. V. A. Malyusov, N. N. Umnik, and N. M. Zhavoronkov, *Khim. Prom.* 5, 36 (1958).
5. V. A. Malyusov, N. A. Malafeev, N. N. Umnik, D. N. Glazunov, and B. S. Belin, *Zavodskaya Lab.* 5, 629 (1959).
6. G. B. Ovakimyan, M. A. Besprozvannyi, and A. A. Beér, *Khim. Nauka i Prom.* **2**, 1, 13 (1957).
7. A. N. Nesmeyanov, A. A. Karapetyan, E. I. Vasil'eva, and R. Kh. Freidlina, *Doklady Akad. Nauk SSSR* **127**, 2, 345 (1959).\*

\* Original Russian pagination. See C. B. translation.

A STUDY OF THE EFFECT OF ADDITIONS OF DISPERSED  
IRON AS ACTIVE FILLER ON THE PHYSICOMECHANICAL  
PROPERTIES OF POLYMERIC MATERIALS

A. M. Smirnova, L. V. Pevzner, T. V. Raikova,  
and V. I. Likhtman

(Presented by Academician P. A. Rebinder, June 18, 1960)

Translated from *Doklady Akademii Nauk SSSR*, Vol. 135, No. 3, pp. 663-666,  
November, 1960

Original article submitted June 1, 1960

Due to the extensive use of polymer materials in various branches of industry the problem of increasing their heat resistance and strength has become very important.

It is well known that the mechanical properties of high molecular compounds can be considerably improved by adding active fillers. In the papers of Rebinder and co-workers [1-3] it was found that the mechanical properties of polymer systems increased as they were filled with an active filler. The authors of these papers showed that with the introduction of comparatively small amounts of filler the mechanical properties of the system are improved due to strengthening of the spatial structure formed by the macromolecules of the polymer. The active particles of the filler, situated at the points of the space lattice, are centers for the development of this structure. With high degrees of filling (80-90%) of the polymer volume [4] the strengthening action is connected with the formation of coagulation structures in which the polymer practically changes to a state of limiting structure films, distributed between the particles of the filler [5].

Of considerable interest is the use of highly dispersed metallic powders as fillers for polymer materials. It can be assumed that for certain high molecular compounds metal is the most active filler. The presence of a very fine layer of oxide on the metal particles does not noticeably affect the formation of strong adsorption-chemical bonds between the metal and polymer.

In the present work we studied the effect of additions of iron powder on the strength and thermal resistance of some polymer materials. The objects used in the investigation were crystalline polymers - polyamide resin-68, polyethylene (high pressure) and also amorphous phenolformaldehyde resin (resol). The filler was iron powder with a specific surface  $S = 1.2 \text{ m}^2/\text{g}$ , prepared electrolytically (in the A. T. Vagramyan laboratory). To prepare specimens of a certain composition the required amount of iron powder was introduced into the polymer solution. The specimens obtained after extrusion were tested for strength and thermal stability. The strength of extruded specimens of polyethylene and polyamide resin-68 were evaluated from tests in which a 1 mm diameter cylinder was pressed into them. The strength of specimens based on phenolformaldehyde resin was evaluated by the monoaxial compression of the specimens. The thermal stability was judged from the thermo-mechanical curves of compression [6, 7], obtained with a constantly acting load at a rate of heating of  $50^\circ$  per hour.

Figure 1 shows the relationship between the strength of the polymers and the concentration of the iron powder addition. As can be seen from Fig. 1, the additions of filler in all the cases mentioned strengthen the polymer system but the character of the dependence of strength on the concentration of iron powder is different.

Thus, in the case of polyamide resin-68 (curve 1) of the crystalline polymer, with the introduction of 5% iron powder the system is strengthened by about 20%. Further increase in the filler does not affect the strength. In the case of polyethylene (curve 2) in which the amount of the crystalline phase does not exceed 50-75%, at first the strength increases very slightly with increase in the concentration of filler to 60%, after which there is intensive strengthening of the system and the maximum strength corresponds to 85-90% content of filler. The numerical values (85-90%) which we have given for the filling of the polymer system causing the maximum strengthening are relative since the effect of a high degree of filling depends to a large extent on the degree of dispersion of the filler and the method with which it is introduced. Thus, it can be assumed that the vibrating action during the introduction of the filler will considerably improve the properties of the filled polymer.

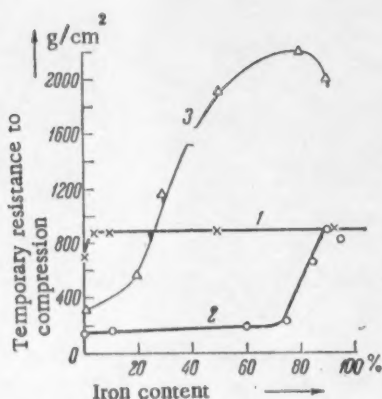


Fig. 1. Mechanical strength of polymer materials in relation to the concentration of the iron powder filler: 1) compositions based on polyamide resin-68; 2) polyethylene; 3) phenolformaldehyde resin (resol).

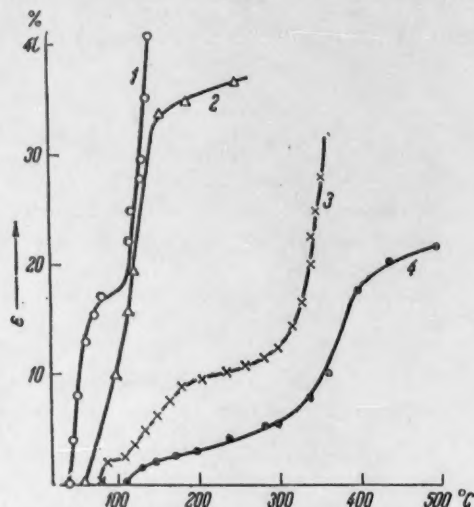


Fig. 2. Relationship between deformation and temperature for a resol resin with varying content of iron powder. 1) 0%; 2) 10%; 3) 50%; 4) 80%.

The strength of specimens based on phenolformaldehyde resin increases in parallel with the increase in concentration of the filler. Considerable strengthening of the system (two-fold) takes place on the addition of 30% filler. With a content of 50% iron powder the strength is increased six-fold. The optimum strengthening of seven-fold corresponds to 75-80% filling. These results show that the mechanism of strengthening of polymer systems varies with the introduction of iron powder filler and depends on the chemical nature of the polymer. The temperature dependence of the deformations of monoaxial compression of polymer specimens filled to varying degrees with iron powder is shown by the thermomechanical curves of Figs. 2 and 3.

Figure 2 gives curves for specimens based on phenolformaldehyde resin. The specific load on the specimen was 8 kg/cm². With increase in concentration of the filler the vitrification temperature ( $T_v$ ) of the material increases, which indicates the formation of transverse chemical bonds between the macromolecules. The deformability of the specimens is sharply reduced. Thus, with increase in temperature the specimen is strongly deformed and at 150° the deformation reaches 40% (curve 1) whereas a specimen which is 10% filled (curve 2) is deformed by 32% at this temperature and a specimen which is 50% filled is only deformed by 8%. Material with 80% filling is deformed by 6% at 300°, and its decomposition occurs after 400°. In the presence of iron powder the formation of a space lattice is apparently accelerated, characteristic for thermo-setting resins at high temperatures. As a result, the material becomes much more thermally stable in the presence of the filler.

Figure 3 shows thermomechanical curves for specimens based on polyethylene. In this case, the load on the specimen was high and was 40 kg/cm², which caused the polyethylene to flow without filler at 40°

(curve 1). With increase in filler content the temperature of "flow" \* was somewhat increased, but the character of the relationship between deformation and temperature remained the same even with 80% filling. Only when starting with a concentration of 90% iron powder was the shape of the curve seriously altered. The deformation of the specimen at 150° was only 8%, after which with further increase in temperature to 400° it became constant. This indicates the sharp change in properties of the material on increasing its thermal stability. This is shown by the curves for heating [8], giving an idea of the phase composition of the polymer. In Fig. 4 the continuous line shows the heating curve for polyethylene without a filler and the dotted line shows polyethylene with 90% iron powder filler. The specimen was preliminarily extruded and heated to 220°. On the dotted curve a new effect appeared at 300°, not present on the continuous curve. It is apparently connected with a phase transformation, the fusion of a specially ordered crystalline phase, which appears in the material when it is filled with iron powder and subsequently extruded.

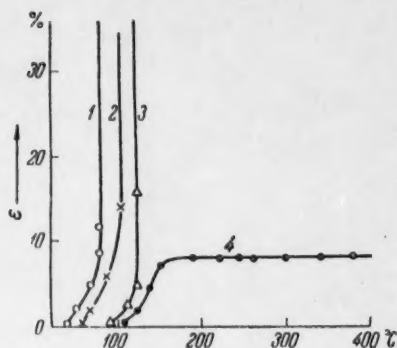


Fig. 3. Relationship between deformation and temperature for polyethylene filled with iron powder. 1) 0; 2) 50; 3) 80; 4) 90 wt. % of iron powder.



Fig. 4. 1) Thermogram of polyethylene (high pressure); 2) thermogram of polyethylene containing 90 wt. % of iron powder.

In these experiments the weight of the specimen remained constant up to 400°. The considerable increase in strength and thermal stability of specimens based on polyethylene, observed only with a high degree of filling, indicates that this is connected with the change in properties of the material, when it is in the state of a limiting ordered orientated film. These films are probably fastened on the surfaces of the solid fillers and are held to them by adsorption-chemical bonds.

#### LITERATURE CITED

1. P. A. Rebinder and V. B. Margaritov, *Zhur. Rezinovoi Prom.* **12**, 991 (1935).
2. P. A. Rebinder, G. A. Ab, and S. Ya. Veiler, *Doklady Akad. Nauk SSSR* **31**, 5, 444 (1941).
3. A. S. Koloanovskaya, P. A. Rebinder, and O. I. Luk'yanova, *Kolloid. Zhur.* **12**, 3, 208 (1950).
4. B. L. Tsetlin, L. P. Yanova, G. K. Sibirskaya, and P. A. Rebinder, *Doklady Akad. Nauk SSSR* **114**, 1, 146 (1957). \*\*

\* Since we did not study the restoration processes after unloading, the temperature of "flow" has an arbitrary character.

\*\* Original Russian pagination. See C. B. translation.

5. B. Ya. Yampol'skii and Wu Shu-ch'iu Kolloid. Zhur. 20, 3, 382 (1958).\*
6. V. A. Kargin and T. I. Sogolova, Zhur. Fiz. Khim. 23, 15, 530 (1949).
7. B. L. Tsetlin, V. I. Gavrilov, N. A. Velikovskaya, and V. V. Kochkin, Zavodskaya Lab. 3, 352 (1956).
8. N. V. Mikhailov and V. O. Klesmok, Kolloid, Zhur. 4, 272 (1954).\*

---

\* Original Russian pagination. See C. B. translation.

# THE PROBLEM OF REDUCING BASICITIES TO A SINGLE STANDARD STATE

## AN INVESTIGATION OF THE BASICITY OF ACETONE

Yu. L. Khaldna and V. A. Pal'm

Tartu State University

(Presented by Academician V. N. Kondrat'ev, June 6, 1960)

Translated from Doklady Akademii Nauk SSSR, Vol. 135, No. 3, pp. 667-670,

November, 1960

Original article submitted May 27, 1960

In considering various problems of the kinetics, mechanism and equilibrium of heterogeneous reactions taking place in solution, it is necessary to know the degree of protonization of the base in the solvent to which a strong acid has been added. This quantity may be calculated if the concentration constant,  $K_{aB}^s$ , of the base B is known under the given conditions:

$$K_{aB}^s = \frac{[B]}{[BH^+]} a_{H^+} \quad (1)$$

together with the value of the activity of the proton,  $a_{H^+}$ . Since no free protons exist in the solution, the quantity  $a_{H^+}$  cannot be given such a direct physical significance as, for example,  $a_{Cl^-}$ . In transferring our attention from one solvent to another, the values of  $a_{H^+}$  cannot in general be equated to the activity of the solvated proton, since we are then dealing with particles of different composition and structure, depending on the nature of the solvent. Hence, the value of  $a_{H^+}$  must be given a distinct significance, which may be performed in the following way [1, 2]:

$$a_{H^+} = K_{aS}^0 \frac{[SH^+]}{[S]} \frac{\gamma_{SH^+}}{\gamma_{0S}} = K_{aB}^0 \frac{[BH^+]}{[B]} \frac{\gamma_{BH^+}}{\gamma_{0B}} = \dots, \quad (2)$$

where  $[S]$ ,  $[B]$ ,  $[SH^+]$  and  $[BH^+]$  are the concentrations of the bases S and B and their respective conjugate acids  $SH^+$  and  $BH^+$ ;  $\gamma_0$  etc. refer to single neutral activity coefficients [3]; and  $K_{aS}^0$  and  $K_{aB}^0$  are the thermodynamic basicity constants of the bases S and B respectively. In the standard solvent, for which purpose water is taken,  $\gamma_{0H_3O^+} = \gamma_{0H_2O} = \gamma_{0B} = \gamma_{0BH^+} = 1$ ,  $a_{H^+} = [H_3O^+]$ , and, consequently,  $K_{aH_2O}^0 = [H_2O]$  and  $K_{aB}^{H_2O} = K_{aB}^0$ .

So as to calculate the value of  $K_{aB}^0$  in any arbitrary solvent S, it is necessary to know the magnitude of  $K_{aS}^0$ ,  $K_{aB}^0$ ,  $K_{aS}^s$ ,  $\gamma_{0S}$ ,  $\gamma_{0B}$ ,  $\gamma_{0SH^+}$  and  $\gamma_{0BH^+}$ , since:

$$K_{aB}^s = \frac{K_{aB}^0}{K_{aS}^0} K_{aS}^s \frac{\gamma_{0S} \gamma_{0BH^+}}{\gamma_{0SH^+} \gamma_{0B}}. \quad (3)$$

In general, numerical values are only known for  $K_{aB}^0$  and  $K_{aS}^s$ . In the case of media for which the concept of the acidity function,  $H_0$ , may be employed, the calculation is considerably simplified because of the fact that the ratios of the type  $\frac{\gamma_B B}{\gamma_{BH^+}}$  are equal for all bases [4]. However, for the majority of organic solvents this condition is not fulfilled, and such a method of calculation can not be employed.

In the current work, the role of the nonstandard solvent has been filled by acetone, and the base B was p-nitroaniline.

Values of  $K_{aB}^0$  for p-nitroaniline at various temperatures are given in [5]. The value of  $K_{aB}^s$  was determined by one of us, together with V. Kh. Malmvere, and is given by:

$$pK_{aB}^s = \frac{7150}{4,575T} - \frac{17,78}{4,575}. \quad (4)$$

We have investigated the basicity of acetone in aqueous solutions with the object of determining  $K_{aS}^0$ . Measurement of the ultraviolet absorption spectrum only permitted of the determination of the order of magnitude of  $K_{aS}^0$  ( $-pK_{aS}^0 = 0.2 - 1.2$ ), since the molar extinction coefficient of the protonized form of acetone does not remain constant with increase in the concentrations of hydrochloric or sulfuric acids [7]. An investigation of the kinetics of the bromination of acetone has given values of  $K_{aS}^0$  of the same order [7, 8]. Having regard for the magnitude of the possible experimental errors, and the approximations which have been made, it is not possible to obtain more precise values of  $K_{aS}^0$  starting with the kinetic data.

In this connection we have worked out a new method for the determination of the basicity of electrically neutral bases in media consisting of water and hydrochloric, and water and sulfuric acids, based on the differing electrical conductivities of the  $H_3O^+$  and  $BH^+$  ions. The experimental work was carried out using the apparatus constructed by V. A. Reiben for the measurement of the conductivity of electrolytes, which permitted of the measurement of the electrolytic resistance under the conditions of our experiments with a sensitivity of  $\pm 5 \times 10^{-3} \%$  at a frequency of  $10^3$  hertz.

The experimental part of the work consisted of the measurement of the resistance of well thermostatted ( $\pm 0.003^\circ$ ) aqueous solutions of hydrochloric or sulfuric acids, both with and without the addition to these of small quantities (1-2%) of the base under investigation, B. The effect of the base B on the electrical conductivity of the acid solution is characterized by the quantity  $\gamma$ :

$$\gamma = \frac{1}{[B]_0} \left( \frac{k}{R_0 + \Delta R} - \frac{k}{R_x} \right) = \frac{1}{[B]_0} (\kappa_1 - \kappa_2), \quad (5)$$

where  $k$  is the cell constant (in  $\text{cm}^{-1}$ );  $[B]_0$  is the concentration of the added base (in mole  $\cdot$  liter $^{-1}$ );  $R_0$  and  $R_x$  are the resistances of the electrolyte before and after addition of the base B;  $\Delta R$  is the change in the resistance of the electrolyte owing to the dilution of the solution (in ohms). In calculating the value of  $\Delta R$ , we used the change in the resistance of the electrolyte when the equivalent quantity of pure water was added instead of the base B. In order to bring the volume of added acetone to the equivalent volume of water, the contraction of the solution was also taken into account. The quantity  $\frac{k}{R_0 + \Delta R} = \kappa_1$  is the expected value of the equivalent conductivity of the solution if the addition of the base B is equivalent in strength to the addition of the equivalent volume of water. The experimentally measured value of the specific conductivity of the solution,  $\frac{k}{R_x} = \kappa_2$ , does not coincide with the expected value  $\kappa_1$ , and the difference,  $\kappa_1 - \kappa_2$ , is proportional to the concentration of the added base B. If we postulate that the difference between  $\kappa_1$  and  $\kappa_2$  is due to the protonization of the base B, we obtain:

$$1000 (\kappa_1 - \kappa_2) = [BH^+] (\lambda_{H_3O^+} - \lambda_{BH^+}), \quad (6)$$

where  $\lambda_{H_3O^+}$  and  $\lambda_{BH^+}$  are the equivalent conductivities of  $H_3O^+$  and  $BH^+$ , respectively. The difference between  $\kappa_1$  and  $\kappa_2$  is due to the difference in the equivalent conductivities of the ions  $H_3O^+$  and  $BH^+$ . As we should expect, it proves that  $\lambda_{H_3O^+}$  is greater than  $\lambda_{BH^+}$ . Substituting Eq. (6) in Eq. (5), we obtain:

$$y = \frac{[BH^+]}{[B]_0} (\lambda_{H_3O^+} - \lambda_{BH^+}) \cdot 10^{-3}, \quad (7)$$

where  $[B]_0 = [B] + [BH^+]$ . It is possible by means of Eq. (7) to determine the value of the ratio  $B/BH^+$  in relationship to the acidity of the medium, if it can be supposed that  $\lambda_{H_3O^+} - \lambda_{BH^+}$  remains practically constant within the range considered for the concentrations of the hydrochloric and sulfuric acids. The value of  $\lambda_{H_3O^+} - \lambda_{BH^+}$  may be determined, if  $[BH^+] \gg [B]$ , and  $[BH^+] \sim [B]_0$ , a situation which obtains in media of acidity  $H_0 < pK_{aB} - 1$ . The value of  $(\lambda_{H_3O^+} - \lambda_{BH^+}) \cdot 10^{-3}$  are taken to be equal to the maximum value of  $y$ , since in certain cases, with further increase in the concentrations of the hydrochloric and sulfuric acids, after the attainment of a maximum value, it is found that  $y$  commences to fall.

TABLE 1

Base Constants for p- and o-Nitroanilines and for Acetone

Base and medium	Temp. ° C	$pK_{aB}^0$	
		electrical conductivity method	spectrophotometric method [5]
p-nitroaniline in the system $H_2O - HCl$	40	+0,90	+0,91
o-nitroaniline in the system $H_2O - H_2SO_4$	60	-0,49	-0,43
Acetone in system $H_2O - HCl$	5	-0,55	
	15	-0,60	
	25	-0,66	
	40	-0,81	

In order to confirm the suitability of the method here described, the values of  $pK_{aB}^0$  have been determined for p- and o-nitroanilines. The results obtained are in good agreement with the values given in [5] (see Table 1 and Fig. 1), which confirms the applicability of the method for determination of the base constants of electrically neutral bases. The method has therefore been used for the determination of the base constant of acetone. The values of  $pK_{aS}^0$  obtained at various temperatures are given in Table 1, and may be expressed by the relationship:

$$pK_{aS}^0 = \frac{2624}{4,575T} - \frac{11,89}{4,575}. \quad (8)$$

The values of  $pK_{aS}^0$  obtained from (8) have been inserted into the equation describing the kinetics of the bromination of acetone [8]. Accounting for the effect of the activity coefficients (that is, taking  $f_{SH} + f_{Cl^-} / f_{\neq} = f_{BH} + f_{Cl^-} / f_B$ ), the values of  $k_1$  have been evaluated. The magnitudes of  $f_{BH} + f_{Cl^-} / f_B$  have been taken from [1]. The greatest deviation of the calculated values of  $k_1$  from the experimental values is found for the region  $-H_0 = 0.5 - 2.0$ , but these do not amount to more than 30% of  $k_{1exp}$  at 35°, nor to more than 50% at 15°. When the activity coefficients are applied, so as to give greater precision, new results are obtained for the values of  $k_{H_2O}$  and  $k_{Cl^-}$ , different from those used in [8]. These are:  $k_{H_2O} = 6.96 \cdot 10^{10} \cdot \exp^{-22340/RT}$ , and  $k_{Cl^-} = 8.20 \cdot 10^6 \cdot \exp^{-15190/RT}$ .

It should be observed that the reaction in which a proton is transferred from  $H_3O^+$  to acetone is not exothermic, as we reported earlier in [8], but endothermic:  $-\Delta H_0 = 2.6$  kcal/mole.

We have also determined values of  $\gamma_{0B}$  for p-nitroaniline, starting from the appropriate values of the solubilities and the distribution coefficients. We have used a "chain" of solutions of p-nitroaniline in the

solvents acetone, glycerol, carbon tetrachloride and water, according to the scheme: pure acetone - (1) - saturated solution of glycerol in acetone - (2) - saturated solution of acetone in glycerol - (3) - pure glycerol - (4) - saturated solution of carbon tetrachloride in glycerol - (5) - saturated solution of glycerol in carbon tetrachloride - (6) - p-nitroaniline (solid phase) - (7) - water. The processes 2, 5, 6, and 7 have been investigated experimentally, while the remainder have been estimated on the basis of the assumption that the solution can be treated as ideal. The values of  $\gamma_{0B}$  so obtained are given in Table 2.

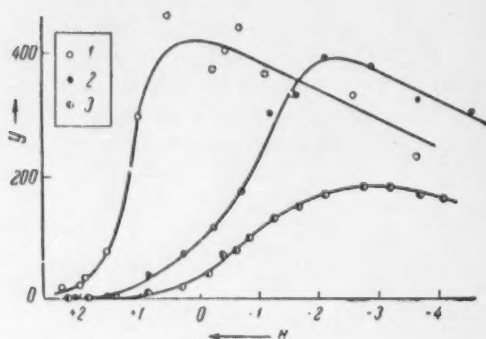


Fig. 1. Relationship between  $\gamma$  and the acidity of the medium. 1) p-Nitroaniline at 40° in the system  $H_2O - HCl$ ; 2) o-nitroaniline at 60° in the system  $H_2O - H_2SO_4$ ; 3) acetone at 25° in the system  $H_2O - HCl$ .

TABLE 2

Values of

Temp. °C	$\gamma_{0B} \cdot 10^3$	$\gamma_{0S}$	$\gamma_{0SH}/\gamma_{0BH^+}$
15,0	0,93	0,70	5700
25,0	1,11	0,67	3550
35,0	1,86	0,64	1500
45,0	3,04	0,61	600

In addition to this we have calculated values of  $\gamma_{0S}$  according to Eq. (9) below, for the equilibrium between the liquid and the vapor in the acetone-water system, taking the appropriate values from [9-12]:

$$\gamma_{0S} = \frac{p_{S0}}{[S]^S} \lim_{[S] \rightarrow 0} \frac{[S]}{p_S}, \quad (9)$$

where  $p_{S0}$  is the pressure of acetone vapor over pure acetone;  $[S]^S$  is the concentration of pure acetone (in mole/liter);  $[S]$  is the concentration of acetone in its aqueous solution (in mole/liter), and  $p_S$  is the pressure of acetone vapor above its aqueous solution. The values obtained for  $\gamma_{0S}$  are given in Table 2.

Using Eqs. (3), (4), and (8), and taking for  $\gamma_{0B}$  and  $\gamma_{0S}$  the values set out in Table 2, we have calculated the values of  $\frac{\gamma_{0SH^+}}{\gamma_{0BH^+}}$ , also given in Table 2. For this purpose the values of  $K_{AB}^0$  are taken from [5].

Thus, the change in value of the dissociation constant of the acid  $p-NO_2-C_6H_4-NH_3^+$  in moving from solutions in water to those in acetone is connected with the changes in the values of all the activity coefficients entering into Eq. (3), in which no mutual compensation takes place in the variations of  $\gamma_{0S}$  and  $\gamma_{0B}$ , on the one hand, or  $\gamma_{0SH^+}$  and  $\gamma_{0BH^+}$  on the other. In this connection, however, the solution of the problem of calculating  $K_{AB}^S$  cannot be obtained with our present insufficient knowledge of the values of  $K_{AB}^0$ ,  $K_{AS}^0$ ,  $K_{AS}^S$ .

$\gamma_{0B}$  and  $\gamma_{0S}$ , and it is necessary to carry out further experimental work to determine these, or the ratio  $\frac{\gamma_{0SH^+}}{\gamma_{0BH^+}}$ .

#### LITERATURE CITED

1. M. I. Vinnik, R. N. Krugnov, and N. M. Chirkov, *Zhur.Fiz. Khim.* **30**, 4, 827 (1956).
2. V. A. Pal'm, *Zhur. Fiz. Khim.* **32**, 2, 380 (1958).
3. N. A. Izmailov, *Doklady Akad. Nauk SSSR* **127**, 1, 104 (1959).\*
4. L. P. Hammett and A. J. Deyrup, *J. Am. Chem. Soc.* **54**, 2721 (1932).
5. A. I. Gel'bshtein, G. G. Shcheglova, and M. I. Temkin, *Doklady Akad. Nauk SSSR* **107**, 1, 108 (1956).\*
6. V. Kh. Maimvere and Yu. L. Khaldna, *Nauchn. Zap. Tartusk. Gos. Univ.* **95**, 37 (1960).
7. Yu. L. Khaldna, *Nauchn. Zap. Tartusk. Gos. Univ.* **95**, 6 (1960).
8. Yu. L. Khaldna, A. I. Tal'vik, and V. A. Pal'm, *Doklady Akad. Nauk SSSR* **126**, 1, 119 (1959).\*

\*Original Russian pagination. See C. B. translation.

9. G. S. Hartley, Trans. Farad. Soc. 27, 26 (1931).
10. D. S. Morton, J. Phys. Chem. 33, 389 (1929).
11. W. G. Beare, G. A. McVicar, and J. B. Ferguson, J. Phys. Chem. 34, 1310 (1930).
12. A. E. Taylor, J. Phys. Chem. 4, 290, 355 (1900).

1123 22

# HYPERFINE STRUCTURE OF THE EPR SPECTRUM IN A ONE-ELECTRON SYSTEM WITH TWO POTENTIAL WELLS

A. I. Burshtein

Institute of Chemical Kinetics and Combustion, Siberian Branch of the  
Academy of Sciences of the USSR

(Presented by Academician V. N. Kondrat'ev, June 13, 1960)

Translated from *Doklady Akademii Nauk SSSR*, Vol. 135, No. 4, pp. 886-889,  
December, 1960

Original article submitted June 8, 1960

We will consider an electron in a system of two symmetrical potential wells (Fig. 1), for which the Hamiltonian has the form

$$H_0 = \hat{H}_0 + \hat{H}'; \quad (1)$$

$$\hat{H}_0 = \hat{E}_0 - \beta_0 \hat{S}_z H_z - \beta \left[ \sum_{l=1}^{n'} I_z^l H_z + \sum_{l'=1}^{n'} I_z^{l'} H_z \right], \quad (2)$$

$$\hat{H}' = \hat{V} + \hat{R} = \hat{V} - \frac{16\pi\beta_0\beta}{3c} \left[ \sum_{l=1}^n \delta(\mathbf{r} - \mathbf{r}_l) \hat{S}_l \hat{I}_z^l + \sum_{l'=1}^{n'} \delta(\mathbf{r} - \mathbf{r}_{l'}) \hat{S}_l \hat{I}_z^{l'} \right]. \quad (3)$$

The first term in (2) represents the operator for the orbital movement of an electron in a separate well, the second gives the interaction between the magnetic moment  $\beta_0 \hat{S}$  of the electron and the constant external magnetic field  $H_z$  and the third is the energy of the nuclear magnetic moments  $\beta_l \hat{I}^l$  in this same field; the index  $l$  marks the nucleus in the right potential well and  $l'$  that in the left one. The first term in the perturbation operator represents the additional small energy resulting from the presence of the adjacent well and this energy can be treated as a perturbation, because the barrier is supposed to be high. The remainder  $\hat{R}$  of the perturbation is connected with the hyperfine interaction between the electron spin and the nuclei. It is supposed that we have to deal with pure spin magnetism and in the hyperfine interaction only the Fermi contact term occurs.

We will choose the eigenvectors of the operators  $\hat{E}_0, \hat{S}_z, \hat{I}_z^l, \hat{I}_z^{l'}$  as a starting point and characterize them by  $\psi(k, s, i_l, i_{l'})$ , where  $s, i_l$  and  $i_{l'}$  are the eigenvalues of the operators  $\hat{S}_z, \hat{I}_z^l$ , and  $\hat{I}_z^{l'}$  and  $k$  can take only the values 1 and 2 corresponding to the two possible coordinate functions

$$\psi_1(\mathbf{r}) = \frac{1}{\sqrt{2}} [\psi(\mathbf{r}) + \psi(-\mathbf{r})], \quad \psi_2(\mathbf{r}) = \frac{1}{\sqrt{2}} [\psi(\mathbf{r}) - \psi(-\mathbf{r})], \quad (4)$$

where  $\hat{E}_0 \psi(\pm \mathbf{r}) = E_0 \psi(\pm \mathbf{r})$ .

In this representation the Hamiltonian of the unperturbed problem is diagonalized and each of its terms are doubly degenerate with respect to the orbital quantum number  $k$ :

$$\langle k, s, i_l, i_{l'} | \hat{H}_0 | k', s', i'_l, i'_{l'} \rangle = \left\{ E_0 - \beta_0 H s - \beta H \left[ \sum_{l'=1}^n i_l + \sum_{l'=1}^{n'} i_{l'} \right] \right\} \times \\ \times \delta_{kk'} \delta_{ss'} \delta_{i_l i'_l} \delta_{i_{l'} i'_{l'}}. \quad (5)$$

Of course, the matrix of the operator  $\hat{V}$  is diagonal with respect to all spin variables. Moreover, because the coordinate wave functions have been chosen in the form of (4), the said matrix is also diagonal in the variable  $\underline{k}$ , since

$$\langle k, s, i_l, i_{l'} | \hat{V} | k', s', i'_l, i'_{l'} \rangle = (-1)^k b \delta_{kk'} \delta_{ss'} \delta_{i_l i'_l} \delta_{i_{l'} i'_{l'}} \quad (6)$$

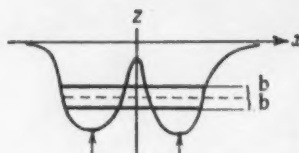


Fig. 1

and under certain known conditions the value of  $b$  can be calculated quasiclassically [2]. Generally, the interaction with the internal field is much stronger than the hyperfine coupling (Paschen-Back effect) and, therefore, the product  $\hat{S}\hat{I}^l$  in the operator  $\hat{R}$  permutes with  $\hat{S}_z \hat{I}_z^l$ . This makes the operator  $\hat{R}$  diagonal in the variables  $\underline{s}, \underline{i}$  and  $i_{l'}$  and by a straightforward calculation using (3) and (4) its elements which are different from zero are found to be equal to:

$$\langle k, s, i_l, i_{l'} | \hat{R} | k, s, i_l, i_{l'} \rangle = \sum_{l=1}^n \delta_l s i_l + \sum_{l'=1}^{n'} \delta_{l'} s i_{l'}; \quad (7a)$$

$$\langle k, s, i_l, i_{l'} | \hat{R} | k', s, i'_l, i'_{l'} \rangle = \sum_{l=1}^n \delta_l s i'_l - \sum_{l'=1}^{n'} \delta_{l'} s i_{l'} = t(s, i_l, i'_{l'}); \quad (7b)$$

the hyperfine structure constants

$$\delta_l = -\frac{16\pi\beta_0\beta}{3c} \frac{1}{2} |\psi(r_l)|^2 > 0; \quad \delta_{l'} = -\frac{16\pi\beta_0\beta}{3c} \frac{1}{2} |\psi(r_{l'})|^2 \quad (8)$$

correspond to an electron equally distributed over both wells.

The energy spectrum of the system is found by solving the secular equation. Since  $H'$  is diagonal in all spin variables, this means that the appropriate coordinate functions  $\psi^0(\underline{r}, \underline{s}, i_l, i_{l'})$  of the zero order approximation and the corresponding energy corrections  $\Delta E(\underline{r}, \underline{s}, i_l, i_{l'})$  must be sought. The variable  $\underline{r}$ , just as  $\underline{k}$ , takes only the two values 1 and 2; it quantizes the total energy  $H$ .

Because of (6) and (7) the secular equation has the form

$$\begin{vmatrix} -b + \sum_{l=1}^n \delta_l s i_l + \sum_{l'=1}^{n'} \delta_{l'} s i_{l'} & t(s, i_l, i'_{l'}) \\ t(s, i_l, i'_{l'}) & b + \sum_{l=1}^n \delta_l s i_l + \sum_{l'=1}^{n'} \delta_{l'} s i_{l'} \end{vmatrix} = 0. \quad (9)$$

The energy corrections are [1]:

$$\Delta E(1, s, i_l, i_{l'}) = \sum_{l=1}^n \delta_l s i_l + \sum_{l'=1}^{n'} \delta_{l'} s i_{l'} - \sqrt{b^2 + t^2}; \quad (10a)$$

$$\Delta E(2, s, i_l, i_{l'}) = \sum_{l=1}^n \delta_l s i_l + \sum_{l'=1}^{n'} \delta_{l'} s i_{l'} + \sqrt{b^2 + t^2}, \quad (10b)$$

and the elements of the matrix  $C_k^T$ , which accomplishes the canonical transformation of the initial state to that sought for, are:

$$C_1^1 = \sqrt{\frac{t}{2|t|} \left[ 1 + \frac{b}{\sqrt{b^2 + t^2}} \right]}; \quad C_2^1 = -\sqrt{\frac{|t|}{2t} \left[ 1 - \frac{b}{\sqrt{b^2 + t^2}} \right]}; \quad (11a)$$

$$C_1^2 = \sqrt{\frac{t}{2|t|} \left[ 1 - \frac{b}{\sqrt{b^2 + t^2}} \right]}; \quad C_2^2 = \sqrt{\frac{|t|}{2t} \left[ 1 + \frac{b}{\sqrt{b^2 + t^2}} \right]}. \quad (11b)$$

The denotations have been chosen in such a way that at  $b \gg t > 0$  the new representation coincides with the old one

$$\psi^0(r, s, i_l, i_{l'}) = \sum_{k=1}^2 C_k^r \psi(k, s, i_l, i_{l'}) = C_1^r \psi(1, s, i_l, i_{l'}) + C_2^r \psi(2, s, i_l, i_{l'}). \quad (12)$$

From (12), (11), and (4) it follows that at  $b \gg t$  the stationary wave function corresponds to an electron equally distributed over both wells and at  $b \ll t$  to an electron localized in only one of them. At  $t = 0$  ( $\sum_l^n \delta_{il} = \sum_{l'}^{n'} \delta_{l'i_{l'}}$ ) the electron is always equally distributed over both wells regardless of the value of  $\underline{b}$ .

We are interested in the electron transitions which in the system considered are induced by a variable magnetic field. In this case  $\beta_0 H_x(t) \hat{S}_x$  is the time dependent part of the Hamiltonian and, in accordance with the correspondence principle, the intensities of the induced spectral lines are determined by the relation

$$I(r, s, i_l, i_{l'} \rightarrow r', s', i'_l, i'_{l'}) = \gamma |\langle r, s, i_l, i_{l'} | \hat{S}_x | r', s', i'_l, i'_{l'} \rangle|^2 = \\ = \gamma |\langle r | r' \rangle_s|^2 \delta_{ss' \pm 1} \delta_{i_l i'_l} \delta_{i_{l'} i'_{l'}} \quad (13)$$

where because of (12) and the orthogonality of  $\psi(k, s, i_l, i_{l'})$

$$\langle r | r' \rangle_s = 2\psi^{0*}(r, s, i_l, i_{l'}) \hat{S}_x \psi^0(r', s \pm 1, i_l, i_{l'}) = \\ = C_1^r(s) C_1^{r'}(s \pm 1) + C_2^r(s) C_2^{r'}(s \pm 1). \quad (14)$$

According to (11), (13), and (14), only those transitions which satisfy the selection rules  $\Delta i_l = \Delta i_{l'} = 0$ ,  $\Delta s = \pm 1$  are allowed and they belong to two separate groups with intensities

$$I_{i_l, i_{l'}}(r | r) = \gamma \frac{b^2}{b^2 + t^2}, \quad (15a)$$

$$I_{i_l, i_{l'}}(r | r') = \gamma \left( 1 - \frac{b^2}{b^2 + t^2} \right). \quad (15b)$$

It is striking that within each group the intensity of all lines is not equal but depends via  $t(1/2, i_l, i_{l'})$  upon the orientation of the nuclear spins in the molecule which undergoes a given transition. Meanwhile, however, the total intensity corresponding to a given  $\underline{t}$  is constant:  $I_{i_l, i_{l'}}(r | r) + I_{i_l, i_{l'}}(r | r') = \gamma = \text{const}$ . It is evident that formulas (15) give only the integrated intensities of the hyperfine spectral components, which at a monochromatic excitation have a resonance character with a width depending upon relaxation processes.

Obviously, the frequencies of the lines which belong to the two separate groups are equal to

$$h\nu_{i_l, i_{l'}}(1 | 1) = \beta_0 H_x + \sum_{l=1}^n \delta_{li_l} + \sum_{l'=1}^{n'} \delta_{l'i_{l'}} = h\nu_{i_l, i_{l'}}(2 | 2); \quad (16a)$$

$$\begin{aligned}
h\nu_{i_l i_{l'}}(1|2) &= \beta_0 H_z + \sum_{l=1}^n \delta_l i_l + \sum_{l'=1}^{n'} \delta_{l'} i_{l'} - 2\sqrt{b^2 + t^2}; \\
h\nu_{i_l i_{l'}}(2|1) &= \beta_0 H_z + \sum_{l=1}^n \delta_l i_l + \sum_{l'=1}^{n'} \delta_{l'} i_{l'} + 2\sqrt{b^2 + t^2}.
\end{aligned}
\tag{16b}$$

To illustrate the results the spectra of a system having only one nuclear spin  $i$  and  $i'$  with the value  $1/2$  in each potential well is shown in Fig. 2 for the three different cases:  $b \gg t$ ,  $b = t$ ,  $b \ll t$ . The outer lines in these spectra belong to allowed transitions of the second group [formulas (15b) and (16b)] and the other ones to the first group [formulas (15a) and (16a)], while the center of the spectrum is taken by two transitions whose frequencies coincide. As  $b$  decreases, the latter transitions become forbidden and the central line disappears, while the outer lines, on the other hand, increase in intensity and converge to the two median lines with which they are united at  $b \rightarrow 0$ . The lines with varying intensities (the central and the outer ones) are connected with transitions in which  $i = -i'$  and this corresponds to wells differing in the orientation of the nuclear spin. However, the median lines, which remain unchanged at any relation between  $b$  and  $t$ , correspond to transitions with  $i = i'$ , which take place in molecules with complete spatial symmetry.

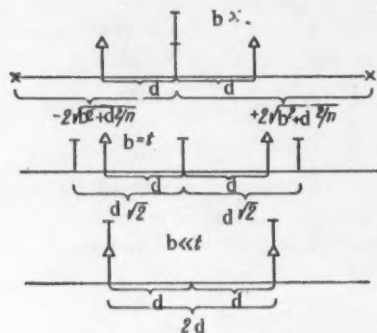


Fig. 2

$i = -i'$ ), for which the said statement is true, make their appearance, but also the median lines ( $i = i'$ ), which in any case correspond to an equally distributed electron.

Of course, it should be kept in mind that any electron distribution in the molecule is maintained during a time of the order of  $\frac{T_1}{n + n'}$ , where  $T_1$  is the longitudinal nuclear relaxation time. After this lapse of time  $t(1/2, i_l, i_{l'})$  changes and, correspondingly, the electron density is redistributed. The hyperfine structure of the spectrum in the intermediate case ( $b \sim t$ ) is very complicated. Starting from it  $b$  may be calculated using (15) or (16). It is regrettable, but the change of the spectrum for  $b \gg t$  into that for  $b \ll t$  takes place in such a narrow energy range that it is very difficult to detect it in an experiment. Therefore, until now only the limiting cases have been investigated in detail [2].

It can easily be seen that in the most general case the statement: "the electron is present in the two wells" only means that  $b \gg t$ . In the opposite case ( $b \ll t$ ) the interaction on the system disturbs the symmetry of the wells and localizes the electron in that well in which it has the lowest energy. In the case of an unperturbed molecule (at  $b \gg t$ ) the electron is "equally distributed" between the wells and performs a periodic transition between them with a frequency of  $2b/h$ . This process differs from the radioactive decay of a particle surmounting the nuclear barrier by the fact that the electron cannot go outside the boundaries of the system and for this reason its movement has a periodic character.

The author expresses his deep gratitude to V. V. Voevodskii, Corresponding Member of the Academy of Sciences of the USSR, to S. P. Solodovnikov and V. M. Chibrikov for suggesting the subject and fruitful discussions in the course of the study. The author also acknowledges his sincere appreciation to V. L. Ginzburg, Corresponding Member of the Academy of Sciences of the USSR, for his interest in the work and a discussion of the results.

#### LITERATURE CITED

1. L. Landau and E. Lifshits, Quantum Mechanics [in Russian] (Moscow-Leningrad, 1948), Part 1.
2. V. V. Voevodskii, S. P. Solodovnikov, and V. M. Chibrikín, Doklady Akad. Nauk SSSR 129, 1082 (1959).\*

---

\* Original Russian pagination. See C. B. translation.

2-22-77

## THE EFFECT OF CORROSION INHIBITORS ON MECHANICO-CORROSIONAL ABRASION

E. M. Zaretskii, I. M. Katser, and O. A. Petrova

The Scientific-Research Institute for Auxiliary Attachments and Spare Parts for Textile Equipment

(Presented by Academician P. A. Rebinder, June 24, 1960)

Translated from *Doklady Akademii Nauk SSSR*, Vol. 135, No. 4, pp. 890-892, December, 1960

Original article submitted June 1, 1960

It is a well-known fact that the nature of the surrounding medium greatly influences the character and intensity of metallic abrasion. The lubricating action of the medium, its ability to bring about a reduction of hardness through adsorption [1], and its corrosional interaction with the metal are all factors which affect the extent of abrasion. Metallic abrasion in dry air is usually accompanied by oxidation, new metallic surfaces being continually exposed through the scaling off of the oxide film which was formed earlier. It has been shown that the rate of abrasion of steel diminishes in an oxygen-free atmosphere [2]. Processes of electrochemical corrosion must also be taken into account in the operation of friction joints in electrolytes or in moist air.

In the first case, for example machining, the corrosional factor is not significant since the shaving which is removed has a depth many times greater than that of the natural oxide film. In the second case, the rate of abrasion is so low that the corrosional and mechanical effects are of the same order. An instance of this type would probably be the operation of the ring - roller combination in the wet spinning of flax.

The layer of metal removed from the surface of a  $4 \times 13$  nitrocemented steel ring by one rotation of a steel roller has an average depth of only 2-3 Å. Here, account must be taken, not only of the formation of a brittle oxide layer, but also of possible electrochemical corrosion under the action of a thin film of water. The third case of movement of an aggressive electrolyte containing an abrasive is one in which metal breakdown arises principally from corrosional processes, the mechanical factor being of secondary importance. Evidence of the participation of electrochemical processes in abrasion can be found in the fact that the use of a protective covering will reduce the frictional wear of steel against a textolite bearing in sea water [3].

The present work is a study of the possible use of corrosion inhibitors to diminish the mechanocorrosional abrasion of a  $4 \times 13$  nitrocemented steel in Moscow tap water. These experiments were carried out at  $40^\circ \text{C}$  in a Kh2M apparatus [4] where a rotating disk of high speed R9 steel wore down a test bar in an electrolyte, forming a depression in its surface. The volume of material worn away was calculated from the dimensions of this depression and served as a criterion of the abrasion resistance. The specimen was under a load of 2.25 kg in each experiment and the disk rotated at 600 rpm.

It had been shown earlier that the composition and pH of the water exert a considerable effect on the resistance of steels [5, 6].

The first series of experiments was designed to determine the effect of anodic and cathodic polarization on abrasion of the  $4 \times 13$  steel, and thus bring out the role of electrochemical processes. A platinum foil served as the second electrode. Each of the reported values of the abrasion corresponds to a separate experiment and each series of experiments was carried out on a single specimen.

Mean results are presented in the curves of Figs. 1 and 2.

The curves of Fig. 1 show that anodic polarization increased the mechanocorrosional abrasion by 25%. The volume abrasional loss of the  $4 \times 13$  steel after 3000 revolutions diminished from approximately  $75 \cdot 10^{-3}$  to  $45 \cdot 10^{-3} \text{ mm}^3$  under cathodic polarization, i.e., decreased by approximately 40%. Thus, the corrosional and the mechanical factors were fully commensurate under these conditions, the experiments on cathodic protection showing the role of the one to be approximately the same as that of the other. On this basis, it could be anticipated that corrosion inhibitors might lower the abrasion rate considerably.

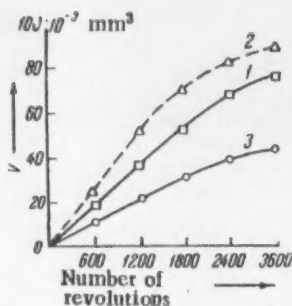


Fig. 1. The effect of polarization on the volume abrasion ( $v$ ) of  $4 \times 13$  steel in tap water: 1) without polarization; 2) under anodic polarization at  $D_a = 1 \text{ ma/cm}^2$ ; 3) under cathodic polarization at  $D_c = 0.1 \text{ ma/cm}^2$ .

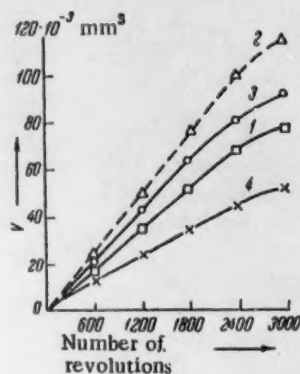


Fig. 2. The effect of corrosion inhibitors on the abrasion of  $4 \times 13$  steel: 1) without inhibitor; 2) with addition of sodium nitrite at 500 mg/liter; 3) with addition of soluble glass at 500 mg/liter; 4) with addition of sodium hexametaphosphate at 200 mg/liter.

Anodic corrosion inhibitors are known to diminish the corrosion of steel in neutral solutions, generally as the result of formation of a protective oxide film [7]. Such corrosion inhibitors could be expected to increase the rate of mechanocorrosional abrasion by reducing the deformability of the oxide film.

It can be seen from Fig. 2 that abrasion was increased markedly by the addition of sodium nitrite, a typical anodic corrosion inhibitor, or soluble glass, to the water. Sodium nitrite increased the rate of abrasion by 50%.

Sodium sulfite and sodium hexametaphosphate are cathodic inhibitors for steel corrosion, retarding those corrosion processes which proceed with oxygen depolarization [8, 9]. The first of these is oxidized with relative ease in aqueous solutions by atmospheric oxygen; at a concentration of 1000 mg/liter it lowered the rate of mechanocorrosional abrasion by approximately 25%. Figure 2 also shows results from experiments which were carried out with and without addition of sodium hexametaphosphate. The curves make it clear that it is possible to diminish abrasion by approximately 25% by addition of this compound.

Thus, these experiments lend support to the hypothesis that electrochemical processes play an essential role in mechanocorrosional abrasion and bring out the possibility of diminishing the rate of wear of  $4 \times 13$  steel in aqueous solution by addition of sodium hexametaphosphate, a cathodic corrosion inhibitor.

The authors wish to express their thanks to M. A. Babichev for his advice on the technique of these experiments.

#### LITERATURE CITED

1. P. A. Rebinder, Jubilee Collection in Honor of the 30th Anniversary of the Great October Socialist Revolution [in Russian] (1947) Vol. 1, p. 533; P. A. Rebinder, L. A. Shreiner, and K. F. Zhigach, Hardness Reducers for Boring [in Russian] (Izd. AN SSSR, 1944).
2. N. D. Tomashev and V. G. Sapozhnikova, Sudostroenie 4-5, 228 (1940).
3. S. J. Rosenberg and L. Jordan, Trans. Am. Soc. Metals 23, 577 (1935).
4. M. M. Khrushchov and M. A. Babichev, Collection: Friction and Abrasion in Machines [in Russian] (Izd. AN SSSR, 1955) Collection 10.
5. M. M. Khrushchov and M. A. Babichev, Friction and Abrasion in Machines [in Russian] (Izd. AN SSSR, 1958) Collection 12.
6. M. P. Kalyanova, The Technology of the Treatment of Parts of Textile Machines [in Russian] (Moscow, 1957), No. 3.
7. I. L. Rozenfel'd, Corrosion Inhibitors in Neutral Media [in Russian] (Izd. AN SSSR, 1953).
8. I. V. Krotov and E. I. Gurovich, Zhur. Obshch. Khim. 16, 12 (1946).
9. I. É. Apel'tsin and E. F. Zolotova, Studies on Water Treatment [in Russian] (1955).

22-11-11

## THE STRUCTURE AND PROPERTIES OF ISOTACTIC POLYACRYLIC ACID AND ITS SALTS\*

Academician V. A. Kargin, S. Ya. Mirlina, V. A. Kabanov,  
G. A. Mikheleva, and A. V. Vlasov

M. V. Lomonosov Moscow State University

Translated from *Doklady Akademii Nauk SSSR*, Vol. 135, No. 4, pp. 893-895,  
December, 1960

Original article submitted July 27, 1960

The synthetic polyelectrolytes are capable of undergoing extensive structural and chemical changes when acted on by relatively weak forces and thus can serve as models for the study of certain properties of biological polymers. This is particularly true of the stereoregular synthetic polyelectrolytes which resemble the other stereoregular polymers in manifesting clearly that diversity and individuality of secondary structural formations which is so characteristic of biological systems.

The present work has involved the preparation of stereoregular isotactic polyacrylic acid (PAA) and a study of the secondary structures which arise in this acid and its salts. The isotactic PAA was obtained by alkaline hydrolysis of a previously prepared isotactic polyisopropylacrylate. The degree of hydrolysis was controlled by either potentiometric titration, or by titration with phenolphthalein indicator. Hydrolysis was carried to completion. The resulting isotactic PAA precipitated from solution as a white crystalline powder on addition of concentrated HCl, crystallization being proven by x-ray analysis. Thermogravimetric experiments with the crystalline isotactic PAA were carried out on continuous weighing analytical balances and the results combined with microanalytical data to show that crystallization produced a hydrate containing one water molecule for every two monomer links.

The structures of the isotactic PAA and its salts were studied on a JEM-5Y electron microscope with a resolving power of 10 Å at a direct electrooptical magnification of 18,000-80,000. This microscope was so constructed that it was possible to obtain electron diffraction patterns of the rear portions of the specimen which was under observation. The specimens of isotactic PAA were carefully purified by electrodialysis. Objectives were prepared by evaporation of the solvent from a drop of a dilute solution of the polymer deposited on a colloxylin backing.

Salts of the isotactic PAA were obtained by potentiometric titration of a 1% aqueous hydrate solution with barium and sodium oxides and tetramethylammonia. These titrations were carried out with a LP-5 lamp and scale potentiometer and a glass electrode. Electron microscopic studies were carried out on specimens of isotactic PAA obtained from aqueous solutions whose concentrations ranged from 0.01 to 0.00001%. These showed that the polymer formed either separate molecular globules or aggregates of such globules, depending on the solution concentration, just as had been observed earlier in work on atactic PAA [2].

\* A brief note concerning the synthesis of isotactic polyacrylic acid by hydrolysis of polytertiarybutylacrylate appeared in the literature [1] after the present work had been completed.

The amorphous structure of these aggregates was evident from their electron diffraction patterns. It has already been pointed out above that the isotactic PAA crystallized and precipitated from aqueous solution on addition of concentrated hydrochloric acid. Study of the crystalline PAA was carried out on specimens deposited on a platinum grid by dropwise addition of redistilled 6 N hydrochloric acid to a 100° aqueous solution of the polyacid. Evaporation of the solvent was at 100° also. Crystalline bundles (Fig. 1a), spiral ribbons (Fig. 1b), and individual monocrystals (Fig. 1c) were observed in the specimens obtained from dilute solutions (0.0001-0.00001%).

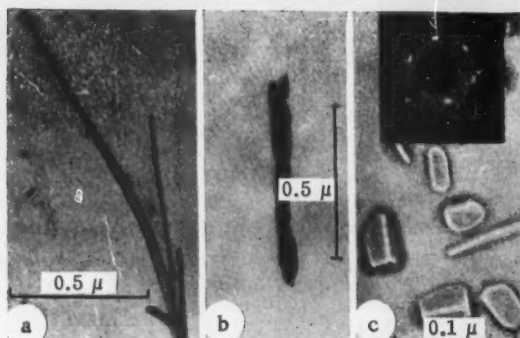


Fig. 1. Crystalline polyacrylic acid: a) crystalline bundles ( $C \approx 0.00001\%$ ); b) spiral ribbons ( $C \approx 0.0005\%$ ); c) individual monocrystals ( $C \approx 0.0001\%$ ); d) electron diffraction pattern of a monocrystal of PAA.

10.7 were used for electron microscopic study. Parallel measurements on the viscosities of these barium salt solutions were also carried out.

The crystalline structure of these formations was proven by the electron diffraction method (Fig. 1d). The fact that isotactic PAA crystallized readily in the presence of HCl was due to the complete suppression of the carboxyl group dissociation with elimination of chemical irregularities in the chain resulting from the  $\text{COO}^-$  groups of the partially dissociated compound. For this reason, the isotactic acid behaved as an ordinary stereoregular polymer in acid medium.

Specimens of the barium salt of PAA obtained from solutions in which the pH ranged from 4.2 to

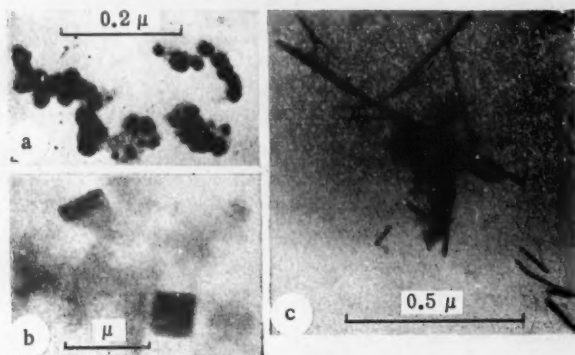


Fig. 2. Salts of isotactic polyacrylic acid: a) Ba salt; b) Na salt at pH 6.75; c) Na salt at pH 7.35.

The electron microscopic photographs showed dense compacted globule formations over the entire pH interval (Fig. 2a). The viscosity of the barium polyacrylate solutions was less than the viscosity of the isotactic PAA solutions (at pH 5:  $\eta_{\text{spec. PABa}} = 0.07$ ;  $\eta_{\text{spec. PAA}} = 0.12$ ), a higher degree of compaction of the spherical molecular globules being indicated.

An entirely different situation was observed in the study of specimens of the sodium salt of isotactic PAA which had been prepared by titrating PAA solutions to pH values ranging from 4.2 to 11.5. The electron microscopic photographs at the lower pH values (i.e., at the lower degrees of neutralization) showed formations of molecular globules, less compact, it is true, than those of barium polyacrylate. There was an unwinding of the molecular globules at pH 6.75, as the result of increased dissociation of the carboxyl groups and enhanced electrostatic repulsion of the  $\text{COO}^-$ 's within the molecule. Bundle-like (fibril) structures built up by parallel superposition of straightened molecular chains could be seen on the corresponding electron microscopic photographs (Fig. 2b). Practically all of the carboxyl groups of the polymer were dissociated at pH 7.5. The

molecular chains acquired the same chemical regularity as was seen in the case of completely undissociated PAA. This condition was sufficient for crystallization within the bundle and for formation of structured forms of high order ranging all the way to individual monocrystals when the chains contained a regular sequence of asymmetric atoms (Fig. 2c). In this same pH interval, the curve relating pH and specific viscosity of the polyelectrolyte solutions passed through a maximum corresponding to maximum degree of unwinding of the molecular chains, or chain aggregates, in solution. The excess of low-molecular ions present at the higher pH values screened-in negative charges of the macromolecule and thereby reduced the intramolecular electrostatic repulsion. The chains assumed the form of globules with a statistical distribution corresponding to maximum entropy. Formations of the globular type were observed once more on the electron microscopic photographs.

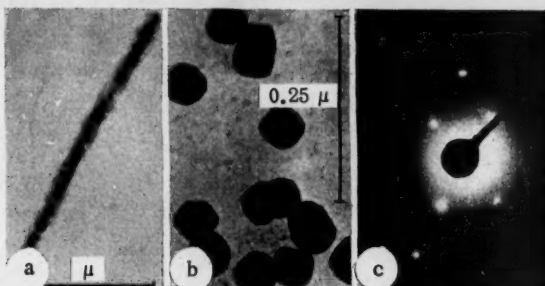


Fig. 3. Isotactic tetramethylammonia polyacrylate: a) fibril type of structure; b) individual monocrystals; c) electron diffraction pattern of a monocrystal.

The phenomena described above for isotactic sodium polyacrylate appeared again, and even more clearly, with isotactic tetramethylammonia polyacrylate. Here electron microscope photographs taken near neutralization showed the formation of fibril type structures whose degree of perfection approached that of biopolymers. Figure 3a shows a transverse banded ribbon built up of individual bundles and Fig. 3b, individual monocrystals of the polymeric salt. The corresponding electron diffraction patterns were fine-banded and thus indicative of a high degree of ordering of the structural elements in the formations in question (Fig. 3c). A very interesting

effect was observed when films of tetramethylammonia polyacrylate were studied under the polarizing microscope. These specimens were prepared by 100° evaporation of the solvent from a drop of aqueous polymer solution which had been deposited on a slide. Observations were made at 40-60° in order to avoid uptake of atmospheric moisture by the hygroscopic polymer.

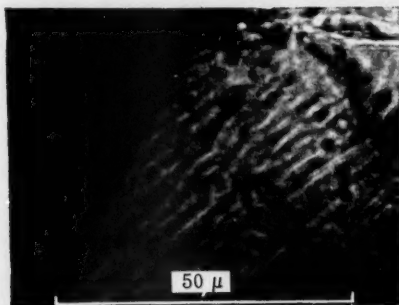


Fig. 4. Photomicrograph of film of isotactic tetramethylammonia polyacrylate in polarized light.

Figure 4 is a photomicrograph of a thin film of isotactic tetramethylammonia polyacrylate viewed in polarized light. It is clear that the film consisted entirely of coarse combinations of rhombic monocrystals whose dimensions sometimes reached 100 μ. The fine folded structure of the monocrystals were well defined. These crystals broke down under the influence of atmospheric moisture when the specimen was cooled to 20° under the microscope. This breakdown began with a deepening and widening of the folds. Double refraction disappeared rapidly

and the concretion of monocrystals was converted into a swollen polymeric film. The monocrystals appeared again and in exactly the same form, dimensions, and mutual arrangement as before when the film was warmed without changing its position under the microscope. It was possible to repeat this operation several times. This effect can be explained only if it is assumed that the swollen polyelectrolyte film (gel) retained coarse structural units arranged in a strictly defined pattern.

The potentiometric titration curves for the isotactic polyacrylic acid were used to calculate dissociation constants and  $\Delta pK$  values which determine the conformations of the monomer units.

The value of  $pK_{i_1}$  for the titration of isotactic PAA by hydrated sodium oxide proved to be 5.5 while  $pK_{i_2}$  for titration with the hydrated tetramethylammonia oxide was 6.3. Assuming the ionization constant for the isolated carboxyl group to be  $K_a = 10^{-4.86}$  gave:

$$\Delta pK_1 = pK_{i_1} - pK_0 = 5.5 - 4.86 = 0.64;$$

$$\Delta pK_2 = pK_{i_2} - pK_0 = 6.3 - 4.86 = 1.44.$$

Thus, isotactic PAA and its salts are characterized by the same basic types of structure, the globular and fibril, which have been established earlier for the atactic PAA.

Here, however, there is a regular sequential arrangement of asymmetric atoms in the macromolecule and when the polyelectrolyte chain is chemically uniform, the fibril structures show a higher degree of multiplicity and a perfection of form approaching the regular structures of the biopolymers.

#### LITERATURE CITED

1. M. L. Miller, M. C. Botty, and C. E. Rauhut, *Colloid. Sci.* **15**, 83 (1960).
2. V. A. Kargin and N. F. Bakeev, *Kolloid. Zhur.* **29**, 133 (1957).\*

\* Original Russian pagination. See C. B. translation.

# THE ROLE OF LONGITUDINAL MIXING IN EXCHANGE COLUMNS FOR ISOTOPIC SEPARATION

Academician B. P. Konstantinov and L. V. Kotova

Physicotechnical Institute of the Academy of Sciences of the USSR

Translated from *Doklady Akademii Nauk SSSR*, Vol. 135, No. 4, pp. 896-898,  
December, 1960

Original article submitted August 1, 1960

The stationary-state concentration gradient of one of the two components in an exchange column is generally described by an equation of the form [1, 2]:

$$H \frac{dC}{dz} = \epsilon C (1 - C) - \frac{i(C_k - C)}{I}, \quad (1)$$

in which  $C$  is the mole fraction of that component which is being separated out of the binary mixture,  $\epsilon$  is the coefficient of enrichment,  $C_k$  is the concentration in the take-off,  $I$  is the flow in one of the phases,  $\underline{1}$  is the flow in the take-off, and  $H$  is the height equivalent to one theoretical plate (H.E.T.P.).

The height equivalent to one theoretical plate is independent of the concentration  $C$ , but varies with the flow  $I$ , the construction and diameter of the column, the type of head, and the dimensions of the latter. Column theory aims at expressing  $H$  as a function of  $I$  and predicting its value for columns and heads of various constructions and dimensions.

The development of such theory is a complex problem and for practical purposes we generally resort to empirical formulas which are of limited validity. The present note aims at establishing the effect of longitudinal phase mixing on the value of  $H$ .

Equation (1) and all of the assumptions upon which it is based will be assumed to be valid in what follows. More especially, the equilibrium distribution of isotopes between phases I and II will be determined from the relation:

$$\beta_1 = \alpha \beta_2, \quad (2)$$

where  $\beta_1$  and  $\beta_2$  are the isotopic ratios in phases I and II, respectively,  $\beta = \left( \frac{c}{1-c} \right)$   $\alpha$  is the separation factor, and  $\alpha = 1 + \epsilon$ ,  $\epsilon \ll 1$ .

An expression of the concentration difference can be obtained from Eq. (2) by neglecting  $\epsilon^2$  and has the form:

$$C_1 - C_2 = \epsilon \bar{C} (1 - \bar{C}), \quad (3)$$

$\bar{C}$  being some value lying between  $C_1$  and  $C_2$ .

The rate of isotopic exchange per unit column length is determined by the equation:

$$J = I_0 [\epsilon \bar{C} (1 - \bar{C}) - (C_1 - C_2)], \quad (4)$$

in which  $J$  is the flow of the light component from phase II into phase I and  $I_0$  is the exchange current.

The stationary-state flow of the light component along the column is determined by:

$$i_l = IC_1 - (I - i)C_2 - D_{s1} \frac{dC_1}{dz} - D_{s2} \frac{dC_2}{dz}, \quad (5)$$

the flow of the light component resulting from longitudinal phase mixing being fixed by the third and fourth members on the right. These members differ from zero when  $\frac{dC}{dz} \neq 0$ .

The alteration in the flow of the light component with phase I per unit column length is equal to the flow of this same component from phase II into phase I and, according to Eq. (4):

$$\frac{d}{dz} (IC_1 - D_{s1} \frac{dC_1}{dz}) = I_0 [\epsilon \bar{C} (1 - \bar{C}) - (C_1 - C_2)]. \quad (6)$$

The conditions of actual column operation are such that  $(C_1 - C_2) \leq \epsilon \bar{C} (1 - \bar{C})$ . The concentration difference along the entire length of the column  $(C_k - C_0)$  can, at the same time, be of the order of one unit. From this it follows that:

$$\frac{dC_1}{dz} = \frac{dC_2}{dz} = \frac{dC}{dz} \quad (7)$$

is sufficiently precise. The last two members of the right-hand side of Eq. (5) can then be replaced by the one term,  $D_3 \frac{dC}{dz}$ ,  $D_3 = D_{s1} + D_{s2}$  being the coefficient of longitudinal mixing, a process parameter which takes account of effects in both phases.

The usual practice will be followed in the further steps of the derivation of the column equation, and terms containing second derivatives with respect to  $C$  will be neglected in the left-hand member of (6). Solving (5) for the difference  $C_1 - C_2$  and inserting the result into (6) gives:

$$\left( \frac{I}{I_0} + \frac{D_3}{I} \right) \frac{d\bar{C}}{dz} = \epsilon \bar{C} (1 - \bar{C}) - \frac{i_l - i\bar{C}}{I}. \quad (8)$$

The quantity  $C_2$  has been replaced by  $\bar{C}$  in this transformation. This is permissible since  $\frac{i}{I} \approx \epsilon$ .

Evaluation of  $\frac{d^2C}{dz^2}$  from (8) shows that the accuracy in question justifies neglect of members of (6) containing this term.

Examination of (8) shows the expression for the H.E.T.P. to have the form:

$$H = \frac{I}{I_0} + \frac{D_3}{I}. \quad (9)$$

This quantity is given by  $\frac{I}{I_0}$ , i.e., by the ratio between phase flow and exchange current per unit column length when the longitudinal mixing is slight and  $\frac{D_3}{I} \ll \frac{I}{I_0}$ . The value of the exchange current

$I_0$  is determined by the degree of dispersion of the phases (the surface area of phase contact) and by the chemical or diffusional exchange kinetics.

The determination of the individual contributions to the H.E.T.P. arising from mass exchange and the longitudinal mixing is a matter of importance for the experimenter and the designer, especially the latter. The experimental methods which are commonly applied to the study of columns do not permit such determination for either the stationary state or the operating regime. Each such experiment gives no more than a value of  $H$ , i.e., the sum  $\frac{I}{I_0} + \frac{D_3}{I}$ .

It is possible to set up more exact experiments for determining the effect of longitudinal mixing. In particular, for operation without take-off,  $i = 0$  and Eq. (5) goes over into:

$$D_{31} \frac{dC_1}{dz} + D_{32} \frac{dC_2}{dz} = I(C_1 - C_2). \quad (10)$$

The mixing coefficients  $D_{31}$  and  $D_{32}$  can be evaluated by solving two equations obtained by measuring  $(C_1 - C_2)$ ,  $\frac{dC_1}{dz}$  and  $\frac{dC_2}{dz}$  at two points in the column. This method and others similar to it are very difficult to carry out in practice since they impose quite high requirements on the precision of isotopic analysis. In our opinion, the following would be a feasible method of determining the coefficients  $D_{31}$  and  $D_{32}$ .

A definite additive would be introduced into each of the phases as it entered the column. It would be necessary that such additive not pass over into the other phase. A determination of the distribution of the additive along the column at various times, or of the time variation of the amount of additive in the phase take-off from the column, would permit  $D_{31}$  and  $D_{32}$  to be obtained separately.

If, it is assumed that the additive was originally concentrated in a sufficiently narrow section of the column, the diffusion equation can be solved to give [3]:

$$C(z, t) = \frac{Q}{2a\sqrt{\pi t}} e^{-\frac{(z-v_1 t)^2}{4a^2 t}}, \quad (11)$$

$z$  being a coordinate measured along the column,  $t$  is the time,  $Q$  is the amount of the additive introduced,  $v_1$  is the linear rate of movement of the phase, and  $a^2 = D$ .

The  $C(L, t)$  curve covered by Eq. (11) is obtained by introducing the additive at the phase input into the column and measuring its concentration at various times at the other end where  $z = L$ . The coefficient of longitudinal mixing,  $D$ , can be found from this curve and Eq. (11). The equation for  $D$  assumes the simple form:

$$D = \frac{1}{4\pi} \cdot \frac{Q^2}{C^2(L, T) \frac{L}{v_1}}, \quad (12)$$

at the time  $T = \frac{L}{v_1}$ .

It should be noted that  $D$  and  $v_1$  can be determined in a single experiment by observing the time corresponding to maximum concentration at the point  $L$ , as given by the equation:

$$T_{\max} = \frac{L}{v_1} \left[ \sqrt{1 + \left( \frac{a^2}{v_1 L} \right)^2} - \frac{a^2}{v_1 L} \right], \quad (13)$$

and making use of Eq. (11).

Thus, with this analysis of the column equation and the proposed methods for the determination of the longitudinal mixing, it is possible to fix the true value of the mass exchange per unit column length and the contribution to the H.E.T.P. resulting from longitudinal mixing.

#### LITERATURE CITED

1. M. Benedict, Collection: The Physical Chemistry of the Separation of Mixtures [Russian translation] (IL, 1949) No. 1, p. 11.
2. K. Cohen, The Theory of Isotope Separation as Applied to the Large-scale Production of  $U^{235}$  (1957).
3. F. Frank and R. Mizes, Differential and Integral Equations of Mathematical Physics [in Russian] (Moscow, 1937) Chap. II.

## THE EFFECT OF METALLIC IONS ON THE CORROSION OF STAINLESS STEEL IN CONCENTRATED $\text{HNO}_3$ SOLUTIONS

M. M. Kurtepov and A. S. Gryaznova

Institute of Physical Chemistry, Academy of Sciences of the USSR

(Presented by Academician V. I. Spitsyn, June 25, 1960)

Translated from *Doklady Akademii Nauk SSSR*, Vol. 135, No. 4, pp. 899-901,  
December, 1960

Original article submitted June 22, 1960

It is known that the passive state of stainless steels can be broken down in solutions of high oxidation-reduction potential and that corrosion will then proceed rapidly according to a mechanism of overpassivation. This effect is observed when the steel is at high positive potentials and is due to a loss of protective ability of the film as a result of the formation of metallic ions of higher valency [1-6]. Concentrated solutions of nitric acid at the boiling point are special instances of media of high oxidation-reduction potential. Thus, the potential of a 12-14 N nitric acid solution measured against platinum is 1.4-1.48 v. Corrosion of stainless steel in these solutions will lead to the accumulation of ions of those metals which were alloyed in the steel. The formation of compounds containing metals of higher valency ( $\text{Cr}^{6+}$ ,  $\text{Mn}^{7+}$ ,  $\text{Mn}^{4+}$ ,  $\text{Fe}^{3+}$ ) is possible here.

Under these conditions, ions of higher valency can be formed either by the oxidation of lower valence ions in the body of the solution or by oxidation of the protective oxide film and the surface layers of the steel. It is to be understood that there is a possibility of reduction of metallic ions of higher valency and participation of the products of reduction of the medium in the corrosion process. Thus, boiling concentrated  $\text{HNO}_3$  solutions containing metallic ions of variable valency are complex oxidation-reduction systems.

The present communication is devoted to an elucidation of the effect of metallic ions of variable valency on the corrosion of stainless steel in boiling solutions.\* Insufficient attention has been given to this problem despite its undoubted interest [7-9]. It is to be expected that the corrosion products from the steel would have a pronounced effect on the corrosion process.

The high resistance of stainless steel to corrosion in  $\text{HNO}_3$  is known to be related to the stability of the passive state over a wide interval of potentials. The most pronounced corrosion of the steel is observed in boiling concentrated  $\text{HNO}_3$  solutions. Corrosion is accompanied by a displacement of the potential of the steel into the region of high potentials (the stationary potential of the steel in 14 N acid is in the neighborhood of 1.3 v, for example) and the cathodic and anodic processes are facilitated thereby. Displacement of the potential of the steel into the region of high positive values results in a breakdown of the passive state and corrosion then proceeds at high velocity according to a mechanism of overpassivation. It will be shown below that the corrosion products function as corrosion accelerators in such case. It should be noted that cathodic reduction of nitric to nitrous acid proceeds on a passive surface at low temperatures, and on a metallic surface in the region of overpassivation in boiling concentrated solutions.

\* A tempered 1Kh18N9T steel was used in these studies. Metallic ions were introduced into the 12-16 N  $\text{HNO}_3$  solutions in the form of nitrates and  $\text{K}_2\text{Cr}_2\text{O}_7$ .

The corrosion of stainless steel in boiling concentrated nitric acid solutions is increased by the presence of  $\text{Cr}^{3+}$  ions. The corrosion rate increases with the concentration of the acid, with the amount of  $\text{Cr}^{3+}$  added to the acid, and with the time of contact with the solution (Fig. 1). Increase in the corrosion rate is accompanied by a displacement of the steel potential toward positive values (Fig. 2) which are so high that corrosion can follow a mechanism of overpassivation. The observed rise in the corrosion of the stainless steel with time resulting from the presence of  $\text{Cr}^{3+}$  ions is to be explained by an increase in the depolarizing ability arising from the formation of higher oxides of chromium in the body of the solution and from oxidation of the steel surface.

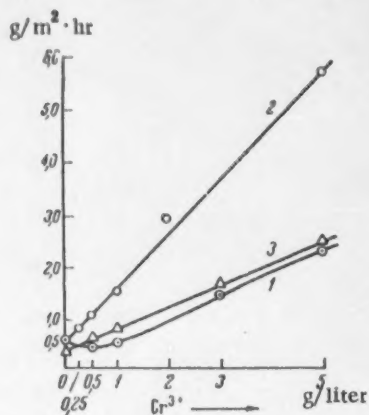


Fig. 1. The effect of  $\text{Cr}^{3+}$  on the rate of corrosion of stainless steel in boiling solutions of 12-14 N  $\text{HNO}_3$  as a function of time: 1) 5 hours, 14 N; 2) 10 hours, 14 N; 3) 10 hours, 12 N.

The resulting  $\text{Cr}^{6+}$  ions are effective depolarizers and cause enhanced corrosion of the steel. There is ample opportunity for the formation of compounds containing chromium of higher valencies in boiling concentrated  $\text{HNO}_3$  [5, 10] since the potentials of these solutions are higher than the equilibrium potential for the reaction  $\text{Cr}^{3+} = \text{Cr}^{6+}$ .

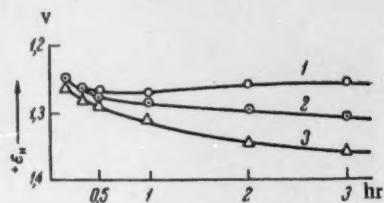


Fig. 2. Curves showing potential as a function of holding time of stainless steel in boiling 14 N  $\text{HNO}_3$  containing  $\text{Cr}^{3+}$ : 1) without addition; 2) 1 g/liter  $\text{Cr}^{3+}$ ; 3) 5 g/liter  $\text{Cr}^{3+}$ .

This fact was confirmed by our other experiments. Thus, the introduction of  $\text{Cr}^{3+}$  into boiling concentrated  $\text{HNO}_3$  solutions in the form of  $\text{Cr}_2\text{O}_3$  (this oxide is known to be sparingly soluble in acids) considerably increases the rate of corrosion of the steel. In addition, it should be remembered that corrosion will reduce the  $\text{Cr}^{6+}$  to  $\text{Cr}^{3+}$  which will then be reoxidized to the higher oxide in the body of the solution.

It has been shown repeatedly in our laboratory that the introduction of  $\text{Cr}^{6+}$  into nitric acid solutions leads to an increase in the rate of corrosion of stainless steel. Corrosion proceeds quite rapidly in boiling concentrated  $\text{HNO}_3$  solutions containing  $\text{Cr}^{6+}$  at high positive potentials of 1.3-1.4 v. The curve showing corrosion rate as a function of time passes through a maximum. The rate of corrosion eventually levels off at a value which is dependent on the concentration of chromium ions in solution. The existence of such a relationship is clearly tied up with the oxidation-reduction processes which take place in the solution and on the steel surface, i.e., with the eventual establishment of a  $\text{Cr}^{6+} = \text{Cr}^{3+}$  equilibrium.

Corrosion of the stainless steel causes a large amount of iron to pass into solution where it exists as  $\text{Fe}^{3+}$ , the medium being a strong oxidizing agent. Experiment shows that the presence of the  $\text{Fe}^{3+}$  ions in boiling concentrated nitric acid solutions leads to a pronounced corrosion of the steel. The corrosion rate increases with the  $\text{Fe}^{3+}$  concentration of the solution (Fig. 3). At lower temperatures (down to 100°) no increase in the rate of corrosion of the steel is noted in these solutions, the steel being in the passive state. There is also pronounced corrosion of the steel in boiling dilute  $\text{HNO}_3$  solutions which contain considerable quantities of  $\text{Fe}^{3+}$ . In each case, acceleration of corrosion is accompanied by a displacement of the potential to positive values which are high enough to facilitate the cathodic processes and permit corrosion to proceed according to a mechanism of overpassivation (Fig. 4).

Our work has shown that addition of  $\text{MnO}_4^-$  to nitric acid solutions will accelerate the corrosion of stainless steel markedly, even at low temperatures. No similar effect is observed on adding  $\text{Mn}^{2+}$  to these solutions.

On the other hand,  $Mn^{2+}$  is readily oxidized to ions or compounds of higher valency in boiling concentrated nitric acid solutions and thereby increases the corrosion rate. This rise in the corrosion rate is accompanied by a displacement of the potential into the region of high positive values and the cathodic process is markedly promoted.

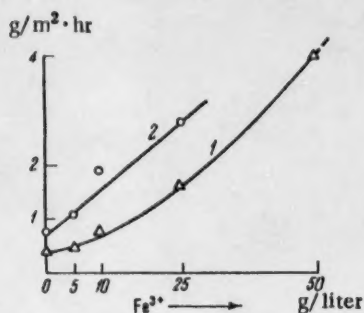


Fig. 3. The effect of  $Fe^{3+}$  on the rate of corrosion of stainless steel in boiling  $HNO_3$  solutions (duration of experiments, 10 hours): 1) 12 N; 2) 14 N.

$Ni^{2+}$  ions impede the cathodic process and reduce the corrosion rate of stainless steel in those cases where corrosion follows a mechanism of overpassivation.

Thus, the observed increase in the rate of corrosion of stainless steel in boiling concentrated nitric acid solutions with the passage of time is the result of an accumulation in solution of corrosion products in the form of metallic ions of variable valency (Cr, Mn, Fe).

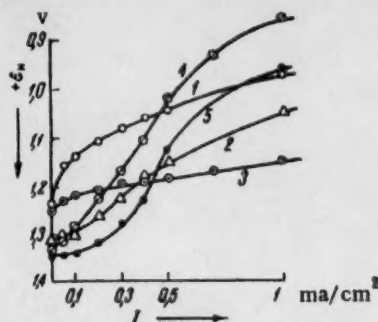
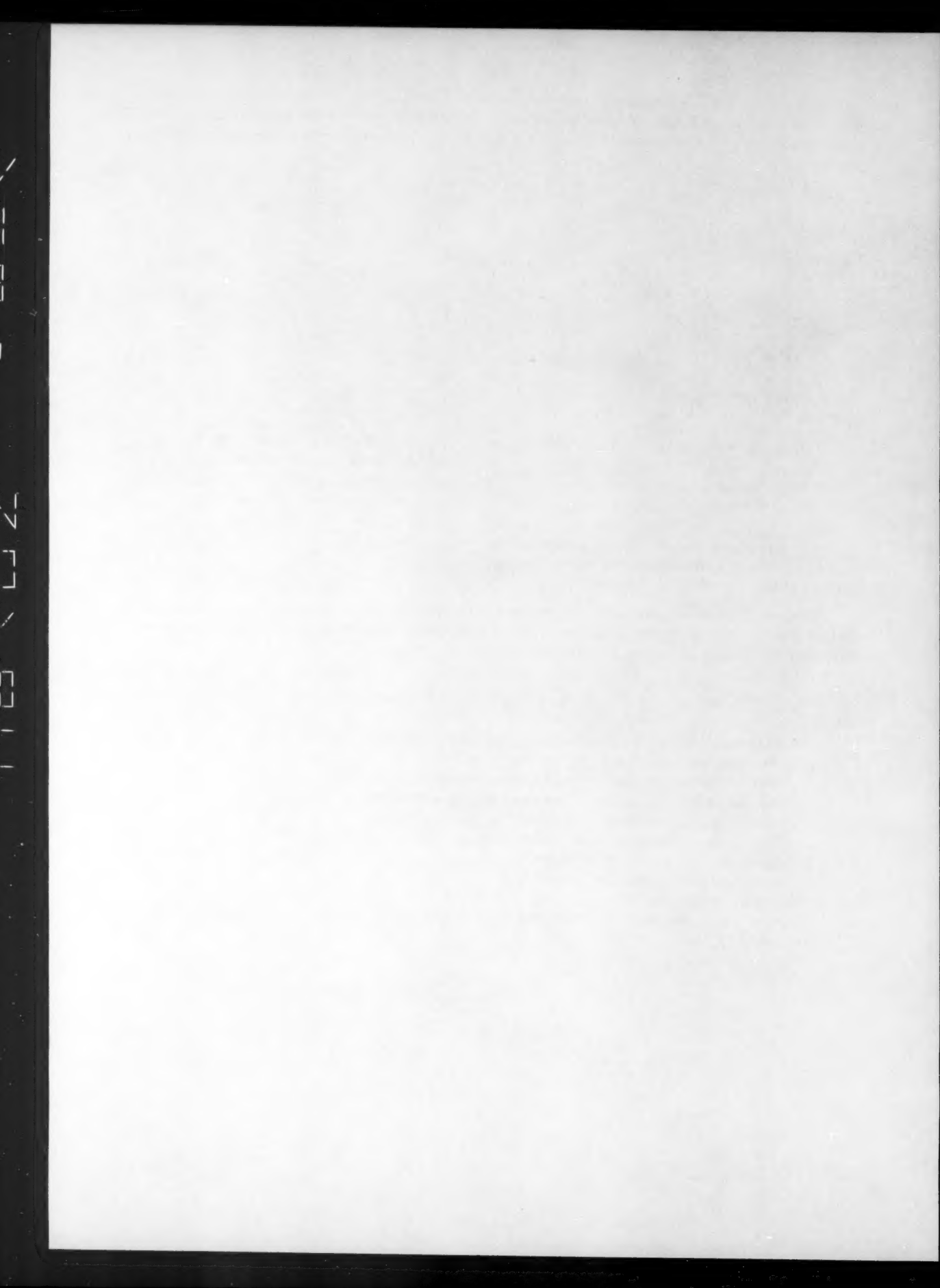


Fig. 4. The effect of metallic ions (25 g/liter) on cathodic polarization of stainless steel in boiling 12 N  $HNO_3$  solutions: 1) without addition; 2)  $Fe^{3+}$ ; 3)  $Mn^{2+}$ ; 4)  $Cr^{3+}$ ; 5) 1 g/liter  $Cr^{6+}$ .

#### LITERATURE CITED

1. M. M. Kurtepov and G. V. Akimov, *Doklady Akad. Nauk SSSR* **87**, 1, 93 (1952); **87**, 5, 795 (1952).
2. J. M. Defranoux, *Rev. métallurgie* **49**, 9, 664 (1952).
3. V. P. Batrakov and G. V. Akimov, *Doklady Akad. Nauk SSSR* **89**, 2, 321 (1952).
4. N. D. Tomashov and G. P. Chernova, *Doklady Akad. Nauk SSSR* **98**, 3, 435 (1954).
5. A. M. Sukhotin and É. I. Antonovskaya, *Zhur. Fiz. Khim.* **31**, 1521 (1957); **32**, 1842 (1958).
6. Ya. M. Kolotyrkin, *Problems of Physical Chemistry* [in Russian] (Moscow, 1958).
7. J. E. Truman, *J. Appl. Chem.* **4**, 5, 273 (1954).
8. H. T. Shirley and J. E. Truman, *J. Iron and Steel Inst.* **171**, 345 (1952).
9. M. Streicher, *J. Electrochem. Soc.* **106**, 3, 161 (1959).
10. V. Latimer, *The Oxidation States of the Elements and Their Potentials in Aqueous Solutions* [Russian translation] (IL, 1954).



# THE RADIOLYTIC REDUCTION OF TETRAVALENT CERIUM IN THE PRESENCE OF MONOVALENT THALLIUM UNDER IRRADIATION AT HIGH DOSAGE RATES

A. K. Pikaev and P. Ya. Glazunov

Institute of Physical Chemistry, Academy of Sciences of the USSR

(Presented by Academician V. I. Spitsyn, June 21, 1960)

Translated from Doklady Akademii Nauk SSSR, Vol. 135, No. 4, pp. 902-905,  
December, 1960

Original article submitted June 7, 1960

We have shown earlier [1-3] that overlapping of the tracks of ionizing particles in irradiation at dosage rates of approximately  $10^{21}$  ev/ml·sec, or higher, alters the yield of radical and molecular products from the radiolysis of water and thereby leads to a marked diminution in the yield of  $\text{Fe}^{3+}$  in irradiation of aqueous sulfuric acid solutions of ferrous sulfate in air and to an increase in the yield of  $\text{Ce}^{3+}$  in irradiation of aqueous sulfuric acid solutions of ceric sulfate. The study of the effect of high dosage rates on the course of radiolytic transformations in aqueous solutions has been extended by investigating the radiochemical processes in sulfuric acid solutions of mixed  $\text{Ce}^{4+}$  and  $\text{Tl}^+$  sulfates at dosage rates ranging up to approximately  $10^{23}$  ev/ml·sec.

These high dosage rates were obtained through single monoenergetic pulses of 0.8 Mev electrons which were produced in the accelerating tube of a linear accelerator [2, 3]. The experimental technique and method of measuring the dosage rate have been described in our previous communications [2, 3]. Doubly distilled water was used in each experiment. The following reactants were employed: ceric sulfate ("pure" grade) recrystallized twice from doubly distilled water to which a small amount of sulfuric acid had been added; thallous sulfate (analytical grade) recrystallized from doubly distilled water; cerous sulfate (analytical grade) and sulfuric acid

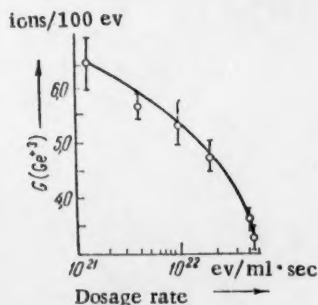


Fig. 1. The relation between  $G(\text{Ce}^{3+})$  and dosage rate in the  $\text{Ce}^{4+} - \text{Tl}^+$  system ( $\text{Ce}^{4+}$  concentration,  $2 \cdot 10^{-4}$  M;  $\text{Tl}^+$  concentration,  $10^{-2}$  M).

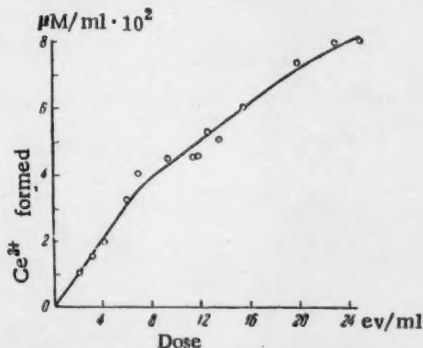


Fig. 2. The relation between the reduction of  $\text{Ce}^{4+}$  in the presence of  $10^{-2}$  M  $\text{Tl}^+$  and the dose at a dosage rate of  $5 \cdot 10^{22}$  ev/ml·sec.

(chemically pure grade), neither of which were subjected to preliminary purification. These solutions were irradiated in a glass cell with a glass membrane approximately 60  $\mu$  thick. The irradiated volume was 7 ml and the depth of the liquid layer, 5 mm.

The amount of  $Ce^{3+}$  formed by irradiation was determined spectrophotometrically. The molar extinction coefficient of  $Ce^{4+}$  in 0.8 N  $H_2SO_4$  was assumed to be equal to 5580 at 320 m $\mu$  [4]. The  $Tl^{3+}$  was determined indirectly. The amount of  $Ce^{4+}$  in the irradiated solution was first determined spectrophotometrically and a  $10^{-3}$  M solution of Mohr's salt in 0.8 N  $H_2SO_4$  then added. A certain amount of  $Fe^{2+}$  was oxidized by the  $Tl^{3+}$  and the  $Ce^{4+}$ . Knowing the amount of  $Ce^{4+}$  in the solution, the  $Tl^{3+}$  content could be obtained from a spectrophotometric determination of the  $Fe^{3+}$  concentration. This method proved to be satisfactory for irradiation at dosage rates up to about  $10^{22}$  ev/ml·sec. It was not sufficiently precise at higher dosage rates where the  $Tl^{3+}$  concentration was very low.

Use was made of an air-saturated 0.8 N sulfuric acid solution containing  $2 \cdot 10^{-4}$  M  $Ce^{4+}$  and  $10^{-2}$  M  $Tl^{+}$  in studying the effect of high dosage rates on the  $G(Ce^{3+})$  value for mixed  $Ce^{4+} - Tl^{+}$  solutions. The value of  $G(Ce^{3+})$  for  $Co^{60}$   $\gamma$ -irradiation at dose rates of  $2.5 \cdot 10^{15}$  ev/ml·sec is 7.9 ions/100 ev [5] and is independent of the  $Tl^{+}$  concentration over the range from  $10^{-2}$  to  $10^{-5}$  M. Our experiments on the irradiation of mixed  $Ce^{4+} - Tl^{+}$  solutions of the concentration indicated with a continuous electron current of 0.9 Mev and a dose rate of  $9.4 \cdot 10^{15}$  ev/ml·sec gave a value of  $G(Ce^{3+})$  of  $7.6 \pm 0.2$  ions/100 ev. The slight difference between this result and the value of [5] obviously arises from the fact that our dosage rate was greater by a factor of four.

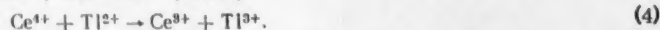
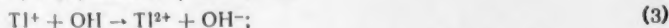
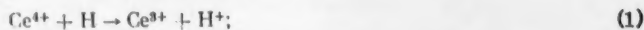
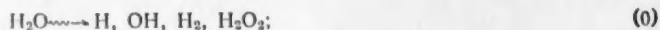
There was a pronounced diminution in the value of  $G(Ce^{3+})$  with increasing dose rate in electron pulse irradiation of  $Ce^{4+} - Tl^{+}$  solutions. The results are presented in Fig. 1. The  $Ce^{4+} - Tl^{+}$  solutions were irradiated with from 1 to 50 electron pulses, depending on the dosage rate.\* Each value of  $G(Ce^{3+})$  represents the mean of 5-15 measurements.

Figure 2 shows the relation between the formation of  $Ce^{3+}$  in 0.8 N sulfuric acid solution with  $2 \cdot 10^{-4}$  M  $Ce(SO_4)_2$  and  $10^{-2}$  M  $Tl_2SO_4$  and the dosage in impulse irradiation at a dose rate of  $5 \cdot 10^{22}$  ev/ml·sec. The value of  $G(Ce^{3+})$  is somewhat dependent on the initial  $Tl^{+}$  concentration at the high dosage rates. It is to be seen from Fig. 3 that  $G(Ce^{3+})$  rises with increasing  $Tl^{+}$  concentration and is proportional to the logarithm of the  $Tl_2SO_4$  concentration. Addition of  $Ce^{3+}$  to the  $Ce^{4+}$  solution diminishes the value of  $G(Ce^{3+})$ . Figure 4 shows the relation between  $G(Ce^{3+})$  and the concentration of the  $Ce_2(SO_4)_3$  added to the solution originally containing  $2 \cdot 10^{-4}$  M  $Ce^{4+}$ , the dosage rate being approximately  $5 \cdot 10^{22}$  ev/ml·sec; data from [5] for a dose rate of  $2.5 \cdot 10^{15}$  ev/ml·sec are also included for comparison.

Our values of  $G(Tl^{3+})$  at high dosage rates are presented below, each being the mean of 5-12 measurements; from them it is clear this quantity diminishes markedly as the dose rate rises.

Dose rate, ev/ml·sec	$\sim 10^{21}$	$5 \cdot 10^{22}$
$G(Tl^{3+})$ , ions/100 ev	$1.5 \pm 0.15$	$0.4 \pm 0.2$

According to [5], the mechanism of radiolytic reaction of  $Ce^{4+}$  and  $Tl^{+}$  in 0.8 N sulfate solutions can be expressed by:



\* There was a certain averaging out of the dose rate over the volume of the solution in these experiments. This would not essentially affect the value of  $G(Ce^{3+})$ .

It follows that

$$G(\text{Ce}^{3+})_{\text{Tl}^+} = G_{\text{H}} + G_{\text{OH}} + 2G_{\text{H}_2\text{O}_2} \quad (5)$$

and

$$G(\text{Tl}^{3+}) = G_{\text{OH}} \quad (6)$$

$G_{\text{H}}$ ,  $G_{\text{OH}}$ , and  $G_{\text{H}_2\text{O}_2}$  being the yields of the respective products as obtained in the radiolysis of water.

The present study was set up on the assumption that measurement of the yield from the radiational reactions in the  $\text{Fe}^{2+}$ ,  $\text{Ce}^{4+}$ , and  $\text{Ce}^{4+} - \text{Tl}^+$  systems would permit a quantitative evaluation of the alteration which overlapping of the tracks of the ionizing particles would produce in the yield of radical and molecular products in the water radiolysis. According to [5, 6], at low dosage rates

$$G(\text{Fe}^{3+}) = 3G_{\text{H}} + G_{\text{OH}} + 2G_{\text{H}_2\text{O}_2} \quad (7)$$

for diluted 0.8 N air-saturated aqueous sulfuric acid solutions of  $\text{Fe}^{2+}$  and

$$G(\text{Ce}^{3+}) = G_{\text{H}} - G_{\text{OH}} + 2G_{\text{H}_2\text{O}_2} \quad (8)$$

for diluted 0.8 N aqueous sulfuric acid solutions of  $\text{Ce}^{4+}$ . The following expressions can now be obtained from 5, 7, and 8:

$$G(\text{Ce}^{3+})_{\text{Tl}^+} - G(\text{Ce}^{3+}) = 2G_{\text{OH}} \quad (9)$$

$$3G(\text{Ce}^{3+})_{\text{Tl}^+} - G(\text{Fe}^{3+}) = 4G_{\text{H}_2\text{O}_2} + 2G_{\text{OH}} \quad (10)$$

Substitution of our values of  $G(\text{Fe}^{3+})$ ,  $G(\text{Ce}^{3+})$ , and  $G(\text{Ce}^{3+})_{\text{Tl}^+}$  at dosage rates of approximately  $5 \cdot 10^{22}$  ev/ml · sec into these expressions led to negative values of  $G_{\text{H}_2\text{O}_2}$  at all of the investigated  $\text{Tl}^+$  concentrations.

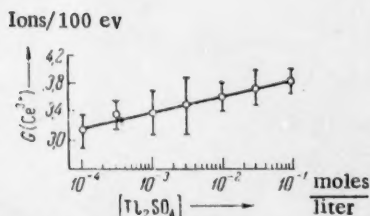


Fig. 3. The relation between  $G(\text{Ce}^{3+})$  and the  $\text{Tl}_2\text{SO}_4$  concentration at a dosage rate of  $4.5 \cdot 10^{22}$  ev/ml · sec ( $\text{Ce}^{4+}$  concentration;  $2 \cdot 10^{-4}$  M).

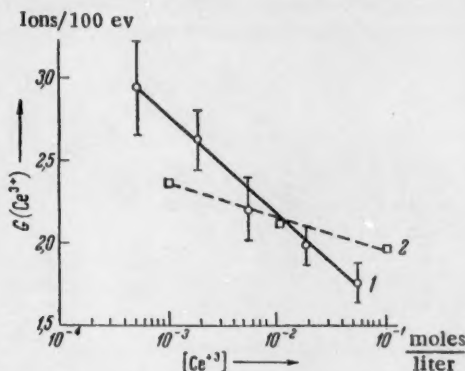


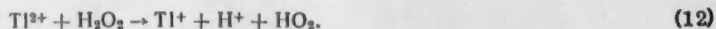
Fig. 4. The relation between  $G(\text{Ce}^{3+})$  and the  $\text{Ce}^{3+}$  concentration at dosage rates of: 1)  $5 \cdot 10^{22}$  ev/ml · sec; 2)  $2.5 \cdot 10^{15}$  ev/ml · sec [5].

\*  $G(\text{Fe}^{3+})$  and  $G(\text{Ce}^{3+})$  had been determined earlier [2, 3].

From this we assumed that at high dose rates the  $Tl^{2+}$  formed through reaction 3 could either interact with  $Ce^{4+}$  according to reaction 4 or enter into side reactions. Chief among these latter reactions would be the reduction of  $Tl^{2+}$  by hydroperoxide radicals or H atoms:<sup>\*</sup>



or, possibly, reduction by hydrogen peroxide:



Disproportionation of the  $Tl^{2+}$  according to



probably plays a very significant role here since, within the limits of experimental error,  $\frac{1}{2}[G(Ce^{3+})_{Tl^+} - G(Ce^{3+})] = G(Tl^{3+})$ .

It is quite likely that there is a reverse reaction involving  $Tl^{3+}$  and hydrogen peroxide when the dosage rate is high:

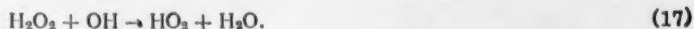


or



This supposition is confirmed by the fact that the relation between the reduction of  $Ce^{4+}$  in the presence of  $Tl^+$  and the dosage is no longer linear when the dosage is high (see Fig. 2). The role of side reactions of  $Tl^{2+}$  ions in the radiational transformation of  $Ce^{4+}$  in the  $Ce^{4+} - Tl^+$  system is a minor one for irradiation at low dosage rates.

The increase in  $G(Ce^{3+})$  with increasing  $Tl^+$  concentration is clearly to be explained in terms of a competition between reactions (3) and (16) and (17):<sup>\*\*</sup>



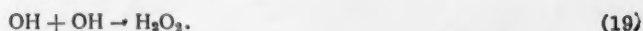
In all likelihood, the decrease of  $G(Ce^{3+})$  with increasing  $Ce^{3+}$  concentration is the result of a competition between (19) and



just as is the case at low dosage rates [5].

\* This reaction clearly leads to a reduction in the value of  $G(Ce^{3+})_{Tl^+}$ .

\*\* The significance of reactions (16) and (17) for radiolytic transformations in aqueous solutions increases markedly at high dosage rates where there is overlapping of the tracks of the ionizing particles, and the same is true of:



It should be noted that the relation between  $G(\text{Ce}^{3+})$  and the  $\text{Ce}^{3+}$  concentration is most clear-cut at the high dosage rates. Curves covering these relations at dose rates of approximately  $5 \cdot 10^{22}$  and  $2.5 \cdot 10^{15}$  ev/ml · sec, respectively, intersect. From a  $\text{Ce}^{3+}$  concentration of approximately  $10^{-2}$  M on, the  $G(\text{Ce}^{3+})$  value for a dose rate of approximately  $5 \cdot 10^{22}$  ev/ml · sec is greater than the corresponding value for a dose rate of  $2.5 \cdot 10^{15}$  ev/ml · sec. Thus, it is necessary to introduce about  $10^{-2}$  M of a  $\text{Ce}^{3+}$  salt into a solution containing  $\text{Ce}^{4+}$  in order to suppress the formation of those additional quantities of  $\text{H}_2\text{O}_2$  which would result from (19) by overlapping of the tracks of ionizing particles. At  $\text{Ce}^{3+}$  concentrations in excess of  $10^{-2}$  M, the principal alteration in  $G(\text{Ce}^{3+})$  at high rates of dosage is that due to the diminution of  $G_{\text{H}}$  resulting from the overlapping of the tracks of the ionizing particles.

Thus, competition between radical-radical and radical-dissolved substance interactions, and side reactions between the intermediates, become increasingly significant to transformations in aqueous solutions as the dosage rate is increased and the radical concentration rises.

#### LITERATURE CITED

1. A. K. Pikaev and P. Ya. Glazunov, *Izvest. Akad. Nauk SSSR, Otdel. Khim. Nauk* **12**, 2244 (1959).\*
2. P. Ya. Glazunov and A. K. Pikaev, *Doklady Akad. Nauk SSSR* **130**, 1051 (1960).\*
3. A. K. Pikaev and P. Ya. Glazunov, *Izvest. Akad. Nauk SSSR, Otdel. Khim. Nauk* **5**, 940 (1960).\*
4. C. Hochanadel and J. Ghormley, *J. Chem. Phys.* **21**, 880 (1953).
5. T. Sworski, *Radiation Res.* **4**, 483 (1956).
6. A. O. Allen, *Collection: Reports of Foreign Scientists at the Geneva Conference* [Russian translation] (Moscow, 1956).

\* Original Russian pagination. See C. B. translation.



## THE PROBLEM OF THE PENETRATION OF SILVER INTO TUNGSTEN

V. I. Rakhovskii, A. P. Lyubimov, and V. M. Garmash

V. I. Lenin All-Union Electrotechnical Institute and

I. V. Stalin Moscow Steel Institute

(Presented by Academician P. A. Rebinder, June 22, 1960)

Translated from *Doklady Akademii Nauk SSSR*, Vol. 135, No. 4, pp. 906-908,  
December, 1960

Original article submitted June 14, 1960

The life of electrical contacts in heavy-current apparatus is determined principally by the thermal stresses which arise under working conditions. These stresses are largely conditioned by the thermal stability and conductivity of the contact material and by its rate of vaporization, a factor which depends on the melting point as well as on the other characteristics which have been mentioned above. For this reason, there have been repeated attempts to develop complex multicomponent contact alloys having both high thermal conductivity and high melting point. Silver and tungsten have usually served as the basic elements in these alloys. Here the problem of possible penetration of silver into tungsten by diffusion, or by other processes proceeding at temperatures of the order of 1000°, takes on great significance. The phase diagram for the Ag-W system has been studied only inadequately, but Hansen has claimed in his monograph [1] that silver and tungsten do not form solutions in either the liquid or the solid state. It should be noted, however, that this claim of Hansen's was based on the work of [2] and [3] which was based, in turn, on techniques of relatively low sensitivity.

We are, furthermore, now familiar with certain processes such as the aggregation of solid tungsten particles in molten silver which are consistent with the supposition that tungsten does dissolve.

We have used radioactive isotopes in an attempt to establish the possibility of penetration of silver into tungsten. For this purpose tungsten sheets were held in liquid radioactive silver at elevated temperatures for extended periods. Measurements of the sample activity were then used to determine the total amount of silver which had penetrated into the tungsten.

The experimental procedure was as follows. Sheets of rolled technically pure W,  $0.015 \times 0.4 \times 1.2$  cm<sup>2</sup>, were embedded in silver which had been enriched with the Ag<sup>110</sup> radioactive isotope and contained 0.01% Si, 0.01% Fe, 0.01% Cu, and 0.001% Al. The resulting block was placed in a quartz crucible which was then inserted into the tube of the apparatus (see Fig. 1). This tube was evacuated to a pressure of the order of  $10^{-4}$  mm Hg and then filled with helium to a pressure somewhat in excess of atmospheric. A tubular furnace in which the desired working temperature had been already established was then moved up over this system. The tungsten was kept immersed in the liquid radioactive silver for periods ranging from 4 to 24 hours. A fine tungsten wire was sealed to each tungsten plate at the outset and was used to withdraw it into the cold region of the tube at the end of the holding period.

A chromel-alumel thermocouple in circuit with a PPTV-1 potentiometer was used to control the furnace temperature during an experiment. The working temperature was held constant to within  $\pm 1.5^\circ$  by manual adjustment, using a LATR-2 autotransformer. The low inertia of the furnace and careful check on the rate of heating made it possible to hold the temperature constant to within the limits indicated above.

The specimen was cooled, taken out of the experimental tube, and the excess silver covering its surface removed by treatment with dilute  $\text{HNO}_3$  in a TS-15 M thermostat at  $40^\circ$ . After acid treatment and repeated washing in dilute  $\text{HNO}_3$  and distilled water, the sample was dried and its activity determined on a VSP counter. Completion of removal of the adhering silver was shown by a preliminary experiment in which the tungsten sample was embedded in silver enriched with the radioactive isotope and removed without heating. Such procedure assured that there would be practically no penetration of silver into the tungsten. The count on these samples, after the above-described chemical treatment, was no higher than that of the background. In addition, a number of preliminary experiments were carried out to evaluate the effect of various secondary factors which might tend to increase the activity of the specimens during preliminary treatment. These experiments involved heating at  $1000^\circ$  for 8, 16, and 24 hours, and at  $1080^\circ$ , for 4, 8, 12, and 16 hours.

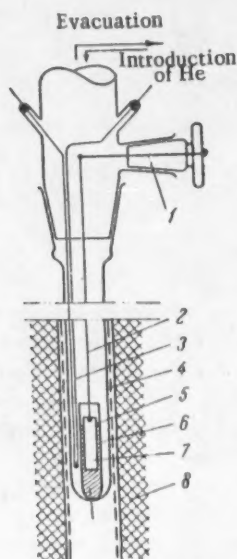


Fig. 1. Schematic representation of the experimental tube: 1) cock for raising sample; 2) fine wire support for plate; 3) thermocouple; 4) experimental tube; 5) crucible; 6) liquid silver; 7) tungsten plate; 8) tubular furnace.

Measurements of the activity of the samples took account of the alteration of the background, the time rate of decrease in the sample activity, self-absorption,  $\beta$ -irradiation, and the formation of secondary  $\beta$ -electrons through  $\gamma$ -irradiation. The resulting data permitted an

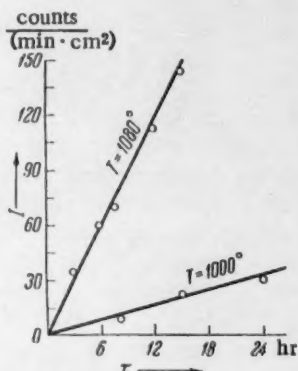


Fig. 2. The relation between the sample activity and the time of heating in liquid silver.

evaluation of the number of counts per unit of sample surface per unit time. These data are presented in Fig. 2. The specific activity of the silver was combined with the count coefficient to determine the total amount of silver which had "penetrated" through the tungsten surface at each temperature.

Since the specimens were far from being saturated with silver even after a 24-hour heating, there was no possibility of relating the silver contained in the tungsten to the entire sample mass. A rough evaluation of the depth of penetration of the silver into the tungsten was made by removing a layer  $20 \mu$  deep from both sides of the plate. Count on this sample proved to be no higher than the background itself. Figure 2 shows that there is a linear relation between the number of counts per unit surface per unit time and the duration of heating at each of the temperatures. This justifies the assertion that this is not a case of diffusion. Clearly some other process of penetration comes into play here. This differs from diffusion insofar as it is characterized by a constant rate of penetration at fixed temperature, the value of which is  $7.62 \cdot 10^{-8} \text{ g/cm}^2 \cdot \text{sec}$  at  $1080^\circ$ . The energy of activation,  $E$ , of this process was calculated from the slope of the experimental straight lines and proved to be equal to  $825,000 \text{ cal/g-at}$ .

An additional factor which might aid in explaining the penetration of the silver into the tungsten is the marked diminution in the hardness of the latter during extended heating in molten silver. This led to disintegration of the tungsten plate in a number of instances. In this light, penetration of Ag into W could be

explained as a process of attack of the tungsten grain boundaries by molten silver. The silver atoms then penetrate into the resulting "pores". This process should be linearly dependent on time and would, therefore, be reflected in the experimental curves. Numerous cases of such disintegration of metals during heating in a foreign metallic liquid has been observed.

#### LITERATURE CITED

1. M. Hansen, The Structures of Binary Alloys [Russian translation] (Moscow-Leningrad, 1941).
2. F. A. Bernoulli, Pogg. Ann. 111, 587 (1860).
3. M. V. Schwarz, Metall- und Legierungskunde (Stuttgart, 1929) p. 73.



# EFFECT OF THE NATURE OF THE CATION ON THE KOLBE ELECTROSYNTHESIS

M. Ya. Fioshin, Yu. B. Vasil'ev, and E. G. Gaginkina

Institute of Electrochemistry, Academy of Sciences of the USSR

(Presented by Academician A. N. Frumkin, June 26, 1960)

Translated from *Doklady Akademii Nauk SSSR*, Vol. 135, No. 4, pp. 909-912,  
December, 1960

Original article submitted July 6, 1960

It has been reported in the literature that the cation of the salt of carboxylic acid has a considerable effect on the yield of products formed at the anode during Kolbe electrosynthesis [1-3]. The effect of the nature of the cations on the anode process has also been observed in a number of other anode reactions which occur at high potentials. Izgaryshev et al. reported that the nature of the cations has an effect on the yield of persulfuric acid during the anode oxidation of sulfuric acid and associated this effect with a change in the degree of hydration of hydrosulfate ions [4, 5]. Erdey-Gruz and Safarik consider that cations added to sulfuric acid in the form of sulfates change the oxygen overvoltage on the anode due to their effect on water molecules adsorbed in the double layer [6, 7].

The Kolbe electrosynthesis proceeds at high anode potentials and, as in the case of the electrosynthesis of persulfuric acid, involves dimerization of free radicals formed as a result of discharge of anions [8]. However, while a series of regularities in the change of anode polarization and product yields in relation to the nature of the cation were observed in the electrosynthesis of persulfuric acid and attempts were made to explain the phenomena observed, this cannot be said of the Kolbe electrosynthesis. Though it has been reported that there is a connection between the hydrocarbon yield and the nature of the cation of the carboxylic acid salt, no regular relation could be observed and there is no satisfactory explanation of this connection in the literature. It therefore seemed interesting to study the effect of cations on the anode process in the Kolbe electrosynthesis.

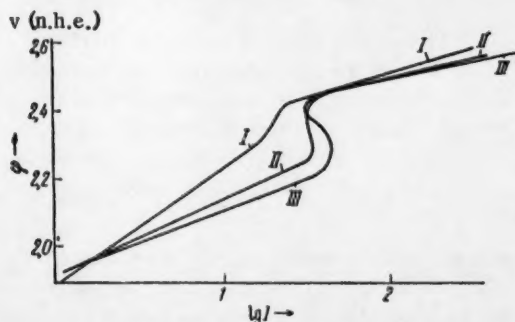


Fig. 1. Polarization curves of  $\phi$  against  $\lg I$  for 0.1 N alkali metal acetates. I)  $\text{KOOCCH}_3$ ; II)  $\text{NaOOCCH}_3$ ; III)  $\text{LiOOCCH}_3$ .

Using the procedure we described previously [8], we studied the behavior of acetates of the following cations on a rotating platinum anode:  $\text{Li}^+$ ,  $\text{Na}^+$ ,  $\text{K}^+$ ,  $\text{NH}_4^+$ ,  $\text{Rb}^+$ ,  $\text{Cs}^+$ ,  $(\text{CH}_3)_4\text{N}^+$ ,  $\text{Mg}^{2+}$ ,  $\text{Ca}^{2+}$ ,  $\text{Sr}^{2+}$ ,  $\text{Ba}^{2+}$ ,  $\text{Tl}^+$ ,  $\text{Tl}^{3+}$ ,  $\text{Co}^{2+}$ ,  $\text{Mn}^{2+}$ ,  $\text{Pb}^{2+}$ . At the same time, we studied the effect of the nature of the cations on the yield of the main products from the Kolbe electrosynthesis, namely, carbon dioxide and ethane, on a smooth, stationary platinum electrode on an apparatus which made it possible to analyze the gas at separate points on the polarization curve.

As we established previously [8], the Kolbe electrosynthesis proceeds at potentials which are more positive than the potentials corresponding to oxygen liberation. On the polarization curve, the

beginning of anode discharge of carboxylate anions is preceded by the wave of oxygen liberation and maximum, whose appearance is associated with retardation of oxygen liberation as a result of adsorption of anions. As the polarization curves showed, the nature of the cation strongly affected the first section, corresponding to oxygen liberation as a result of the discharge of water molecules, and this led to a sharp change in the maximum current (Fig. 1). The effect on the second part of the curve, corresponding to the discharge of acetate ions, was very slight.

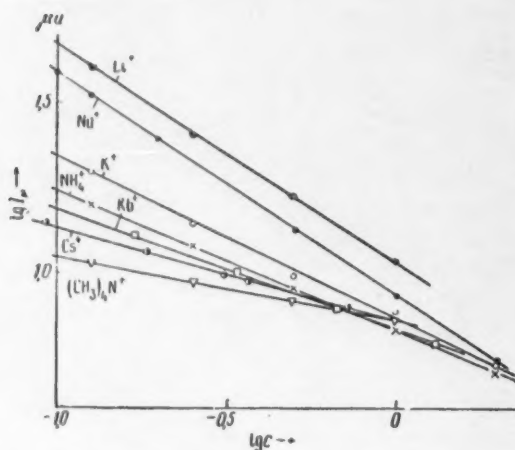


Fig. 2. Relation of the logarithm of maximum current to the logarithm of acetate concentration.

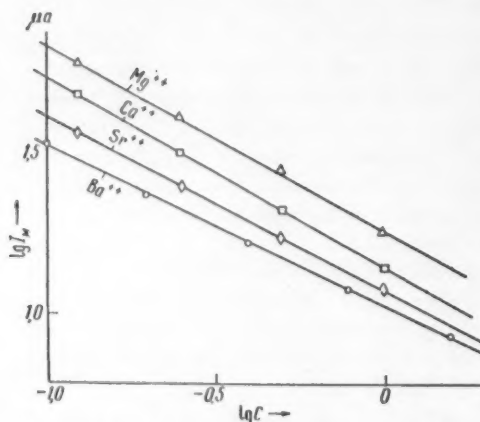


Fig. 3. Relation of the logarithm of maximum current to the logarithm of the concentration for acetates of divalent metals.

Figures 2 and 3 show the relation of the logarithm of the maximum current to the logarithm of the acetate concentration. The nature of the cation had little effect on the maximum current in concentrated solutions. However, the more dilute the solution, the greater was this effect and this was difficult to explain by the dehydrating action of the cation on the anion.

Starting with these considerations, we chose 0.2 N acetate solutions for carrying out electrolyses to collect and analyze the gases.

An examination of the relation of the maximum current and the nature of the cation clearly shows the connection between this phenomenon and the cation radius. The greater the radius of the cation, the lower is the maximum current, i.e., retardation of oxygen liberation and the discharge of acetate ions begin earlier. Thus, it is to be expected that electrolysis of the acetate whose cation has the maximum radius will give the maximum yield of the main products from the Kolbe electro-synthesis. The nature of the cation affects not only the maximum current, but also its relation to the concentration, expressed by the equation  $I_{\max} = \frac{A}{C^n}$  [8], i.e., the value of  $A$  and  $n$ . The greater the cation radius, the lower is the maximum current and the less it depends on concentration. Table 1 clearly illustrates the effect of the nature of the cation on the anode process in the Kolbe synthesis with respect to the magnitude of the cation radius.

From Table 1 it follows that the maximum yield of Kolbe electrosynthesis products is obtained in the electrolysis of acetates whose cations have the greatest radius. The attainment of maximum yield corresponds to the greatest fall in maximum current, i.e., to the strongest suppression of oxygen liberation.

The effect of the nature of cations on the anode process is probably connected with the adsorption of cations in the double electrical layer. To elucidate this question, we measured the displacement in the electrode potential from the initial value in the potential region from 0.5 to 2.0 v relative to a normal hydrogen electrode when cations were added to solutions of acetates of other cations. In a study of the addition of cations  $K^+$ ,  $Rb^+$ ,  $Cs^+$  and  $(CH_3)_4N^+$  to 0.1 N lithium acetate and 1 N sodium acetate, it was observed that there is a linear relation between the adsorption displacement  $\Delta\varphi$  and the logarithm of the concentration of added cation, i.e.,  $\Delta\varphi = b \log C$ . An analogous relation was found by Erdey-Gruiz and Safarik [7]. This relation was observed only at very low additive concentrations (from  $10^{-6}$  to  $10^{-2}$  N). At an additive concentration above a definite value, further increase in concentration produced no further potential displacement.

The greater the difference in the radii of the cations of the base electrolyte and of the acetate introduced, the stronger was the potential displacement in a positive direction produced by adsorption. The greater the cation radius, the lower was the concentration at which no further potential displacement was observed.

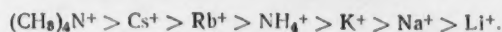
TABLE 1

Relation of Carbon Dioxide and Ethane Yield to the Nature of the Cation, Anode Current Density 10 amp/dm<sup>2</sup>, Acetate Concentration 0.2 N

Cation	$i_{\max}$ at $C=0.1$ N, $\mu\text{A}$	$n$	Current yield of dimethylization product $\text{C}_2\text{H}_6$ , %	Cation radius $r$ , $\text{\AA}$	Cation	$i_{\max}$ at $C=0.1$ N, $\mu\text{A}$	$n$	Current yield of dimethylization product $\text{C}_2\text{H}_6$ , %	Cation radius $r$ , $\text{\AA}$
$\text{Li}^+$	46,8	0,63	64,0	0,60	$(\text{CH}_3)_4\text{N}^+$	11,2	0,205	76,2	—
$\text{Na}^+$	38,9	0,63	66,2	0,95	$\text{Mg}^{2+}$	61,5	0,54	—	0,65
$\text{K}^+$	22,4	0,49	68,2	1,33	$\text{Ca}^{2+}$	51,1	0,56	61,1	0,99
$\text{NH}_4^+$	17,35	0,42	68,7	1,43	$\text{Sr}^{2+}$	38,9	0,515	61,7	1,13
$\text{Rb}^+$	15,85	0,380	(66,4)	1,48	$\text{Ba}^{2+}$	30,9	0,46	68,3	1,35
$\text{Cs}^+$	13,5	0,280	—	1,99					

There was an analogous change in the maximum current corresponding to retardation of oxygen liberation. It was observed that the acetate introduced reduced the maximum current only if the radius of its cation was greater than the radius of the cation of the acetate forming the base electrolyte. For example, if tetramethylammonium or cesium acetates were added to sodium acetate solution, there was a sharp decrease in the maximum current. If acetates whose cations had a smaller radius than the base electrolyte cations were introduced, then this gave no effect at all, i.e., no change in the maximum current or potential displacement was observed.

It is probable that the observed phenomenon can only be explained by assuming that cations form part of the electrical double layer at the anode. The introduction into the solution of the acetate of a cation with a large radius and, consequently, a high adsorption power on the given electrode apparently leads to its predominant adsorption on the electrode. The addition of a cation with a lower adsorption power than the base electrolyte cation leads to no change in the structure of the double layer or a potential displacement. Consequently, the cations may be arranged in the following series with respect to adsorption activity on smooth platinum:



In the work of Obrucheva [9], it was concluded that cations whose electron shell did not have the configuration of noble gases may show strongly expressed specific adsorption. Specific adsorption of  $\text{Cs}^+$  on a Hg surface on which  $\text{F}^-$  ions were adsorbed was detected in the work of Damaskin, Nikolaeva-Fedorovich, and Frumkin [10].

We also studied the specific action of variable-valence cations  $\text{Ti}^+$ ,  $\text{Co}^{2+}$ ,  $\text{Mn}^{2+}$ ,  $\text{Pb}^{++}$  and it was shown that the action of these cations is connected not with their activity as "catalysts of hydrogen peroxide decomposition," as was proposed by Glasstone and Hickling [1], but with the change in the state of the electrode surface in the presence of these cations. The surface changes due to the formation on the electrode of deposits of oxides of these metals ( $\text{MnO}_2$  and  $\text{PbO}_2$ ). It is also possible that a new electrode process occurs on the electrode ( $\text{Co}^{2+} - e \rightarrow \text{Co}^{3+}$ ,  $\text{Ti}^+ - 2e \rightarrow \text{Ti}^{3+}$ ).

#### LITERATURE CITED

1. S. Glasstone and A. Hickling, *Electrolytic Oxidation and Reduction* (London, 1935) p. 279.
2. O. Walker and J. Weiss, *Trans. Farad. Soc.* **31**, 1011 (1935).
3. F. Fichter and R. Zumbrunn, *Helv. Chim. Acta* **10**, 878 (1927).
4. N. Isgarischew and S. Berkman, *Z. Elektrochem.* **28**, 40 (1922).
5. N. A. Izgaryshev and A. A. Petrova, *Zhur. Fiz. Khim.* **24**, 881 (1950).

6. T. Erdey-Gruz and I. Safarik, Proceedings of the Fourth Conference on Electrochemistry [In Russian] (Moscow, 1959) p. 263.
7. T. Erdey-Gruz and I. Safarik, Acta Chem. Acad. Sci. Hung. 13, 159 (1957).
8. M. Ya. Fiozhin and Yu. B. Vasil'ev, Doklady Akad. Nauk SSSR 134, 879 (1960).\*
9. A. D. Obrucheva, Doklady Akad. Nauk SSSR 120, 1072 (1958).\*
10. B. B. Damaskin, N. V. Nikolaeva-Fedorovich, and A. N. Frumkin, Doklady Akad. Nauk SSSR 121, 129 (1958).\*

\* Original Russian pagination. See C. B. translation.

# INVESTIGATION OF ENERGY TRANSFER ALONG A $\sim\text{CH}_2\sim$ CHAIN BY LUMINESCENCE QUENCHING

V. I. Gusynin and V. L. Tal'roze

Institute of Chemical Physics, Academy of Sciences of the USSR

(Presented by Academician V. N. Kondrat'ev, June 23, 1960)

Translated from *Doklady Akademii Nauk SSSR*, Vol. 135, No. 5, pp. 1160-1163,

December, 1960

Original article submitted June 18, 1960

The luminescence of organic solutions of luminophores under  $\gamma$ -radiation and ultraviolet excitation plays an important part in the study of energy transfer processes in material. By making use of luminescence (in particular, quenching of luminescence) it is possible to find the cross sections (or values proportional to the cross sections) of elementary reactions involving excited molecules in solutions [transfer of excitation energy from solvent molecules to molecules of the fluorescing substance (activator) or quencher, luminescence of activator molecules, etc.].

Up to now, luminescence methods have been used usually for investigating intermolecular transfer of excitation energy (see appropriate literature in [1, 2]). However, in principle, it is possible to use the luminescence method for investigating intramolecular energy transfer along molecular chains of different types. For this purpose one could try to choose substances in which the molecular chain interesting us is connected to a functional group capable of either emitting energy absorbed by the molecule (or transferred to the molecule by a "neighbor") or having a quenching action. It is precisely this second variant which was used by the authors on the example of the quenching of luminescence of terphenyl in dioxane by alcohols with aliphatic chains of various lengths (methyl, ethyl, propyl, hexyl, and nonyl alcohols). The luminescence was produced by weak  $\gamma$ -radiation from an external source.

Let us examine a formal scheme of all the processes which may occur in principle with excited molecules in such a solution, which has first been freed from dissolved oxygen (Table 1). In the table, S, F, and Q denote solvent, activator, and quencher molecules, respectively, and a star marks the excited state.

Processes 1-3 are primary excitation processes; due to the low concentrations of activator and quencher used in our experiments, processes 2 and 3 have a weak effect on the light yield of the solution and we may neglect them for the present. In the case of terphenyl, process 13 can also be neglected [3].

From a consideration of the general scheme, it is possible to obtain the following kinetic equations:

$$\begin{aligned}\frac{dn_s^*}{dt} &= N - (p_4 + p_5 + p_6 + p_7 + p_8 + p_9) n_s^*, \\ \frac{dn_f^*}{dt} &= p_9 n_s^* - (p_{10} + p_{11} + p_{12} + p_{14}) n_f^*,\end{aligned}\tag{1}$$

where  $n_s^*$  and  $n_f^*$  are the concentrations of excited solvent and activator molecules;  $N$  is the number of solvent molecules excited per second per unit volume;  $p_4 - p_{12}$  and  $p_{14}$  are the specific rates of the corresponding processes where  $p_7 = k_7 n_f$ ,  $p_8 = k_8 n_q$ ,  $p_9 = k_9 n_f$ ,  $p_{14} = k_{14} n_q$ ;  $k_7$ ,  $k_8$ ,  $k_9$ , and  $k_{14}$  are the rate constants of the corresponding elementary reactions;  $n_f$  and  $n_q$  are the concentrations of activator and quencher molecules.

TABLE 1

1. $S \rightarrow S^*$	Formation of excited solvent molecules by the action of $\gamma$ -radiation.
2. $F \rightarrow F^*$	Formation of excited activator molecules by the action of $\gamma$ -radiation.
3. $Q \rightarrow Q^*$	Formation of excited molecules of quenching agent by the action of $\gamma$ -radiation.
4. $S^* \rightarrow S + \text{photon}$	Luminescence of excited solvent molecules
5. $S^* \rightarrow S$	Spontaneous deactivation of excited solvent molecules (radiationless transition)
6. $S^* + S \rightarrow S + S$	Self-quenching of excited solvent molecules
7. $S^* + F \rightarrow S + F$	"Quenching" of excited solvent molecules by activator molecules
8. $S^* + Q \rightarrow S + Q$	Quenching of excited solvent molecules by molecules of quenching agent
9. $S^* + F \rightarrow S + F^*$	Transfer of excitation energy from solvent molecules to activator molecules
10. $F^* \rightarrow F + \text{photon}$	Luminescence of excited activator molecules
11. $F^* \rightarrow F$	Spontaneous deactivation of excited activator molecules (radiationless transition)
12. $F^* + S \rightarrow F + S$	Quenching of excited activator molecules by solvent molecules
13. $F^* + F \rightarrow F + F$	Self-quenching of excited activator molecules (concentration quenching)
14. $F^* + Q \rightarrow F + Q$	Quenching of excited activator molecules by molecules of quenching agent

For stationary states, the ratio of the light yields of solutions I and II with concentrations  $n_{sI}$ ,  $n_{fI}$ , and  $n_{qI}$  and  $n_{sII}$ ,  $n_{fII}$ , and  $n_{qII}$ , respectively, of solvent, activator, and quencher from Eq. (1) equals

$$\frac{I_I}{I_{II}} = \frac{n_{fI} (1 + yn_{qII} + zn_{fII}) (1 + xn_{qII}) n_{sI}}{n_{fII} (1 + yn_{qI} + zn_{fI}) (1 + xn_{qI}) n_{sII}}, \quad (2)$$

where

$$x = \frac{k_{14}}{p_{10} + p_{11} + p_{12}}, \quad y = \frac{k_8}{p_4 + p_5 + p_6}, \quad z = \frac{k_7 + k_9}{p_4 + p_5 + p_6}.$$

By measuring  $I_I/I_{II}$  for different combinations of  $n_{fI}$ ,  $n_{qI}$ ,  $n_{fII}$  and  $n_{qII}$ , it is possible to use (2) to determine successively  $z$ ,  $y$ , and  $x$ .

#### EXPERIMENTAL AND RESULTS

The photometric cell was charged with 5 ml of quencher solution and 10 ml of activator solution in dioxane at a definite concentration; the mixture obtained was flushed with nitrogen for 5-7 minutes to remove oxygen. The light detector was a FEU-19 photomultiplier, fed with a potential of 1400 v from a stabilized, high-voltage rectifier. The geometry was strictly constant for all the measurements. The  $\gamma$ -radiation source was the isotope  $Co^{60}$ . The dose strength was approximately 5.4 r/hr in all experiments. A measure of the relative light yield of the solution was the photomultiplier current, which was measured with a class 0.5 microammeter. The sensitivity of the photomultiplier was checked before each measurement with a standard (stilbene crystal) and an appropriate correction introduced.

The experiments were carried out at room temperature. The relative light yield of the solutions in our experiments was measured for three terphenyl concentrations ( $2.89 \cdot 10^{-3}$ ;  $7.23 \cdot 10^{-3}$ ;  $2.89 \cdot 10^{-2}$  mole/liter).

The ranges of quencher concentrations were as follows: methanol 0.21-1.03, ethanol 0.14-0.73, propanol 0.11-0.56; hexanol 0.07-0.34, and nonanol 0.05-0.24 mole/liter.

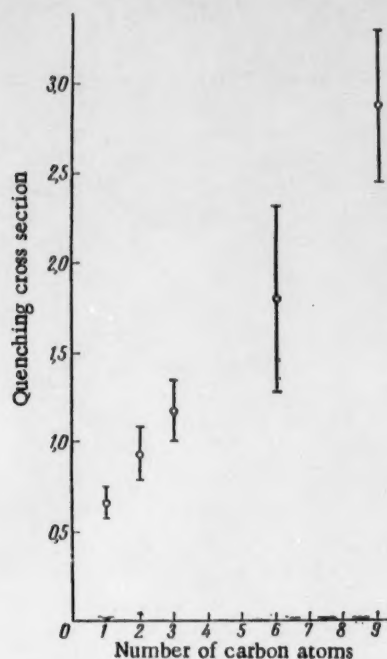


Fig. 1. Relation of quenching cross section of solvent in arbitrary units to the length of the  $\sim\text{CH}_2\sim$  chain.

The procedures described can be used if the fluorescence spectra of the quenched and unquenched solutions do not differ appreciably. It is known [4] that the emission spectrum of a toluene solution of terphenyl shows no appreciable change when methanol is added (up to 30 vol. %). It may be assumed that this is also the case for the other alcohols we investigated.

Table 2 gives the values of  $\bar{x}$ ,  $\bar{y}$ , and  $\bar{z}$  for the five alcohols and a dioxane solution of terphenyl. Each value is the mean from the results of several determinations by formulas derived from expression (2).

An examination of the data in the table for  $\bar{y}$  and  $\bar{x}$  shows that: 1) the quenching is caused mainly by the reaction of excited solvent molecules with alcohol molecules; 2) the quenching cross section increases linearly (within the limits of experimental errors) with the length of the  $\sim\text{CH}_2\sim$  chain (number of carbon atoms) in the alcohol molecule. For clarity, this relation is illustrated graphically (see Fig. 1).

The increase in quenching cross section with an increase in the length of the  $\sim\text{CH}_2\sim$  chain might be ascribed to the capacity of the chain itself to show a quenching action. Special experiments were carried out in which an equivalent number of moles of the corresponding hydrocarbon was added to the solution instead of alcohol. It was found that there was hardly any quenching.

Thus, in the given case there is apparently justification for the energy transfer scheme in which the  $\sim\text{CH}_2\sim$  chain acts as an

TABLE 2\*

Quencher		Luminescing solution	$\bar{z}$ , liter/mole	$\bar{y}$ , liter/mole	$\bar{x}$ , liter/mole
Methanol	$\text{CH}_3\text{OH}$	Terphenyl in dioxane	$115 \pm 12$	$0,66 \pm 0,09$	$0,04 \pm 0,02$
Ethanol	$\text{C}_2\text{H}_5\text{OH}$		$115 \pm 12$	$0,93 \pm 0,15$	$0,07 \pm 0,02$
Propanol	$\text{C}_3\text{H}_7\text{OH}$		$115 \pm 12$	$1,18 \pm 0,16$	—
Hexanol	$\text{C}_6\text{H}_{13}\text{OH}$		$115 \pm 12$	$1,82 \pm 0,55$	—
Nonanol	$\text{C}_9\text{H}_{19}\text{OH}$		$115 \pm 12$	$2,88 \pm 0,42$	$0,17 \pm 0,05$
Water			$115 \pm 12$	$0,23 \pm 0,03$	—
Carbon tetrachloride		Terphenyl in xylene	62	28	18
"	"		415	217	10

\* For comparison, we give values characterizing quenching by water and carbon tetrachloride of the luminescence of a solution of terphenyl in dioxane (our own measurements) and xylene (results taken from [3]).

"antenna" which receives and transmits energy to the OH group and, in general, produces scattering of this energy in an unknown manner. It is interesting that right up to the longest chain, which consists of nine carbon atoms, the cross section increases linearly with the chain length. This indicates that the probability of energy transfer along such a chain is much greater than the probability of its transfer from the chain to a "neighbor".

Naturally, a scheme in which the capacity of the chain to transfer energy and the capacity of the OH group to scatter it are, so to speak, added is approximate. In actual fact, it is naturally impossible to consider that the system of excitation levels of ROH can be divided into independent systems of R and OH. However, as the chain grows longer, this approximation should apparently become more accurate.

The results obtained on the transfer of energy along the  $\sim\text{CH}_2\sim$  chain naturally may be treated from the point of view of charge transfer as always in kinetic investigations of this type.

#### LITERATURE CITED

1. V. L. Levshin, Usp. Fiz. Nauk 64, 1, 55 (1958).
2. J. B. Birks, J. Chem. Phys. 31, 1135 (1959).
3. M. D. Galanin and Z. A. Chizhikova, Optika i Spektroskopiya 4, 2, 196 (1958).
4. Arno Kunh and Jan Mojzls, Chekhosl. Fiz. Zhur. 6, 4, 401 (1956).

# ADSORPTION OF ALKYL RADICALS ON OXIDE SEMICONDUCTORS

I. A. Myasnikov and E. V. Bol'shun

L. Ya. Karpov Physicochemical Institute

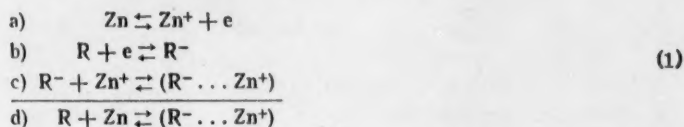
(Presented by Academician S. S. Medvedev, June 22, 1960)

Translated from *Doklady Akademii Nauk SSSR*, Vol. 135, No. 5, pp. 1164-1167, December, 1960

Original article submitted June 17, 1960

In [1] it was shown that the adsorption of atoms and radicals on the surface of semiconducting oxide films of the ZnO type (n-semiconductor) is accompanied by a considerable change in their electrical conductivity. On the basis of these data, in the present work we undertook an investigation of the quantitative relation between the stationary radical concentration and the electrical conductivity of ZnO films lying at various distances from the radical source in various gases. Alkyl radicals (methyl and ethyl) chemisorbed on ZnO decrease its electrical conductivity (the energy of the affinity of a  $\text{CH}_3$  radical for an electron is 25 kcal/mole). This means that this type of active particle forms electron traps (acceptor impurities) on the semiconductor surface.

For a self-activated semiconductor, this phenomenon may be associated with the following processes:

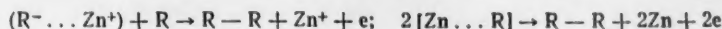


where R is the radical,  $e^-$  is an electron of the conductivity zone,  $\text{Zn}^+$  is an ionized extrinsic zinc atom,  $(\text{R}^- \dots \text{Zn}^+)$  is a surface compound of the radical with the extrinsic atom (the signs plus and minus do not denote the ionic nature of the bond and only indicate the predominant distribution of charges).

Assuming that the rate of the forward reaction (1) is proportional to the concentration of radicals in the gas phase  $n$ , the amount of free surface  $1 - \theta$ , and the concentration of extrinsic zinc atoms, while the rate of the reverse reaction is proportional to the concentration of chemisorbed radicals  $[(\text{Zn}^+ \dots \text{R}^-)]$ , for the stationary process we obtain an expression relating the extrinsic electrical conductivity of the surface layer of the semiconductor to the concentration of radicals in the gas phase.\*

$$\sigma^2/\Delta\sigma = \text{const}/n(1 - \theta), \quad (2)$$

\* With high degrees of filling, expressions (2) and (3) should not apply as in this case there will also be reactions of the type:



(reaction of adsorbed radicals) and, in addition, for high values of  $\theta$  it is necessary to consider the effect of the electrical double layer [2].

where  $\Delta = \sigma_0 - \sigma$ ,  $\sigma_0$  is the electrical conductivity of the sample without radicals on the surface. With the conditions  $\sigma_0 \gg \sigma$  and  $\theta \ll 1$ , formula (2) may be rearranged into the approximate expression

$$\sigma = \text{const}/\sqrt{n}. \quad (3)$$

The accuracy of expression (3) was demonstrated in the present work for the chemisorption of methyl radicals. The methyl radicals were obtained by photolysis of acetone vapor in the reaction vessel illustrated in Fig. 1.

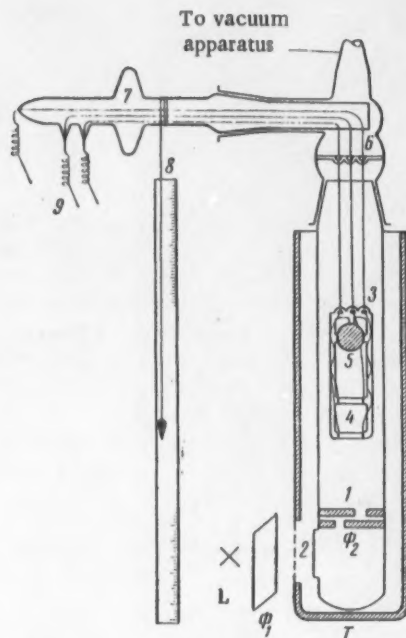


Fig. 1. Photocell (1) with movable quartz frame (3); 2) quartz windows; 4) frames; 5) glass-covered plumb; 6) guide; 7) ground joint; 8) ruler; 9) sealed-in contacts;  $\phi_1$ ) filter for incident light;  $\phi_2$ ) movable black filter; L) PRK-2 lamp; T) thermostat.

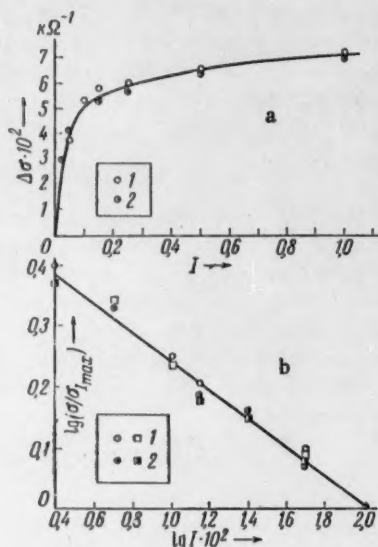
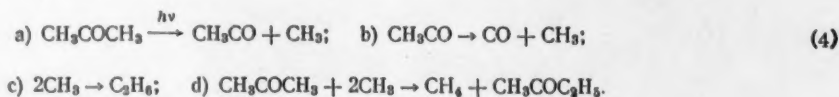


Fig. 2. Relation of ZnO conductivity during photolysis of acetone to light intensity  $I$  (in relative units) at  $t = 300^\circ$ ,  $P_{\text{acetone}} = 5 \text{ mm Hg}$ , a) for  $\Delta\sigma = \sigma_0 - \sigma$  (1) increase in  $I$ , 2) decrease in  $I$ ; b) for two film samples differing in thickness by a factor of 1.5 (1) increase in  $I$ , 2) decrease in  $I$ .

The acetone vapor pressure was varied from 0.1 to 100 mm Hg, the inert gas pressure from 1 to 200 mm, and the temperature from  $200^\circ$  to  $300^\circ$  (the value of  $\theta$  is low at high temperatures). The distance of the ZnO films from the radical source (distance from the filter  $\phi_2$ ) was varied from 1 to 15 cm. The thickness of the ZnO films, which were deposited on the rod of a quartz frame 4, was approximately  $5 \mu$ .

According to data in [3], during the photolysis of acetone under the given conditions (temperature and pressure), the following main reactions occur:



The quantum yield of the primary photolysis process is close to unity. The destruction of methyl radicals is mainly bimolecular according to reaction c [4].

The change in the stationary concentration of radicals with the intensity of the absorbed light  $I$  with this condition follows the law  $n \sim \sqrt{I}$ . By substituting this expression in (3), we obtain a relation for  $I$  and the electrical conductivity ( $\sigma$ ) of the semiconductor film, i.e.,

$$\sigma = \text{const}/\sqrt{I}. \quad (5)$$

An experimental check of formula (5) is shown in Fig. 2. The slope of the line in Fig. 2b is  $-0.26$ . This means that formula (5) is obeyed satisfactorily. This, in its turn (for the case examined) indicates the accuracy of formulas (2) and (3).

To estimate the sensitivity of semiconductor films to methyl radicals, we calculated the concentration of radicals under stationary conditions from measurements of the energy of the incident and absorbed light. For the established process of acetone photolysis, the following expression applies:

$$(I_0/V)(1 - e^{-\alpha dp}) = k_1 n^2 + k_2 np, \quad (6)$$

where  $V = 20$  cc is the volume of the irradiated zone,  $\alpha = 0.94 \cdot 10^4$  cm<sup>2</sup>/mole is the absorption coefficient ( $\lambda = 3100$  Å),  $d = 3$  cm is the thickness of the absorbing layer,  $P = 5$  mm Hg is the acetone vapor pressure,  $I_0 = 3 \cdot 10^{15}$  quanta/sec is the energy of the incident light (the absorption of energy per cc was approximately  $1 \cdot 10^{12}$  quanta/sec),  $k_1 = 5 \cdot 10^{13}$  mole<sup>-1</sup> · cc · sec<sup>-1</sup> and  $k_2 = 10^8$  mole<sup>-1</sup> · cc · sec<sup>-1</sup> are the rate constants of reactions 4c and 4d for  $t = 300^\circ$  [4, 5].

The calculation shows that the stationary radical concentration  $n$  at the maximum light intensity in our experiments was not more than  $10^{10}$  radicals/cm<sup>3</sup>. The electrical conductivity of the ZnO film ( $t = 300^\circ$ ) thereupon changed by 300-400% relative to the dark. Consequently, [in accordance with formula (3)], by means of a semiconductor indicator it may be possible to measure radical concentrations of  $10^6$ - $10^7$  radicals/cm<sup>3</sup>, i.e., seven orders lower than by methods existing at present. This high sensitivity of ZnO films to alkyl radicals is also confirmed by comparing data on the activation energies of the electrical conductivity of ZnO in the presence of oxygen molecules [6] (the energy of the affinity of O<sub>2</sub> for an electron is 20 kcal/mole) and methyl radicals [1] (the energy of the affinity of CH<sub>3</sub> for an electron is 25 kcal/mole). Experiment shows that in an oxygen atmosphere at a pressure of  $10^{-6}$  mm ( $10^{10}$  molecules/cm<sup>3</sup>), the electrical conductivity of ZnO films decreases by 30-50% and consequently, under otherwise equal conditions, in the presence of CH<sub>3</sub> radicals the same change in conductivity should correspond to a radical concentration of less than  $10^{10}$  radicals/cm<sup>3</sup>.

An increase in the acetone pressure under photolysis conditions (the frame was moved into the lower part of the vessel) first led to a decrease in electrical conductivity (the dark electrical conductivity was practically unchanged), indicating an increase in the radical concentration due to an increase in the absorption of active radiation, and then to an increase, which was associated with an increase in the rates of reactions 4c and 4d and the reaction of acetone vapor with chemisorbed radicals. An increase in the pressure of inert gases under analogous conditions led only to an increase in the electrical conductivity (see Fig. 3) and there was a symbatic relation between the activity of the inert gas with respect to the increase in the conductivity of the film under acetone photolysis conditions and the atomic weight of the gas. The increase in  $\sigma$  with the inert gas pressure is most probably associated with the fact that in addition to processes (4), ternary collisions of two radicals with an inert gas atom as the third body play a part in the destruction of CH<sub>3</sub> radicals. From this point of view, the symbatic relation may be explained by the fact that with an increase in the atomic weight in the series He - Ne - Xe, there is an increase in the kinetic diameter of the particles (2.20; 2.60; 4.91 Å) and the number of ternary collisions  $Z_{III} \sim d_{1,2}^6 m_1^{1/2}$ . As a result,  $Z_{III}$  increases from He to Xe.

Figure 4 shows the change in  $\sigma$  of the film with an increase in the distance ( $x$ ) from the bottom of the vessel (Fig. 4a) and the inert gas pressure (Fig. 4b). The radical concentration  $n_0$  at the bottom of the vessel was kept constant during these experiments.

According to data in [7], under these conditions the relative concentration of radicals ( $n_x/n_{x=0}$ ) changes with distance in the following way:  $n_x/n_{x=0} = \exp [-(\beta\gamma^{1/2}x)]$  - surface recombination of the first order;  $n_x/n_{x=0} = [1 + (n_{x=0}bp/6D)^{1/2}x]^{-2}$  - space recombination (ternary collision), where  $b$  and  $\gamma$  are the recombination coefficients,  $\beta = (\bar{v}C/4SD)^{1/2}$ ;  $\bar{v}$  is the mean velocity of the radicals,  $p$  is the gas pressure, and  $C$  and  $S$  are the perimeter and section of the reaction vessel, respectively.

If a semiconductor film is used as a probe, then in accordance with formula (3), these formulas may be rearranged to the following:  $(\sigma_{x=0} / \sigma_x)^2 = \exp [-(\beta \gamma^{1/2} x)]$  and  $(\sigma_x / \sigma_{x=0}) = 1 + (n_{x=0} b p / 6D)^{1/2} x$  or  $\Delta \sigma = (b p / 6D)^{1/2} k x$ , where  $\Delta \sigma = \sigma_x - \sigma_{x=0}$ ,  $k = \text{const}$  [see formula (2)]. For the space bimolecular reaction of methyl radicals, the value  $b p$  should be replaced by the recombination constant of methyl radicals.

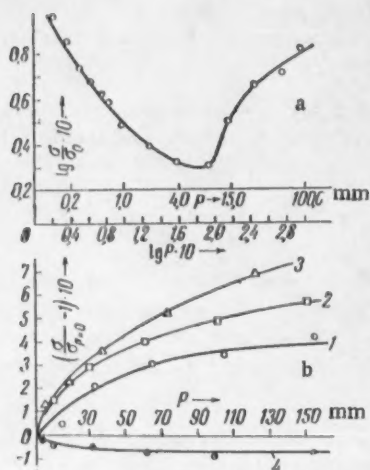


Fig. 3. Relation of ZnO conductivity during acetone photolysis to the pressure: a) of acetone; b) of inert gases ( $P_{\text{acetone}} = 5 \text{ mm Hg}$ ) at  $t = 300^\circ$  (frame at bottom of vessel). 1) He; 2) Ne; 3) Xe; 4) dark conductivity.

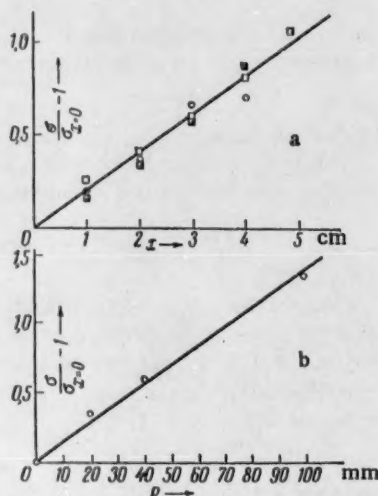


Fig. 4. Relation of conductivity of ZnO films: a) to distance  $x$  to  $\Phi_2$ ; b) to neon pressure at  $t = 300^\circ$ ,  $P_{\text{acetone}} = 5 \text{ mm Hg}$ ,  $\sigma_{x=0} (n_{x=0}) = \text{const}$  (frame at top of vessel).

As yet, the relations derived have only been checked for alkyl radicals for space recombination. Figure 4 shows that the relation derived is confirmed adequately by experiment. This means that semiconductor probes may be used to investigate recombination processes and the reactivity of radicals in the presence of various gases.

The method proposed may also be used to study active particles arising during the pyrolysis or radiolysis of chemical substances and in some heterogeneous reactions. Experiment shows that different alkyl radicals behave differently as regards effect on the conductivity of films and therefore there is the possibility of identifying them at extremely low concentrations.

The authors would like to thank Professor S. Ya. Pshezhetskii and the group in the laboratory for valuable help in discussing the results of the work.

#### LITERATURE CITED

1. I. A. Myasnikov, Doklady Akad. Nauk SSSR **120**, 1298 (1958).\*
2. K. Hauffe, Angew. Chem, **7**, 189 (1955).
3. W. A. Noyes and L. M. Dorfman, J. Chem. Phys. **16**, 788 (1948).

\* Formula (2) should be used at low values of  $\Delta \sigma$ .

\*\* Original Russian pagination. See C. B. translation.

4. R. Gomer and G. B. Kistiakowsky, J. Chem. Phys. 19, 85 (1951).
5. A. F. Trotman-Dickenson and E. W. Steacie, J. Chem. Phys. 18, 1097 (1950).
6. I. A. Myasnikov, Zhur. Fiz. Khim. 31, 1721 (1957).
7. W. V. Smith, J. Chem. Phys. 11, 110 (1943).



# ON A CERTAIN POSSIBILITY IN THE QUANTUM THEORY OF CHEMISORPTION

V. I. Osherov

L. Ya. Karpov Physicochemical Institute

(Presented by Academician V. A. Kargin, June 24, 1960)

Translated from *Doklady Akademii Nauk SSSR*, Vol. 135, No. 5, pp. 1168-1171,  
December, 1960

Original article submitted June 23, 1960

Most of the quantum theoretical studies of chemisorption aim at investigating the levels of localized electron states (see, for instance [1, 2]). However, these levels have no direct connection with any observable property. The heat of adsorption, for which a proper theory still is absent, is an important observable property. An attempt to calculate this heat has been done in the study [3].

The aim of the present paper is to extend the study [3] and to establish a definite procedure for the calculation of chemisorption heats which may be particularly useful in the adsorption of complicated atoms and molecules.

We consider the shift in electron energy of the crystal resulting from the formation of defects and use a method which is convenient in the special case of adsorption.

We introduce complete many-electron wave functions  $\Psi_0$  and  $\Psi$ , which obey equations of the form

$$(H_0 - E_0) \Psi_0 = 0; \quad (1)$$

$$(H_0 + \lambda V - E) \Psi = 0; \quad (2)$$

$$H_0 = -\frac{\hbar^2}{2m} \sum_i \nabla_i^2 + \sum_i v_0(r_i) + \frac{1}{2} \sum_{i,h}' \frac{e^2}{|r_i - r_h|}; \quad (3)$$

$$V = \sum_i v(|r_0 - r_i|); \quad (4)$$

$v_0(r_i)$  is the average of the periodic lattice potential;  $V$  is the perturbation produced by the defect; the sums are extended over all electrons.

Now, we use the relation

$$E = E_0 + \int_0^\lambda \langle \Psi | V | \Psi \rangle d\lambda, \quad (5)$$

which upon normalizing  $\langle \Psi | \Psi \rangle = 1$  is an obvious consequence of the fact that the ground state of the perturbed system is stationary with respect to variations in the wave function. The relation (5) in principle enables the energy shift to be found, when  $\Psi(\lambda)$  is known. Let us use now a one-electron approximation. This

considerably simplifies the problem, in particular in the part which concerns the possibility of forming localized states. We will neglect the mutual interaction between the electrons. Then

$$E = E_0 + 2 \sum_i \int_0^\lambda \langle \psi_{\epsilon_i} | v | \psi_{\epsilon_i} \rangle d\lambda; \quad (6)$$

here  $\psi_{\epsilon_i}$  are one-electron wave functions obeying the equation

$$\left( -\frac{\hbar^2}{2m} \nabla^2 + v_0 + \lambda v - \epsilon_i \right) \psi_{\epsilon_i} = 0. \quad (7)$$

We restrict the spectrum of the unperturbed equation

$$\left( -\frac{\hbar^2}{2m} + v_0 - \epsilon_k \right) \psi_k = 0 \quad (8)$$

to the upper valence band ( $\mathbf{k}$  is the wave vector inside this band;  $\psi_k$  is the corresponding Bloch function).

Let us consider the main region of the lattice  $N$ ; then the spectrum of  $\epsilon_k$  will be quasicontinuous and we may write Eq. (7) in the form

$$\psi_{\epsilon_i} = \frac{1}{1 - \lambda K_{\epsilon_i} v} \psi_k; \quad (9)$$

$$K_{\epsilon_i} = (1 - P_k) \frac{1}{H - \epsilon_i}. \quad (10)$$

Here  $H = -\frac{\hbar^2}{2m} \nabla^2 + v_0$ ;  $P_k$  is the projector on the state  $\psi_k$ . In the limit  $N \rightarrow \infty$  [4]

$$\psi_{\epsilon_i} = A \frac{1}{1 - \lambda G_{\epsilon_i} v} \psi_k. \quad (11)$$

Here  $A$  represents a phase factor of no importance for us;  $G_{\epsilon_i}$  is a Green's function, which is so defined that it satisfies the requirements of the evolution principle and which we write in the form of an integral over the whole band

$$G_{\epsilon_i}(\mathbf{r} - \mathbf{r}') = N \frac{2\pi i}{(2\pi)^3} \int \delta_+(e_i - \epsilon_k) \psi_k(\mathbf{r}) \bar{\psi}_k(\mathbf{r}') d\mathbf{k}. \quad (12)$$

In the case of a local perturbation which interests us the wave functions  $\psi_{\epsilon_i}$  are normalized [5] and, therefore, the relations (5) and (6) can be used, which gives  $(\Delta E = E - E_0 \sim$  the components of the heat in the case of adsorption)

$$\Delta E = 2 \sum_i \int_0^\lambda \left\langle \psi_k \left| v \frac{1}{1 - \lambda G_{\epsilon_i} v} \right| \psi_k \right\rangle d\lambda. \quad (13)$$

Now we represent  $\psi_k(\mathbf{r})$  as a Fourier series of Wannier functions  $a_n(\mathbf{r})$  localized near the lattice points

$$\psi_k(\mathbf{r}) = \frac{1}{N^{1/2}} \sum_n e^{i\mathbf{k}\mathbf{n}} a_n(\mathbf{r}). \quad (14)$$

We expand the operator  $\frac{1}{1 - \lambda G_{\epsilon_i} v}$  in a power series of  $\lambda$ . Using (14) we write the term of the  $(p+1)$ th order in the matrix element as follows

$$\begin{aligned} \lambda^p \langle \psi_k | v (G_{\epsilon_i} v)^p | \psi_k \rangle = \\ = \frac{\lambda^p}{N} \sum_{n, m_1, \dots, m_p, n'} e^{ik(n-n')} v_{nm_1} I_{\epsilon_i} (m_1 - m_2) \dots I_{\epsilon_i} (m_{p-1} - m_p) v_{m_p n'}. \end{aligned} \quad (15)$$

Here we have introduced Green's function for a limited space

$$I_{\epsilon_i} (m - m') = \frac{2\pi i}{(2\pi)^3} \int e^{ik(m-m')} \delta_+( \epsilon_i - \epsilon_k ) dk, \quad (16)$$

$$v_{nn'} = \langle a_n | v | a_{n'} \rangle. \quad (17)$$

Following [6] we take only the very greatest term of the matrix elements namely;  $\alpha = v_{n_0 n_0}$ ;  $n_0$  is the point which of all  $n$  is nearest to  $r_0$ .

Then

$$\lambda^p \langle \psi_k | v (G_{\epsilon_i} v)^p | \psi_k \rangle = \frac{\lambda^p}{N} I_{\epsilon_i}^p (0) \alpha^{p+1}. \quad (18)$$

Summing up the series thus obtained we find

$$\langle \psi_k | v \frac{1}{|1 - \lambda G_{\epsilon_i} v|} | \psi_k \rangle = \frac{1}{N} \frac{\alpha}{|1 - \lambda \alpha I_{\epsilon_i} (0)|^2}. \quad (19)$$

In this same approximation one finds for two identical defects situated at a distance  $R$  from each other that

$$\langle \psi_k | v \frac{1}{|1 - \lambda G_{\epsilon_i} v|} | \psi_k \rangle = \frac{2}{N} \alpha \left| \frac{1 - [I_{\epsilon_i} (0) - \cos kR I_{\epsilon_i} (R)] \lambda \alpha}{(1 - I_{\epsilon_i} (0) \lambda \alpha)^2 - I_{\epsilon_i} (R) \lambda \alpha} \right|^2. \quad (20)$$

After substituting (19) in (13), we get ( $\lambda = 1$ )

$$\Delta E = \frac{2}{N} \sum_i \frac{1}{\text{Im } I_{\epsilon_i} (0)} \arctg \frac{\alpha \text{Im } I_{\epsilon_i} (0)}{1 - \alpha \text{Re } I_{\epsilon_i} (0)}, \quad (21)$$

where according to (16)

$$\text{Im } I_{\epsilon_i} (0) = \frac{1}{(2\pi)^3} \int \delta(\epsilon_i - \epsilon_k) dk, \quad \text{Re } I_{\epsilon_i} (0) = \frac{1}{(2\pi)^3} P \int \frac{dk}{\epsilon_i - \epsilon_k}. \quad (22)$$

Within the bounds of the spectrum  $\text{Im } I_{\epsilon_i} (0) = 0$ , since starting from a certain  $\alpha$  (in the three-dimensional case) at a definite  $\epsilon$

$$1 = \alpha \text{Re } I_{\epsilon_i} (0). \quad (23)$$

If one now takes into account that  $\text{Re } I_{\epsilon_i} (0)$  is discontinuous, when the boundary of the spectrum is crossed, then it becomes clear that the energy found from (23) corresponds to a localized boundary state  $\psi_g$ . In this case it undergoes resonance scattering

$$\psi_{\epsilon_i} = \psi_g + N (\epsilon_0 - \epsilon_g) \int \frac{\psi_k dk}{\epsilon_0 - \epsilon_k}; \quad (24)$$

depending upon the sign of  $\alpha$ ,  $\epsilon_g$  is the upper or the lower boundary of the band. So we obtain finally

$$\Delta E = 2(\epsilon_0 - \epsilon_g) + \frac{2}{(2\pi)^3} \int \frac{1}{\text{Im } I_{\epsilon_k}(0)} \arctg \frac{\alpha \text{Im } I_{\epsilon_k}(0)}{1 - \alpha \text{Re } I_{\epsilon_k}(0)} dk; \quad (25)$$

the integral is taken over the Fermi impulse  $k_F$ .

For the shift in the vibrational part of the lattice free energy an analogous relation has been found by I. M. Lifshits [6, 7].

When using the simplest molecular orbital method one obtains in the case of adsorption

$$\alpha = \frac{z}{\epsilon_0 - \epsilon_2} + \alpha_2, \quad (26)$$

where

$$z = \langle a_2 | v_1 | a_{1n} \rangle \langle a_{1n} | v_2 | a_2 \rangle; \alpha_2 = \langle a_{1n} | v | a_{1n} \rangle; \epsilon'_2 = \epsilon_2 + \alpha_1, \alpha_1 = \langle a_2 | v_1 | a_2 \rangle;$$

$\epsilon_2$  is the energy of the electron in the atom before adsorption. The indices 1 and 2 refer to the lattice and the adsorbed atom, respectively.

When  $|\alpha| \ll \beta$  ( $\beta$  is the band width)  $\Delta E \sim \alpha$ , and, when  $|\alpha| \gg \beta$  it no longer depends upon  $\alpha$ , but in this case a greater number of localized states may be formed and a more detailed discussion is needed. Relation (25) also shows that in both extremes (an almost filled or an almost empty band)  $\Delta E \sim \epsilon_F$ .

Further, we note that between two adsorbed atoms there exists, according to (20), an "interaction," which at great mutual distances  $R$  behaves as  $\text{const}/R^2$ .

So, we come to the important conclusion that for calculating heats of adsorption one may use the wave functions (11), which essentially are solutions of the Schroedinger equation for the case of scattering and can be found with a sufficient degree of accuracy also for the adsorption of complicated systems.

I express my thanks to Professor M. I. Temkin and V. V. Tolmachev for a valuable discussion of the paper.

#### LITERATURE CITED

1. J. Koutecky, *Trans. Farad. Soc.* **54**, 1038 (1958).
2. T. B. Grimley, *Proc. Phys. Soc.* **72**, 103 (1958).
3. V. I. Osherov, *Doklady Akad. Nauk SSSR* **132**, 884 (1960).\*
4. B. S. De Witt, *Phys. Rev.* **103**, 1565 (1956).
5. B. S. De Witt, *Phys. Rev.* **100**, 905 (1955).
6. I. M. Lifshits, *Uspekhi Matem. Nauk* **7**, 171 (1952).
7. I. M. Lifshits, *Nuovo Cim.* **3**, 4, Suppl. X, 716 (1956).

\* Original Russian pagination. See C. B. translation.

# A METHOD FOR DETERMINING THE RATES AND THE KINETIC CONSTANTS OF COMPLICATED CHEMICAL REACTIONS IN A FLOW SYSTEM

G. M. Panchenkov and Yu. M. Zhorov

I. M. Gubkin Moscow Institute of Petrochemical and Gas Industry

(Presented by Academician A. V. Topchiev, June 21, 1960)

Translated from *Doklady Akademii Nauk SSSR*, Vol. 135, No. 5, pp. 1172-1175,  
December, 1960

Original article submitted June 18, 1960

As we have shown in [1], the rate of a chemical reaction can be easily derived from the experimentally determined dependency between the conversion of a substance fed and its feed rate, even if one does not know the kinetic equation of the process. From the way in which the reaction rate at a given constant conversion of the substance fed depends upon temperature the activation energy of the process can be determined. From the activation energy of the heterogeneous-catalytic reaction one may judge in which region (kinetic, internal diffusion or external diffusion) the reaction proceeds.

The method proposed, which has been discussed for examples of simple reactions [1], is only correct, as can easily be seen, in those cases where the rate is a function of the degree in which the substance fed is converted and does not depend upon the number of moles  $n_0$  fed into the reactor per unit time; the conversion degree  $x$  is expressed in relative units so that in those cases the rate  $W = f(x)$ .

Since the reaction rate is a function of the partial pressures  $P_{A_i}$  of the reactants, the dependency of  $W$  upon  $n_0$  will be determined by the relation between  $P_{A_i}$  and  $n_0$ . As has been shown in [2], the latter may be expressed as a function of the degree of conversion for one of the reactants by means of the relation

$$P_{A_i} = \frac{\frac{n_{0A_i}}{n_{0A_1}} - \frac{\nu_i}{\nu_1} x_{A_1}}{\frac{\sum n_{0A_i}}{n_{0A_1}} - \frac{\sum \nu_i}{\nu_1} x_{A_1}} P_0, \quad (1)$$

where  $\nu_i$  are the stoichiometric coefficients;  $P_0$  is the total pressure in the reactor.

From Eq. (1) it is obvious that  $P_{A_i}$  does not depend upon  $n_0$  in the following two cases: 1) when only a single substance reacts, and 2) when several substances react, but in all experiments the composition of the reacting mixture is kept constant and only the rate of feeding a reactant mixture with a given composition is varied.

In the more general case where several substances react and the composition of the reactant mixture is different in each experiment, the reaction rate will be a function not only of the conversion degree  $x$  but also of the feed rate  $n_0$ . Therefore, applying to the previously obtained equation for a heterogeneous-catalytic reaction [1]

$$-\frac{S_0 l}{n_0^2} = \frac{d}{dn_0} \int_0^x \frac{dx}{W} \quad (2)$$

the rule of differentiating a definite integral with respect to a parameter we obtain

$$-\frac{S_0 l}{n_0^2} = \int_0^x \frac{\partial}{\partial n_0} \left( \frac{1}{W} \right) dx + \frac{1}{W} \frac{dx}{dn_0}, \quad (3)$$

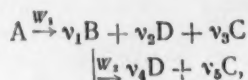
where  $S_0$  is the catalyst surface area per unit of bed length,  $l$  is the length of the catalyst bed,

When  $W$  does not depend upon  $n_0$ , Eq. (3) goes over in the previously derived relation [1]

$$W = -\frac{n_0^2}{S_0 l} \frac{dx}{dn_0} = \frac{1}{S_0 l} \frac{dx}{d(1/n_0)}. \quad (4)$$

We have used this relation to determine the kinetic parameters in the case of simple reactions. The method developed may be applied with success also for a kinetic description of complicated reactions.

Many reactions of importance in industry (cracking of separate hydrocarbons or oil fractions, dehydrogenation of hydrocarbons, dehydration of alcohols etc.) proceed via the formation of a stable intermediary product. For instance, catalytic cracking follows the scheme:



where  $A$  is the substance fed,  $B$  is the intermediary product,  $C$  and  $D$  are end products. The reaction rates  $W_1$  and  $W_2$  are determined from the conversions of  $A$  and  $B$ .

The kinetic analysis of the first stage in a consecutive reaction gives no troubles. To obtain relations for the kinetic analysis of the second stage we define the relative conversion degree of substance  $B$  as  $y$ , the relative yield of  $B$  as  $u$  and the relative yield of reaction product  $C$  as  $z$  (all three are expressed as fractions of the amount of substance  $A$  fed per unit time). Then the rate of the second reaction stage may be written in the form

$$W_2 = \frac{n_0 dy}{S_0 dl}. \quad (5)$$

Taking into account that

$$W_2 = k_2 \sigma_B, \quad (6)$$

where  $\sigma_B$  is the degree in which the surface is covered by substance  $B$  and that  $\sigma_B$  does not depend upon  $n_0$ , that is

$$\sigma_B = \varphi_1(x, y) = \varphi_2(x, u), \quad (7)$$

and applying the procedure described above [we integrate (5) and differentiate the equation obtained with respect to  $n_0$ ], we find:

$$W_2 = -\frac{n_0^2}{S_0 l} \frac{dy}{dn_0}. \quad (8)$$

However, the experiment does not give  $\underline{y}$ , but  $\underline{u}$ , the relative yield of the intermediary product B. For the case under consideration  $u = \nu_1 x - y$ . In order to transform from the variable  $\underline{y}$  to  $\underline{u}$  we search for the difference  $\nu_1 W_1 - W_2$ . On account of the formulas (4) and (8)

$$\nu_1 W_1 - W_2 = -\frac{n_0^2}{S_0 l} \frac{\nu_1 dx - dy}{dn_0} = -\frac{n_0^2}{S_0 l} \frac{du}{dn_0}, \quad (9)$$

from which follows

$$W_2 = -\frac{n_0^2}{S_0 l} \left( \frac{\nu_1 dx}{dn_0} - \frac{du}{dn_0} \right) = \frac{1}{S_0 l} \left[ \frac{\nu_1 dx}{d(1/n_0)} - \frac{du}{d(1/n_0)} \right]. \quad (10)$$

The value of  $\frac{du}{dn_0}$  may be found from the experimental relation between the yield of intermediary product B and the feed rate of the raw material A. In the special case where the yield of intermediary product goes through a maximum,  $\frac{du}{dn_0} = 0$  so that the relation is

$$W_2 = \nu_1 W_1. \quad (11)$$

When the reaction rate is known at various temperatures and product concentrations, it is not difficult to find also the other kinetic parameters. For instance, the activation energy of the second stage may be found from the way in which the reaction rate changes with temperature at constant  $\sigma_B$ . But since  $\sigma_B$  is determined from the variables  $\underline{x}$  and  $\underline{y}$  or, which is the same,  $\underline{x}$  and  $\underline{u}$ , such a degree of conversion  $\underline{x}$  must be chosen for the calculation so that at all temperatures an equal value is obtained for  $\underline{u}$  (see Fig. 1). If such a conversion degree has been found, it is not difficult to calculate the activation energy after having determined the rates for the points selected. The inaccuracy of this determination will be somewhat higher than that in the analysis of the first reaction stage, because the errors of  $\underline{x}$  and  $\underline{u}$  are superposed.

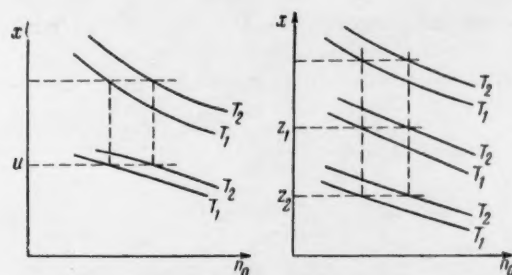
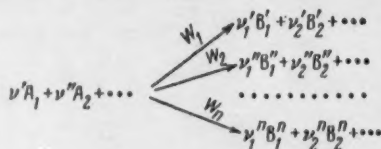


Fig. 1. Selection of the points for determining the activation energy of the second stage in a consecutive reaction (left) or in a complex of parallel reactions (right).

If one of the reaction products is formed in the second stage only (for instance, the product C,  $\nu_3 = 0$ ), then the rate of the second stage may be expressed in the relative yield of this product. Since in this case  $y = \frac{\nu_1}{\nu_3} z$ , we find by substituting its relation into (8)

$$W_2 = -\frac{(\nu_1/\nu_3) n_0^2}{S_0 l} \frac{dz}{dn_0} = \frac{\nu_1/\nu_3}{S_0 l} \frac{dz}{d(1/n_0)}. \quad (12)$$

As a further example we consider parallel reactions of the type:



The rate of each stage in such reactions referred to any substance (for instance,  $A_1$ ) may be expressed in the yield of a product in the stage considered (for instance,  $B_1^i$ ). Designating the yield of this product by  $z_i$  we may write:

$$W_i = \frac{(\nu'/\nu_1^i) n_{0A_1} dz_i}{S_0 dl} \quad (13)$$

If the composition of the reactant mixture for the whole series of experiments with different feed rates is not varied, then by applying the method described above, we obtain

$$W_i = - \frac{(\nu'/\nu_1^i) n_{0A_1}^2}{S_0 l} \frac{dz_i}{dn_{0A_1}} = \frac{\nu'/\nu_1^i}{S_0 l} \frac{dz_i}{d(1/n_{0A_1})} \quad (14)$$

Consequently, the kinetic characteristics of any stage in such a reaction can be determined by examining the changes in relative yield of the reaction products found when varying the feed rate of the reactant mixture. When taking into account that  $W_i = k \Pi \sigma_{A_1}$  it is clear that the activation energy of any stage in the complex, of parallel reactions can be determined only at such degrees of  $A_1$  conversion that correspond to equal yield of each reaction product (Fig. 1).

The methods of determining the reaction rate from yields of the end product can be applied not only in complicated but also in simple reactions. In the latter case they may be used even to verify the accuracy of the experiment, for instance, by comparing the activation energy calculated from curves of over-all conversion degrees with that from curves for the relative yields of products or by verifying whether at a given temperature the ratio of the rates calculated at equal feed rates from the curves mentioned is constant.

All relations derived remain also valid for homogeneous reactions. In this case in all equations obtained  $S_0$  must be replaced by the reactor cross section  $\rho$ .

#### LITERATURE CITED

1. G. M. Panchenkov and Yu. M. Zhorov, Doklady Akad. Nauk SSSR **130**, 1280 (1960).\*
2. G. M. Panchenkov and Yu. M. Zhorov, Collection: J. Phys. Chem., Kinetics and Catalysis [in Russian] (Izd. AN SSSR, Moscow, 1960) p. 3.

\* Original Russian pagination. See C. B. translation.

# ELECTRON DENSITY DISTRIBUTION IN GERMANIUM

Academician of the Academy of Sciences, Beloruss SSR,

N. N. Sirota and A. U. Sheleg

Division of Physics of the Solid State and Semiconductors, Academy of Sciences,  
Belorussian SSR

Translated from *Doklady Akademii Nauk SSSR*, Vol. 135, No. 5, pp. 1176-1178,  
December, 1960

Original article submitted September 10, 1960

In our laboratory we have carried out a systematic investigation of electron density distributions in elementary and compound semiconductors. In the present paper some results, obtained when determining the atomic scattering factor for various values of  $\sum_i h_i^2$  and the electron density distribution in germanium, are recorded.

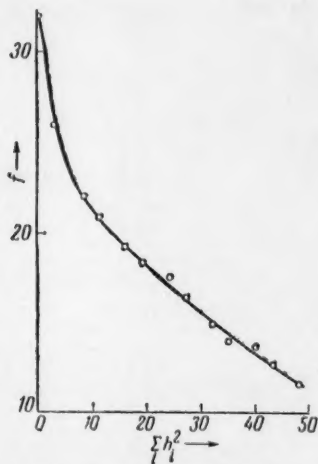


Fig. 1. The atomic scattering factor of Ge plotted versus the sum over the squared indices of the diffraction maxima  $\sum_i h_i^2$ .

Together with the investigation of the electron density distribution in diamond [1-3] and silicon [4, 5] it is of considerable interest to study this distribution in germanium, which also belongs to the fourth group of

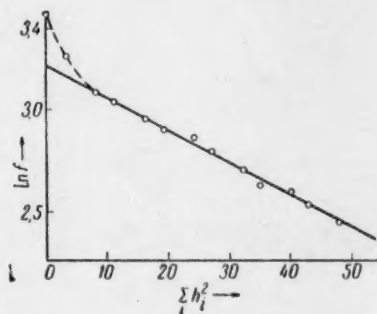


Fig. 2. The logarithm of the atomic scattering factor of germanium as a function of  $\sum_i h_i^2$ .

the periodic system and is of practical importance as a semiconducting material. The investigation of electron density distribution in the sequence diamond-silicon-germanium is also of considerable interest in order to find the nature of the interatomic interaction in elementary semiconductors and establish the connection between the character of the electron density distribution and the semiconducting properties. Only relative values, which

do not allow drawing any quantitative conclusion about the electron density distribution in germanium, are given in the paper of Yu. N. Shuvalov [6].

We have investigated germanium powder, which was obtained by pulverizing single crystal germanium in an agate mortar and thereafter elutriating in toluene to a particle size of  $5-8 \mu$ . A n-germanium single crystal with a specific resistivity of  $60 \Omega/\text{cm}$  was used for the preparation of the powders. The x-ray measurements were carried out at room temperature with  $\text{CuK}\alpha$ -radiation in the recording apparatus URS-501 provided with a Geiger-Müller counter. Nickel foil,  $20 \mu$  thick and placed in front of the counter, was used as a filter. The intensities of the  $I_{\text{hkl}}$  reflexes were determined from the peak areas recorded by the automatic electronic potentiometer ÉPP-09.

In order to obtain absolute values we have determined the intensity  $I_0$  of the primary radiation and, moreover, used the method of comparing the  $hkl$  line intensities of germanium with that of the 220 and 311 reflection in silicon and NaCl, which were taken as standards.

To determine the absorption coefficient of germanium we have measured the decrease in intensity of the primary radiation caused by passing through slabs with various thicknesses between 50 and 200  $\mu$ . The slabs were prepared by pressing without using any binding agent.

The curve of the atomic scattering factor was constructed from the experimental data obtained. In this construction a correction for dispersion was applied and the other factors were taken into account in the usual way. Since the powders used in the x-ray measurements had a sufficiently high degree of dispersion and the absorption coefficient is relatively great, extinction was left out of consideration.

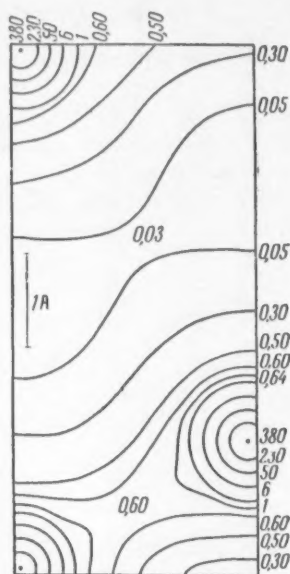


**Fig. 3. Map of the electron density distribution in one-fourth of the (110) plane in the elementary cell of germanium.**

In Fig. 1 the curve found for the atomic scattering factor of germanium as a function of  $\sum_i h_i^2$  is plotted for values up to  $\sum_i h_i^2 = 48$ . The experimental points lie relatively well on a smooth curve. The fact that the points corresponding to the lines 422; 531; 620 deviate

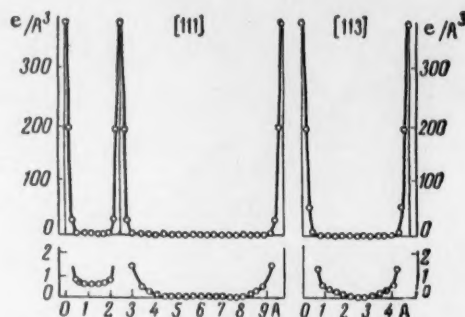


**Fig. 4. Electron density distribution for the [111] and [113] directions in the (110) plane of the germanium elementary cell.**

somewhat from the smooth curve may be imputed to experimental errors. All points are averages of five experimental values.

Since the electron distribution close to the nucleus where it is highest can be approximated by a Gauss' function, most of the points corresponding to values  $\sum_i h_i^2 > 8$ , in the plot of  $\ln f$  versus  $\sum_i h_i^3$ , lie on a straight line (Fig. 2).

From the data of this  $f$ -curve the electron density distribution in the elementary cell was calculated by means of the method described previously [3]. A map of the electron density of germanium in the (110) plane of the elementary cell is shown in Fig. 3. The distribution in the [111] and [113] directions between adjacent atoms in the elementary cell is given in Fig. 4.

A discussion of the data obtained enables us to draw several conclusions about the nature of the electron density distribution and the radius of germanium ions. The germanium ion radius found from the  $1.5 \text{ e}/\text{\AA}^3$  density contour is equal to  $0.5 \text{ \AA}$ ; here six electrons lie outside this volume. The ion radius determined from the  $0.05 \text{ e}/\text{\AA}^3$  contour has the value  $2 \text{ \AA}$ ; outside this volume there is only a very small number of electrons. We note that the ionic radii determined in this way for diamond are  $0.20$ - $0.25$  and  $1.25 \text{ \AA}$ , for silicon  $0.4$  and  $1.75 \text{ \AA}$ , respectively.

At the point  $\frac{3}{4} \frac{3}{4} \frac{3}{4}$  in the [111] direction the electron density is small and does not exceed  $0.03 \text{ e}/\text{\AA}^3$ . Between the points  $0, 0, 0$ , and  $\frac{1}{4} \frac{1}{4} \frac{1}{4}$  the lowest electron density is  $0.6 \text{ e}/\text{\AA}^3$ .

From the map of the [111] direction it is clear that the region between  $0, 0, 0$  and  $\frac{1}{4} \frac{1}{4} \frac{1}{4}$  corresponds to a certain electron "bridge" of raised density. Between the points  $\frac{1}{2} \frac{1}{2} \frac{1}{2}$  and  $\frac{3}{4} \frac{3}{4} \frac{3}{4}$  the electron density has a minimum ("trench") with a value which is practically zero.

#### LITERATURE CITED

1. R. Brill, et al., *Naturwiss.* **26**, 479 (1938).
2. R. Brill, et al., *Ann. Phys.* **34**, 393 (1939).
3. N. N. Sirota, N. M. Olekhovich, and A. U. Sheleg, *Doklady Akad. Nauk SSSR* **132**, 160 (1960).\*
4. S. Göttlicher, et al., *Z. Phys. Chem. Neue Folge* **21**, 133 (1959).
5. N. N. Sirota, N. M. Olekhovich, and A. U. Sheleg, *Doklady Akad. Nauk Beloruss SSR* **4**, 4 (1960).
6. Yu. N. Shuvalov, *Fiz. Tverd. Tela* **1**, 208 (1959).

\* Original Russian pagination. See C. B. translation.



## MICELLE FORMATION IN SOLUTIONS OF SURFACE-ACTIVE SUBSTANCES

A. B. Taubman and S. A. Nikitina

Institute of Physical Chemistry, Academy of Sciences of the USSR

(Presented by Academician P. A. Rebinder, July 5, 1960)

Translated from *Doklady Akademii Nauk SSSR*, Vol. 135, No. 5, pp. 1179-1182, December, 1960

Original article submitted June 24, 1960

It is characteristic both of natural soaps and of synthetic soap-like surface-active substances that there exists for them a critical concentration corresponding to the formation of micelles ( $C_c$ ), above which these particles exist in solution partially in the form of micelles, which are in thermodynamic equilibrium with the separate molecules or ions which give rise to them [1]. It is usually assumed that the process of formation of spherical micelles, such as are obtained in dilute aqueous solutions, begins and ends within such a narrow concentration range that it may for practical purposes be considered as a single concentration, corresponding to the value of  $C_c$  [2-4].

On the other hand, it has been established for a number of investigations that a single substance may give rise, not merely to one but to several values of  $C_c$ , associated with a more complicated relationship between the process of molecular association and the concentration [5]. In other cases this result has been attributed to the presence of impurities in the substances investigated [6], or to peculiarities in the methods of measurement which have been employed [7, 10].

It thus appears that the question whether surface-active substances truly possess a critical concentration range, within whose limits the process of micelle formation takes place, so that two (or more) values of  $C_c$  may be defined, and what meaning is to be attached to these points, is as yet not fully elucidated.

The formation of micelles is accompanied by an abrupt change in the properties of the solutions, and it is this change which is exploited in the determination of the values of  $C_c$ . This may be done by measuring the turbidity or surface tension, by titration with dyestuffs or by other methods [8-10].

Among these methods, measurements of surface tension occupy an important place, since they permit of the establishment of the link between micelle formation in the bulk of the solution, and the process of formation of the adsorption layer at its surface: as we have been able to show by simultaneous measurement of the static ( $\sigma_s$ ) and dynamic ( $\sigma_d$ ) surface tensions of solutions of surface active substances [11]. In Table 1, below, data are given which we obtained during the determination of  $C_c$  for solutions of surface-active substances of anionic, cationic and nonionic types within an adequate concentration range, using various methods. The turbidity of the solutions was measured by means of a nephelometer (model FÉK-N-57), and was represented by the values of the optical density (D); the surface tension was also measured by a stalagmometric method, with times of duration for the surface of separation of  $\tau = 2$  minutes and  $\tau = 2$  seconds [12]; titration with dyestuffs was performed using pinacyanolchloride and eosin. \*

\* N. E. Khokhlova took part in this work.

Figure 1 presents curves showing the relationship between the optical density and the logarithm of the concentration, and between both the static and the dynamic surface tension and the logarithm of the concentration, for the solutions of one of the surface-active substances which we have investigated: the sodium salt of the diethyldihexyl ester of sulfosuccinic acid (aerosol OT). It is seen that the curve showing the relationship between D and log C has two break points, which evidently indicate the presence of definite concentration limits within which micelle formation takes place in dilute solutions.

TABLE 1

The Critical Concentration for Micelle Formation (for systems 1-4 in moles/liter, and for system 5 in percent).

Surface-active substance	Method of determining $C_C$				measurement of surface tension	
	nephelometer		titration with dyestuff			
	$(C_C)_1$	$(C_C)_2$	$(C_C)_1$	$(C_C)_2$	$(C_C)_1$	$(C_C)_2$
Sodium salt of diethyldihexyl ester of sulfosuccinic acid (aerosol OT)	0.0025	0.0049	0.0026*	0.0050*	0.0027	0.0052
Sodium salt of dihexyl ester of sulfosuccinic acid (aerosol MA)	—	—	0.014*	0.031*	—	—
Sodium salt of didecyl ester of sulfosuccinic acid	—	—	0.00022*	0.00045*	—	—
Dodecylaminoacetate (Amak 1120)	0.0020	0.013	0.0024**	0.012**	0.0030	0.010
Material DB ***	0.025	0.095	0.023*	0.075*	0.026	0.085

\* Nitration with pinacyanolchloride.

\*\* Titration with eosin.

\*\*\* Material DB is a polyoxyethylene ether, predominantly ditertiarybutylphenol,  $C(CH_3)_3 \cdot C(CH_3)_3 \cdot C_6H_4O(C_2H_4O)_6 C_2H_4OH$ .

The first of these points corresponds to the development, in a solution which formerly contained only molecules or ions, of micelles: this, therefore, corresponds to the usually accepted significance of  $C_c$  [13], which ought therefore to be considered as the initial concentration, defining the left hand boundary of the critical region. We therefore consider it as the first critical concentration and denote it by  $(C_c)_1$ .

The second point of inflection on the curve, which corresponds to the sudden appearance of a maximum, clearly defines the right-hand boundary of the region of micelle formation, and under our notation appears as  $(C_c)_2$ . It is necessary to stress that, although the reduction in turbidity in the concentration range above  $(C_c)_2$  is difficult to explain,\* it is still true that this magnitude, which is associated with definite peculiarities of the micelle formation process, possesses a real physical meaning. This follows clearly from the fact that this, like the magnitude  $(C_c)_1$ , can be determined not only by the nephelometric method, but also by all the other methods.

Actually, it appears from Fig. 1 that, for solutions of aerosol OT, there exists a strict quantitative correspondence between the positions of the points  $(C_c)_1$  and  $(C_c)_2$ , as determined from curve 1, representing the relationship between D and log C, and the points of inflection on the surface tension isotherms, determined under static (curve 2a) and dynamic (curve 2b) conditions respectively. The mean values for these points are 0.0026 and 0.0050 mole/liter.

It is also important to note that the minimum equilibrium values,  $\sigma_s \min$  and  $\sigma_d \min$  on both the curves 2a and 2b correspond to each other; this signifies that, for solution concentrations  $\geq (C_c)_2$ , the rate of reduction of the surface tension and, consequently, the rate of formation of the adsorption layer are practically independent

\* The maximum on the curve showing the relationship between turbidity of the solutions and the concentration has also been obtained for the nonionic compound triton-X-100 [14].

of the duration of the existence of the separation surface [11].\*

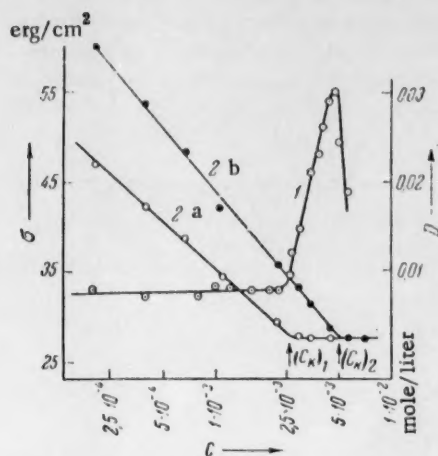


Fig. 1. Relationship between the optical density and the concentration for solutions of aerosol OT (1). Isotherms for the static (2a) and dynamic (2b) surface tensions of the same solutions.

solution to be adsorbed into micelles. This process corresponds to the abrupt rise in the  $D - \log C$  curve to the maximum value of  $D_m$  when  $C = (C_c)_2$ , when increase in the number of micelles comes to an end.

Thus,  $(C_c)_1$  determines at the same time two associated changes in the molecular condition both of the bulk of the solution (the development of micelles) and of its surface layer (cessation of the formation of the adsorption layer). In addition to this, under the dynamic (kinetic) conditions for which  $\tau = 2$  seconds (which is easily attained experimentally), saturation of the layer occurs not at  $(C_c)_1$  but at  $(C_c)_2$ , at which point  $\sigma_d$  also assumes its minimum value, which is also the same as the corresponding value of  $\sigma_s \min$ .\*\* On the other hand (see Fig. 1), as  $C$  approaches  $(C_c)_2$ , not only does micelle formation come to an end but the rate of adsorption, which increases rapidly, becomes (at the point of intersection of the  $\sigma_s - \log C$  and  $\sigma_d - \log C$  isotherms) practically independent of  $\tau$ .

It must evidently be supposed that the diminution in the rate of attainment of adsorption equilibrium in the critical concentration region between  $(C_c)_1$  and  $(C_c)_2$  (see curves 2a and 2b) is associated with a reduction in the rate of formation and destruction of the micelles in the bulk of the solution (see, for example [15]), which

Table 1 shows that similar results were obtained with the other substances studied; in all cases independently of the chemical composition and molecular structure of the surface-active substance, and also of contamination with impurities, two values of  $C_c$  were obtained in excellent agreement with the results of measurements obtained by other methods. The fact that the second critical point is determined on the basis of the nonequilibrium isotherm for the dynamic surface tension ( $\sigma_d - \log C$ ), by the point of intersection of this with the static (equilibrium) isotherm ( $\sigma_s - \log C$ ), makes it possible to base the interpretation of the course of the process of formation of micelles in solutions of aerosol OT, within the concentration range bounded by  $(C_c)_1$  and  $(C_c)_2$ , on kinetic premises.

Within the concentration range between zero and  $(C_c)_1$ , the formation of the adsorption layer proceeds progressively with increase in  $C$ , and in the body of the solution the surface-active material is found in the molecular (or ionic) condition. When  $C$  reaches the value  $(C_c)_1$ , saturation of the adsorption layer is attained ( $\Gamma \rightarrow \Gamma_m$ ), and the minimum value of the static surface tension is, consequently, reached ( $\sigma_s = \sigma_{\min}$ ). After this, further increase in  $C$  causes the excess number of molecules (or ions) in the body of the

\* It should be pointed out that, for the  $\sigma_s - \log C$  isotherm, the lowest value of  $\sigma_s$  corresponds to an equilibrium value which is characteristic for each method of measurement, but is not the static value which, as we have shown, can only be obtained by means of truly static methods, such as the suspended drop method [12]. This is evidently due to the fact that in the use of semistatic methods (such as the stalagmometric, or the method of the greatest pressure of bubble formation), the boundary surface (whether of drop or bubble) undergoes deformation during the process of its formation, even when the lifetime is very great ( $\tau \rightarrow \infty$ ), which hinders the attainment of the static value for the surface tension.

\*\* The values of  $\sigma_s \min$  is the region where  $C > (C_c)_1$  remain practically constant, which provides a distinction between the course of the surface tension isotherms of micelle forming substances, from that of surface-active substances of a nonsoaplike type (organic acids, alcohols and others). The reason for this is found in the fact that, beginning at the concentration  $(C_c)_1$ , all the molecules (or ions) of the surface-active substance are autosolubilized.

displaces toward the right the equilibrium of the process "adsorption  $\rightleftharpoons$  desorption". However, with increase in the concentration to a value  $C = (C_C)_2$ , the dynamic equilibrium between these two processes, proceeding in the bulk and in the surface layer respectively, is established with very great velocity. Notwithstanding the complexity of a more detailed theoretical analysis of the problem here considered, the aggregate of the data obtained confirms the opinion that the processes of micelle formation and of adsorption are due to one and the same tendency of solutions of long-chain soaplike surface-active substances: that is, the tendency to a reduction in the free surface energy at the water-air boundary, or at the water-hydrocarbon chain surface, the two being directly linked to each other.

In conclusion we wish to express our thanks to Academician P. A. Rebinder for his great kindness in giving us valuable advice.

#### LITERATURE CITED

1. J. W. McBain, *Colloid Science* (Boston, 1942) p. 240; D. G. Davies and C. R. Bury, *J. Chem. Soc.* 2263 (1930).
2. A. E. Alexander and P. Johnson, *Colloid Science* (Oxford, 1949) Vol. 2, p. 667.
3. G. S. Hartley, *J. Chem. Soc.* 1968 (1938).
4. P. A. Rebinder and K. A. Pospelova, *Acta Phys. Chim.* 16, 71 (1942).
5. P. Ekwall, *Kolloid Z.* 136, 37 (1954).
6. E. F. Williams, N. T. Woodberry, and J. K. Dixon, *J. Colloid Sci.* 12, 5, 454 (1957).
7. M. L. Miller and J. K. Dixon, *J. Colloid Sci.* 13, 5, 411 (1958).
8. A. Shvarts and D. Perri, *Surface-Active Substances* [Russian translation] (IL, Moscow, 1953).
9. M. L. Corrin and W. D. Harkins, *J. Am. Chem. Soc.* 69, 679 (1947).
10. A. B. Taubman, V. V. Konstantinova, and A. S. Kryukova, *Chemistry and Technology of Fuels and Oils* [in Russian] (1960) No. 3, p. 61.
11. S. A. Nikitina and A. B. Taubman, *Doklady Akad. Nauk SSSR* 116, 1, 113 (1957).\*
12. S. A. Nikitina, *Dissertation* [in Russian] (Moscow, 1957).
13. P. Debye, *Ann. N. Y. Acad. Sci.* 51, Art. 4 (1949).
14. T. M. Doscher, G. E. Myers, and D. C. Atkins, *J. Colloid Sci.* 6, 223 (1951).
15. T. Nash, *J. Colloid Sci.* 14, 59 (1959).

\* Original Russian pagination. See C. B. translation.

## THE CAPACITY OF THE ELECTRICAL DOUBLE LAYER IN MOLTEN SALTS

E. A. Ukshe, N. G. Bukun, and D. I. Leikis

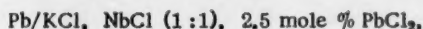
Institute of Electrochemistry, Academy of Sciences of the USSR;  
Bereznikov Branch of the All-Union Aluminum-Magnesium Institute  
(Presented by Academician A. N. Frumkin, July 6, 1960)

Translated from *Doklady Akademii Nauk SSSR*, Vol. 135, No. 5, pp. 1183-1186,  
December, 1960

Original article submitted July 2, 1960

The structure of the electrical double layer in molten salts has up to now hardly been studied at all, in spite of the fact that the problem is of considerable importance both from a theoretical and from a practical standpoint. Some data on the capacity of the double layer at the mercury electrode in nitrate melts, and at the platinum electrode in chlorides, have been published by Randles and White [1], and by Laitinen and his collaborators [2]. These data, however, afford no possibility of arriving at the basic peculiarities of the structure of the double layer in melts.

We have recently undertaken a systematic study of the capacity of the electrical double layer in molten salts. The present article is a preliminary statement of the results which have been achieved. The experiments were carried out in an argon atmosphere at 700-800° C. The cell used in the measurements was a quartz vessel, closed by means of a cover made of molybdenum glass in a ground socket. The electrodes were mounted in the cap. A quartz tube was used as holder for the electrode under study, and the end of the tube was bent upward and drawn out into a capillary. The tube was filled with the liquid metal under investigation, the working surface of which had the form of a hemisphere bounded by the glass capillary. The electrodes for polarization by direct and alternating current were rods of spectroscopically pure graphite, the side surfaces of which were protected by means of quartz tubes. The comparison electrode was the lead electrode:



which was placed in a quartz tube with a capillary aperture. The potential of this electrode on the chlorine scale of potentials was 1.39 v. In all experiments, the electrolyte consisted of an equimolar molten mixture of sodium and potassium chlorides. The measurements of the capacity and resistance of the cell under a given potential were carried out by means of an impedance bridge at frequencies from 20 to 200 kh.

Figure 1 gives curves showing the relationship between the capacity and the potential for lead and cadmium electrodes at a frequency of 200 kh. In all cases the relationship between capacity and potential possessed a sharply defined minimum, for which the potential corresponding to minimum capacity was determined by the nature of the metal and did not depend on the frequency of the alternating current or (with a range of 100°) on the temperature. The capacity and resistance of the cell depended on the frequency, in that the dispersion gradually diminished to zero with increase in the frequency (see Fig. 2). We assumed that the dispersion of capacity with frequency near to the minimum was connected with the flow of the electrolyte between the walls of the capillary and the liquid metal. With increase in the frequency of alternation of the current, the part of the metal surface screened by the walls of the capillary gradually separates, and the capacity falls. A similar cause for the dispersion was established by Graham [3] by means of his measurements of the

capacity of the double layer in aqueous solutions. It is only necessary to remark that, since molten electrolytes possess conductivities of the order of a hundred times higher than their solutions, the dispersion effect in our experiments was considerably more strongly expressed, and was maintained up to higher frequencies, than is the case in solutions.

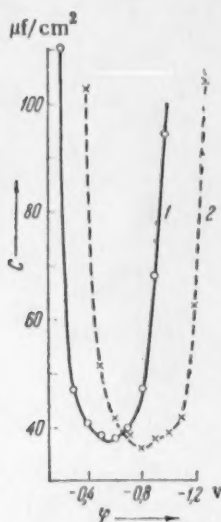


Fig. 1. Relationship between the capacity of the double layer and the potential for liquid metal electrodes in a KCl-NaCl melt at 700° and a frequency of 200 kh. 1) Pb; 2) Cd.

Taking into account the nature of the relationship between capacity and frequency, we have taken as the true value of the capacity of the electrical double layer for the electrode under investigation the value determined at 200 kh. For the working surface of the electrode at this frequency we have taken the surface of a hemisphere of diameter equal to that of the capillary. To confirm the validity of this determination of the specific capacity we have measured the capacity of cadmium electrodes of different surface area. From the data set out in Fig. 2, the following ratios emerge:  $C'_{Cd}/C''_{Cd} = 1:2.36$ ;  $S'_{Cd}/S''_{Cd} = 1:2.28$ . It can therefore be taken that, at a frequency of 200 kh, it is permissible to neglect the screening effect on the electrode surface by the walls of the container. In this case the specific capacity of cadmium at potential  $\varphi = -0.8$  v amounts to  $36 \mu f/cm^2$ . For lead at potential  $\varphi = -0.55$  we obtained a value close to  $38 \mu f/cm^2$ .

Table 1 gives the values of the potentials at the maxima of the electrocapillary curves, and the minima of the capacity curves for a range of metals. It can be seen from the data given in Table 1 that the potential corresponding to the minimum capacity is close to the potential corresponding to the maximum of the electrocapillary curve of the same metal [4, 5].

When our data are compared with those of S. V. Karpachev and A. G. Stromberg [4, 5], it should be borne in mind that these authors used a stationary lead electrode as their comparison electrode, the potential of this at 700° being some  $200 \pm 20$  mv more positive than the potential of the comparison electrode used by ourselves. The data of S. V. Karpachev and A. G. Stromberg are given in Table 1 after conversion to the scale of potentials used by us.

The fact that the potentials corresponding to minimum capacity correspond to the potentials at the maxima of the electrocapillary curves makes it possible to make use of the method of measuring capacity in

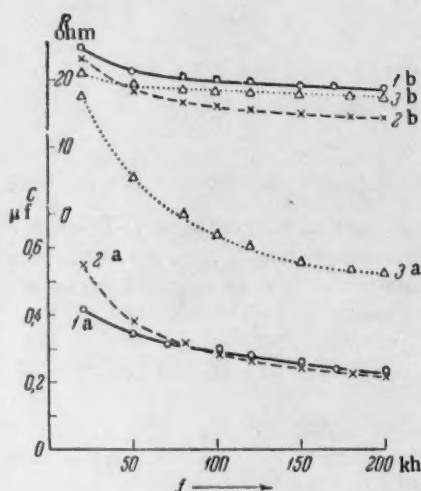


Fig. 2. Dispersion of capacity and resistance for liquid electrodes in molten potassium chloride-sodium chloride mixtures. 1a) Capacity for lead electrode ( $S = 4.9 \cdot 10^{-3} cm^2$ ); 1b) resistance for the same electrode; 2a) capacity for cadmium electrode ( $S = 6.2 \cdot 10^{-3} cm^2$ ); 2b) resistance for the same electrode; 3a) capacity for cadmium electrode ( $S = 14.1 \cdot 10^{-3} cm^2$ ); 3b) resistance for the same electrode.

melts for the determination of the null points of metals. In addition, it would be expected that, if the capacity measured by us is the capacity of the electrical double layer, then double integration of the  $C - \varphi$  curves would result in obtaining electrocapillary curves which ought to coincide with the experimental curves. Such a correspondence would be impossible if an appreciable part of the measured capacity consisted of pseudocapacity, or if the specific capacity per unit surface had been obtained incorrectly by us.

TABLE 1

Metal	Electrolyte	Temp. °C	$\varphi$ at the max. of electrocapil- lary curve, v	Metal	Electrolyte	Temp. °C	$\varphi$ at min. of capacity curve, v
Lead	KCl - LiCl	450	$-0,58 \pm 0,02$	Lead	KCl - NaCl	700	$-0,55$
Cadmium	KCl - LiCl	450	$-0,82 \pm 0,02$	Cadmium	KCl - NaCl	700	$-0,80$
Thallium	KCl - LiCl	420	$-0,85 \pm 0,02$	Thallium	KCl - NaCl	700	$-0,87$
Antimony	KCl - LiCl	1050	$-0,10 \pm 0,02$	Antimony	KCl - LiCl	500	$-0,92$
	KCl - LiCl	750	$0,00 \pm 0,02$		KCl - NaCl	700	$-0,17$
Tin	KCl - LiCl	420	$-0,43 \pm 0,02$	Tin	KCl - NaCl	700	$-0,32$
Bismuth	KCl - LiCl	420	$-0,48 \pm 0,02$	Bismuth	KCl - NaCl	700	$-0,32$

Figure 3 gives the electrocapillary curves obtained by graphical integration of the capacity curves shown in Fig. 1, on the basis of the following limiting conditions [5]:

for lead at  $\varphi = -0.55$  v,  $\sigma = 444$  dyne/cm;

for cadmium at  $\varphi = -0.80$  v,  $\sigma = 568$  dyne/cm.

The experimental points plotted on the same graph are also taken from publication [5]. Taking account of some difference in the experimental conditions, the agreement between the calculated and experimental data can be regarded as satisfactory.

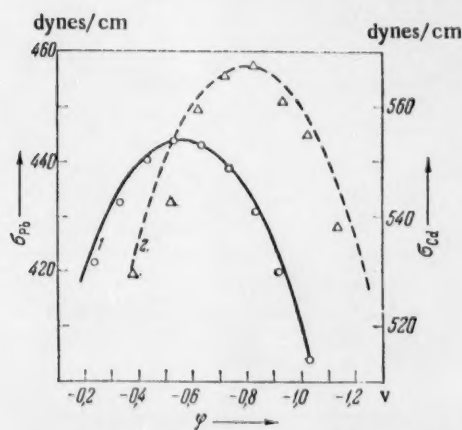


Fig. 3. Electrocapillary curves for lead (1) and cadmium (2) obtained by integration of the  $C - \varphi$  curves of Fig. 1. The points represent the experimental data taken from paper [5].

from the pre-electrode layer). When a large shift of potential occurs in a positive or a negative direction, it seems that the phenomenon of pseudocapacity arises, owing to the occurrence of autosolution of the electrode, or to discharge of cations of the alkali metals. The possibility of the reduction of sodium or potassium ions at potentials more positive than the standard potentials of the two metals is, we should suppose, connected with the depolarization produced at the expense of the energy of formation of the mixed melt [6].

We may therefore draw the following conclusions on the basis of the results obtained. The capacity of the electrical double layer in molten electrolytes is a minimum at the potential at which the charge on the metal is zero. The minimum in the  $C - \varphi$  curve in the melts corresponds to a capacity of  $36-38 \mu\text{f}/\text{cm}^2$ . The existence of a minimum capacity on the  $C - \varphi$  curves requires special elucidation. It is questionable whether the minimum obtained can be explained in a way similar to that used for dilute aqueous solutions in terms of the diffuse double layer, since, in the first place, the presence of diffusion in such concentrated ionic systems, of a kind which is found in dilute salt solutions, is improbable, and, in the second place, the minimum capacity in the case under consideration is so great that the thickness of the electrical double layer cannot be significantly greater than one ionic diameter.

The increase in the capacity of the double layer with increase in the charge on the surface of the metal may be connected with deformation of the electronic environment of the ions, and also with the compression of the structure of the molten salt (that is, the displacement of the "holes"

We would like to express our deep thanks to Academician A. N. Frumkin and Professor B. N. Kabanov for their valuable advice and discussion of the present work.

#### LITERATURE CITED

1. J. Randles and W. White, *Z. Elektrochem.* 59, 666 (1955).
2. H. Laitinen, et. al., *J. Electrochem. Soc.* 102, 598 (1955); 104, 730 (1956).
3. D. Grahame, *J. Am. Chem. Soc.* 68, 301 (1946); 71, 2975 (1949).
4. S. V. Karpachev and A. G. Stromberg, *Zhur. Fiz. Khim.* 18, 47 (1944).
5. A. G. Stromberg and T. N. Chukina, *Zhur. Fiz. Khim.* 18, 234 (1944).
6. M. Sittig, *Sodium* (Reinhold Publ. Corp., 1956).

# THE SIMULTANEOUS DISCHARGE OF METALLIC IONS IN REAL CONJUGATE SYSTEMS

A. T. Vagramyan and T. A. Fatueva

Institute of Physical Chemistry, Academy of Sciences of the USSR

(Presented by Academician V. I. Snitsyn, June 20, 1960)

Translated from *Doklady Akademii Nauk SSSR*, Vol. 135, No. 6, pp. 1413-1416,  
December, 1960

Original article submitted June 15, 1960

The condition governing the simultaneous reduction of several types of metallic ions is that their discharge potentials shall be equal:

$$\varphi_1^0 + \frac{RT}{nF} \ln a_1 - \eta_1 = \varphi_2^0 + \frac{RT}{nF} \ln a_2 - \eta_2, \quad (1)$$

where  $\varphi_1^0, a_1, \eta_1$ ;  $\varphi_2^0, a_2, \eta_2$  are, respectively, the standard potentials, activities and overpotentials of the first and second type of metallic ion. For simplicity we shall use the concentrations of the ions instead of their activities in the following development.

We have already shown [1] that electrochemical reactions taking place simultaneously at electrodes are conjugate, and hence that Eq. (1) does not completely characterize the conditions obtaining during simultaneous discharge, since it does not take account of the mutual interaction of the ions undergoing reduction. In particular, it ignores the change in the condition of the electrode surface, the changes in the concentrations of the ions undergoing discharge in the electrical double layer, and the change in the condition of the ions in the solution.

The rate of reduction of metal ions is known to depend on the concentration of the ions in the electrical double layer, and not on that in the bulk. For the case of hydrogen ion discharge, A. N. Frumkin [2] has proposed a relationship connecting the surface and bulk concentrations of the ions by the formula  $[H_s] = [H]e^{-F\psi_1/RT}$ . It must be recognized that, in the case of simultaneous discharge of metallic ions under given conditions of electrode polarization, the concentration of each type of ion in the double layer will be reduced, according to the number of ionic types and their concentrations, as a result of the partial displacement of some ions by others.

When the fact is recognized that, during simultaneous reduction, both the nature of the deposit on the cathode, and its surface condition (the degree of passivation) will be changed, it can be seen that account must then be taken of the overpotential relevant to the discharge of the given ion on the deposited alloy ( $\eta^{al}$ ), and not of the overpotential which would arise during separate deposition of the metals ( $\eta$ ). In order to determine the conditions for simultaneous discharge of the ions in real conjugate systems, it is necessary to take account of the fact that, when several types of ions enter into the electrical double layer, that part of the polarization attributable to each type of ion will be characterized by the fractions of the ions penetrating into the electrical double layer, in relation to the total number of ions causing the polarization. If we denote the concentration of each type of ion by  $C_i$ , and denote the coefficient which defines the power of each type of ion to penetrate into the electrical double layer by  $\alpha_i$ , the reduction in the polarization due to the entry of other ions into the

double layer may be expressed by the quantity  $-\frac{RT}{nF} \ln \frac{\sum \alpha_i C_i}{\alpha_1 C_1}$ . A change corresponding to this will occur in the rate of discharge of the various ions.

Since Eq. (1) does not take account of the influence of the overpotential factor, an equation which purports to describe the conditions for simultaneous discharge of ions must be expressed in the following way:

$$\varphi_1^0 + \frac{RT}{nF} \ln C_1 - \frac{RT}{nF} \ln \frac{\sum \alpha_i C_i}{\alpha_1 C_1} - \eta_1^{al} = \varphi_2^0 + \frac{RT}{nF} \ln C_2 - \frac{RT}{nF} \ln \frac{\sum \alpha_i C_i}{\alpha_2 C_2} - \eta_2^{al} \quad (2)$$

or,

$$\varphi_1^0 + \frac{RT}{nF} \ln \frac{\alpha_1 C_1}{\sum \alpha_i C_i} C_1 - \eta_1^{al} = \varphi_2^0 + \frac{RT}{nF} \ln \frac{\alpha_2 C_2}{\sum \alpha_i C_i} C_2 - \eta_2^{al} \quad (3)$$

No account is here taken of the fact that the activity of each type of ion in the mixture will be different from its activity when each ion is reduced by itself.

It is assumed in Eq. (3) that the formation of the alloy does not appreciably alter the normal potentials of the metals.

A calculation of the depolarizing effect of the deposit during simultaneous discharge has been presented by A. I. Krasovskii [5]. It follows from Eq. (3) that, during the electrodeposition of two or more types of ions differing appreciably in their normal electrode potentials, the change in the concentrations of the ions being deposited cannot sensibly cause their discharge potentials to approximate to each other. It follows that the principal regulating factor must be the magnitude of the overpotential. Since simultaneous discharge, accompanied by a change in the nature of the deposit, may cause either increase or decrease in the overpotential, then, under actual conditions, the simultaneous deposition of the metals may take place in the following possible ways:

1. When

$$\eta_1^{al} + \eta_2^{al} \ll \varphi_1^0 + \frac{RT}{nF} \ln \frac{\alpha_1 C_1}{\sum \alpha_i C_i} C_1 + \varphi_2^0 + \frac{RT}{nF} \ln \frac{\alpha_2 C_2}{\sum \alpha_i C_i} C_2,$$

the rate of separation of the metal with the more positive deposition potential is greater than the rate of discharge of ions whose reduction takes place at a more negative potential.

2. When

$$\eta_1^{al} > \eta_2^{al}, \quad \varphi_1^0 + \frac{RT}{nF} \ln \frac{\alpha_1 C_1}{\sum \alpha_i C_i} C_1 - \left( \varphi_2^0 + \frac{RT}{nF} \ln \frac{\alpha_2 C_2}{\sum \alpha_i C_i} C_2 \right) \ll \eta_1^{al} - \eta_2^{al},$$

the rate of separation of the metal with the more negative potential is greater than the rate for the more positive ion.

Thus, in real conjugate systems, because of the influence of the nature of the deposit on the magnitude of the overpotential, change in the rate of reduction is possible both for the more positive and for the more negative metallic ions, within a wide range.

If there is considerable reduction in the overpotential for simultaneous deposition (case 2), we should expect an inverse relationship for the velocities: that is, the rate of reduction of the ions with the more positive potential ought to exceed the rate of reduction of the ions with the more negative potential.

In order to confirm this suggestion, we have investigated the simultaneous discharge of ions of iron and nickel. The study was carried out using 1 N solutions of the lower sulfates of iron and nickel, with the addition of 30 g/liter of boric acid at a pH 1.9, and at various temperatures, which were controlled to a precision of  $\pm 0.5^\circ$ . The method of investigation has been described in previous articles [1].

Figure 1 gives the polarization curves for simultaneous and separate deposition of nickel and iron, and the corresponding partial curves, obtained from the solutions indicated at a temperature of 25°. As can be seen from these curves, the reduction potential for nickel ions (4) for its separate deposition is appreciably more positive than that for iron (7). However, when the discharge takes place simultaneously, the rate of deposition of the nickel ions (9) is appreciably less than the

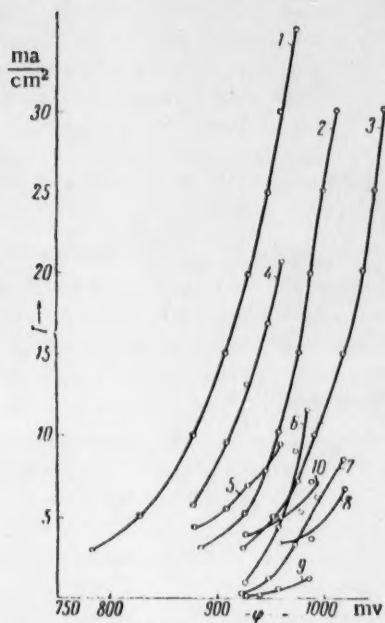


Fig. 1. Relationship between the rate of reduction of iron and nickel ions and the electrode potential (measured against the saturated calomel electrode). Over-all polarization curves for: 1) discharge of  $\text{Ni}^{2+}$  and  $\text{H}^+$  from 1 N nickel sulfate solution; 2) discharge of  $\text{Ni}^{2+}$ ,  $\text{Fe}^{2+}$ , and  $\text{H}^+$  from a solution 1 N with respect to nickel sulfate and 1 N with respect to ferrous sulfate; 3) discharge of  $\text{Fe}^{2+}$  and  $\text{H}^+$  in 1 N ferrous sulfate solution. Partial polarization curves: 4 and 5) discharge of  $\text{Ni}^{2+}$  and  $\text{H}^+$ , respectively, obtained on the basis of curve 1; 7 and 8) discharge of  $\text{Fe}^{2+}$  and  $\text{H}^+$  respectively, obtained on the basis of curve 3; 6, 9, and 10) discharge of  $\text{Fe}^{2+}$ ,  $\text{Ni}^{2+}$ , and  $\text{H}^+$  respectively, obtained on the basis of curve 2.

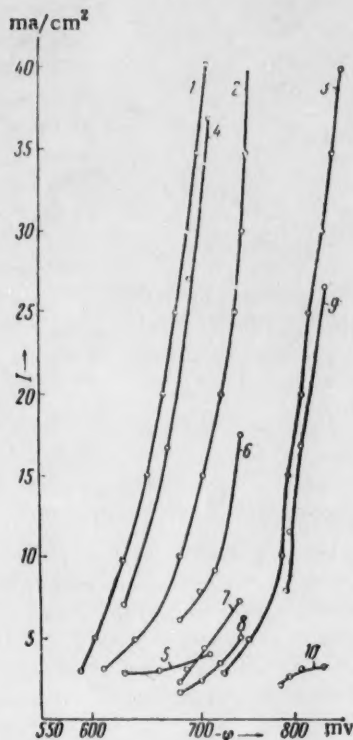


Fig. 2. Relationship between the rate of reduction of iron and nickel ions and the electrode potential (measured against the saturated calomel electrode), at pH = 1.9. Over-all polarization curves for: 1) separation of  $\text{Ni}^{2+}$  and  $\text{H}^+$ ; 2) separation of  $\text{Fe}^{2+}$ ,  $\text{Ni}^{2+}$ , and  $\text{H}^+$ ; 3) separation of  $\text{Fe}^{2+}$  and  $\text{H}^+$ . Partial polarization curves: 4 and 5) for discharge of  $\text{Ni}^{2+}$  and  $\text{H}^+$ , respectively, obtained on the basis of curve 1; 6, 7, and 8) for discharge of  $\text{Ni}^{2+}$ ,  $\text{Fe}^{2+}$ , and  $\text{H}^+$ , respectively, obtained on the basis of curve 2; 9 and 10) for discharge of  $\text{Fe}^{2+}$  and  $\text{H}^+$  respectively, obtained on the basis of curve 3.

rate of deposition of the iron ions [6]. This "anomalous phenomenon" (as it is called) is sometimes explained by supposing that the iron is deposited as a result of depolarization arising from the alloy formation. It should be remarked that, if a depolarization effect were found, the reduction of potential ought to take place for both

metals according to their concentrations in the alloy. The experimental results clearly show that such a reduction of the separation potentials for the two metals is absent, and therefore the explanation just referred to is unacceptable.

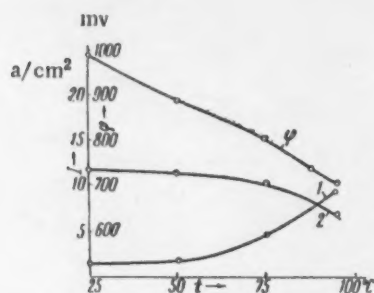


Fig. 3. Relationship between the rate of reduction of  $\text{Ni}^{2+}$  (1) and  $\text{Fe}^{2+}$  (2) ions together with discharge and the temperature and change of the electrode potential  $\phi$ .

It is known that, during the electrodeposition of nickel, an abrupt retardation of the process of reduction of the ions occurs if adsorption of hydroperoxides occurs, while during the electrodeposition of iron atoms of hydrogen are preferentially adsorbed [3]. When simultaneous discharge of iron and nickel occurs, a reduction of the overpotential should be observed for the reduction of the iron ions, since the alloy will have a smaller absorbing power for hydrogen than iron when deposited alone. There should, however, occur an increase in the overpotential for the reduction of nickel ions when these are deposited simultaneously with iron, in view of the increased adsorption of hydroxides on the surface of the alloy, in comparison with that which occurs when nickel is deposited alone — arising from the fact that hydroxide formation for iron arises in a more acid medium than for nickel.

When the electrodeposition of these metals is carried out at higher temperatures, there is a great reduction in the adsorption both of hydrogen and of hydroxide, so that the content of foreign particles in the deposit is appreciably diminished. Under these circumstances also there is a great reduction of the overpotentials accompanying the deposition of these metals.

Figure 2 gives the polarization curves for separate and simultaneous discharge of iron and nickel ions, and the corresponding partial curves for the same solutions, obtained when the temperature is increased to  $95^\circ$ . It can be seen from these curves that, in contrast to those shown in Fig. 1, the rate of deposition of the nickel, during the simultaneous electrodeposition of iron and nickel at high temperatures, is greater than that of iron in the alloy. It is clear that the increased temperature and reduced overpotential for the deposition of these metals caused the reduction of the ions to be controlled essentially by the quantity

$$\varphi_i^0 + \frac{RT}{nF} \ln \frac{\alpha C}{\sum \alpha_i C_i} C;$$

and therefore the rate of deposition of the metal with the more positive normal potential will be greater than that of the one with the more negative value, in accordance with condition (1).

Figure 3 gives the change in the rate of discharge of nickel and iron ions during simultaneous electrodeposition, using the same solutions as in Fig. 2, as a function of the temperature. It can be seen from these curves that increase in the electrolyte temperature causes the rate of reduction of the nickel ions to be increased, while that of the iron ions is diminished, so that at a temperature above  $90^\circ$  the nickel content of the alloy is greater than the iron content.

The experimental results which have been produced show that the theory of real conjugate systems makes it possible to calculate the regularities observed in the simultaneous deposition of metallic ions.

The observed anomaly of the greater rate of deposition of the ions of metals having the more negative reduction potential, in comparison with those having a more positive value, is connected with a change in the overpotential of the deposition of the metals when these are deposited simultaneously, arising from a change in the nature of the deposit on the electrode.

#### LITERATURE CITED

1. A. T. Vagramyan and T. A. Fatueva, *Zhur. Neorg. Khim.* 6, 1281 (1959); T. A. Fatueva and A. T. Vagramyan, *Doklady Akad. Nauk SSSR* 128, 4 (1959).\*

\* See C. B. translation.

2. A. N. Frumkin, V. S. Bagotskii, Z. A. Iofa, and B. N. Kabanov, The Kinetics of Electrode Processes [in Russian] (Moscow, 1952).
3. A. T. Vagramyan and Yu. S. Petrova, The Physicomechanical Properties of Deposits [in Russian] (Izd. AN SSSR, 1960).
4. A. I. Krasovskii, Transactions of the Fourth Congress on Electrochemistry [in Russian] (Moscow, 1959).



## THE INFLUENCE OF MONOLAYERS ON THE EVAPORATION OF DROPS

Corresponding Member of the Academy of Sciences of the

USSR B. V. Deryagin, S. P. Bakanov, and Yu. S. Kurgin

Institute of Physical Chemistry, Academy of Sciences of the USSR

Translated from *Doklady Akademii Nauk SSSR*, Vol. 135, No. 6, pp. 1417-1420,

December, 1960

Original article submitted July 14, 1960

**1. Introduction.** It has been known for a long time [1] that the evaporation of water may be impeded by films of certain surface-active substances, such as stearic and oleic acids and, especially, cetyl alcohol. The theory of this process was developed by Langmuir, who suggested that the presence of a monolayer on the water surface created a resistance to the evaporation of the water [2]. Langmuir represented by means of a single phenomenological parameter — the condensation coefficient,  $\alpha$  — two different phenomena: the penetration of the monolayer by the water molecules; and evaporation from the monolayer surface. Bradley [3] explained in a similar way the retardation of the evaporation of liquid drops by means of insoluble monolayers, ascribing the reduction to values of  $\alpha$  of the order of  $10^{-6}$ .

The theory set out below consists in essentials of the separation of the two effects underlying the influence of films on the rate of evaporation of liquids.

**2. The quasi-stationary evaporation of drops covered by an insoluble film of a foreign substance.** We shall determine the rate of evaporation of an immobile drop placed in an infinite space, the radius of the drop being  $a$ , when the drop is covered by an insoluble liquid film of a foreign substance whose thickness is  $\delta$ ; in terms of the change in the mass of the drop per unit time,  $-dM/dt$ .

A stationary diffusion process occurs in the film, owing to the dissolution in it of the substance of which the drop is composed, which may be described by means of a Laplace equation:

$$\Delta C_1 = 0, \quad a < r < a + \delta, \quad (1)$$

where  $C_1$  is the number of molecules of the material composing the drop in  $1 \text{ cm}^3$  of the film.

Molecules of the liquid evaporate into the atmosphere from the surface of the film. Through a region in direct contact with the surface of the film of thickness  $\lambda$  [6] of the order of the mean free path of the molecules of the vapor in air, the vapor is transferred into a molecular stream and subsequently, beginning at the surface of a sphere of radius  $a + \delta + \lambda$ , diffuses into the atmosphere.

The stationary diffusion of the vapor in the atmosphere is described by the equation:

$$\Delta C_2 = 0, \quad r > a + \delta + \lambda, \quad (2)$$

where  $C_2$  is the concentration of the vapor in the air.

Since the problem possesses spherical symmetry, the solution of Eqs. (1) and (2) emerges in the form:

$$\begin{aligned} C_1 &= A_1/r + B_1, & a < r < a + \delta; \\ C_2 &= A_2/r + B_2, & r > a + \delta + \lambda. \end{aligned} \quad (3)$$

From the condition that a state of equilibrium shall exist between the liquid in the drop and the solution of the liquid in the film at the boundary where  $r = a$ , we arrive at the conclusion that, at this boundary, the concentration of the solution of the liquid in the film,  $C_1$ , is equal to the concentration of the saturated solution of the liquid in the film,  $C_p$ :

$$C_1|_{r=a} = C_p. \quad (4)$$

At the boundary for which  $r = a + \delta$ , the solution of the liquid in the film must be in equilibrium with the vapor of concentration  $C_0$ .

Starting from Henry's Law, we obtain the limiting condition at the boundary for which  $r = a + \delta$ :

$$C_1|_{r=a+\delta} = \frac{C_p}{C_0} C_0', \quad (5)$$

where  $C_0$  is the concentration of the vapor, when this is saturated at the temperature of the drop.

If  $C_2|_{r=a+\delta+\lambda}$  is the concentration of the vapor at a distance  $\lambda$  from the surface of the film, then the molecular stream of vapor from the film is equal to  $\alpha \frac{\bar{v}}{4} (C_0' - C_2|_{r=a+\delta+\lambda})$ , where  $\bar{v}$  is the mean velocity of the vapor molecules. The coefficient of "adhesion",  $\alpha$ , shows that, of the molecules of vapor evaporated from the surface of the film, the portion  $\alpha$  of the molecules passes into the film, while the remaining portion,  $1 - \alpha$  of the molecules rebounds reversibly into the vapor.

From the equation at the boundary for which  $r = a + \delta$ , between the diffusion current of the dissolved liquid in the film and the molecular stream of vapor, we obtain the limiting condition:

$$-D_1 \frac{dC_1}{dr} \Big|_{r=a+\delta} = \alpha \frac{\bar{v}}{4} (C_0' - C_2|_{r=a+\delta+\lambda}), \quad (6)$$

where  $D_1$  is the diffusion coefficient of the liquid molecules in the film.

From the equation at the boundary for which  $r = a + \delta + \lambda$ , between the molecular and the diffusion currents of the vapor in the air, we obtain the limiting condition,

$$4\pi (a + \delta)^2 \alpha \frac{\bar{v}}{4} (C_0' - C_2|_{r=a+\delta+\lambda}) = 4\pi (a + \delta + \lambda)^2 \left( -D_2 \frac{dC_2}{dr} \Big|_{r=a+\delta+\lambda} \right), \quad (7)$$

where  $D_2$  is the diffusion coefficient of the vapor in the air.

The concentration of vapor in the air at infinite distance from the drop is given by:

$$C_2|_{r=\infty} = C_{\infty}. \quad (8)$$

From the five limiting conditions given in Eqs. (4) to (8) the four constants  $A_1$ ,  $A_2$ ,  $B_1$ , and  $B_2$ , and the concentration of the equilibrium vapor,  $C_0'$  are determined.

The rate of evaporation of the drop is equal to the diffusion current of the vapor through the surface of a sphere of radius  $r = a + \delta + \lambda$ :

$$-\frac{dM}{dt} = m 4\pi (a + \delta + \lambda)^2 \left( -D_2 \frac{dC_2}{dr} \Big|_{r=a+\delta+\lambda} \right).$$

If we insert in this relationship the value of  $C_2(r)$  found, we obtain the equation for the rate of the quasi-stationary evaporation of the drop covered with a film of thickness  $\delta$ ,

$$-\frac{dM}{dt} = \frac{4\pi a D_2 (C_0 - C_\infty) m}{\frac{D_2}{\alpha \bar{v}/4} \frac{a}{(a+\delta)^2} + \frac{a}{a+\delta+\lambda} + \frac{D_2 C_0}{D_1 C_p} \frac{\delta}{a+\delta}} \quad (9)$$

In the absence of the film (that is, when  $\delta = 0$ ), Eq. (9) reduces to the known Fuchs equation for the rate of evaporation of a drop of pure liquid:

$$-\frac{dM}{dt} = \frac{4\pi a D_2 (C_0 - C_\infty) m}{D_2/\alpha \frac{\bar{v}}{4} a + \frac{a}{a+\lambda}}$$

We shall assume that the relevant equation for the rate of evaporation of the drop through a monolayer may be obtained from Eq. (9) for the limiting transition from a macroscopic film of thickness  $\delta$  to a monolayer for which  $\delta \ll a$ ; we then obtain:

$$-\frac{dM}{dt} = \frac{4\pi a^3 (C_0 - C_\infty)}{\frac{C_0}{C_p} \frac{\delta}{D_1} + \frac{1}{\alpha \bar{v}/4} + \frac{1}{D_2} \frac{a^2}{a+\lambda}} \quad (10)$$

Equation (10) gives the relationship for the rate of quasi-stationary evaporation of the liquid of a drop covered with a monolayer. The component parts of the denominator in Eq. (10) may be considered as partial resistances to evaporation:  $\frac{1}{D_2} \frac{a^2}{a+\lambda}$  is the resistance due to diffusion of vapor into the air;  $\frac{1}{\alpha \bar{v}/4}$  is the resistance due to the molecular current near to the surface of the drop;  $\frac{C_0}{C_p} \frac{\delta}{D_1}$  is the partial diffusion resistance of the monolayer, which is increased with diminution of the solubility of the liquid in the film.

The description of the effect of the monolayer on the rate of the evaporation by means of the two phenomenological parameters  $\alpha$  and  $\frac{1}{C_p} \frac{\delta}{D_1}$  is equivalent to ascribing to the monolayer simultaneously both a coefficient of repulsion and a coefficient of absorption for the molecules of the liquid.

The theoretical result which we have obtained shows that under conditions for which

$$\frac{C_0}{C_p} \frac{\delta}{D_1} + \frac{1}{\alpha \bar{v}/4} < \frac{1}{\alpha_{H_2O} \bar{v}/4}, \quad (11)$$

where  $\alpha_{H_2O} = 0.034$ , the coefficient of condensation of water, the monolayer ought to increase the rate of evaporation of water.

This paradoxical-seeming case is actually observed experimentally [4, 5]. In a way similar to that for the evaporation from a planar liquid surface, we obtain:

$$I_0 = \frac{m(C_0 - C_L)}{\frac{L-\lambda}{D_2} + \frac{1}{\alpha \bar{v}/4} + \frac{C_0}{C_p} \frac{\delta}{D_1}} \quad (12)$$

where  $C_L$  is the concentration of vapor in air at a distance  $L$  from the liquid surface.

**3. Nonstationary evaporation of a drop covered by an insoluble monolayer of a foreign substance.**  
We shall consider the nonstationary evaporation of the liquid of a drop of radius  $a$ , when this is covered by an insoluble monolayer of a foreign substance of thickness  $\delta$ , when  $\delta \ll a$ .

The nonstationary character arises because of the nonequilibrium initial condition for the introduction of the drop into the atmospheric medium, when the constant concentration of the vapor in the air is  $C_\infty$ , this being different from the equilibrium value, the density of the vapor being much lower than the density of the liquid,  $\gamma$ . That is,  $mC_\infty \ll \gamma$ .

The rate of evaporation is given by:

$$I = -\frac{dM}{dt} = m 4\pi (a + \lambda)^2 \left( -D_2 \frac{\partial C}{\partial r} \Big|_{r=a+\lambda} \right). \quad (13)$$

Inserting in (13) the expression for the mass of the drop,  $M = \frac{4}{3} \pi a^3 \gamma$ , we obtain the equation for the rate of movement of the boundary,

$$\frac{da}{dt} = \frac{mC_\infty}{\gamma} D_2 \left( \frac{a+\lambda}{a} \right)^2 \frac{1}{C_\infty} \frac{\partial C}{\partial r} \Big|_{r=a+\lambda},$$

from which it can be seen that, when  $mC_\infty/\gamma \ll 1$  the Leclé number is small, and the phase boundary may be regarded as immobile [7].

Since equilibrium in the monolayer is set up rapidly, in a time  $T \sim \delta^2/D_1 \sim 10^{-11}$  sec, it may be supposed that equilibrium is only absent in the gas phase, and the effect of the monolayer may be attributed to the change in the concentration of the equilibrium vapor,  $C'_0$ , at the boundary for which  $r = a$ , in comparison with the concentration,  $C_0$ , of the saturated vapor when evaporation occurs from a pure liquid surface.  $C'_0$  is found by the solution of the present quasi-stationary problem; that is, from the system of equations given in (4) to (8):

$$C'_0 = \frac{\frac{C_\infty}{C_p} \frac{\delta}{D_1} + \frac{1}{\alpha \bar{v}} \frac{1}{4} + \frac{1}{D_2} \frac{a^2}{a+\lambda}}{\frac{C_0}{C_p} \frac{\delta}{D_1} + \frac{1}{\alpha \bar{v}} \frac{1}{4} + \frac{1}{D_2} \frac{a^2}{a+\lambda}} C_0. \quad (14)$$

The nonstationary diffusion of the vapor in air is described by the equation,

$$D_2 \Delta C = \frac{\partial C}{\partial t}, \quad r > a + \lambda, \quad t > 0, \quad (15)$$

where  $C$  is the concentration of the vapor in air.

From the equation at the boundary for which  $r = a$  between the molecular vapor current and the diffusion vapor current, we obtain the limiting condition,

$$4\pi a^2 \alpha \frac{\bar{v}}{4} (C'_0 - C \Big|_{r=a+\lambda}) = 4\pi (a + \lambda)^2 \left( -D_2 \frac{\partial C}{\partial r} \Big|_{r=a+\lambda} \right). \quad (16)$$

We write the initial condition in the form,

$$C(r, 0) = C_\infty, \quad r > a + \lambda. \quad (17)$$

From Eqs. (13) to (17) we obtain an expression for the rate of the nonstationary evaporation of the drop covered with a monolayer:

$$I = I_0 f(t),$$

$$f(t) = (1 + \nu) \sqrt{\frac{D_2 t}{\pi}} \frac{a + \lambda}{(a + \lambda)^2 + (1 + \nu) D_2 t} e^{-(a + \lambda)^2 / 4 D_2 t} + \\ + \frac{1 + \nu}{2} \frac{(a + \lambda)^4 + (\nu + 2)(a + \lambda)^2 D_2 t + 2(1 + \nu) D_2^2 t^2}{[(a + \lambda)^2 + (1 + \nu) D_2 t]^2} \left[ 1 - \operatorname{erf} \left( -\frac{a + \lambda}{2 \sqrt{D_2 t}} \right) \right] - \\ - \frac{D_2 t}{2} (1 + \nu) \frac{(a + \lambda)^2 + 2(1 + \nu) D_2 t}{[(a + \lambda)^2 + (1 + \nu) D_2 t]^2} e^{1 + \nu + \left( \frac{1 + \nu}{a + \lambda} \right)^2 D_2 t} \left[ 1 - \operatorname{erf} \left( \frac{a + \lambda + 2 \frac{1 + \nu}{a + \lambda} D_2 t}{2 \sqrt{D_2 t}} \right) \right], \quad (18)$$

where  $\nu = \frac{\alpha \bar{v}/4}{D_2} \frac{a^2}{a + \lambda}$ ;  $J_0 = \frac{4\pi a^3 (C_0 - C_\infty) m}{C_0 \frac{\delta}{D_1} + \frac{1}{\alpha \bar{v}/4} + \frac{1}{D_2} \frac{a^2}{a + \lambda}}$  = the rate of the quasi-stationary evaporation

of the drop.

When  $t \gg (a + \lambda)^2 / D_2$   $f(t) \rightarrow 1$ ,  $J = J_0$ , i.e., the initial nonequilibrium condition is resolved, and there is established a quasi-stationary situation for the evaporation at a time given by  $T \sim (a + \lambda)^2 / D_2$ .

The rate of evaporation of the drop at the initial moment is given by:

$$J|_{t=0} = J_0 \left( 1 + \frac{\alpha \bar{v}/4}{D_2} \frac{a^2}{a + \lambda} \right).$$

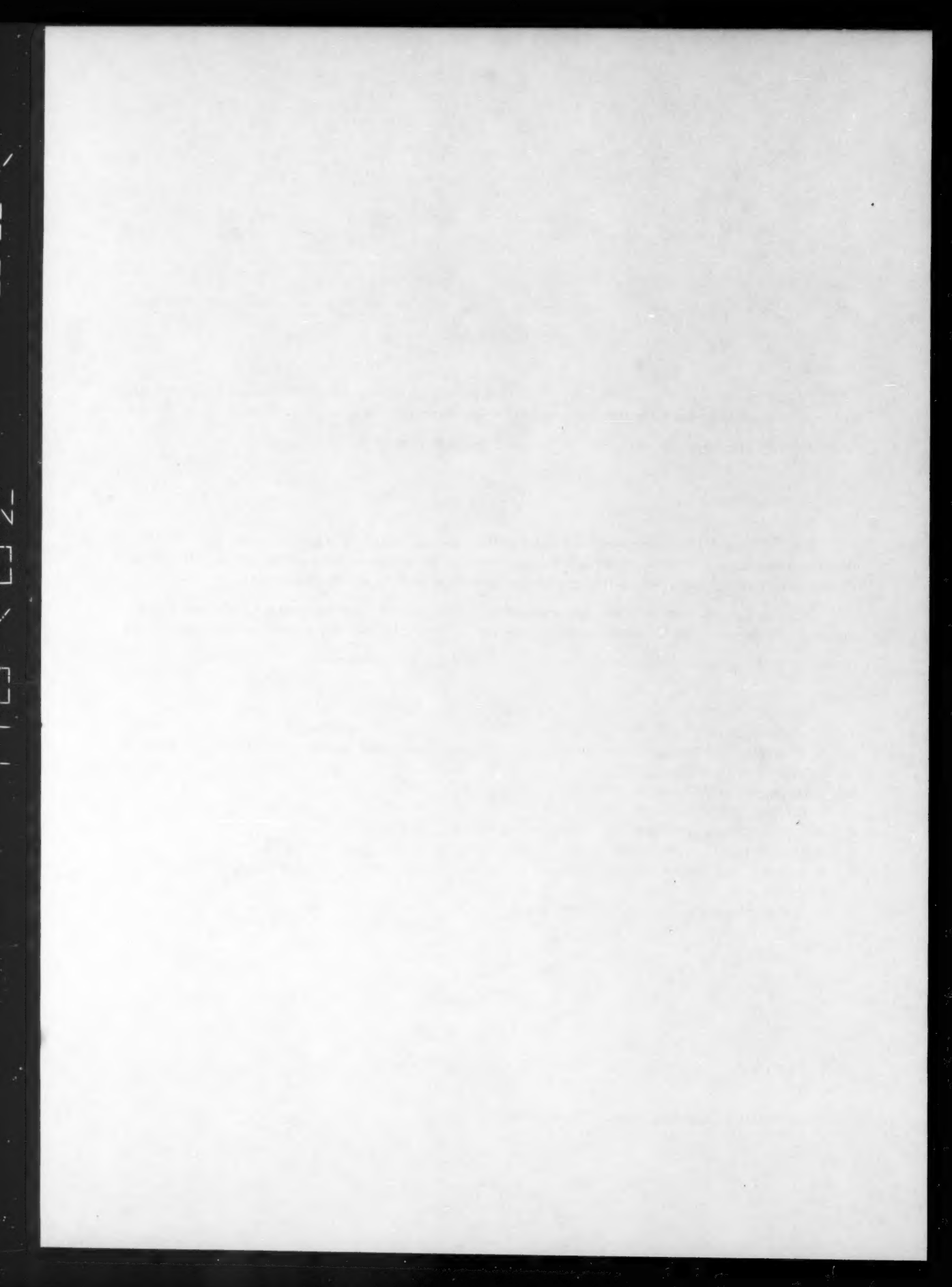
If the presence of the monolayer on a water surface leads to a value of  $\alpha$  greater than  $\alpha_{H_2O} = 0.034$ , the rate of evaporation of the water through the monolayer at the initial moment will be greater than the rate of evaporation of pure water, which is in qualitative agreement with the results given in [4].

According to the experimentally determined rate of stationary evaporation from a  $1 \text{ cm}^2$  plane liquid surface, and the corresponding nonstationary evaporation at the initial moment of nonstationary conditions, it is possible to determine the parameters  $\alpha$  and  $\frac{1}{C} \frac{\delta}{D_1}$  for any given monolayer.

#### LITERATURE CITED

1. N. K. Adam, *Physics and Chemistry of Surfaces* [Russian translation] (Moscow, 1947) Chap. 2, Sect. 36, p. 140.
2. J. Langmuir and V. Schaefer, *J. Franklin Inst.* **235**, 119 (1943).
3. R. Bradley, *J. Coll. Sci.* **10**, 571 (1955).
4. M. V. Tovbin and E. V. Savinova, *Zhur. Fiz. Khim.* **31**, 2717 (1957).
5. G. I. Izmailova, P. S. Prokhorov, and B. V. Deryagin, *Koll. Zhur.* **19**, 556 (1957).\*
6. N. A. Fuks, *The Evaporation and Growth of a Drop in a Gaseous Medium* [in Russian] (Izd. AN SSSR, 1958) Sect. 5.
7. H. L. Frisch and E. C. Collins, *J. Chem. Phys.* **21**, 2158 (1953).

\* Original Russian pagination. See C. B. translation.



# DESTRUCTION AND FORMATION OF STRUCTURES OF NATURAL PROTEINS DURING THEIR TRANSFER THROUGH NONPOROUS MEMBRANES

Academician V. A. Kargin, P. V. Kozlov, S. Ya. Mirlina,  
and Z. A. Kapralova

M. V. Lomonosov Moscow State University

Translated from *Doklady Akademii Nauk SSSR*, Vol. 135, No. 6, pp. 1421-1424,  
December, 1960

Original article submitted August 20, 1960

All the various life phenomena are usually determined by the chemical and physicochemical properties of the substances which make up the living organisms and by their reaction with the substances of the surrounding medium in a manner specific to the biological processes. However, to understand these processes it is also very important to study structural problems, i.e., the laws of formation and destruction of structures in living organisms, the characteristics of types of structures, their morphology, and nature. It seemed interesting therefore to study the nature of the destruction and formation of microstructures of natural proteins by studying the well-known phenomenon of the transfer of proteins through nonporous (cellophane) membranes during electro-dialysis.

For this purpose, we used a high voltage, multichamber electro-dialyzer, which has the advantage that due to the presence of "electric traps," the dynamic equilibrium in a system with a very small fraction of disperse material is gradually displaced toward dissociation to elementary structural units [1]. The subjects of the investigation were fibrillar and globular proteins: gelatin, myosin (in the form of finely ground muscular tissue), egg albumen (in the form of denatured hen egg white), and edestin. The main investigation method in this work was electron microscopy with a JEM-5Y electron microscope with a direct magnification of 15,000 to 85,000.

Destruction of the structure of natural proteins and their transfer through nonporous membranes during electro-dialysis. During a previous study of the processes of electro-dialysis [2] it was noticed that some proteins of comparatively high molecular weight are able to pass through nonporous polymer membranes. This phenomenon occurred in the electro-dialysis of the proteins investigated in a five-chamber, high-voltage electro-dialyzer. The globular proteins (edestin and denatured hen egg white) and also one of the fibrillar proteins, namely, myosin, passed into the neighboring chamber through the membrane in insignificant amounts, while quite large amounts of gelatin were transferred under the given conditions.

This observation necessitated a more detailed study of this phenomenon with gelatin solutions. For this purpose, we investigated the effect of gelatin concentration (from 1.5 to 10%) and temperature (from 25 to 90°) on the transfer processes with various potentials on the electrodes of the electro-dialyzer (from 0.05 to 2.5 kv). It was found that a rise in concentration and temperature caused an increase in the transfer of the gelatin through the membrane into the neighboring chamber of the electro-dialyzer.

Many experiments showed that by using the temperature factor, it was possible to obtain a gelatin transfer through the membrane of 30-40%. There naturally arose the question of the reasons for this phenomenon. The transfer of small initial amounts of gelatin and the other proteins investigated was apparently caused by the

presence in the proteins of fractions of comparatively low molecular weight, which were capable of passing through nonporous membranes during electrodialysis. To find the reasons for the transfer of large amounts of gelatin, we carried out special experiments to determine the molecular weights of the starting gelatin and that transferred into the neighboring chamber of the electrodialyzer. The mean molecular weight of the starting gelatin was 41,350 and after electrodialysis it fell to 23,590, while the molecular weights of gelatin fractions transferred through the membrane were 23,140 at  $t = 60^\circ$  and 22,680 at  $t = 80^\circ$ . Thus, the transfer of gelatin through the membrane was not associated with the fall in the molecular weight of the gelatin as, had this been the case, the whole of the gelatin should have been transferred through the membrane during electrodialysis as the molecular weights of gelatin which underwent electrodialysis and did not pass through the membrane and the gelatin which passed through the membrane coincided.

Special experiments were then carried out to determine the role of pH of the gelatin solutions and the effect on the transfer process of a change in the acid-alkali equilibrium. It was found that the transfer of gelatin was not increased by a large addition of sulfuric acid. The position changed sharply if very small amounts of surface-active substances were introduced into the system with the starting protein after the transfer of protein through the membrane had ceased completely in the electrodialysis process. We used both surface-active electrolytes (dihexyl ester of sodium sulfosuccinate) and also surface-active nonelectrolytes (OP-10). When a few drops of a solution of one of the surface-active substances were added, the transfer of protein slowly recommenced and this applied equally to all the fibrillar and globular proteins we investigated. Electrodialysis of gelatin in urea solutions also increased the amount of product transferred through the membrane, as was shown in a special series of experiments. In this case, even at low temperatures and voltages, the gelatin transfer reached 80% of the original weight of gelatin undergoing electrodialysis in a comparatively short time.

This surprising phenomenon sheds light on the transfer of proteins through nonporous membranes and also compels us to reexamine the usual ideas on the structure of protein molecules. Svedberg [3] observed reversible dissociation of the protein molecule into separate elements, namely, units which are connected to each other in a single chain by bonds that are readily broken and renewed under definite conditions. Such a primary structure of protein molecular formations agrees well with contemporary experimental data on the decomposition of proteins and synthesis of complex structures from them, obtained by means of isotopic tracers [4]. The transfer of proteins through nonporous membranes during electrodialysis is apparently connected with precisely these characteristics of the complex formation of primary protein structures. In the five-chamber electrodialyzer, there is continuous decomposition of primary protein structures to separate, small molecules, namely, units which are readily transferred through the membranes into the side chambers at a high rate. An increase in temperature and applied voltage facilitates decomposition of the structures. The action of surface-active substances, which sharply increase the transfer of protein through the membranes, may be likened to the action of soaps.

Structure-formation processes and the nature of secondary protein structures transferred through nonporous membranes during electrodialysis. To study the formation of secondary protein structures from their elements which had passed through a nonporous membrane through electrodialysis, we used direct observation of the structures formed under an electron microscope. It was possible to use this method under two conditions: a high resolving power of the electron microscope and prevention of the formation of thin protein films, which could not be examined under an electron microscope as they did not have the necessary contrast for observing structural characteristics of the object. The resolving power of the JEM-5Y electron microscope, which equals 8-10 Å, satisfied the first condition. The second condition was satisfied by using solutions of very low concentrations (down to 0.003%) and drying them at temperatures above the gelling point. Gelatin solution was dried at  $40^\circ$ . No gel was formed in this case and it was possible to observe the secondary structural formations of the protein produced after drying the solution.

By observing the above conditions, it was possible to obtain electron microscope photographs of the secondary structural formations of the starting fibrillar proteins, gelatin and myosin, which have a globular character. Figure 1 shows globules of gelatin. Similar globules, which differed only in the least dimensions, were formed by myosin. The formation of globules by gelatin molecules in dilute solutions has been studied quite well [2]. In the present investigation, this phenomenon was again confirmed by direct electron microscope observations. In the investigation of proteins passing through the membrane, it was possible to observe the whole sequence of the elaboration of secondary structural formations, beginning from globules and bundles of chains and ending with combination of the bundles in fibrils and the fibrils in more complex structures. Among the

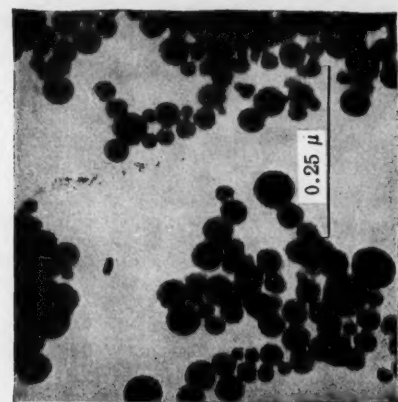


Fig. 1.

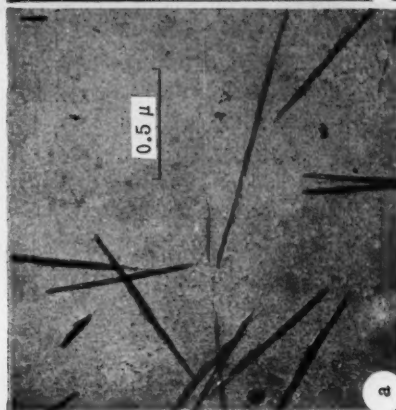


a



b

Fig. 2.

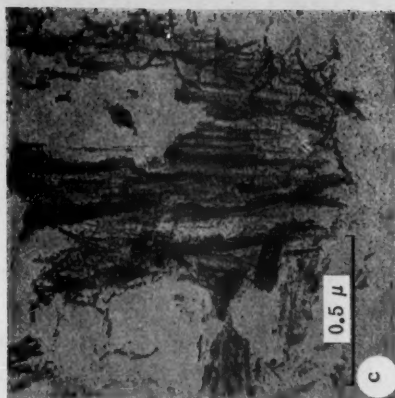


a



b

Fig. 3.



c

Fig. 4.

numerous electron microscope photographs of secondary structural formations, the most characteristic for gelatin are given in Fig. 2a (supermolecular formation of fibrils) and Fig. 2b (structure of individual fibrils) and for myosin in Fig. 3a (fibrils) and Fig. 3b (structure of fibrils). In Fig. 2a, there are well-differentiated fibrils of gelatin, 10 to 40,000 Å in length, without the details of their fine structure. The thickness of these fibrils was approximately the same. We also obtained gelatin fibrils which were very similar to collagen fibrils with their characteristic transverse band structure along the fibril axis (Fig. 2b). It is difficult to determine the method of packing of bundles of gelatin chains in the fibrils, but the photograph presented shows fibrils of spiral form, which combine to form more complex structural systems.

The most coherent and complete picture of the ordering of the structures was observed for myosin. Figure 3a shows the fibrillar structure of the protein which is characteristic of myosin. With sufficient magnification, we observed a clearly expressed discrete build-up of fine structural formations (Fig. 3b). An analogous picture was observed in the case of denatured egg albumen which had passed through a membrane. Figure 4 shows the clearly defined complex structural formations produced after this product had passed through a membrane.

Thus, after destruction of protein structures and the transfer of the elements of these structures through nonporous membranes in electrodialysis, these elements again combine into the most diverse forms of secondary and more complex structural formations.

It is remarkable that regardless of the fibrillar or globular nature of the protein, depending on certain experimental conditions (concentration, temperature, the introduction of surface-active and similar substances, etc.), the synthesis of secondary structural formations may yield both globules and fibrils with subsequent elaboration of supermolecular structures. The processes of destruction and reformation of structures in living organisms apparently are also associated with the role of semipermeable membranes and the action of the corresponding factors and components of the organism. Therefore, the investigation of such processes on model systems is of undoubted interest in extending our ideas on the nature of the whole diversity of life processes.

#### LITERATURE CITED

1. V. A. Kargin and T. A. Matveeva, *Doklady Akad. Nauk SSSR* **105**, 294 (1955).
2. I. I. Zhukov, *Electrokinetic Properties of Capillary Systems* [in Russian] (Izd. AN SSSR, 1956) p. 296; A. A. Tager and V. A. Kargin, *Zhur. Fiz. Khim.* **15**, 10 (1941); P. I. Zubov, Z. N. Zhurkina, and V. A. Kargin, *Doklady Akad. Nauk SSSR* **67**, 659 (1949).
3. T. Svedberg and K. O. Pedersen, *The Ultracentrifuge* (Oxford, 1940); J. B. Eriksson-Quansel and T. Svedberg, *Biol. Bull.* **71**, 498 (1936).
4. G. M. Frank and V. A. Engel'gardt, *Collection: Philosophic Problems of Contemporary Natural Science* [in Russian] (Izd. AN SSSR, 1959) p. 316.

EFFECTS OF DISCRETENESS OF CHARGE AND PROPERTIES  
OF THE DOUBLE LAYER AT A METAL - SOLUTION  
INTERPHASE (CONSIDERATION OF THE DISCRETE  
STRUCTURE OF THE CHARGE OF SPECIFICALLY  
ADSORBED IONIC LAYERS)

Corresponding Member V. G. Levich, V. A. Kir'yanov,  
and V. S. Krylov

Institute of Electrochemistry, Academy of Sciences of the USSR

Translated from Doklady Akademii Nauk SSSR, Vol. 135, No. 6, pp. 1425-1428,  
December, 1960

Original article submitted September 26, 1960

The possibility of a substantial effect of the discreteness of charge on the properties of the double layer was pointed out some time ago by A. N. Frumkin [1]. In recent years, the need for considering these effects in the theory of the double layer has also been emphasized by a number of other authors [2, 3, 6]. This problem has assumed special interest in connection with experimental investigations [2-4] and subsequently those of other authors [13]. As a result of these investigations, it was shown that experimental data on the effect of surface-active electrolytes on the electrocapillary maximum potential cannot be explained by Stern's theory, starting from a one-dimensional model of the layer and using mean values of the characteristics (potential, field, etc.).

These circumstances indicate the inadequacy of the double layer model with a uniformly "spread" charge and the need for systematic consideration of the discrete structure of the charge of specifically adsorbed ionic layers.

Attempts at a theoretical examination of the effects of the discreteness of the charge in the double layer on the basis of various models of the layer have been made previously in [2, 5, 6]. A thermodynamic analysis of the effect of adsorption of surface-active substances on the properties of the double layer was given in [7]. However, the results obtained in [2, 5, 6] are of a qualitative nature and leave unsolved problems associated with calculation of the discrete structure of the double layer in the presence of specific adsorption of ions.

The present work was devoted to a quantitative examination of the effects of discreteness of the charge in the double electrical layer at a metal - solution interphase. On the basis of the theory developed in the work, an examination was also made of charged interphases and an adsorption isotherm derived for anions on metal.

Let us examine a metal - electrolyte solution interphase. The solution occupies the space on one side of a plane  $x > 0$ , where  $x$  is the coordinate characterizing the distance from the interphase ( $x = 0$ ). Due to the small effective radius of specific adsorption forces, it may be assumed that the centers of gravity of all the adsorbed charges are in the same plane, lying at a distance  $x = \beta$  from the interphase.

With allowance for the discrete nature of the charge distribution in the ionic adsorbed layer, the equations for determining the potential in the inner ( $0 \leq x \leq \beta + \gamma$ ) and outer (diffuse) regions of the double layer, respectively, assume the form:

$$\Delta\psi(r) = -\frac{4\pi}{D} \sum_i e_0 z_i \delta(r - r_i); \quad (1)$$

$$\Delta\varphi(r) = -\frac{4\pi}{D_0} \sum_{1 \leq a \leq M} e_0 z_a n_a \exp\left\{-\frac{e_0 z_a \varphi(r)}{kT}\right\}, \quad (2)$$

where  $D$  and  $D_0$  are the dielectric constants in these regions,  $z_a$  is the valence and  $n_a$  the mean density of ions of the given sort in the bulk of the solution,  $\delta(r)$  is the three-dimensional  $\delta$ -function. The summation in (1) is made for all charges of the layer in the plane  $x = \beta$ .

In the case of a metal-solution interphase, the solution of Eqs. (1) and (2) must obey the limiting conditions:

$$\begin{aligned} \psi(0, y, z) &= \psi_0; \quad \varphi(\infty, y, z) = 0; \\ \psi(\beta + \gamma, y, z) &= \varphi(\beta + \gamma, y, z); \quad D \partial\psi/\partial x = D_0 \partial\varphi/\partial x \quad (x = \beta + \gamma), \end{aligned} \quad (3)$$

which indicate the continuity of the potential and the normal component of the electric induction vector at the boundary of the inner and diffuse regions of the double layer ( $\psi_0 = \text{const}$  denotes the over-all potential drop between the metal and the depth of the solution).

For calculating the mean values of the characteristics (in particular, the potential drop, etc.), in the work we derived the relation

$$\begin{aligned} \overline{\Phi} = \overline{\Phi}(x) &= \lim_{\substack{N \rightarrow \infty \\ S \rightarrow \infty}} \left\{ \frac{1}{S} \iint_S \Phi(x, y, z) dy dz \right\} = \frac{2\pi\sigma}{e} \eta(0, x); \\ \Phi(x, y, z) &= \sum_n \sum_n \int_0^\infty \eta(\lambda, x) J_0(\lambda \sqrt{(y - y_m)^2 + (z - z_n)^2}) \lambda d\lambda, \end{aligned} \quad (4)$$

where  $\sigma$  is the mean charge density of the surface adsorbed layer and  $J_0(\lambda)$  is the Bessel function of the first kind and zero order.

Due to the briefness of the present communication, we present here the main results obtained in the work. Starting from the solutions for the appropriate limiting cases, found by means of Green's functions, we calculated the potential drop in the inner and outer (diffuse) regions of the double layer and the micropotential  $\psi^A$  (potential at the point where the fixed ion is adsorbed) as functions of the degree of filling of the surface adsorbed layer, the dielectric permeabilities of the phases, the values of the component of electronic charge  $q$  on the metal, and other characteristics. It was shown that with an arbitrary charge distribution in the adsorbed layer, the potential drop  $\delta\psi_a$  created by a layer of specifically adsorbed anions at the electrocapillary maximum (e.c.m.) equals

$$\delta\psi_a = \psi_0 = -\frac{4\pi\sigma}{D} \gamma, \quad (5)$$

where  $\sigma$  is the mean charge density in the adsorbed layer,  $D$  is the dielectric constant of the inner region,  $\beta$  and  $\beta + \gamma$  are the distances of maximum approach to the metal of the anion and cation, respectively.

This and subsequent results refer to the case of predominant specific adsorption at the interphase of ions of one sign, namely, anions.

If the phases at whose interphase the double layer arises are not electrically neutral as a whole (charged interphase), then together with the potential drop produced by the ionic component of the charge  $\delta\psi_a$ , there also arises the potential component  $\delta\psi_q$ , caused by the presence of the electronic charge  $q$  on the metal (per unit surface). The over-all potential drop  $\delta\psi$  in the inner region of the double layer is then given by the equation

$$\delta\psi = \psi_0 = \delta\psi_a + \delta\psi_q; \quad \delta\psi_q = -\frac{4\pi q}{D}(\beta + \gamma). \quad (6)$$

The micropotential of the layer  $\psi^A$  for a system of point charges, localized at the points of a planar hexagonal lattice with the parameter  $r_0$  for any degree of filling  $\theta$ , is given by the expression

$$\psi^A = \frac{\gamma}{\beta + \gamma}(\delta\psi_a + \delta\psi_q) + \psi_{iz} + \alpha\delta\psi_a, \quad (7)$$

where  $\psi_{iz}$  is a function independent of  $r_0$  (it is, figuratively speaking, a system of "reflections" of the point charge from two equipotential planar surfaces):

$$\psi_{iz} = \frac{e}{D} \int_0^\infty \{e^{-\lambda\gamma} \text{sh } \lambda\beta + e^{-\lambda\beta} \text{sh } \lambda\gamma\} \text{sh}^{-1}\lambda(\beta + \gamma) d\lambda \simeq \frac{e}{D\gamma} \ln 2, \quad (8)$$

and the coefficient  $\alpha$  with  $\delta\psi_a$  in the last term equals

$$\alpha = \alpha(\beta, \gamma, r_0) = 1,656 \frac{r_0^2}{\gamma(\beta + \gamma)} \left\{ \sum_{m=1}^\infty \sum_{p=1}^\infty \sin^2\left(\frac{\beta}{r_0} \xi p\right) \cdot K_0(mp\xi) + \right. \\ \left. + \sum_{m=2}^\infty \sum_{n=1}^{m-1} \sum_{p=1}^\infty \sin^2\left(\frac{p}{r_0} \xi p\right) \cdot K_0(\xi p \sqrt{m^2 + n^2 - mn}) \right\}. \quad (9)$$

Here  $K_0(\lambda)$  is the MacDonald function (cylindrical function from the imaginary argument of zero order),  $-e$  is the charge of the anion, and  $\xi = \pi r_0 / (\beta + \gamma)$ . The micropotential of the layer at the electrocapillary maximum is determined by the preceding formula with  $q = 0$ .

An investigation of the series (9) shows that with real degrees of filling of the surface adsorbed layer, which do not exceed 25-30% according to electrocapillary measurements [4], the last term in the first part of (7) is practically negligible ( $\alpha \ll 1$ ) and consequently, in this region of values of  $\theta$

$$\psi^A = \psi_{iz} + \frac{\gamma}{\beta + \gamma}(\delta\psi_a + \delta\psi_q). \quad (10)$$

The potential  $\psi(r)$  in the inner region of the double layer thereupon changes mainly according to a linear law.

The results obtained confirm in this region of degrees of filling the qualitative ideas on the structure of a discrete double layer put forward in the work of D. Grahame [2].

A substantial deviation from (10) occurs at considerably higher degrees of filling, corresponding to values of the parameter  $(\beta + \gamma)/2r_0$  equal to approximately 0.3-0.4, which correspond to values of  $\theta$  close to unity. Strictly speaking, these results are accurate with the assumption that the inner Helmholtz plane (limit of the approach of the cation to the metal) is an equipotential of the field and the adsorbed ions are rigidly held in fixed positions.\*

It was shown that with allowance for the thermal motion of the ions in solution and rejection of the limitation associated with the assumption that the inner Helmholtz plane is equipotential, the results obtained above remain practically effective at sufficiently high bulk solution concentrations and with a considerable difference in the dielectric constants of the inner and outer regions of the double layer. Thus, for example, the potential drop  $\delta\psi_a$  in the inner region of the double layer at the electrocapillary maximum is found to equal

\* As an approximate calculation shows, allowance for the thermal motion of the ions in the adsorbed layer does not have an appreciable effect on the results presented.

$$\delta\psi_a = -\frac{4\pi\sigma}{D}\gamma - \frac{4\pi}{D}\sigma\frac{D}{D_0\kappa}\left(\frac{D/D_0 + \kappa\gamma}{D/D_0 + \kappa(\beta + \gamma)}\right) \quad (11)$$

instead of (6), where  $\kappa$  is the reciprocal Debye length, depending on temperature and solution concentration. The corrections to the micropotential of the layer and other characteristics are analogous.

Starting from the calculated values of the micropotential of the layer  $\psi^A$ , it is possible to determine the relation of the potential drop  $\delta\psi_a$  to the concentration (activity  $a_{\pm}$ ) of anions in solution or, what is equivalent, to calculate the value  $\partial(\delta\psi_a)/\partial \ln a_{\pm}$  as a function of  $\delta\psi_a$ :

$$\frac{\partial(\delta\psi_a)}{\partial \ln a_{\pm}} = \left( \frac{RT}{F\delta\psi_a} - \frac{\partial\psi^A}{\partial(\delta\psi_a)} \right)^{-1} \frac{RT}{F}. \quad (12)$$

Relation (12) was derived on the assumption that the relation  $\sigma = \sigma(a_{\pm}, \psi^A)$  is determined with respect to  $\psi^A$  mainly by the Boltzmann factor

$$\sigma = ka_{\pm} \exp \left\{ -\frac{\psi^A F}{RT} \right\}, \quad (13)$$

and the potential drop in the diffuse region of the double layer may be neglected.

If we also consider the potential drop in the diffuse region of the double layer, then according to [2],  $\partial(\delta\psi_a)/\partial \ln a_{\pm}$  is determined in terms of  $\psi^A$  by the relation

$$\frac{\partial(\delta\psi_a)}{\partial \ln a_{\pm}} = \left[ \frac{RT}{F\delta\psi_a} - \frac{\partial\psi^A}{\partial(\delta\psi_a)} - \frac{\partial(\varphi_{\beta+\gamma} - \varphi^*)}{\partial(\delta\psi_a)} \right]^{-1} \left( 1 + \frac{\partial \ln(\gamma/D)}{\partial \ln a_{\pm}^2} \right) \frac{RT}{F}, \quad (14)$$

where  $\varphi^*$  is the statistical mean of the values of  $\varphi(x)$  in the diffuse region of the double layer.

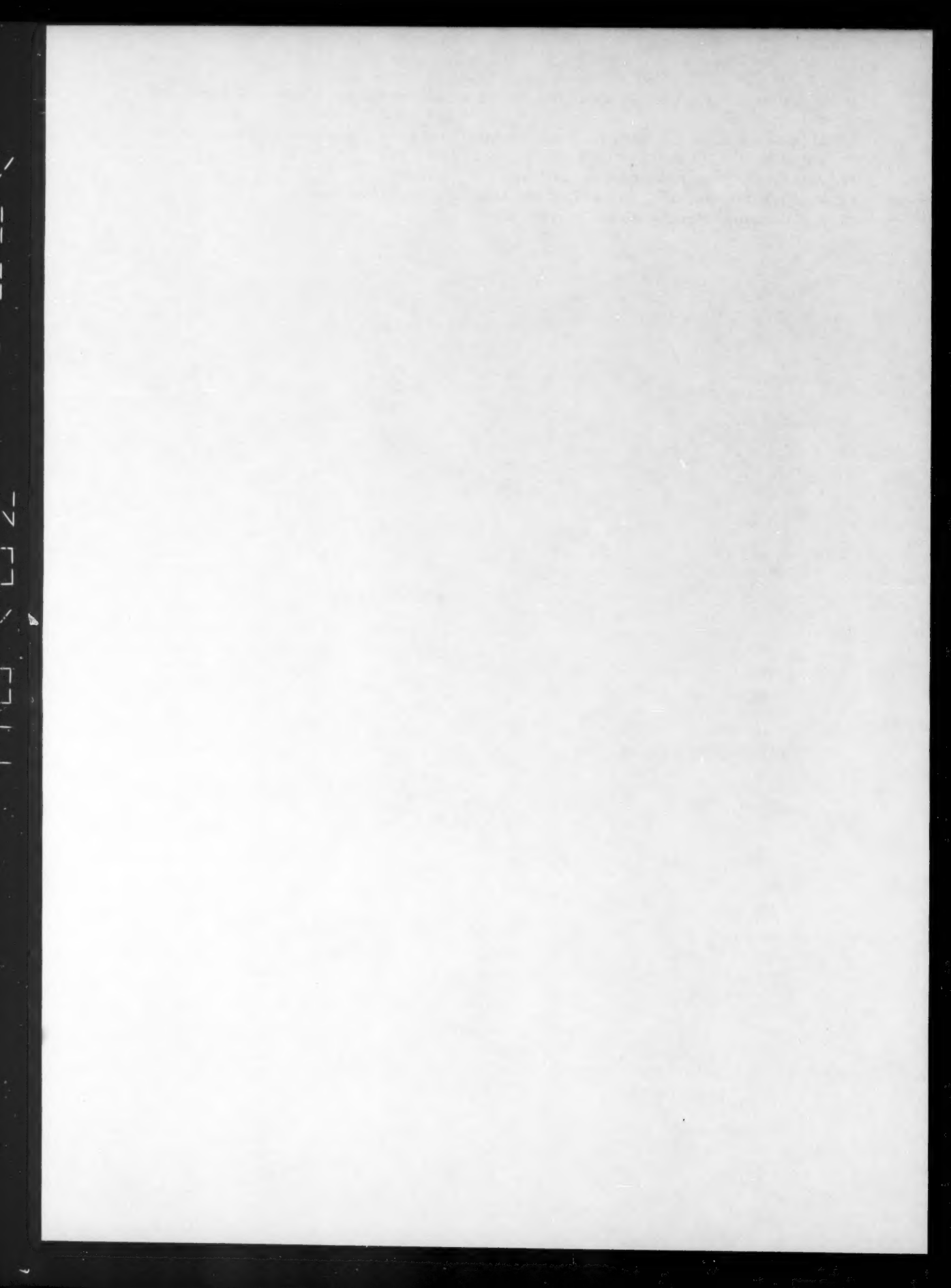
An approximate determination of the values  $\beta$  and  $\gamma$  from data on ionic radii and calculation of  $\partial(\delta\psi_a)/\partial \ln a_{\pm}$  from formula (12) shows that there is quite close agreement between the theoretical results and experimental data on the mercury - solution interphase [13]. An examination of the effects of the discreteness of the charge on a dielectric - solution interphase will be given in a separate communication.

The authors would like to thank Academician A. N. Frumkin for very valuable discussion of the results of the present work.

#### LITERATURE CITED

1. A. N. Frumkin, *Zhur. Fiz. Khim.* **17**, 308 (1943); *Proc. Second International Congress of Surface Activity* (1958) Vol. 3.
2. D. C. Grahame, *Chem. Rev.* **41**, 441 (1947); *Z. Elektrochem.* **62**, 264 (1958); *J. Chem. Phys.* **18**, 903 (1950); *J. Am. Chem. Soc.* **68**, 301 (1946); **63**, 1207 (1941); **71**, 2975 (1949); **80**, 4201 (1958).
3. O. A. Esin and B. F. Markov, *Zhur. Fiz. Khim.* **13**, 318 (1939).
4. Z. A. Iofa and A. N. Frumkin, *Zhur. Fiz. Khim.* **18**, 268 (1944).
5. O. A. Esin and V. M. Shikhov, *Zhur. Fiz. Khim.* **17**, 236 (1943).
6. B. V. Ershler, *Zhur. Fiz. Khim.* **20**, 679 (1946).
7. R. Parsons, *Trans. Farad. Soc.* **51**, 1518 (1955); *Proc. Second International Congress of Surface Activity* (1958) Vol. 3; P. Devanathan and R. Parsons, *Trans. Farad. Soc.* **49**, 404 (1953); **49**, 675 (1953).
8. D. P. Benton and G. A. H. Elton, *Proc. Second International Congress of Surface Activity* (1958) Vol. 3.

9. A. Watanabe, F. Fsuyl, and Sh. Veda, Proc. Second International Congress of Surface Activity (1958) Vol. 3.
10. M. A. Gerovich, see L. D. Gil'man, Electrophoresis of Gas Bubbles, Dissertation [in Russian] (L. Ya. Karpov Institute, 1944).
11. A. Craxford, Trans. Farad. Soc. 34, 85 (1940).
12. Z. Iofa, B. Ustinskiĭ, and F. Éiman, Zhur. Fiz. Khim. 13, 934 (1939).
13. B. S. Gurenkov, Zhur. Fiz. Khim. 30, 1830 (1956).



## DETERMINATION OF THE ELECTROCAPILLARY MAXIMUM POTENTIAL OF SILVER

D. I. Leikis

Institute of Electrochemistry, Academy of Sciences of the USSR

(Presented by Academician A. N. Frumkin, July 14, 1960)

Translated from *Doklady Akademii Nauk SSSR*, Vol. 135, No. 6, pp. 1429-1431,  
December, 1960

Original article submitted July 8, 1960

There are a series of values for the electrocapillary maximum potential of silver in the literature and these differ substantially. A value of  $\varphi_{e.m.}^*$  for silver equal to + 0.05 v was obtained from adsorption measurements [1]. Values of + 0.05 v [2] and - 0.15 v [3] were obtained from capacity measurements. From observations on the smoothing of silver it follows that  $\varphi_{e.m.} \approx - 0.3$  v [4]. An electrocapillary maximum potential of - 0.6 v was obtained for silver by plotting electrocapillary curves in melts (by calculation using the value of  $\varphi_{e.m.}$  for lead) [5]. Despite the calculation, the latter method seems to be one of the most reliable methods of determining  $\varphi_{e.m.}$ , as the measurements are made on liquid metal, whose surface is naturally more homogeneous than the surface of a solid metal. Data obtained by this method for almost all the metals investigated agree well with data obtained by other methods in aqueous solutions at room temperature. Silver is the exception. To elucidate these contradictions, we considered it profitable to measure  $\varphi_{e.m.}$  of silver in aqueous solutions by plotting curves of the capacity of the double layer against potential in solutions of various compositions. This method has been used successfully to determine the electrocapillary maximum potential of Pb [6, 7], Cd [6], Tl [6], and  $PbO_2$  [8]. The measurement procedure with an alternating current was the same as that described previously [7, 8]. The measurements were carried out on a silver wire sealed in molybdenum glass. Before measurements, the electrode was cleaned with a fine, wet glass powder and defatted by boiling in alkali for 1 minute, after which it was carefully washed with doubly distilled water and subjected to cathode polarization at a potential of - 0.5 v. The data obtained are illustrated in Fig. 1. As this figure shows, curves 1 and 2, which were plotted in dilute solutions of  $Na_2SO_4$ , show a well-expressed minimum at  $\varphi = - 0.7$  and the minimum deepened with dilution. For comparison, we present curve 3, which was plotted in 1 N solution. In accordance with the theory of the double layer, the capacity minimum observed in dilute solutions was not present in the latter curve over the potential range from - 0.6 to - 0.8 v. On the basis of the data presented, we concluded that for silver  $\varphi_{e.m.} = - 0.7 \pm 0.05$  v.

To confirm the accuracy of this conclusion we considered it necessary to make a comparison of data obtained in dilute  $K_2SO_4$  solutions with data obtained in dilute KCl and KBr solutions, i.e., in solutions containing anions of different surface activities. It might have been expected that  $\varphi_{e.m.}$  would be displaced in a negative direction with successive replacement of  $SO_4^{2-}$  by  $Cl^-$  and  $Br^-$ . Figure 2 gives curves plotted in 0.01 N solutions of  $K_2SO_4$  (curve 1), KCl (curve 2), and KBr (curve 3). As Fig. 2 shows, the anticipated phenomenon was actually observed. It should be noted that the accuracy of our determination of  $\varphi_{e.m.}$  may be questioned if it is assumed that the  $SO_4^{2-}$  ion has a high surface activity with respect to silver and that in actual fact  $\varphi_{e.m.}$  of silver has a more positive value than follows from Fig. 1. However, the absence of the

\* All potentials are relative to a normal hydrogen electrode.

displacement of the potential minimum in a positive direction when the solution is diluted (curves 1 and 2, Fig. 1) contradicts this hypothesis.

In addition to the measurements given, for additional confirmation of the accuracy of our determination of  $\varphi_{e.m.}$ , we measured the differential capacity of the double layer on silver in the presence of hexanol. As is known, hexanol is adsorbed close to the electrocapillary maximum and is desorbed at sufficiently high negative and positive surface charges so that desorption peaks are observed on either side of  $\varphi_{e.m.}$  [9]. Although this method cannot be used to determine  $\varphi_{e.m.}$  accurately as the orientation of the adsorbed dipolar molecule may differ somewhat on different metals, due to the great discrepancy between previous results and between the latter and the value we obtained, we con-

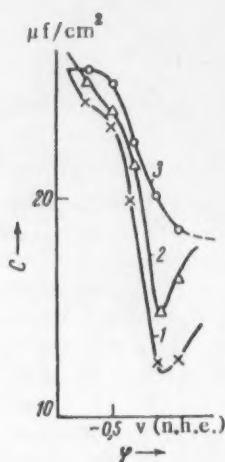


Fig. 1. Potential dependence of the capacity of a silver electrode: 1) in 0.002 N  $\text{Na}_2\text{SO}_4$ ; 2) in 0.01 N  $\text{Na}_2\text{SO}_4$ ; 3) in 1 N  $\text{Na}_2\text{SO}_4$ .

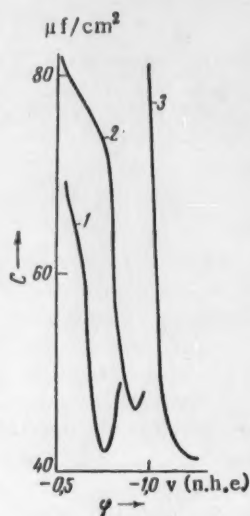


Fig. 2. Potential dependence of the capacity of a silver electrode: 1) in 0.01 N  $\text{K}_2\text{SO}_4$ ; 2) in 0.01 N  $\text{KCl}$ ; 3) in 0.01 N  $\text{KBr}$ .

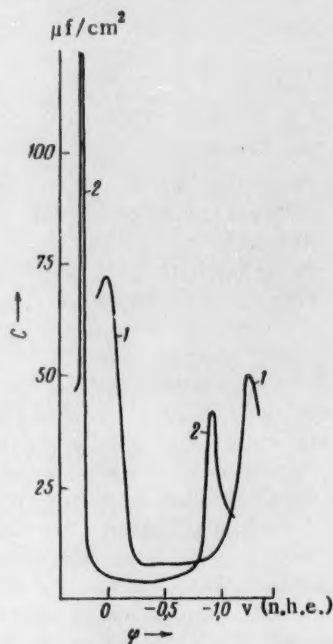


Fig. 3. Potential dependence of the capacity of a silver (1) and mercury (2) electrode in 1 N  $\text{Na}_2\text{SO}_4$  solution, saturated with hexanol.

sidered it valuable to make these additional measurements which can show the region in which  $\varphi_{e.m.}$  lies by an independent method.

Figure 3 gives curves obtained on silver (curve 1) and mercury (curve 2) in 1 N  $\text{Na}_2\text{SO}_4$  solutions, saturated with hexanol, at a frequency of 2 kh.\* The desorption peaks on silver were somewhat less clearly expressed than on mercury (this is probably associated with heterogeneity of the solid metal), but they were sufficiently clear (see Fig. 3). The value of  $\varphi_{e.m.}$  of silver we found ( $-0.7$  v) lay within the potential range between the desorption peaks. It should be noted that the desorption peaks on silver were approximately 0.3 v more negative than on mercury, from which it may be concluded that  $\varphi_{e.m.}$  of silver is more negative than  $\varphi_{e.m.}$  of mercury, which equals  $-0.2$  v.

On the basis of what has been presented, we consider that the electrocapillary maximum potential of silver equals  $-0.7 \pm 0.05$  v. The value of  $\varphi_{e.m.}$  we obtained agrees with the results of measuring  $\varphi_{e.m.}$  by means of electrocapillary curves in melts [5], with the same accuracy as for other metals.

\* The measurements on mercury were carried out in the Electrochemistry Department of Moscow State University by Satiya Narayana, whom we would like to thank.

In studying the potential dependence of the capacity of the double layer on silver, we observed that strong cathode polarization in  $\text{Na}_2\text{SO}_4$  and  $\text{K}_2\text{SO}_4$  solutions has an effect on the properties of the silver surface. Thus, in particular, polarization of silver in the potential region from  $-1.3$  to  $-1.4$  v led to irreversible changes in the properties of the silver surface. Therefore, the silver was not cathodically polarized at such negative values in the measurements.

In conclusion, we should like to thank Academician A. N. Frumkin and Professor B. N. Kabanov for valuable advice which helped with this work.

#### LITERATURE CITED

1. V. I. Veselovskii, *Zhur. Fiz. Khim.* 13, 1543 (1939).
2. V. L. Kheifets and B. S. Krasikov, *Doklady Akad. Nauk SSSR* 109, 586 (1956).
3. T. I. Borisova, Transactions of the Conference on Electrochemistry [in Russian] (Moscow, 1953) p. 386.
4. M. Fleischman, J. Sowerby, and H. Thirsk, *Trans. Farad. Soc.* 53, 91 (1957).
5. S. Karpachev and A. Stromberg, *Zhur. Fiz. Khim.* 18, 47 (1944).
6. T. I. Borisova and B. V. Érshler, *Zhur. Fiz. Khim.* 24, 337 (1950).
7. D. I. Leikis and B. N. Kabanov, *New Methods for Physicochemical Investigations* [in Russian] (Moscow, 1957) Coll. 2, p. 5.
8. B. N. Kabanov, I. G. Kiseleva, and D. I. Leikis, *Doklady Akad. Nauk SSSR* 99, 805 (1954).
9. V. I. Melik-Gaikazyan, *Zhur. Fiz. Khim.* 26, 560 (1952).



## MECHANISM OF THE ANODE SOLUTION OF INDIUM AMALGAM IN ACID SOLUTIONS

V. V. Losev and A. I. Molodov

L. Ya. Karpov Physicochemical Institute

(Presented by Academician A. N. Frumkin, July 8, 1960)

Translated from *Doklady Akademii Nauk SSSR*, Vol. 135, No. 6, pp. 1432-1435,

December, 1960

Original article submitted July 7, 1960

The solution of metals in highly acid solutions in the absence of oxygen proceeds as a result of the independent occurrence of two connected electrochemical reactions, namely, anode ionization of the metal and cathode liberation of hydrogen [1]. The increase in the metal solution rate with a decrease in pH, which is usually observed under these conditions, is normally explained by an increase in the rate of the cathode process, which leads to a displacement of the stationary potential of the metal in a positive direction and, as a secondary effect, produces an increase in the rate of the anode process. As regards the kinetics of the anode process itself, at first glance it seems that the rate of ionization of the metal at a given potential should not depend on the acidity of the solution in sufficiently acid solutions in which the metal is not passivated. Nonetheless, the results of polarization measurements on an iron electrode in solutions of  $\text{HClO}_4 + \text{NaClO}_4$  obtained in the work of Bonhoeffer and Heusler [2] indicate that the rate of anode solution of iron at a given potential decreases strongly with an increase in acidity over the pH range from 0 to 4.\* An analogous effect was observed in the anode solution of nickel [4].

Since the question of the effect of pH on the rate of anode ionization of metals is of considerable importance in understanding the mechanism of this process, we studied the effect of solution acidity on the kinetics of anode and cathode processes at an electrode of indium amalgam\*\* which has a low exchange current [5].\*\*\* By combining polarization measurements with radiochemical measurements on a stationary amalgam electrode [5, 7], we studied the relation of the anode and cathode processes and exchange current to the solution acidity (from  $9.5 \cdot 10^{-4}$  M to 3.3 M  $\text{HClO}_4$ ) on 0.1 M indium amalgam in 0.01 M  $\text{In}(\text{ClO}_4)_3$  solution with added  $\text{NaClO}_4$  to maintain a constant ionic strength (3 M) with vigorous stirring of the amalgam and solution.

Figure 1 shows the potential dependence of the rate of the true anode process  $i_a$  (found radiochemically by means of the radioactive isotope  $\text{In}^{114}$ ) together with the normal polarization curves plotted on the current.

\* The authors explain this effect by the catalytic action of hydroxyl ions on the anode solution of iron; they based this on the results of Kabanov and Leikis [1, 3], who showed that hydroxyl ions participate in the limiting stage of anode solution of iron in alkaline solutions.

\*\* The use of an amalgam electrode in a solution of a salt of the same metal makes it possible to study the effect of pH not only on the anode solution of metal, but also on the kinetics of the corresponding reverse process, namely, discharge of metal ions. In addition, this eliminates the effect of the liberation of hydrogen, which, in the case of iron and nickel electrodes, may be adsorbed on the metal surface and affect the kinetics of the anode process.

\*\*\* In addition, from polarographic data [6], it is clear that the wave of indium ion discharge becomes more reversible with an increase in pH and it might have been expected that in the region of the equilibrium potential, the kinetics of the ionization-discharge process would depend on pH.

There was a linear relation between the potential and  $\log i_a$  and the slope of the anode curve ( $\varphi, \log i_a$ ) was practically independent of the acid concentration and was given by  $b_a = 0.027$  v, which corresponds to a transport coefficient  $\beta = 2.2$  [5]. With an increase in acid concentration from  $9.5 \cdot 10^{-4}$  M to 0.5 M, the exchange current  $i_0$  fell by a factor of 500 (from  $1 \cdot 10^{-3}$  to  $2 \cdot 10^{-6}$  amp/cm<sup>2</sup>).

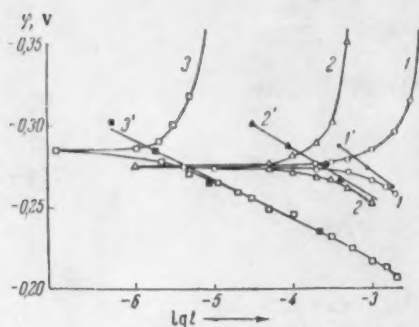


Fig. 1. Relation of the true anode curves (1', 2', 3') and polarization curves (1, 2, 3) to acid concentration (1 and 1')  $9.5 \cdot 10^{-4}$  M; 2 and 2') 0.016 M; 3 and 3') 0.5 M  $\text{HClO}_4$ .

Figure 2 gives anode and cathode polarization curves for solutions with different acidities. For a quantitative determination of the effect of  $\text{HClO}_4$  concentration on the rate of the anode process, Fig. 2a shows a broken line at the potential  $\varphi = -0.250$  v; the points of intersection of the anode curves with this line are the values of  $i_a$  at constant potential. Figure 3 shows the relation of the values of  $i_a$  found in this way to the  $\text{HClO}_4$  concentration.\* Over the range of  $\text{HClO}_4$  concentrations (C) of  $5 \cdot 10^{-3}$  to 0.2 M the relation ( $\log i_a, \log C$ ) was linear with a slope  $p = -1.12$ ; at  $C > 0.2$  M, the rate of the anode process was practically independent of acidity. Figure 3 shows values of the exchange current  $i_0$  (found radiochemically) for  $C < 0.1$  M, i.e., for the range of  $\text{HClO}_4$  concentrations in which the equilibrium potential of the amalgam is independent of acidity; the slope of the line ( $\log i_0, \log C$ ) was  $p = -0.99$ . Since at equilibrium,  $i_0 = i_a = i_c$ , where  $i_c$  is the rate of the true cathode process, this means that the rates of the anode and cathode processes at the equilibrium potential are inversely proportional to the  $\text{HClO}_4$  concentration.\*\*

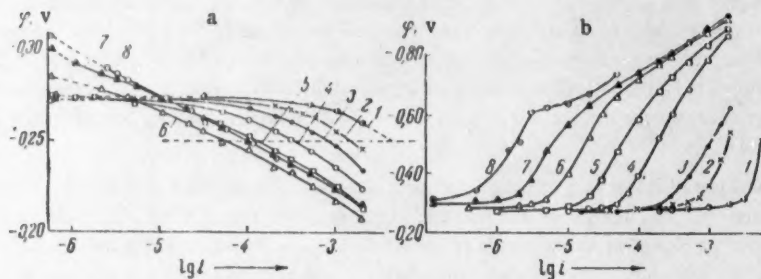


Fig. 2. Relation of anode (a) and cathode (b) polarization curves to acid concentrations: 1)  $2 \cdot 10^{-3}$  M for (a) and  $9.5 \cdot 10^{-4}$  M for (b); 2)  $7.7 \cdot 10^{-3}$  M; 3) 0.016 M; 4) 0.05 M; 5) 0.1 M; 6) 0.5 M; 7) 1.3 M; 8) 3.3 M  $\text{HClO}_4$ .

This conclusion agrees satisfactorily with the result of determining the relation of  $i_a$  to C at  $\varphi = -0.250$  v. If we consider the observed linear relation between  $\varphi$  and  $\log i_a$  and also the proportionality between  $i_a$  and the amalgam concentration at  $\varphi = \text{const}$  [5], then for  $C \leq 0.1$  M it is possible to represent our experimental data by the equation:

$$i_a = k [\text{In}] [\text{H}^+]^{-1} e^{\beta \varphi F / RT}, \quad (1)$$

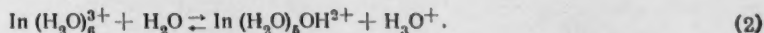
where  $\beta = 2.2$ .

\* Since there was a considerable scatter of the experimental data, Fig. 3 shows not only points from Fig. 2, but also values of  $i_a$  at  $\varphi = -0.250$  v for other experiments.

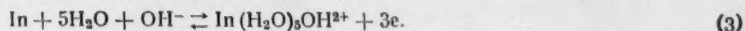
\*\* At  $C < 2 \cdot 10^{-3}$  M, the results of measurements of  $i_a$  and  $i_c$  were distorted due to strong hydrolysis and the formation of  $\text{In}(\text{OH})_3$ .

The relation of the cathode process to acidity is more complex. As Fig. 2b shows, strong retardation of the cathode process with an increase in acidity was observed over the whole range of  $\text{HClO}_4$  concentrations. The slope of the cathode curves was very high (0.4 v) and gradually decreased with a displacement of the potential in a negative direction. It was previously shown [5] that in an acid  $\text{In}(\text{ClO}_4)_3$  solution at an appreciable distance from the equilibrium potential in a negative direction, the normal polarization curves do not correspond to the discharge of indium ions, but apparently reflect the presence of some chemical reaction in solution, which precedes this stage.

In interpreting the results we obtained, it is necessary to consider the high tendency of indium ions for hydrolysis:



By using literature data for the hydrolysis constant of indium salts,\* it is possible to calculate the fraction of hydrolyzed indium ions in solution under our conditions. Thus, when  $C = 2 \cdot 10^{-3} \text{ M HClO}_4$ , the fraction of  $\text{In}(\text{H}_2\text{O})_5\text{OH}^{2+}$  ions is approximately 1.5% and when  $C = 1.6 \cdot 10^{-2} \text{ M}$  to 0.3%, while when  $C = 0.1 \text{ M}$ , it falls to 0.05%. It may be assumed that the electrode process does not involve the cations  $\text{In}(\text{H}_2\text{O})_6^{3+}$ , which predominate in solution, but partly hydrolyzed indium ions:



In this case, the rate of the anode process should be expressed by the equation

$$i_a = k' [\text{In}] [\text{OH}^-] e^{\beta\varphi F/RT} = k' K_w [\text{In}] (\text{H}_3\text{O}^+)^{-1} e^{\beta\varphi F/RT}, \quad (4)$$

where  $K_w = [\text{H}_3\text{O}^+] [\text{OH}^-]$ , which agrees with our experimental data [see Eq. (1)]. The expression for the rate of the cathode process should have the form

$$i_k = k'' [\text{In}(\text{H}_2\text{O})_5\text{OH}^{2+}] e^{-\alpha\varphi F/RT} = k'' K_h [\text{In}(\text{H}_2\text{O})_6^{3+}] [\text{H}_3\text{O}^+]^{-1} e^{-\alpha\varphi F/RT}$$

This equation agrees with the results of determining the relation of exchange current at  $\varphi = \text{const}$  to the  $\text{HClO}_4$  concentration (Fig. 3) and with data on the relation of the exchange current to amalgam concentration [5]. The unusually high slope of the cathode polarization curves is apparently caused by the fact that at sufficiently high current densities, the cathode process begins to be limited by the rate of the preceding reaction in which hydrolyzed indium ions are formed [Eq. (2)]. This reaction evidently proceeds slowly both in the bulk of the solution and on the amalgam surface and therefore, with an increase in the electrode potential in a negative direction, its rate increases due to an increase in the concentration of adsorbed indium ions.\*\* The question arises as to why the formation and discharge of hydrolyzed particles of indium proceed much more readily than the corresponding electrode processes for the simple ions  $\text{In}(\text{H}_2\text{O})_6^{3+}$ , which predominate in the solution. Like some other anions [7], the hydroxyl ion is apparently capable of acting as a type of "bridge," which facilitates the transfer of electrons between the electrode surface and the reacting particle.\*\*\*

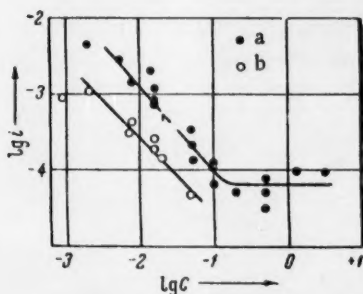


Fig. 3. Relation of the rate of the anode process  $i_a$  (a) at  $\varphi = -0.250 \text{ v}$  and the exchange current  $i_0$  (b) to  $\text{HClO}_4$  concentration.

\* For  $3\text{MNaClO}_4$   $K_h = [\text{In}(\text{H}_2\text{O})_5\text{OH}^{2+}][\text{H}_3\text{O}^+]/[\text{In}(\text{H}_2\text{O})_6^{3+}] = 10^{-4.4}$  [8].

\*\* Our assumptions on the participation of hydrolyzed indium ions in the electrode process and the slowness of their formation agree with results of measuring the capacity of a mercury electrode in solutions with different pH values, containing trivalent lanthanum ions [9]: it was found that basic lanthanum ions, arising as a result of hydrolysis, have a higher adsorption power than simple cations  $\text{La}^{3+}$  and the hydrolysis proceeds at a finite rate on the mercury surface.

\*\*\* An analogous catalytic effect of  $\text{OH}^-$  ions is also observed in the polarographic reduction of some other multicharged cations [10, 11] and in homogeneous isotopic exchange between cations [12].

A comparison of the results we obtained with the rules for iron and nickel mentioned previously [2, 4] indicates that hydrolyzed metal ions play a substantial part in the electrode process. The main difficulty arising in the interpretation of these results consists of the fact that it is assumed that hydroxyl ions participate in the anode process [see Eq. (3)]. Nevertheless, an approximate calculation [13] shows that the volume concentration of hydroxyl ions in acid solutions is too low for the anode process to occur. It has been suggested [2] that due to the high adsorption power of  $\text{OH}^-$  ions, the equilibrium  $\text{H}_2\text{O} \rightleftharpoons \text{H}^+ + \text{OH}^-_{\text{ads}}$  on the metal surface is displaced toward the right and therefore the surface concentration of  $\text{OH}^-$  ions is considerably greater than that in the volume. Another explanation seemed more probable to us: if it is assumed that the electrode processes of the formation and discharge of multicharged metal cations proceed in stages with the successive removal and addition of electrons, respectively, which is very probable in the case of indium [5], then it is natural to assume that metal ions of lower valence thus formed are also capable of being hydrolyzed. For the case of indium, it has been shown that the limiting stage of the electrode process is the elimination of the last electron [5]; consequently, this stage may be preceded by the hydrolysis of the divalent indium ion  $\text{In}(\text{H}_2\text{O})_m^{2+} + \text{H}_2\text{O} \rightleftharpoons \text{In}(\text{H}_2\text{O})_{m-1}\text{OH}^+ + \text{H}_3\text{O}^+$ , and then the limiting stage will be expressed by the equation  $\text{In}(\text{H}_2\text{O})_{m-1}\text{OH}^+ + \text{H}_2\text{O} \rightleftharpoons \text{In}(\text{H}_2\text{O})_{m+1-1}\text{OH}^{2+} + \text{e}^-$ , where  $m + l = 6$ . It is not difficult to show that in this case, the rate of the anode process is described by Eq. (4) as before.

#### LITERATURE CITED

1. A. N. Frumkin, et al., Kinetics of Electrode Processes [in Russian] (Moscow, 1952).
2. K. F. Bonhoeffer and K. E. Heusler, Z. Phys. Chem. 8, 390 (1956); K. E. Heusler, Z. Elektrochem. 62, 582 (1958).
3. B. N. Kabanov and D. I. Leikis, Doklady Akad. Nauk SSSR 58, 1685 (1947).
4. M. Hollnagel and R. Landsberg, Z. Phys. Chem. (DDR) 212, 94 (1959).
5. G. M. Budov and V. V. Losev, Doklady Akad. Nauk SSSR 129, 1321 (1959)\*.
6. D. Cozzi and S. Vivarelli, Z. Elektrochem. 57, 408 (1953).
7. V. V. Losev and A. I. Molodov, Doklady Akad. Nauk SSSR 130, 111 (1960)\*.
8. F. I. C. Rossotti and H. Rossotti, Acta Chem. Scand. 10, 779 (1956).
9. B. B. Damaskin and N. V. Nikolaeva-Fedorovich, Nauch. Dokl. Vysh. Shkoly, Khim. i Khim. Tekhnol. 1, 43 (1959).
10. A. Vloek, Collection 24, 181 (1959); S. Misumi and J. Yasuchi, Bull. Chem. Soc. Japan 32, 1159 (1959).
11. J. M. Kolthoff and Y. Okinaka, J. Am. Chem. Soc. 81, 2296 (1959).
12. R. W. Dodson, et al., J. Am. Chem. Soc. 73, 2890 (1951); J. Phys. Chem. 56, 846 (1952).
13. K. Vetter, Z. Elektrochem. 56, 931 (1952); P. Delahay, J. Am. Chem. Soc. 74, 3497 (1952).

\* Original Russian pagination. See C. B. translation.

## DESTRUCTION OF MOLECULAR CHAINS AND DISRUPTION OF CROSS LINKS DURING AGING OF VULCANIZATES

L. I. Lyubchanskaya and A. S. Kuz'minskii

Scientific Research Institute of the Rubber Industry

(Presented by Academician P. A. Rebinder, July 6, 1960)

Translated from *Doklady Akademii Nauk SSSR*, Vol. 135, No. 6, pp. 1436-1438,  
December, 1960

Original article submitted June 30, 1960

In sulfur vulcanizates, the energy of the bond between sulfur atoms in cross links may differ substantially from the energy of bonds in the molecular chains of the polymers and therefore, as is known [1], the thermal disruption of polysulfide bonds may be produced at much lower temperatures than the disruption of molecular chains in vulcanizates. One of us [2] established that the thermal disruption of sulfur bonds in vulcanizates produces inhibition of oxidation developing in polymer chains. Consequently, it cannot be considered that the destruction of chains and the disruption of cross links are independent processes. However, the difference in the rates of destruction and disruption is so great that these processes may be distinguished.

In the literature there are various points of view on the elements in the structure of the vulcanizates that propagate the aging processes. Tobolsky [3] stated that chemical relaxation of stress is produced by oxidative destruction of the vulcanizate polymer chain regardless of its structure. In contradiction to this, Watson et al. [4] considered that the disruption of the lattice of vulcanizates is the result of the rupture of chemical cross links.

In the present investigation it was established that both the polymer chains and the cross links forming the three-dimensional lattice of the vulcanizates may be involved in the aging process, depending on the composition of the vulcanizate and the experimental conditions.

It is known that slight chemical conversions of polymers produce substantial changes in the mechanical properties and therefore mechanical methods are sufficiently sensitive in the early stages of aging when chemical methods are not yet able to detect the reaction that has begun.

We investigated the chemical relaxation of stress of vulcanizates that differed both in the nature of the cross links and the reactivity of the polymer chain with respect to oxygen.\*

The chemical relaxation of stress was investigated on a specially designed apparatus, namely, a relaxation meter with axial compression [5]. The degree of deformation of the samples during the whole of the experiment was kept constant and equalled 30 % compression. Before the beginning of an experiment, the samples were kept in the deformed state for two days at room temperature to eliminate physical relaxation.

\* As subjects for investigation we chose vulcanizates based on natural and sodium-butadiene rubbers, prepared from the following recipes: I) rubber - 100.0, stearic acid - 2.0, zinc oxide - 5.0, phenyl- $\beta$ -naphthylamine - 2.0, tetramethylthiuram disulfide - 3.0; II) rubber-100.0, stearic acid - 2.0, zinc oxide-5.0, phenyl- $\beta$ -naphthylamine - 2.0, diphenylguanidine - 1.0, and sulfur 6.0 parts by weight.

Figure 1 presents data on the kinetics of relaxation of stress of vulcanizates based on natural and sodium-butadiene rubbers with a predominant content of monosulfide bonds. With the exception of a small initial section, the kinetic curves of these vulcanizates are described by the equation for a monomolecular reaction ( $\sigma_t = \sigma_0 e^{-kt}$ ), which indicates the disruption of one type of bond. The rate constants of the process, calculated from the equation given above, were  $1.54 \cdot 10^{-3} \text{ hr}^{-1}$  for vulcanizates from natural rubber and  $2.1 \cdot 10^{-4} \text{ hr}^{-1}$  for vulcanizates from sodium-butadiene rubber. Thus, the chemical relaxation process in vulcanizates from natural rubber proceeds eight times faster than in the corresponding vulcanizate from sodium-butadiene rubber. These rubbers are known [2] to differ by a factor of seven in oxidation rate at the same temperature. The rate of chemical relaxation of these vulcanizates decreased sharply when the experiments were carried out in vacuum (Fig. 2). A fall in oxygen concentration from atmospheric to  $10^{-2} \text{ mm Hg}$  led to a decrease in the process rate by a factor of five. The facts presented indicate that in this case the chemical relaxation is determined by oxidative disruption of polymer chains in the vulcanizates.

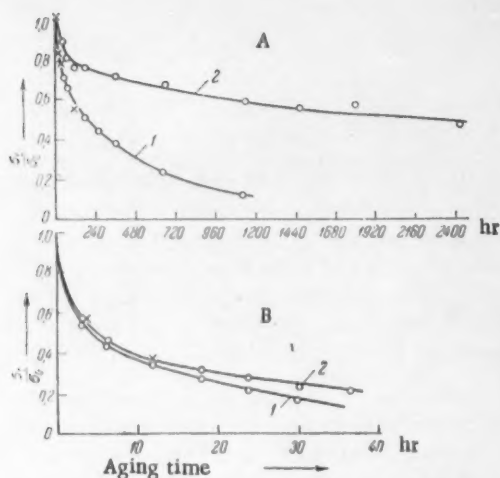


Fig. 1. Effect of nature of polymer on the kinetics of chemical relaxation of vulcanizates containing predominantly monosulfide (A) and polysulfide (B) bonds. Aging temperature  $100^\circ$ , degree of compression 30%. 1) Vulcanizate based on natural rubber; 2) vulcanizate based on sodium-butadiene rubber.

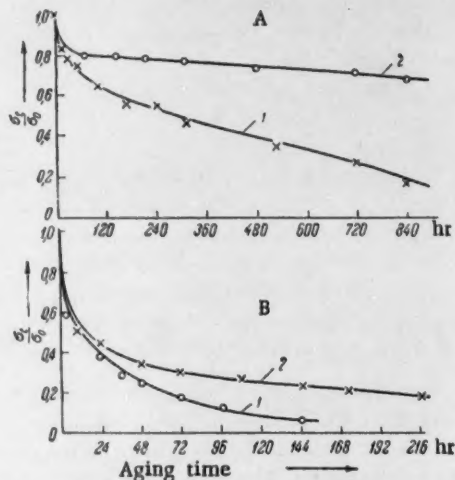


Fig. 2. Effect of oxygen concentration on the kinetics of chemical relaxation of vulcanizates based on natural rubber containing predominantly monosulfide (A) and polysulfide (B) bonds. Compression temperature (B)  $90^\circ$ . Aging temperature  $100^\circ$ , degree of compression 30%. 1) Air; 2) vacuum ( $10^{-2} \text{ mm Hg}$ ).

A completely different picture was observed on investigating the chemical relaxation of stress of vulcanizates with a predominant content of polysulfide bonds.

There was an exponential relation in this case only when the stress in the vulcanizate had fallen to approximately 50% of the original value.

In the initial stage of the process (up to 50% fall in stress), the rates of stress relaxation were the same for the two types of rubber and in the final stage they were  $4.2 \cdot 10^{-2} \text{ hr}^{-1}$  for vulcanizates from natural rubber and  $3.1 \cdot 10^{-2} \text{ hr}^{-1}$  for vulcanizates from sodium-butadiene rubber, i.e., the difference in rates did not exceed 20%. For vulcanizates of this type, carrying out the experiments in the absence of oxygen did not lead to an appreciable decrease in the rate of stress relaxation of the vulcanizates in comparison with corresponding experiments in air.

It should be noted that the disruption of polysulfide bonds depends little on the oxygen concentration and proceeds much more rapidly than the oxidative disruption of molecular chains of the polymer. The rate of chemical relaxation in air of a vulcanizate based on natural rubber with polysulfide bonds was 20 times greater

than the corresponding rate for vulcanizates with monosulfide bonds. In these vulcanizates, oxidative destruction of the polymer chain was unable to develop and lead to an appreciable fall in stress in comparison with thermal disruption of polysulfide bonds and therefore the reactivity of the polymers and the oxygen concentration did not have an appreciable effect on the rate of chemical relaxation.

By analyzing the data presented, it is possible to draw the following basic conclusions. In the aging of vulcanizates, there are two competing tendencies: oxidative destruction of molecular chains of the polymer and thermal disruption of sulfur cross links.

When the vulcanizates contain strong cross links (monosulfides), the chemical relaxation of stress is determined by oxidative destruction of the molecular chains of the polymer and therefore the relaxation rate naturally depends on the reactivity of the polymers and the oxygen concentration.

In cases where the lattice of the vulcanizates is formed by polysulfide bonds, the rate of thermal disruption of the latter is an order higher than the rate of oxidative destruction of polymeric chains and determines the rate of chemical stress relaxation.

A comparison of data on the change in equilibrium modulus (whose value is proportional to the density of cross links) and stress relaxation during aging of the vulcanizates examined showed that with a fall in stress to zero, the equilibrium modulus changed by only 15-20%. This indicates that during aging of vulcanizates in a stressed state, there is not only disruption of bonds, but also subsequent rearrangement of them. Naturally, the rupture of bonds occurs in stressed positions and the formation of new bonds in unstressed parts of the lattice. As a result of this rearrangement, there is a gradual decrease in the number of stressed bonds right up to their complete disappearance, when the total number of bonds remains close to the original value.

#### LITERATURE CITED

1. B. A. Dogadkin and Z. N. Tarasova, *Kolloid. Zhur.* **15**, 5, 347 (1953).
2. A. S. Kuz'minskii, N. N. Lezhnev, and Yu. S. Zuev, *Oxidation of Rubbers and Vulcanizates* [in Russian] (Moscow, 1957).
3. A. Tobolsky, *J. Appl. Phys.* **27**, 7, 673 (1956); *J. Polym. Sci.* **25**, 111, 497 (1957).
4. J. Berry and W. F. Watson, *J. Polym. Sci.* **18**, 88, 201 (1955); W. F. Watson, *J. Polym. Sci.* **25**, 111, 493 (1957).
5. L. I. Lyubchanskaya, A. A. Shlyakhtman, and A. S. Kuz'minskii, *Kauchuk i Rezina* **2**, 31 (1957).

1

2

3

4

5

6

7

8

9

10

11

12

13

14

15

16

# THE ROLE OF DISPERSION IN THE COMBUSTION OF EXPLOSIVES

A. G. Merzhanov

Institute of Chemical Physics, Academy of Sciences of the USSR

(Presented by Academician N. N. Semenov, June 30, 1960)

Translated from *Doklady Akademii Nauk SSSR*, Vol. 135, No. 6, pp. 1439-1441,  
December, 1960

Original article submitted June 20, 1960

A. F. Belyaev [1] in studying the combustion of mercury fulminate under vacuum discovered an interesting new phenomenon — dispersion of condensed phase material during combustion. P. F. Pokhil [2] established as a result of systematic fundamental research that dispersion is an important factor in the mechanism of the combustion of explosives. Dispersion occurs as a result of reaction in the bulk of the condensed phase. Expansion of gaseous products formed in the decomposition zone inevitably causes spattering of unreacted material. According to Pokhil, in the combustion of pyroxylin powder about 30% of the powder decomposes in the condensed phase while the remaining 70% is dispersed and entrained by the gas stream. However, many questions connected with dispersion, specifically those concerning the role of, and the laws describing, dispersion and the "fate" of the dispersed particles, etc., have remained unexplained since these studies were carried out. The latter question has received some elucidation in [3, 4].

In the work presently discussed, a relationship between combustion rate, surface temperature and depth of dispersion factor is derived and a deduction regarding the role of dispersion is made on the basis of the analysis of this relationship.

We will consider dispersion, to a first approximation, as a surface process taking place without a heat effect. The initial set of equations for steady-state conditions, set up using the normal approximations for combustion theory, will be as follows:

$$\lambda \frac{d^2 T}{dx^2} + c\rho u \frac{dT}{dx} + Q\rho k_0 e^{-E/RT} = 0,$$

$$u = u_d + u_{dis}$$

$$u_d = \int_0^\infty k_0 \exp[-E/RT(x, u)] dx.$$

The boundary conditions are:

$$x = 0, \quad T = T_s; \quad x = \infty, \quad T = T_0.$$

Notation:  $T$ ) temperature ( $^{\circ}\text{K}$ );  $T_s$ ) temperature at surface of burning powder ( $^{\circ}\text{K}$ );  $T_0$ ) temperature of powder beyond zone of combustion ( $^{\circ}\text{K}$ );  $x$ ) linear coordinate (cm);  $u$ ) combustion rate (cm/sec);  $u_{dis}$ ) linear rate of dispersion (cm/sec);  $u_d$ ) linear rate of decomposition (cm/sec);  $\lambda$ ) thermal conductivity of powder (cal/cm·sec·deg);  $c$ ) specific heat (cal/gm·deg);  $\rho$ ) density (gm/cm<sup>3</sup>);  $a$ ) thermal diffusivity (cm<sup>2</sup>/sec);  $Q$ ) heat of decomposition of powder (cal/gm);  $k_0$ ) constant factor in exponential term (sec<sup>-1</sup>);  $E$ ) energy of activation (cal/mole).

When dispersion occurs the linear combustion rate is the sum of the linear rate of decomposition and the linear rate of dispersion. By introducing the depth of dispersion factor  $\eta_{dis} = u_{dis}/u$  into the analysis and using results presented in [4], we obtain

$$u^2 = \frac{1}{1 - \eta_{dis}} a k_0 \exp \left[ -E/RT_s \right] \frac{RT_s^2/E}{T_s - T_0 - \frac{Q(1 - \eta_{dis})}{2c}} \quad (1)$$

This formula expresses the relationship between combustion rate, surface temperature and the depth of dispersion factor. As may be seen from (1), the effect of dispersion is equivalent, in one respect, to a reduction of the heat of reaction in the condensed phase ( $Q_{eff} = Q(1 - \eta_{dis})$ ) and, in another respect, to an increase in the velocity constant ( $k_{eff} = \frac{k}{1 - \eta_{dis}}$ ) or in thermal diffusivity.

For combustion without flame, where the process takes place solely due to the heat released in the condensed phase, we have

$$T_s = T_0 + \frac{Q(1 - \eta_{dis})}{c} \quad (2)$$

$$u^2 = \frac{2}{(1 - \eta_{dis})} a k_0 \exp \left\{ -E/R \left[ T_0 + \frac{Q(1 - \eta_{dis})}{c} \right] \right\} \frac{c}{Q} \frac{R}{E} \left[ T_0 + \frac{Q(1 - \eta_{dis})}{c} \right]^2 \quad (3)$$

Since the depth of dispersion factor appears in the exponential term, the rate of flameless combustion is very much dependent on  $\eta_{dis}$ ;  $u$  falls sharply with increase in  $\eta_{dis}$ . \* Thus in a flameless regime the occurrence of dispersion retards the combustion process.

What would be the combustion rates obtaining in the absence of dispersion? Let us consider this question using pyroxylin powder as an example. We will carry out the calculation of combustion rate using formula (3) when  $\eta_{dis} = 0$ . Data available for the calculation are:  $T_0 = 20^\circ \text{C}$ ;  $a = 1 \cdot 10^{-8} \text{ cm}^2/\text{sec}$ ;  $c = 0.35 \text{ cal/gm} \cdot \text{deg}$ ;  $Q = 270 \text{ cal/gm}$  [1];  $k_0 = 10^{17.8} \text{ sec}^{-1}$  and  $E = 44,600 \text{ cal/mole}$  [5]. Calculation yields a very large value for the combustion rate — about 250 cm/sec. This indicates that the heat of decomposition of nitrocellulose, when the velocity constant is relatively large, is quite sufficient to ensure very high combustion rates. The fact that such rates are not observed experimentally is entirely due to the occurrence of dispersion. The heat flow into the condensed phase cannot, in practice, compensate for the loss of potential heat which the undecomposed powder particles take out with them. If decomposition of the powder occurred endothermically, a different result should be expected.

The quantity  $\eta_{dis}$  appears in the expressions from (1) through (3) as a parameter. In fact, the depth of dispersion factor is a complicated function of temperature, pressure and other factors. However, the problem of the laws underlying dispersion remains at present unstudied. No data whatsoever are available on  $\eta_{dis}$  as a function of  $T_s$  and  $p$ , etc. Since dispersion has a marked effect on the process of combustion, the laws determining dispersion may determine (especially at low pressures) the relationships to which the combustion process conforms, i.e., the dependence of combustion rate on pressure and temperature. The problem of the laws of dispersion will become, it would seem, one of the basic problems in the near future in the theory of the combustion of explosive powders.

It is possible to gain some idea of the relationship between  $\eta_{dis}$  and  $T_s$  by employing formula (3) which enables one to calculate depth of dispersion factors from measured rates of flameless combustion at known values of the kinetic constants. With this aim in view, a calculation has been made for pyroxylin powder

\* It should be noted that in the region of fictitiously high values of  $\eta_{dis}$  (about 1) the function  $u = f(\eta_{dis})$  has a minimum value.

from experimental data obtained by P. F. Pokhil [1]. The results of the calculation which are presented in Table 1 show, in the first place, quite a good agreement with experiment (Pokhil experimentally determined by an independent method that  $\eta_{\text{dis}} \approx 0.7$  and  $T_s = 280-300^\circ\text{C}$ ), and secondly that the depth of dispersion factor rises with increase in temperature. It is easy to understand an  $\eta_{\text{dis}} - T_s$  relationship of this kind starting from a picture of dispersion as the spattering out of material in the fluid/viscous reaction layer.

TABLE 1

Experimental data of Pokhil		Calculated values	
$T_0, ^\circ\text{C}$	$u, \text{cm/sec}$	$\eta_{\text{dis}}$	$T_s, ^\circ\text{C}$
90	0.08	0.716	298
120	0.11	0.746	316
140	0.14	0.767	319

The low temperature coefficient of combustion rate in flameless combustion may be explained by the nature of the variation of the depth of dispersion factor with temperature. From (2) and (3)

$$\frac{1}{u} \frac{du}{dT_0} \approx \frac{E_{\text{eff}}}{2RT_s^2},$$

where

$$E_{\text{eff}} = \frac{E}{1 + \frac{Q}{c} \frac{d\eta_{\text{dis}}}{dT_s}}.$$

Since  $d\eta_{\text{dis}}/dT_s > 1$ , then  $E_{\text{eff}} < E$ .

The existence of a positive correlation between  $\eta_{\text{dis}}$  and  $T_s$  prevents a sharp change in surface temperature and, consequently, in combustion rate. In practice, if for any reason  $T_s$  began (for example) to rise, this would automatically lead to an increase in  $\eta_{\text{dis}}$  which would retard the rise in  $T_s$ . Thus, because of the positive correlation between  $\eta_{\text{dis}}$  and  $T_s$  dispersion plays a controlling part in the mechanism of combustion.

The correlation between  $\eta_{\text{dis}}$  and  $p$ , in accordance with the physical significance of  $\eta_{\text{dis}}$ , should be negative. The higher the pressure, the greater the depth in the condensed phase to which decomposition must proceed in order to form dispersed particles and the smaller the depth of dispersion. It should be borne in mind that in combustion conditions  $T_s$  always increases with increase in  $p$  and this prevents sharp variation of  $\eta_{\text{dis}}$ .

#### LITERATURE CITED

1. A. F. Belyaev, Doklady Akad. Nauk SSSR **33**, 41 (1941).
2. P. F. Pokhil, Collection: The Physics of Explosion [in Russian] (1953) Vol. 2, p. 181; Doctoral Thesis, Institute of Chemical Physics [in Russian] (Izd. AN SSSR, 1954).
3. L. N. Gal'perin, V. M. Mal'tsev, and P. F. Pokhil, Doklady Akad. Nauk SSSR **127**, 131 (1959).\*
4. G. B. Manelis, A. G. Merzhanov, and F. I. Dubovitskii, Doklady Akad. Nauk SSSR **133**, 2 (1960).\*\*
5. A. G. Merzhanov and F. I. Dubovitskii, Doklady Akad. Nauk SSSR **129**, 153 (1959).\*
6. K. K. Andreev, The Thermal Decomposition and Combustion of Explosives [in Russian] (1957).

\* Original Russian pagination. See C. B. translation.

\*\* See C. B. translation.



# THE VIBRATIONAL DISTRIBUTION FUNCTION FOR MONATOMIC MOLECULES IN MONOMOLECULAR DECOMPOSITION

E. E. Nikitin

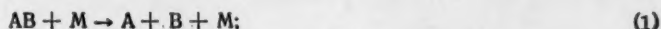
Institute of Chemical Physics, Academy of Sciences of the USSR

(Presented by Academician V. N. Kondrat'ev, June 27, 1960)

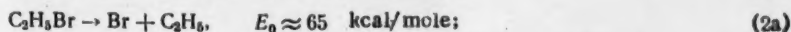
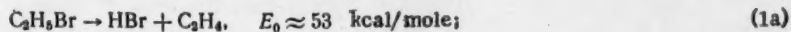
Translated from Doklady Akad. Nauk SSSR, Vol. 135, No. 6, pp. 1442-1445, December, 1960

Original article submitted June 22, 1960

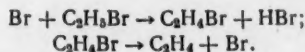
It is known that the thermal decomposition of monatomic molecules follows a monomolecular law at high pressures and a bimolecular law at low pressures, transition from the one to the other being associated with a breakdown of the Boltzmann distribution of decomposing molecules over vibrational energy levels in the neighborhood of the dissociation threshold (see, for example, [1]). Stochastic models have been used in numerous studies of the breakdown of the equilibrium distribution in bimolecular decomposition [2-6]. In monomolecular decomposition, the departure from equilibrium distribution near the dissociation limit is slight and has little effect on the reaction rate. Here, however, secondary reactions can be affected significantly by departures from equilibrium at energies in excess of the dissociation energy  $E_0$ . This is particularly true when the decomposition of molecule AB can follow two different paths such as:



where (2) proceeds with a high dissociation energy and produces active particles which fix the rate of some process, e.g., chain branching, by their secondary reactions. In this case, reaction (1) will result in a decrease in the population of those vibrational energy levels for which  $E > E_0$ , thereby diminishing the rate of reaction (2). An instance of this effect has been noted by E. A. Shilov [7] in his study of the thermal decomposition of ethyl bromide. There the initial reactions are monomolecular decompositions



with the second leading to the chain breakdown represented by:



The general theory of chain reactions indicates that (2a) should result in an increase in the decomposition rate, but such does not prove to be the case. Supplementary introduction of bromine atoms does increase the decomposition rate, however, and thus gives support to the mechanism presented above. Here, study will be made of the breakdown of the equilibrium distribution in the region  $E > E_0$  during monomolecular decomposition of monatomic molecules.

The nonequilibrium distribution function can be developed by solving the kinetic equation describing vibrational relaxation and decomposition and determining the rate of breakdown from the lower characteristic value,  $\mu_0$ , of the stochastic matrix [2-6]. The case of the monatomic molecule is essentially one in which vibrational excitation involves many quanta and the kinetic equation can therefore be written in integral form:

$$\frac{\partial x(\epsilon)}{\partial t} = \int K(\epsilon, \epsilon') d\epsilon' - Z^* x(\epsilon) - k(\epsilon) x(\epsilon), \quad (3)$$

where  $x(\epsilon)$  designates the distribution function expressed in the dimensionless energy units  $\epsilon = E/kT$ ,  $Z^*$  is the number of AB, M collisions which are effective in vibrational relaxation;  $k(\epsilon)$  is the differential decomposition rate; and the kernel function  $K(\epsilon, \epsilon')$  gives a description of the vibrational relaxation with

$\int K(\epsilon, \epsilon') d\epsilon' = Z^*$  [5]. The familiar methods can now be applied [8] to bring (3) into a differential form:

$$\frac{\partial x}{\partial t} = D \frac{\partial}{\partial \epsilon} \left[ \frac{\partial x}{\partial \epsilon} + f'(\epsilon) x \right] - k(\epsilon) x, \quad (4)$$

which will be satisfied by the equilibrium distribution function  $x_0(\epsilon) = \exp[-f(\epsilon)]$  when  $k=0$ . The  $D$  term of this equation represents the mean-square energy transfer to the decomposing molecules per unit time and, therefore,  $D = Z \bar{\epsilon}^2$ , where  $Z$  is the number of AB, M collisions obtained from gas kinetics.  $D$  will be considered as constant in what follows, but all that is really required is that it depend less strongly on  $\epsilon$  than does  $k$ . The lower characteristic value,  $\mu_0$ , of the operator of the right-hand member of Eq. (4) can be obtained by a variational method:

$$\mu_0 = \min \left\{ \frac{\int \exp(-f) [D(\partial \psi / \partial \epsilon)^2 + k \psi^2(\epsilon)] d\epsilon}{\int \exp(-f) \psi^2(\epsilon) d\epsilon} \right\}, \quad (5)$$

$\psi$  being the variational function whose integral normalizing factor appears in the denominator.

A Kassel system of  $s+1$  harmonic oscillators with  $f(\epsilon) = \epsilon - s \ln \epsilon$  [1] can serve as a model of the decomposing molecule; here,  $k(\epsilon) = \nu(1 - \epsilon_0/\epsilon)^s$ , with  $\epsilon_0 = E_0/kT$  and  $\nu \approx 10^{13} \text{ sec}^{-1}$ , a quantity of the order of the frequency of molecular vibration. In the sequence  $Z$  will be expressed in units of  $\nu$  so that it will be presumed that  $\nu = 1$ . Simple variational functions, one identically constant and the other a step function, can be applied and (5) readily carried into

$$\mu_0 = \min \left\{ \begin{aligned} & D \frac{\epsilon_0^s}{s!} \exp(-\epsilon_0), \\ & \exp(-\epsilon_0) \end{aligned} \right. \quad \begin{aligned} & (6a) \\ & (6b) \end{aligned}$$

where (6a) is the expression for the rate of bimolecular decomposition, (6b) is the rate for monomolecular breakdown, and the transition interval between these processes is fixed by the condition  $D \epsilon_0^s / s! \approx 1$ . The nonequilibrium distribution function satisfies the condition:

$$-\mu_0 x = D(x' + f'x)' - kx. \quad (7)$$

This equation can be solved without difficulty when  $\epsilon_0 \gg s$ , which is exactly the case of greatest interest to the experimenter since it corresponds to high energy of activation in molecules which are not overly complex. This condition is identical to that required for validity of the Kassel equation for decomposition rate.

The high pressure case for which  $D \sim 1$  will be considered first. Introducing  $x = y \exp(-f/2)$  into (7) gives:

$$y'' - U(\epsilon) y = 0, \quad U(\epsilon) = \left[ \frac{(f')^2}{4} + \frac{k - \mu_0}{D} \right], \quad (8)$$

$f''$  being neglected in comparison with  $(f')^2$  in  $U(\epsilon)$  on the basis of the inequality  $\epsilon_0/s \gg 1$ . An approximation solution of (8) which allows for a small correction of  $f''$  has the form:

$$y = \frac{\text{const}}{U^{1/4}} \exp\left(-\int \sqrt{U} d\epsilon\right) \quad (9)$$

when the inequality  $U'/U^{3/2} = \chi \ll 1$  is valid. It can be readily shown that the condition  $D \sim 1$  will satisfy this inequality. It can also be easily proven that it is not necessary to take account of  $\mu_0$  in integrating (9).

Thus, the distribution function is expressed by

$$x(\epsilon) = \begin{cases} \exp[-f], & \epsilon \leq \epsilon_0; \\ \sqrt{\frac{(f'_0)^2}{(f')^2 + 4k/D}} \exp\left[-\frac{f}{2} - \int_0^\epsilon \sqrt{\frac{(f')^2}{4} + \frac{k}{D}} d\epsilon\right], & \epsilon \geq \epsilon_0, \end{cases} \quad (10)$$

which takes the form

$$x(\epsilon) = \exp(-f) \exp\left[-\frac{1}{D} \int_{\epsilon_0}^\epsilon \frac{k}{f'} d\epsilon\right], \quad \epsilon \geq \epsilon_0 \quad (11)$$

when  $D$  is sufficiently large. The notation  $f(\epsilon_0) = f_0$ ,  $f'(\epsilon_0) = f'_0$  has been used here and will be employed in what follows.

Equations (10) and (11) show that monomolecular decomposition at pressures far removed from the transition region will result in a lower population of the vibrational levels at  $E > E_0$  than would correspond to equilibrium. This relative diminution,  $\rho$ , in the equilibrium population is determined by the second of the two multiplying factors in (11). When  $E - E_0 = \Delta E \ll E_0$  this factor can be rewritten in ordinary variables as:

$$\rho = \exp\left[-\frac{\nu}{Z} \left(\frac{\Delta E}{E_0}\right)^s \frac{\Delta E \cdot kT}{(s+1) \epsilon_0^2}\right]. \quad (12)$$

Approximation (9) is no longer valid at low pressures since the condition  $\chi \ll 1$  is not fulfilled near the threshold energy. Thus, it is necessary to join the exact solution of Eq. (4) for the region of low  $\Delta \epsilon = \epsilon - \epsilon_0$

$$y'' - \left[ \frac{(f'_0)^2}{4} + \frac{1}{D} \left(\frac{\Delta \epsilon}{\epsilon_0}\right)^s \right] y = 0 \quad (13)$$

with the asymptotic solution (9). Solution of Eq. (13) can be had through the Laplace transform but the general case becomes rather involved. Equation (13) can be replaced by a more simple equation when account is taken of the fact that the pressure is low and  $D \ll 1$ . Bessel functions can be used to obtain solution of this latter equation that satisfies the necessary boundary condition at infinity:

$$y'' - \frac{1}{D} \left(\frac{\Delta \epsilon}{\epsilon_0}\right)^s y = 0, \quad y(\Delta \epsilon) = C \sqrt{\Delta \epsilon} K_{\frac{1}{s+2}} \left( \frac{2\Delta \epsilon^{(s+2)/2}}{(s+2) \sqrt{D \epsilon_0^{s/2}}} \right) \quad (14)$$

In the region  $(f_0)^2/4 \ll (\Delta\epsilon/\epsilon_0)^2/D$  Eq. (13) is satisfied to a certain degree of approximation by the solution (14). The region over which there is an essential difference between the exact and the approximate solutions is determined by the condition:

$$\delta\epsilon \sim \epsilon_0 (D/4)^{1/2}, \quad (15)$$

so that integration of (13) over the interval  $0 < \Delta\epsilon < \delta\epsilon$  with the initial condition  $y(0) = \exp(-f_0/2)$  leads to a multiple of the order of  $\exp\left[-\frac{\epsilon_0}{2} (D/4)^{1/2}\right]$ . The solution (14) can then be extrapolated to  $\Delta\epsilon = 0$  and joined onto the equilibrium distribution function with allowance for the transition interval  $\delta\epsilon$  to obtain the expression:

$$x(\epsilon) = \exp[-f/2] \cdot \sqrt{\frac{2}{\pi}} \sin \frac{\pi}{s+2} [(s+2) \sqrt{D} \epsilon_0^{s/2}]^{1/(s+2)} \times \\ \times \exp\left[-\frac{\epsilon_0}{2} (D/4)^{1/2}\right] K_{\frac{1}{s+2}}\left(\frac{2\Delta\epsilon^{(s+2)/2}}{(s+2) \sqrt{D} \epsilon_0^{s/2}}\right). \quad (16)$$

The relative diminution of the population in the transition interval  $D\epsilon_0^s/s! \approx 1$  can be calculated from this equation, using an asymptotic decomposition of the Bessel function, the result being:

$$\rho \approx \frac{\sqrt{2\pi} e}{s^2} \exp\left[-\frac{s}{e}\right] \exp\left\{-\frac{2}{(s+2) \sqrt{s!}} \left(\frac{\Delta E}{kT}\right)^{s/2+1} + \frac{\Delta E}{2kT}\right\}. \quad (17)$$

Equation (17) agrees to within a constant multiplying factor with (10) in which integration is to be carried out on the assumption that  $(f')^2/4 \ll k/D$  at low values of  $\epsilon$ . This is equivalent to the condition that the solutions in the two intervals join smoothly. The appearance in (17) of an additional multiplying factor whose value is less than unity is quite natural since passage from high pressures at which  $D \sim 1$  to low pressures where  $(D\epsilon_0^s/s! \approx 1)$  increases the degree of departure from the equilibrium distribution. It is to be noted, however, that there are many cases in which the multiplying factor  $\frac{\sqrt{2\pi} e}{s^2} \exp[-s/e]$  is not essential for estimations since the asymptotic solution (10) can be employed even though the inequality  $\chi \ll 1$  is no longer valid.

Quantitative estimations based on (10) and allowing for  $\mu_0 = D\epsilon_0^s/s! \exp(-\epsilon_0)$  show that the distribution function begins to diminish markedly in the immediate neighborhood of the threshold  $\epsilon_0$  at pressures below the transition interval. This fact determines the bimolecular decomposition kinetics.

Thus, the rate constant for reaction (2) can be evaluated from Eq. (6a) or Eq. (6b) by introducing the multiplying factor  $\rho$  to allow for the breakdown in the equilibrium distribution. The rate of reaction (2) proves to be exponentially dependent on the number of collisions, a conclusion which cannot be derived from the formal kinetics of the two-step process represented by (1) and (2). The parameter of the above calculation which cannot be fixed with precision is the mean-square energy transfer,  $\bar{\delta}^2$ . It is clear from what has been said that the value of  $\bar{\delta}^2$  must be related to those vibrationally excited AB molecules whose energies lie close to the threshold value  $E_0$ . Since AB, M collisions principally involve a transfer of many quanta (this is a fundamental difference between the dissociation of monatomic and diatomic molecules) it can be supposed that  $\bar{\delta}^2 \approx (kT)^2$ .

It should be noted that a nonequilibrium distribution function of the type considered here could be basic for calculations on stabilized fluorescence spectra [9]. The vibrational distribution function in a state of electronic excitation should be described by a nonhomogeneous equation similar to (8). In this case, the function  $k(\epsilon)$  would represent the probability factor for radiationless transition. The fact that the intensity of fluorescence is quite dependent on the stabilizing additive is indication of a strong dependence of  $k$  on  $\epsilon$  near a certain threshold, just as in the case of the relation between the energy and cross section in decomposition. The nonequilibrium distribution function should, in principle, affect the form of the high frequency end of the stabilized fluorescence band.

I would like to express my thanks to Professor N. D. Sokolov and to A. E. Shilov for discussion of this work.

#### LITERATURE CITED

1. V. N. Kondrat'ev, The Kinetics of Chemical Gas Reactions [in Russian] (Izd. AN SSSR, 1958).
2. E. E. Nikitin, Doklady Akad. Nauk SSSR 119, 526 (1958).\*
3. E. E. Nikitin and N. D. Sokolov, J. Chem. Phys. 31, 1371 (1959).
4. E. W. Montroll and K. E. Shuler, Adv. in Chem. Phys. 1, 361 (1958).
5. B. Widom, J. Chem. Phys. 31, 1387 (1959).
6. F. P. Buff and D. J. Wilson, J. Chem. Phys. 32, 677 (1960).
7. A. E. Shilov, Dissertation, Institute of Chemical Physics, Acad. Sci. USSR, 1955.
8. S. Chandrasekar, Stochastic Problems in Physics and Astronomy [Russian translation] (IL, 1947).
9. B. S. Neporent, Zhur. Fiz. Khim. 24, 1219 (1950).

\* Original Russian pagination. See C. B. translation.



# THE RELATION BETWEEN THE YIELD OF RADIOCHEMICAL REACTIONS AND THE CONCENTRATION OF DISSOLVED SUBSTANCES

M. A. Proskurnin

L. Ya. Karpov Physicochemical Institute

(Presented by Academician V. A. Kargin, July 7, 1960)

Translated from Doklady Akademii Nauk SSSR, Vol. 135, No. 6, pp. 1446-1449, December, 1960

Original article submitted April 29, 1960

The mechanisms of radiochemical reactions are frequently developed on the basis of experiments involving irradiation of a solution of fixed concentration. This concentration is usually chosen fortuitously and other workers then irradiate similar solutions in order to obtain comparable data. Sometimes study is made over a certain narrow interval of concentrations and the experiments are then broken off without any careful investigation of the relation between concentration and reaction yield. It is readily shown, however, that extensive alteration in the concentration of dissolved substances can result in a marked variation in the radiochemical yield. The effects which are observed do not then fit into the mechanism which was apparently adequate for interpreting the processes occurring at moderate concentration. Reactions of this type include the radiolytic oxidation of ferrous ions, and the reduction of nitrate and ferric ions, in aqueous solution.

It is clear that each free radical which is produced in the radiolysis of the medium (for example, water in aqueous solutions) can either react with other radicals of the same type or with molecules of the dissolved material (acceptor), the probability of each such reaction being proportional to the concentrations and to the reaction cross section. The concentration of radicals along a track falls off rapidly from its initial value and can be evaluated exactly only with the aid of calculating machines. It is possible, however, to use the elementary concepts of track theory and very rough methods of graphical integration to evaluate that concentration of free radicals in the track at which a definite fraction of all of the radicals formed is consumed. On the basis of the Gray [1] model the author has concluded that the first fourth of all radicals ( $\beta$ -particles, accelerated and secondary electrons) will react at a mean concentration  $C_1 = 1.5 \cdot 10^{-5}$  M, the second fourth at  $C_2 = 3 \cdot 10^{-6}$  M, the third at  $C_3 = 5 \cdot 10^{-7}$  M, and the last fourth at  $C_4 = 6 \cdot 10^{-8}$  M. Using  $C_H$  to designate the yield of some type of radical (the hydrogen atom H, for example) expressed as number of radicals per 100 ev of energy absorbed,  $C_{AK}$ ,  $C_{OH}$ ,  $C_H$  to represent the respective mean concentrations of acceptor, OH radicals and H radicals and  $\sigma_{AK+H}$ ,  $\sigma_{H+OH}$ , and  $\sigma_{H+H}$  to indicate the cross sections for reactions involving the given radical, it is possible to obtain the following equation for the yield of the reaction between the H atoms and the dissolved substance:

$$G = G^H \Sigma \frac{C_{AK} \sigma_{H+AK}}{C_{AK} \sigma_{AK+H} + C_{OH} \sigma_{OH+H} + C_H \sigma_{H+H}} \eta.$$

Here  $G$  represents the yield of the reaction between acceptor and H atoms,  $\eta$  is the fraction of all radicals reacting at a given mean concentration, 0.25 in our case, and the summation includes four terms corresponding respectively to the concentrations  $1.5 \cdot 10^{-5}$ ,  $3 \cdot 10^{-6}$ ,  $5 \cdot 10^{-7}$ , and  $6 \cdot 10^{-8}$  M.

The radiochemical yield of H atoms,  $G_H$ , in dilute solutions (lower than  $10^{-2}$  M in concentration) is determined by the value of  $G_{H_2O^+}$ , i.e., by the number of ionized water molecules. The initial portions (left-hand) of the curves of Fig. 1 have been constructed for  $G_H$  equal to  $G_{H_2O^+} = 4$  eq/100 ev. Curve 1 corresponds to the case in which the same cross section is assumed for all reactions and this common value is a maximum, so that there is 100% probability of chemical interaction for each approach of radicals and molecules. This corresponds to the case of the "ideal" acceptor. Curve 2 has been developed on the assumption that the cross section for reaction between radicals (H atoms) and acceptor molecules is only one-hundredth as large as the cross section for the H + AK reaction (poor acceptor). Curves 1 and 2 are of exactly the same form but the one is displaced into the region of higher concentrations of the dissolved substance. Curve 3 was developed on the assumption that there is not only a principal, but a secondary acceptor (the competing AK<sup>•</sup>) as well, and that the concentration of the latter is  $10^{-2}$  M.

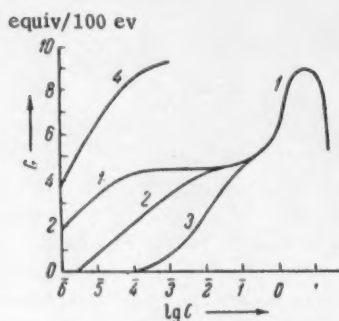


Fig. 1. The relation between the yield of radiochemical reaction and the concentration of acceptor in solution (theoretical calculations): 1) most active acceptor; 2, 3) less active acceptors; 4) in the presence of a supplementary acceptor.

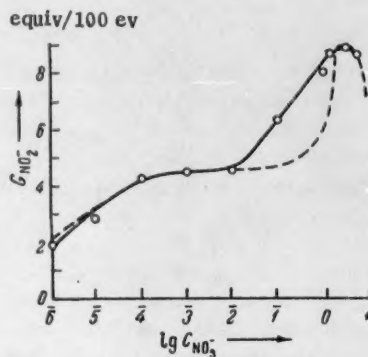


Fig. 2. The relation between the yield from nitrate reduction and the concentration in solutions at pH 14 [3] (the dotted curve was developed theoretically).

The calculations involved in the last of these cases call for the introduction of an additional term,  $G_{AK^{\bullet}} \cdot \sigma_{AK^{\bullet}+H}$ , into the denominator of the expression given above. The curve is S-shaped in semi-logarithmic coordinates and its course is almost independent of the free radical concentration. Curve 4 corresponds to the assumption which is met rather frequently in the foreign literature [2] to the effect that the H and the OH radicals act similarly and that both will oxidize ferrous ions, for instance.

The rise in the right-hand portions of the yield curves of Fig. 1 conforms to our view that excited water molecules participate in this reaction in addition to the ionized molecules. It is to be presumed that an acceptor concentration of approximately 4 M would entail full reaction between the dissolved substance and the dissociation products from 8-9 water molecules. In such case, at least one acceptor molecule would be located within the limits of a single elementary cell of the water. At lower concentrations of the dissolved substance the fraction of excited water molecules entering into reaction would be proportionally smaller if it is assumed that there is no transfer of excitation energy from one water molecule to another over distances of several molecular radii.

Figure 2 presents the earlier published data [3] on the radiochemical reduction of nitrate ions in aqueous solution (full curve) and the theoretical curve (dashed). The initial portions of these curves agree satisfactorily. The rise in the region of higher concentrations begins earlier for the experimental curve and the yield of nitrite reaches a value of 9 eq/100 ev in sodium nitrate solutions. The earlier rise in the region of involvement of excited molecules is obviously to be explained by the fact that the conditions are favorable for a transfer of the excitation energy from the molecules of the medium to the molecules which form the hydrate layer.

The right-hand portions of the curves showing the data of A. I. Chernova on the yield from oxidation of ferrous ions can be interpreted in these same terms (Fig. 3).

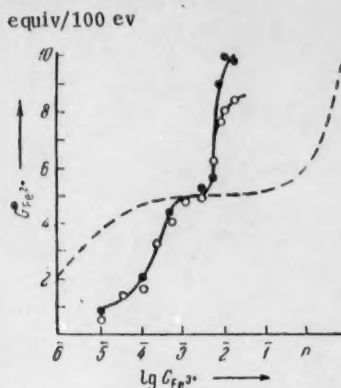


Fig. 3. The relation between the concentration and the yield from reduction of ferric ions in solution of pH 3: 1) Without addition; 2) in the presence of glycerin at 1 M (dashed curve developed theoretically).

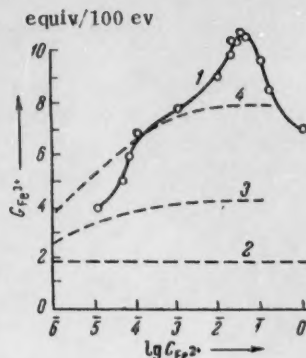


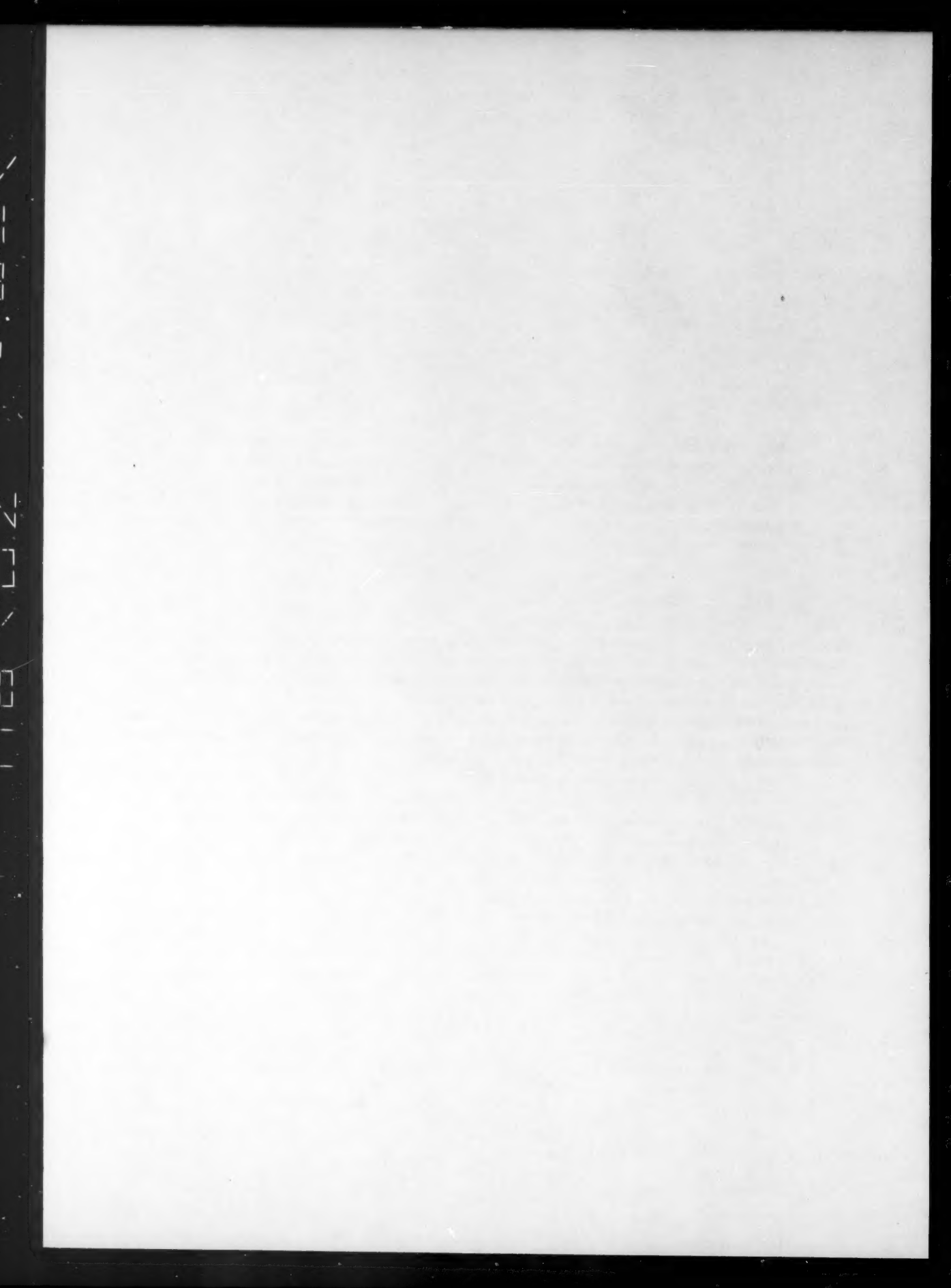
Fig. 4. The relation between the concentration (0.8 N  $H_2SO_4$ ) oxidation of ferrous ions in an atmosphere of nitrogen: 1) experimental relation; 2) oxidation by  $H_2O_2$ ; 3) oxidation by  $H_2O_2 + OH$ ; 4) oxidation by  $H_2O_2 + OH + H_2^+$  according to the Weiss theory.

The S-form of the left-hand portions of these curves indicates the presence of a competing acceptor. Here, the competing acceptor is the  $H^+$  ion; this reacts with atomic hydrogen to form the molecular ion  $H_2^+$  which has a low cross section for interaction with the similarly charged ferric ions. It should be noted in passing that the numerous hypotheses advanced by foreign workers to explain the mechanism of reactions involving  $H_2^+$  ions never take account of electrostatic repulsion between these and other positively charged particles (cations). An example is the Weiss explanation [2] of the high yield from oxidation of ferrous ions in the absence of oxygen as the result of oxidizing action by these molecular hydrogen ions. Such treatment had been generally accepted and has served as a basis for the development of the curves which are shown in Fig. 4. The dotted curve 2 corresponds to the contribution to the oxidation of ferrous ions arising from the molecular products obtained from radiolysis of water (hydrogen peroxide) according to the Allen terminology. Curve 3 also allows for a contribution to the oxidation from interaction with OH radicals. Curve 4 is constructed for the over-all effect of  $H_2O_2$ , OH radicals, and molecular ions  $H_2^+$ . The dashed curve 1 is constructed from the experimental data of A. I. Chernova on the relation between the concentration and the yield in the oxidation of ferrous ions in aqueous solutions saturated with an inert gas. It is easily seen that this curve and the curve developed on the basis of the Weiss-Allen hypothesis agree over only a very narrow interval of concentrations. The course of the former curve and the position of the maximum on it at approximately 11 eq/100 ev are certainly not in agreement with the Weiss-Allen Theory. This is understandable since these workers did not admit the possibility of the participation of excited molecules, but introduced a number of arbitrary assumptions to account for the increased yield in terms of ionized water molecules alone.

#### LITERATURE CITED

1. L. H. Gray, Collection: Radiational Chemistry [Russian translation] (IL, 1953) p. 263.
2. T. Riqq, G. Stein, and J. Weiss, Proc. Roy. Soc. A-211, 375 (1952).
3. V. A. Sharpatyi, V. D. Orekhov, and M. A. Proskurnin, Doklady Akad. Nauk SSSR 122, 825 (1958).\*

\* Original Russian pagination. See C. B. translation.



THE RELATION BETWEEN THE ELECTRICAL CONDUCTIVITY  
OF ORGANIC SUBSTANCES WITH CONJUGATE BONDS AND  
THE ELECTRON MAGNETIC RESONANCE SPECTRA

B. L. Tal'roze and L. A. Blyumenfel'd

Institute of Chemical Physics, Academy of Sciences of the USSR

(Presented by Academician N. N. Semenov, June 25, 1960)

Translated from Doklady Akademii Nauk SSSR, Vol. 135, No. 6, pp. 1450-1452,  
December, 1960

Original article submitted June 23, 1960

Many organic substances show a high electrical conductivity of the nonionic type at room temperature and have a clearly expressed photoconductivity [1, 2].

Recently, interest in organic semiconductors has increased markedly as the result of the development of various polymers which have high electrical conductivity [3-5]. The molecules of such substances usually contain conjugate double bonds.

A study [6] by one of the present authors and his co-workers of a number of polymers which contain conjugate double bonds has disclosed substances showing high electrical conductivity at room temperature. However, most of the investigated materials proved to be typical insulators at room temperature, the "energy of activation",  $E$ , and the frequency factor,  $\sigma_0$ , in the expression for the electrical conductivity,  $\sigma$ , varying over wide limits, depending on the substance in question and the conditions under which it was prepared. The factor  $\sigma_0$  proved to be linearly related to  $E$ , the relationship being less clearly expressed in substances for which  $E$  is low and quite marked for substances in which  $E$  is high.

At the same time, it has been shown in a number of papers [7-9] that there is an anomaly in the magnetic properties of such compounds which can be described as follows. All polymers containing a sufficiently well-developed system of conjugate double bonds show narrow (4-8 oersted) symmetric electron paramagnetic resonance lines with a free spin  $g$ -factor. The signal intensity is independent of the method of preparing the polymer, being completely determined by its degree of conjugation. The signal intensity in the investigated polymers is such as to correspond formally to  $10^{16}$  -  $10^{20}$  unpaired electrons per gram, or  $10^{-4}$  to  $10^{-1}$  unpaired electrons per molecule. This effect persists on dissolution and the number of unpaired electrons per gram is independent of the degree of dilution. The temperature variation of the intensity of the resonance signal indicates that these materials follow the Curie Law exactly, so that the signal arises from the ground state of the system.

Certain of these conjugate bond polymers which contain heteroatoms or electron donor and electron acceptor groups in the conjugated chain also show very wide (500-1000 oersted) asymmetric magnetic resonance lines in the solid state, the  $g$ -factor of such lines being higher than that for the free electron. The integral intensities of these "wide" lines correspond to  $10^{21}$  -  $10^{22}$  unpaired electrons per gram, if true paramagnetism is assumed. The fact that the static magnetic susceptibility is markedly dependent on the external magnetic field strength (clearly expressed saturation effects) indicates, however, that this is not an instance of paramagnetism but of an effect due to collective spin interaction. It has been proposed in [10] that such effect be designated as the "pseudo-ferromagnetism" of the organic structure. This wide line effect disappears on dissolution and is

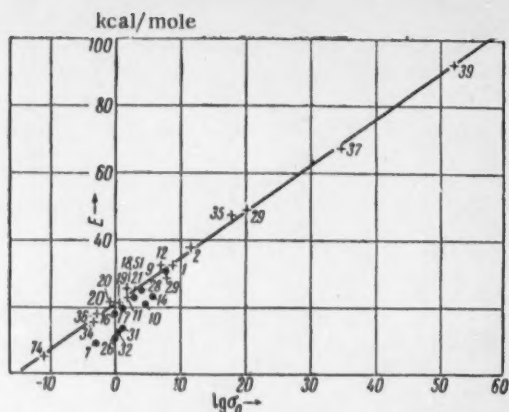
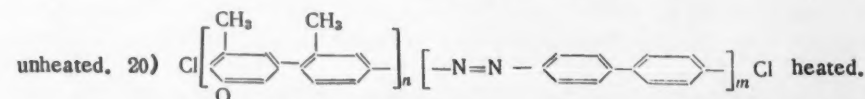
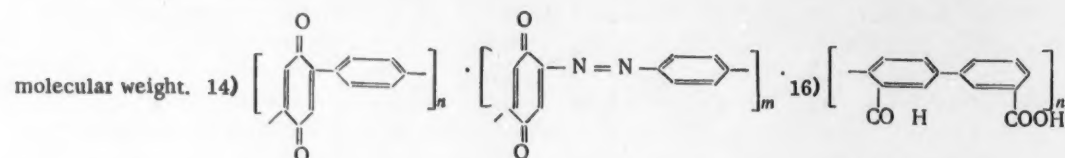
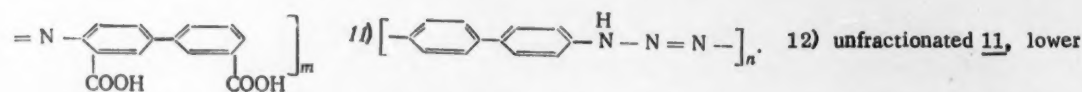
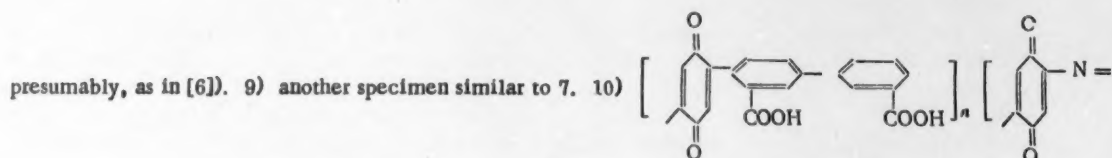
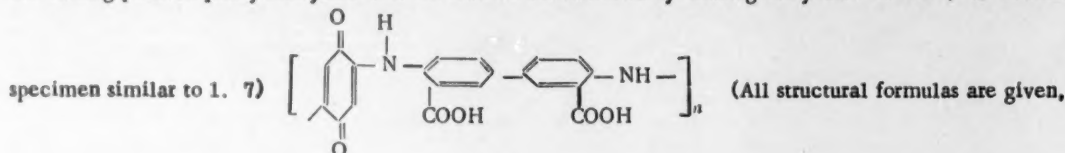


Fig. 1. The relation between the frequency factor and the energy of activation for electrical conductivity.\*

markedly increased by any treatment which increases the degree of order in the packing of the macromolecules [9].

A comparison of the magnetic properties and the electrical conductivity of the substances which we have studied is of interest. Figure 1 presents data on the  $\sigma_0$  and  $E$  values of these materials and certain other substances for which information is available in the literature. The figure also indicates the type of magnetic resonance spectrum in each case. It can be seen that the electrical conductivity at fixed  $E$  of each substance which has a wide electron magnetic resonance line is displaced in the direction of higher values, or enhanced conductivity at room temperature. The linear relation between  $\sigma_0$  and  $E$  is pronounced and clearly applies quite well to all of the materials

\* The plus signs in Fig. 1 denote samples which gave only narrow EPR lines, while the points designate samples giving wide EPR lines. 1) Polyphenylacetylene, a mixture of the yellow form obtained by polymerization at the boiling point of phenylacetylene and the black form obtained by heating the yellow to 400°; 2) another



(Footnote continued on following page.)

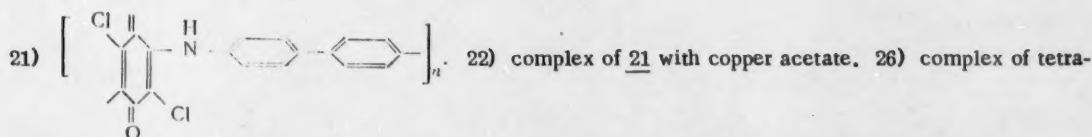
which do not have wide magnetic resonance lines. These results indicate that the correlation is between the conductivity and the pseudo-ferromagnetism of the organic structure rather than between the conductivity and the EPR spectrum of the conjugate system in general.

We cannot give a strict theoretical interpretation of this correlation at the present time. It can only be said that the appearance of "wide lines" gives indication that the sample contains ordered regions with a great number of unpaired electrons. It can be supposed that there is practically no resistance to charge movement in such regions. The transfer of charges between these "ordered regions" is the factor which limits the electrical conductivity in such a case.

#### LITERATURE CITED

1. A. T. Vartanyan, *Acta Phys. Chim.* **22**, 201 (1947).
2. D. D. Eley, et al., *Trans. Farad. Soc.* **49**, 79 (1953).
3. A. V. Topchiev, et al., *Doklady Akad. Nauk SSSR* **128**, 312 (1959).\*\*
4. A. Epstein and B. Wild, *J. Chem. Phys.* **32**, 324 (1960).
5. M. R. Neill and C. E. Weiss, *Austr. J. Chem.* **12**, 643 (1959).
6. E. I. Balabanov, et al., *Doklady Akad. Nauk SSSR* **134**, 3 (1960).\*\*\*
7. A. A. Berlin, et al., *Vysokomolek. Soed.* **1**, 1361 (1959).
8. L. A. Blyumenfel'd, et al., *Vysokomolek. Soed.* **1**, 1647 (1959).
9. L. A. Blyumenfel'd, et al., *Zhur. Strukt. Khim.* **1**, 1 (1960).\*\*\*
10. L. A. Blyumenfel'd and V. A. Benderskii, *Doklady Akad. Nauk SSSR* **133**, 6 (1960).\*\*\*

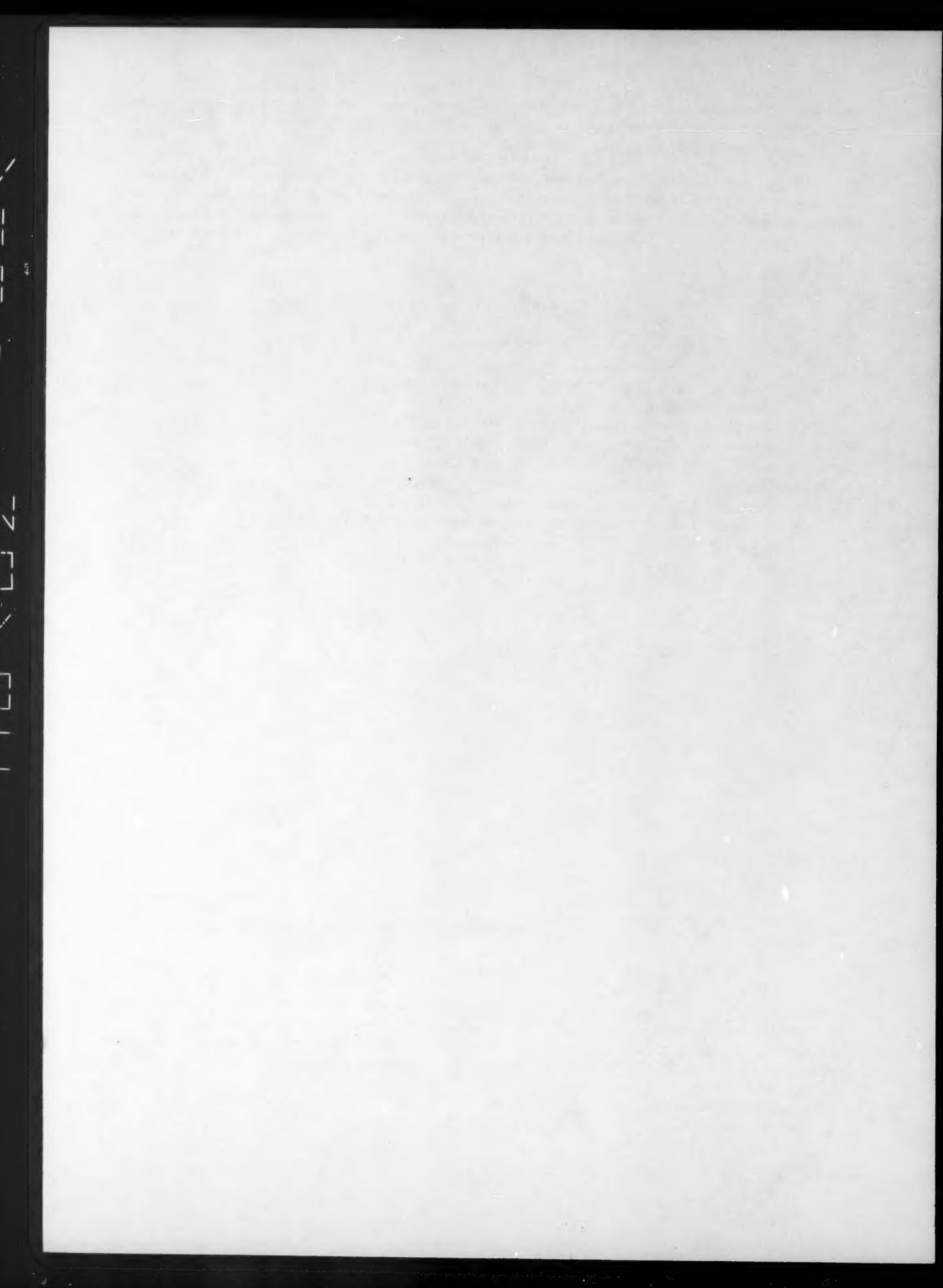
\* (Continued from preceding page).



salicylferrocene with  $\text{Fe}^{++}$ . 29) copolymer of polyphenylacetylene with hexyne. 31) polytetracyanethylene. 32) polytetracyanethylene with cyanethylene. 34) polyphenylacetylene, yellow, pressed at  $200^\circ$  and  $2000 \text{ kg/cm}^2$ . 35) polyphenylacetylene, black, pressed at  $200^\circ$  and  $2000 \text{ kg/cm}^2$ . 36) copolymer of yellow polyphenylacetylene and *n*-diethynylbenzene. 37) complex of acenaphthene with chloranil (1:1). 39) similar to 37 but in ratio 1:2. 74) polyphenylene.

\*\* Original Russian pagination. See C. B. translation.

\*\*\* See C. B. translation.



MISSING PAGES ARE INDEX PAGES  
WHICH HAVE BEEN PHOTOGRAPHED  
AT THE BEGINNING OF THE VOLUME(S)



